Université de Montréal

A Spectroscopic Survey of the WNL Stars in the Large Magellanic Cloud: General Properties and Binary Status

par

Olivier Schnurr

Département de physique

Faculté des arts et des sciences

Thèse présentée à la Faculté des études supérieures

en vue de l'obtention du grade de

Philosophiæ Doctor (Ph.D.)

en physique

Juillet, 2007

Université de Montréal

Faculté des études supérieures

Cette thèse intitulée:

A Spectroscopic Survey of the WNL Stars in the Large Magellanic Cloud: General Properties and Binary Status

présenté par:

Olivier Schnurr

a été évalué par un jury composé des personnes suivantes:

Pierre Bastien,	Président-rapporteur
Anthony F.J. Moffat,	Co-directeur de recherche
Nicole St-Louis,	Co-directrice de recherche
Gilles Fontaine,	Membre du jury
Gregor Rauw,	Examinateur externe

Thèse acceptée le: _____

Sommaire

Cette thèse présente les résultats d'un relevé spectroscopique detaillé de 41 des 47 étoiles Wolf-Rayet (WR) tardives et riches en azote (les étoiles dites WNL) connues dans le Grand Nuage de Magellan (LMC). Pour étudier les six étoiles WNL manquantes, qui se trouvent toutes dans le centre de l'amas stellaire extrêmement dense R136, dans 30 Dor, nous avons dû utiliser la spectroscopie proche infrarouge assistée d'une optique adaptative. Les résultats de cette étude-là seront publiés ailleurs.

Notre relevé conclut l'effort du groupe des étoiles massives de Montréal au cours des dix dernières années pour observer en spectroscopie toutes les étoiles WR dans les Nuages de Magellan afin d'identifier celles qui sont binaires à partir de variations en vitesse radiale (VR). La nature binaire des WR a été le sujet de débats depuis qu'on ait reconnu leur nature évoluée, vers la fin des années mille neuf cent soixante. Les modèles d'évolution stellaire prédisaient une fréquence de binaires WR croissante avec une métallicité décroissante, car les progéniteures ne pourraient pas atteindre la phase WR si elles étaient simples. Notre étude observationelle avait pour but de vérifier cette prédiction.

Après une description générale de l'importance des étoiles massives dans le contexte de l'astrophysique moderne, nous décrivons nos observations. Ensuite, nous expliquons nos méthodes d'analyse incluant la calibration des données et le choix de standards de VR. Nous incluons dans notre analyse des données photométriques ainsi que des données rayons-X. Nous identifions quatre nouvelles binaires, ce qui donne un total de seulement neuf WNL binaires connues, une valeur trop modeste par rapport aux prédictions. Par conséquent, nous rejetons l'hypothèse que la binarité joue un rôle plus important à faible métallicité pour la formation d'une WR.

Curieusement, au moins quelques étoiles WNL riches en hydrogène ne semblent pas être des étoiles WR évoluées, mais plutôt des étoiles non-évoluées, extrêmement massives et lumineuses. En effet, il y a multiples preuves que quelques-unes d'entre elles soient les étoiles les plus massives connues. Huit des neuf binaires identifiées contiennent une WNL de ce type supermassif, ce qui rendra possible la détermination de leur masse à partir d'orbites Képleriennes. Ce dernier point est décisif pour la calibration de modèles stellaires. Une des binaires de notre échantillon, R145, a été étudiée avec plus de détails. Après avoir combiné nos données avec d'autres données publiées et non-publiées, nous établissons, pour la permière fois, l'ensemble des paramètres orbitaux pour ce système, y compris l'angle d'inclinaison orbitale. Nous trouvons alors que R145 contient l'étoile la plus massive connue jusqu'à présent.

Mots clefs:

étoiles: massives, étoiles: Wolf-Rayet, étoiles: évolution, étoiles individuelles: R145

Abstract

This thesis presents the results of an intense, spectroscopic survey of 41 of the 47 known, late-type, nitrogen-rich Wolf-Rayet (WR) stars in the Large Magellanic Cloud (LMC) which could be observed with ground-based, optical telescopes. For the study of the remaining 6 WNL located in the extremely dense central object of 30 Dor, R136, adaptive-optics assisted, near-infrared spectroscopy was required. The results of this study will be published elsewhere.

Our survey concludes the decade-long effort of the Montréal Massive-Star Group to monitor *all* known WR stars in the Magellanic Clouds for radial-velocity (RV) variations due to binarity, a point which has been debated since the true, evolved nature of WR stars has been recognized in the late 1960s. From model calculations, it was expected that with decreasing metallicity, the binary frequency among WR stars increases, or otherwise the progenitor stars could not have turned into a WR star. Our survey set out to observationally test this assumption.

After summarizing the general importance of massive stars, we describe the spectroscopic observations of our program stars. We then detail the data analysis process, which encompasses careful calibration and proper choice of RV standards. We also include publicly available, visible and X-ray photometric data in our analysis. We are able to identify four previously unknown binaries in our sample, bringing the total number of known WNL binaries in the LMC to only nine. As a direct result, we question the assumption that binarity is required to form WR stars at lower metallicity.

At least some of the hydrogen-containing WNL stars in our sample seem not to be genuine, evolved, helium-burning WR stars, but rather unevolved, hydrogen-burning objects. There is ample evidence that some of these stars are the most massive stars known. As a second and

most remarkable result, all but one of our nine binaries harbor such extreme objects; this greatly enlarges the sample of such known binaries, and paves the way for an independent mass determination via Keplerian orbits in further studies, some of which we have already initiated. The results of those studies will be crucial for calibrating stellar models. One of these binaries, R145, is then studied in greater detail, combining previously published and unpublishd data with ours, to present, for the first time, a full set of orbital parameters for both components of the binary system. Since we also determine the orbital inclination angle, we are able to derive the absolute masses of this extreme object. It is found that R145 very likely harbors the most massive star known and properly "weighed" so far.

Key Words:

stars: massive, stars: Wolf-Rayet, stars: evolution, stars: individual: R145.

Table of Contents

List of Figures

List of Tables

Acknowledgements

Before coming to Montréal, I met a former student of Tony's to talk about this weird plan of going to Québec. When he noticed my hesitation, he said, without the slightest trace of doubt in his voice: "You'll have the time of your life." And what shall I say, he was right. It is therefore with deepest sincerity that I would like to thank my two supervisors, Nicole St-Louis and Tony Moffat, for having invited me to come to Montréal and work on this research project. It was an amazing experience in so many ways that I don't know where to start. Science-wise, because I gained a lot of insights in what observations are all about ("The best way not to see... is not to look!"), and of course because I had the privilege to work in a field that I am very much interested in; personality-wise, because I had wonderful experiences and great opportunities to widen my horizon and meet new, different, yet similar, interesting people and places. But on top of that, they gave me all the liberties I wanted and all the support I needed. Thank you for that.

La prochaine chose importante: les amis, évidemment. Je voudrais bien remercier Cédric, Gwen, Fred, Marie-Hélène, Laure, Nathalie, Loïc et André-Nicolas pour les moments drôles, intéressants, tristes, et intriguants que nous avons passés ensembles. Cela dit, je réitère mes remerciement envers Loïc "Général Tao" et André-Nicolas "El Commandante" pour l'incroyable fun qu'on a eu ensemble, à Montréal comme à Hawaii, avec des pizzas livraison comme avec des margouses con baguette y cerveza estivales; et encore une fois André-Nicolas d'avoir été, dès le début une longue nuit à Québec en mars 2001 lorsqu'on ne cessait pas de parler de Dieu et du monde, jusqu'à la fin interminable à Montréal, un des meilleurs amis possible. Et de continuer de l'être. Merci.

Je remercie également les personnes sans lesquelles cette thèse n'aurait pu devenir ce

qu'elle est devenue: Nidia Morrell pour des soirées inoubliables à La Serena et des discussions inspirantes sur tout; Suzanne Talon pour la patience dont elle a fait preuve afin de répondre à toutes mes question à propos de la rotation et la structure interne des étoiles; Antoine Bouchard et Geneviève Despars pour leur incroyable hospitalité en Australie après le petit malheur qui m'est arrivé là-bas; Stéphane Vennes pour les entraînements sur le 74″ à Stromlo qu'il m'a donnes et les observations qu'il a effectuées pour moi pendant que j'étais en route vers Canberra; Michaël Juneau pour sa patience et sa générosité; et last but not least Olivier Chesneau qui m'a beaucoup aidé les premières semaines à Montréal.

I would also like to thank the technical staff at all observatories I used to obtain the data for this project, in particular Angel Guerra & Edgardo Cosgrove (CTIO) and Freddy Marang (SAAO), who did a really great job; Joanna and Thijs who helped me out with last-minute Latex troubles, and Paul Crowther for his patience and his support.

Oh, and what about this guy who talked me into Montréal? Danke, Thomas!

Se non è vero, è ben trovato.

Chapter 1

Introduction

1.1 General Aspects of Massive Stars

Massive stars with initial masses $M_i \gtrsim 20 M_\odot$, i.e., that will appear as O stars on the main sequence (MS), have extremely high temperatures and densities in their central region, thus the dominant hydrogen fusion process is the CNO cycle. For this process, the energy production rate is far more sensitive to temperature than for the pp-cycle: $\varepsilon_{\rm CNO} \propto T^{17}$, while $\varepsilon_{pp} \propto T^5$ (Scheffler & Elsässer 1990). Hence, massive stars quickly run out of fuel, and their lifetimes on the MS are very short, of the order of a few million years. This has two interesting consequences: *i*) although they dominate the light of spiral galaxies, massive stars are very rare, since the initial mass function (IMF) favors low-mass stars (Salpeter 1955), and *ii*) since the formation of the Universe some 13.7 billion years ago, several thousand generations of massive stars have formed, evolved and expired.

Since massive stars are hot and extremely luminous, they account for almost the entire ultraviolet (UV) and far-ultraviolet (FUV) flux of their host galaxies, thus they strongly influence the energetic-radiation balance in their close environments. Moreover, due to the copious amounts of FUV photons they generate, massive stars can drive fast and dense stellar winds at all stages of their lives. These winds inflict severe mass loss to the stars, thereby influencing stellar evolution (see Figure 1.1). Furthermore, massive stars will, despite their

absolute rarity, dominate the feed-back to the local interstellar medium (ISM) in star-forming galaxies via their winds. Thus, they will enrich their environment with both radiation and kinetic energy. While their ionizing radiation inhibits further star formation in their proximity because they blow away the natal molecular cloud (i.e. massive stars are the last to form), the accumulated winds of an entire population of massive stars, so-called superwinds, can trigger star formation by compressing interstellar matter (e.g. Stegman 2002).

Wolf-Rayet (WR) stars have a particularly great influence on their environment. Typical WR stars possess wind densities an order of magnitude larger than massive O stars; also, since most WR stars are evolved objects in the core-helium burning (CHeB) phase, their winds are highly enriched with helium and nitrogen (WN) or carbon and oxygen (WC/WO); moreover, WC stars can form carbon dust when member of a binary system, or, when belonging to the WC9 subgroup, even when they are single (see Marchenko et al. 1999). Thus, given the high turn-over rates due to short lifetimes, massive stars in general and WR stars in particular are the primordial sources of chemical enrichement in the early Universe. This is particularly true since WR stars are considered to be the last observable evolutionary phase of massive stars before they explose in a core-collapse supernova (ccSN), which itself is an important source for kinetic and radiation energy, and of course of heavy, trans-iron elements formed during the explosive nucleosynthesis in a SN. Hydrogen and helium-depleted WR stars have also been proposed as progenitors of long, soft Gamma-Ray Bursts (Woosley & Bloom 2006). In view of the great influence WR stars have on their environment, their formation, in particular at lower metallicities (i.e., at higher redshifts) is a paramount question in modern astrophysics.

1.2 How Do Wolf-Rayet Stars Form?

Classical WR stars are now canonically regarded as the almost bare, helium-burning cores of evolved, massive O stars. Thus, in order to become a WR star, an O star has to shed most of its hydrogen-rich envelope, and how it does so has ever since been one of the most debated problems in massive-star evolution. While it is evident that massive O stars experience mass

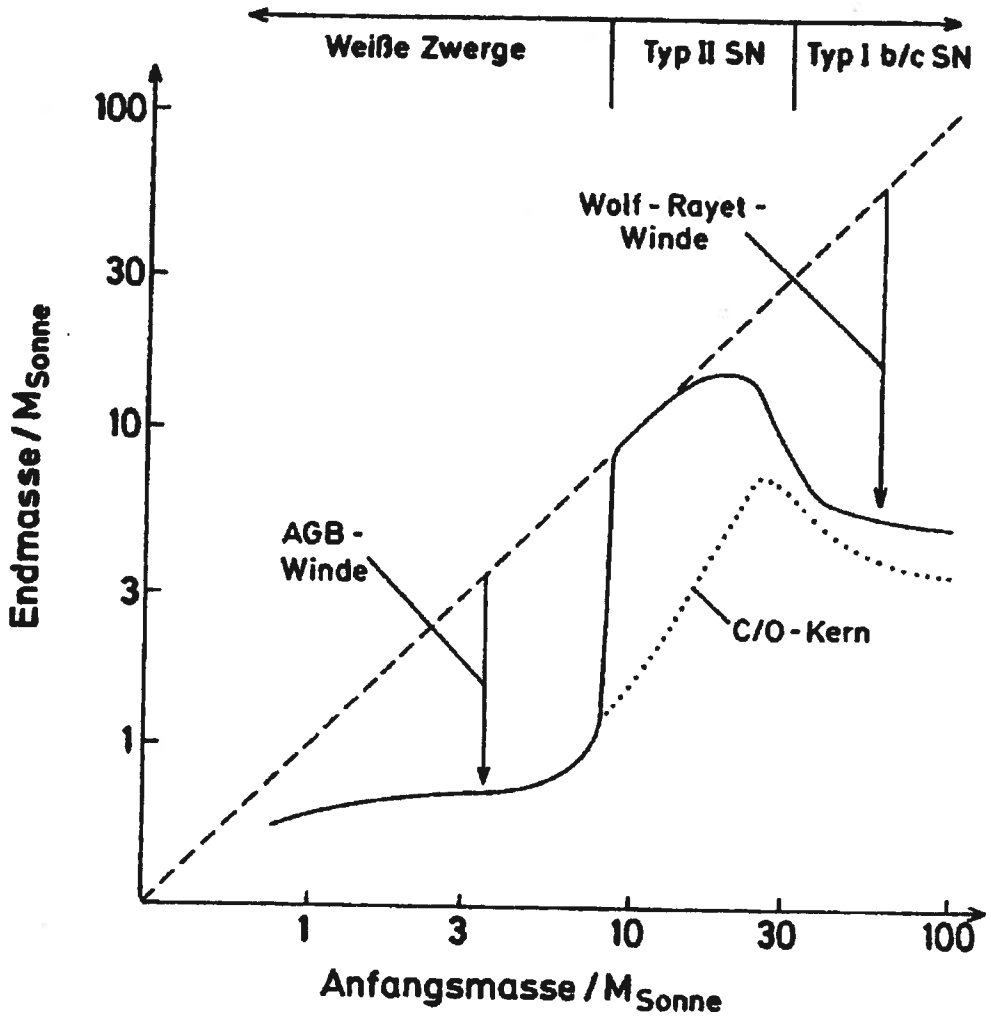

FIGURE 1.1 – Schematic plot of how stellar winds affect the final masses M_f (*"Endmasse"*), depending on the initial mass M_i (*"Anfangsmasse"*) in $M_\odot$ for all stars that shine through nuclear fusion. If no mass loss occurred, initial and final masses would be identical (dashed 45° line). Stars with initial masses $\lesssim 8M_\odot$ are expected to go through the asymptotic giant branch (AGB) phase, during which they experience mass loss through massive winds before turning into white dwarfs (*"Weisse Zwerge"*). Stars with intermediate initial masses ($8M_\odot \lesssim M_i \lesssim 20M_\odot$) go through neither the AGB nor the Wolf-Rayet (WR) phase, i.e. they do not experience significant mass-loss episodes; such stars will have the highest final masses of their C/O core (as is indicated by the dotted line named *"C/O-Kern"*) prior to their explosion in a Type II SN. Stars with initial masses above $\sim 20M_\odot$ experience the absolute highest mass loss. The strong winds experienced during the WR phase (indicated by *"Wolf-Rayet-Winde"*) lower the final core masses before such stars explode in Type Ib,c SNe. However, since this graph has been published, the mass-loss rates of hot, luminous stars have been constantly on the decrease, so that the terminal masses prior to Type Ib,c SNe might be larger. On the other hand, the influence of the luminous blue variables (LBVs) might have been significantly underestimated. Taken from Langer (1995).

loss (see above), it has for a long time not been clear how they could possibly lose enough mass to expose their cores. WR-star masses obtained from Keplerian orbits of eclipsing binaries revealed that classical WR stars have masses $\lesssim 25M_{\odot}$ (e.g. van der Hucht 2001), whereas massive O stars have masses in excess of this value. This mass difference between the unevolved O stars and the evolved WR stars indicates that massive stars have to lose a significant fraction of their initial mass before they reach the CHeB phase.

Several WR formation scenarios were put forward. Since mass-loss rates of O stars were found to be dependent on both luminosity L (and hence, initial mass) and ambient metallicty Z, it was soon realized that probably only the most massive stars, with initial masses in excess of $\sim 60M_{\odot}$ at solar Z, were able to drive strong enough winds to lose all of their envelope by the time they reach the CHeB phase, and thus to expose their cores (Conti 1976). Stars initially less massive were supposed to go through an intermediate stage, which was identified with the red supergiant (RSG) phase. However, it soon was discovered that there is a lack of RSGs with a luminosity corresponding to initial masses higher than $\sim 40M_{\odot}$ (Humphreys & Davidson 1994); instead, the locus in the Hertzsprung-Russell Diagram (HRD) where extreme RSGs were expected, was found to be populated by the enigmatic luminous blue variables (LBVs). Their name already suggests that they are often hot (i.e., blue) and extremely luminous, and that they undergo episodes of eruptive mass loss. How often these episodes occur and how much mass LBV shed during each such episode, or in total during their lifetime, is still highly controversial.

LBVs are canonically considered to descend from stars with initial masses $40M_{\odot} \lesssim M_i \lesssim 60M_{\odot}$ which, while travelling towards the red side of the HRD during and/or shortly after their MS evolution, encountered their limits of radiative stability (the so-called Eddington limit). However, the upper mass limit, if there is one at all, for reaching the LBV phase is only poorly known; the Galactic LBV η Carinae, for instance, might have an initial mass of $\sim 100M_{\odot}$, which would mean that even the most massive stars cannot avoid the LBV phase. It is thought that such massive stars are too luminous to retain their outer layers, which, due

to some as of yet unexplained, but in any case extreme (radiation?) pressure, are expelled. While so far, not much more is understood of these LBVs, it was theorized that after regaining stability, post-LBV stars would turn into WR stars (Wolf et al. 1980).

Stars initially less massive than the canonical lower limit to reach the LBV phase, on the other hand, are supposed to become luminous RSG once they end their MS life, i.e. when they reach shell-hydrogen burning (SHB). It is theorized that during the RSG phase, radiatively-driven mass loss is large enough to rid the stars from their outer, hydrogen-rich envelope, so that they can turn into WR stars once they reach the CHeB phase. However, recent observations suggest that the locus of RSGs in the Hertzsprung-Russell diagram is more consistent with stars whose initial masses are not $25M_{\odot} \lesssim M_i \lesssim 40M_{\odot}$, but rather between $10M_{\odot} \lesssim M_i \lesssim 25M_{\odot}$ (e.g. Massey et al. 2007, and references therein). This in turn means that the LBV phase most likely occur for stars with initial masses all the way down to $\sim 25M_{\odot}$.

This would alleviate major problems with the single-star evolution scenarii, given that radiatively-driven mass-loss rates depend on the ambient metallicity, among other things. Thus, if the metallicity is sufficiently low, a star requires a higher luminosity (i.e., initial mass) if it is to experience the same mass-loss rates and follow the same evolutionary path. However, there is evidence that the IMF does not change its slope with metallicity (e.g., Massey 2003); hence it was theorized that at lower Z, there will simply be fewer single stars that will lose enough mass to reach the WR stage. This means that if significant numbers of WR stars are still observed at very low ambient metallicities, a different formation mechanism from those described above takes over.

Moreover, Fullerton et al. (2006) reported that for O stars, mass-loss rates had possibly to be corrected downwards by factors of $\sim$ 10 up to 100(!). While it is still not clear how this changes our *overall* view on massive-star evolution, for the affected stars the evolutionary path might be completely altered, because these stars then do not lose any significant fraction of their initial mass during their main-sequence lifetime. Thus, if no LBV phase intervened,

such stars could never reach the WR stage and expose their inner, helium-enriched layers. It might thus very well be that the LBV stage is much more important for the evolution of single, massive stars than is currently thought.

1.3 WR Stars and Binarity

The mechanism that was proposed to form WR stars in low-Z environments was Roche-lobe overflow (RLOF) in close, interacting binaries. When a massive star evolves off the MS, it expands its outer layers; this is particularly the case during SHB. Thus, if the star is member of a sufficiently close binary system, it could expand beyond its Roche lobe; gravitational mass loss would then ensue, stripping the star of its hydrogen-rich envelope, and exposing the bare core.

Since binarity is supposed to be independent of ambient Z, it was proposed by Vanbeveren et al. (1998) that RLOF in binaries was the dominant WR formation mechanism in environments with very low metallicity. Indeed, evolutionary models by the Geneva group were unable to reproduce the observed WR populations at different Z without increasing the number of interacting binaries in their models (Maeder & Meynet 1994). It was thus assumed that at low Z, binaries were indeed required to form WR stars.

As will be seen in the forthcoming chapters, in principle this assumption can be observationally tested. In an attempt to conclude the long-standing issue of WR formation at different Z, intense spectroscopic surveys of *all* known WR stars in the Magellanic Clouds were carried out. We here describe our study, the last of three of their kind, that aimed at determining the binary frequency among the late-type, nitrogen-rich subgroup of WR stars, the so-called WNL stars. With the results of our study as well as of the previous studies at hand, we will, for the first time, be able to address the binary frequency among *all* known WR stars in the Magellanic Clouds and thus to obtain statistically viable results to observationally test the influence of metallicity on the evolution of massive stars.

Chapter 2

A SPECTROSCOPIC SURVEY OF WNL STARS IN THE LMC

General Properties and Binary Status

O.Schnurr[1] A.F.J. Moffat[1], N. St-Louis[1]

N.I. Morrell[2]

M.A. Guerrero[3]

To be submitted to MNRAS

[1]Département de Physique, Université de Montréal, C.P. 6128, Succ. Centre-Ville, Montréal, Québec H3C 3J7, Canada; [redacted]

[2]Las Campanas Observatory, Observatories of the Carnegie Institution of Washington, Casilla 601, La Serena, Chile; [redacted]

[3]Instituto de Astrofísica de Andalucía, Consejo Superior de Investigaciones Científicas, Apartado Correos 3004, E-18080 Granada, Spain; [redacted]

2.1 Abstract

We report the results of an intense, spectroscopic survey of all 41 late-type, nitrogen-rich Wolf-Rayet (WR) stars in the Large Magellanic Cloud (LMC) which can easily be reached from ground-based telescopes. This survey concludes the decade-long effort of the Montréal Massive Star Group to monitor every known WR star in the Magellanic Clouds except for the 6 crowded WNL stars in R136, which will be discussed elsewhere. The focus of our survey was to monitor the so-called WNL stars for radial-velocity (RV) variability in order to identify the short- to intermediate-period ($P \lesssim 200$ days) binaries among them. Our results are in line with results of previous studies of other WR subtypes, and show that the binary frequency among LMC WNL stars is statistically consistent with that of WNL stars in the Milky Way. We have identified four previously unknown binaries, bringing the total number of known WNL binaries in the LMC to nine. Since it is very likely that none but one of the binaries are classical, helium-burning WNL stars, but rather superluminous, hence extremely massive, hydrogen-burning objects, our study has dramatically increased the number of known binaries harbouring such objects, and thus paved the way to determine their masses through model-independent, Keplerian orbits. It is expected that some of our binaries will be among the most massive stars known. With the binary status of each WR star now known, we also studied the photometric and X-ray properties of our program stars using archival MACHO photometry as well as *Chandra* and *ROSAT* data. We find that one of our presumably single WNL stars is among the X-ray brightest WR sources known. We also identify a binary candidate from its RV variability and X-ray luminosity which harbours the most luminous WR star known in the Local Group.

2.2 Introduction

Wolf-Rayet (WR) stars are stars whose optical spectra feature broad emission lines from highly-ionized elements like nitrogen (if dominating, the star is then classified as WN), carbon (WC), or oxygen (WO). These emission lines arise in a fast, hot, and dense stellar wind which

is generally optically thick in the inner part, thereby completely veiling the hydrostatic photosphere of the WR star. It therefore took more than a century after their discovery before it became clear that, with few exceptions, most WR stars were evolved objects, displaying fusion products of CNO hydrogen (H) burning (WN) or 3α helium (He) burning (WC and WO) in their winds (Lamers et al. 1991; Maeder & Conti 1994). The exception to this assessment is the superluminous and H-rich subgroup of so-called WN5-7ha stars, for which there is growing evidence, both observational and theoretical, that these are young, unevolved, core-hydrogen burning (CHB) rather than core-helium burning (CHeB) objects (Langer et al. 1994; de Koter et al. 1997; Crowther & Dessart 1998). Their very high luminosities, required to drive WR-like mass-loss rates, merely reflect their very high masses; indeed they are very likely the most massive CHB stars known (Rauw et al. 1996; Schweickhardt et al. 1999; Rauw et al. 2004; Bonanos et al. 2004). In order to distinguish evolved WR stars in the CHeB phase from extreme "Of stars on steroids" (Massey & Hunter 1998), we shall hereafter call "classical" the He-burning WR stars.

Classical WR stars are commonly considered as the almost bare, H-depleted, He-burning cores of stars whose initial mass on the main sequence (MS) was, at solar metallicity, above $\sim 25M_{\odot}$, i.e. that started their lives as O stars. Thus, WR-star progenitors have to lose more or less all of their outer, H-rich envelopes, which also represent a considerable fraction of their initial mass. For single stars at solar metallicity, the canonical evolutionary path follows the "Conti scenario" (Conti 1976; Maeder & Conti 1994): From $25M_{\odot} \lesssim M_{\rm i} \lesssim 40M_{\odot}$, O stars are expected to turn into luminous red-supergiants (RSGs) once they reach the shell-hydrogen burning (SHB) phase[4]. The H-rich envelope is then lost through stellar winds, and the core exposed. The star turns into an H-poor WN star and eventually explodes as a Type Ib core-collapse supernova (cc-SN). More massive stars with $40M_{\odot} \lesssim M_i \lesssim 60M_{\odot}$ apparently do not become RSGs, but rather go through a phase of instability during which they experience huge and episodic mass loss through shell ejection (Humphreys & Davidson 1979, 1994). After

[4]However, recent observational work by Massey et al. (2007) showed that the bulk of RSGs arise only in the intial-mass range $10M_{\odot} \lesssim M_{\rm i} \lesssim 25M_{\odot}$, so that virtually all WR stars require the LBV stage to expose their inner, He-enriched layers, given the reduced mass-loss rates of their progenitor O stars, due to clumping (e.g. Fullerton et al. 2006).

CHeB ignition, these stars are expected to become H-depleted WN stars as well (Wolf et al. 1980) and, since the He-burning cores are massive and thus luminous enough to quickly blow away their CNO-enriched layers and to expose 3α elements, to evolve into WC and WO stars before exploding as a Type Ic cc-SN. Stars initially even more massive, with $M_i \geq 60 M_{\odot}$, suffer from sufficiently high mass-loss rates to reach the WR phase while still in the CHB phase. These stars represent the above mentioned, superluminous WN5-7ha stars. While it is yet unsettled whether these stars reach the classical WR phase by going through the LBV phase as well (Smith & Owocki 2006) or whether they directly evolve into H-poor WN stars (Conti 1976; Maeder & Meynet 2000), they are expected to reach the WC and WO phase before exploding as a Type Ic cc-SN. (Note, however, that the existence of the Galactic LBV η Carinae with a proposed mass of $\sim 100 M_{\odot}$ strongly suggests that even the most massive stars cannot avoid the LBV phase.)

Mass loss through radiatively-driven stellar winds is thus the key to understanding the evolution of single massive stars, because it dominates virtually all evolutionary phases sketched above. For winds which are line-driven, i.e. by radiative pressure on ions through scattering of high-energy photons in resonance lines, mass-loss rates $\dot{M}$ depend on the availbility of line opacity (mainly due to iron-peak elements), i.e. on the initial metallicity Z as $\dot{M} \propto Z^{\alpha}$, where $\alpha = 0.69$ (see Vink et al. 2000, 2001 for details). This means that at lower ambient Z, stars have to be initially more massive to reach the WR stage; Maeder (1998) reports that the lower initial-mass limits for WR formation are 25, 35, and 40 $M_{\odot}$ for solar ($Z_{\odot}$), LMC ($Z_{\rm LMC} \sim 1/3 Z_{\odot}$), and SMC metallicity ($Z_{\rm SMC} \sim 1/5 Z_{\odot}$), respectively. Since the initial-mass function (IMF) has been found to be independent of Z, WR populations change with metallicity (see Massey 2003 and references therein), and so do number ratios involving WR stars, like e.g. WR/O or WN/WC. Because the evolution of WR stars is largely dominated by mass loss rather than by uncertain, hydrodynamical processes like convection (as are e.g. RSGs; Langer & Maeder 1995), WR number ratios at different Z are frequently used as touchstones for stellar-evolution models.

However, it is obviously paramount that the influence of binaries on WR formation, as well as how this influence changes with metallicity, be well understood if those number ratios are to be used. Binary interaction can have a dramatic effect on WR formation and was, in fact, the first ever proposed WR-formation scenario. Paczynski (1967) pointed out that Roche-lobe overflow (RLOF) in close binary systems greatly enhances the removal of the envelope when the primary (i.e., the more evolved and thus initially more massive star) expands its envelope beyond its Roche limits while turning into a RSG during the SHB phase. The large mass loss during this so-called Case B RLOF (Kippenhahn & Weigert 1967) strips the primary almost completely of its H-rich envelope and exposes its bare core. Once the star ignites CHeB, it may turn into a classical WR star, and any residual H is quickly blown away by the WR winds.

Vanbeveren et al. (1998) elaborated on this interacting-binary scenario. They proposed that close O+O binaries with inital periods $P \lesssim 1000$ d cannot escape RLOF if the primary star reaches the RSG stage[5], therefore, exceeds its Roche limits. Since binarity is expected to be Z-independent, the authors expected WR formation through RLOF to become more important for lower Z, since ever fewer O stars are massive enough to reach the WR phase through single-star evolution. Moreover, if the majority of WR stars at low Z, e.g. in distant starbursts, descend from lower-mass stars in binaries, there will be a significant increase in age of the WR population that has to be taken into account, since less massive stars take longer to reach the RSG phase (which, as noted above, is required for Case B RLOF to occur). Additional to that, it might very well be that RLOF is (quasi-)conservative, i.e. that the mass lost by the primary is (almost) entirely accreted onto the secondary, which then in turn might become massive enough to reach the WR phase through single-star evolution, long after the primary has already exploded in a cc-SN (the accreted mass will "rejuvenate" the secondary and reset its nuclear clock, a phenomenon well known from the so-called "blue stragglers" in globular clusters). Clearly, WR formation through binary interaction, in particular the formation of "second-generation" WR stars, may severely distort the derived ages for starbursts as well as chemical and energetic feed-back calculations for star-forming regions at low Z (i.e., in

[5]According to Massey et al. (2007), RSGs have revised initial masses that in general lie below those of O stars, so that Case B RLOF might never occur in an O+O binary.

the early Universe), SN rates, and so forth (see e.g. de Donder et al. 1997; Schaerer & Vacca 1998; de Donder & Vanbeveren 1999; Wellstein & Langer 1999).

Maeder & Meynet (1994), using a grid of non-rotating, stellar-evolution models at different initial Z, were unable to reproduce the observed WR populations without increasing either the then-canonical mass-loss rates through stellar winds by a factor of ~ 2, or the fraction of interacting (RLOF) binaries. From the number of WR stars formed through RLOF that Maeder & Meynet required to match their models to the observations, Bartzakos et al. (2001; updated by Foellmi et al. 2003a) computed the theoretically expected fraction of WR binaries at different metallicities. They found $22 \pm 6\%$ in the Galaxy, whereas for the LMC and the SMC, the values were $52 \pm 13\%$ and $98 \pm 32\%$, respectively. Moreover, model computations of Vanbeveren et al. (1998) and Wellstein & Langer (1999) found that O+O binaries undergoing RLOF (see above) become WR+O binaries with present-day periods $\lesssim$ 200d. The theoretical predictions from Maeder & Meynet (1994) are thus testable within a reasonable amount of time. Therefore, the Montréal group embarked in a project to spectroscopically monitor all known WR stars in the Magellanic Clouds in order to assess the frequency of possible, post-RLOF binaries among the WR population, i.e. those with present-day periods $\lesssim$ 200 d. The Magellanic Clouds are the ideal laboratory for this project: a) The distances to both the SMC and the LMC are well established and $\sim$ constant for all stars (e.g. Keller & Wood 2006); b) reddening towards the Clouds is low and fairly constant, contrary to the Galaxy (e.g. Nikolaev et al. 2004), c) the WR populations in both Clouds are nearly complete (e.g. Massey & Duffy 2001, but see Massey et al. 2003).

In total, the LMC harbours 132 WR stars (Breysacher et al. 1999, hereafter BAT99[6]), while 12 WR stars are known in the SMC (Massey & Duffy 2001; Massey et al. 2003). To search for binaries, the total sample of 144 stars has been split into three distinct studies: Bartzakos et al. (2001) reported the results on the 25 Magellanic Cloud WC/WO stars, while Foellmi et al. (2003a,b) studied the 71 then-known, early-type WNE (=WN2-WN5) stars,

[6]BAT99 lists 134 WR stars in the LMC, but see Moffat (1991) and Niemela et al. (2001) for the revised WR status of BAT99-4 and BAT99-6, respectively.

with the exception of the H-rich WNE stars in and around the R136 cluster in the 30 Dor region. The observations of a 72nd WNE star, which was newly discovered by Massey et al. (2003) in the SMC, were reported by Foellmi (2004). We here present the results of the third and last part of this project, the study of the 41 late-type WNL (=WN5-11) stars known in the LMC (the two WN6 stars in the SMC were studied by Foellmi et al. 2003a), including those stars in the periphery of R136 which could be reached by normal, ground-based telescopes. For the 6 superluminous, WN5-7ha stars in the core of R136, AO-assisted, near-infrared spectroscopy using VLT/SINFONI was used; those results will be reported elsewhere (Schnurr et al., in preparation).

The aim of our study is twofold. First, we will, for the first time, be able to assess the binary frequency among the almost complete WR population of the LMC, and to address the implications of our finding for the evolution of massive stars at different metallicities. Second, we will also be able to discuss general properties of those WR stars in the context of their binary status, and compare with publicly available photometric and X-ray data. Third, binaries identified in this study will pave the way to determine their respective masses by using model-independent, Keplerian orbits. Masses of WR stars are of greatest importance in the context of calibration of both atmospheric and evolutionary models, in particular for the most massive stars. We have ample reason to believe that at least some H-rich WNL stars in our sample belong to the subgroup of very massive, possibly even the most massive stars known in the Local Group.

The paper is organized as follows: In Section 2.3, we will describe the observations of our program stars. In Section 2.4, we will briefly describe the data reduction. In Section 2.5, we will in detail describe how we analysed our spectroscopic, photometric, and X-ray data and the results we obtained. These results will be discussed in Section 2.6. Section 2.7 summarizes and concludes this paper.

2.3 Observations

2.3.1 Spectroscopic Data

Target stars were selected from *The Fourth Catalogue of Population I Wolf-Rayet Stars in the Large Magellanic Cloud* (Breysacher et al. 1999; hereafter BAT99). This catalogue lists 134 WR stars of which 47 fall into the WNL (= WN6-11) class, including the two "slash-star" types O3If/WN6 (supposedly H-burning; Crowther & Bohannan 1997) and Ofpe/WN9 (supposedly linked to the LBV phenomenon; see Stahl et al. 1983; Stahl 1987; Crowther et al. 1995; Nota et al. 1996; Pasquali et al. 1997). 41 of these 47 stars were observed with conventional spectrographs, and the results of those observations are reported here.

The goal of our study is to identify binary systems with orbital periods in the range 1 d $\lesssim P \lesssim$ 200 d from radial-velocity (RV) variations. To establish their binary nature, about 30 good-quality spectra per star, covering timescales from ~1 to ~500 days, are required. Given the high luminosity of WNL stars, the apparent magnitudes of our programme stars range from $11 \lesssim V \lesssim 15$, with most objects around $V \sim 13$, thus relatively small, 2m-class telescopes were sufficient.

Our observations were organized in three different campaigns or "epochs" between 2001 and 2003 to maximize the time coverage, and were carried out during 13 runs at 6 different, 2m-class, southern telescopes. The following observatories were used: Complejo Astronómico El Leoncito (CASLEO), Argentina; Mount Stromlo Observatory (MSO), Australia; Cerro Tololo Inter-American Observatory (CTIO), Chile; South African Astronomical Observatory (SAAO), South Africa; Siding Spring Observatory, Australia; Las Campanas Observatory (LCO), Chile. In total, 99 nights were allocated, but due to bad weather conditions or technical problems, not all nights were useful. Long-slit spectrographs were used at all telescopes. The exact wavelength coverage of the spectra depended on the respective instrument used, but all sets of data included the wavelength range from 4000 to 5000 Å , thereby comprising the strategic emission lines HeIIλ4686 and NIVλ4058. To maximize the flux reaching the de-

tector and thus achieve good S/N, a slit width of 1.5″ was used during the first two years. The obtained linear dispersion varied from 0.65 Å/pixel (SSO) to 1.64 Å/pixel (CASLEO), but all data were uniformly rebinned to 1.65Å/pixel during data reduction, thereby yielding a conservative 3-pixel resolving power of $R \sim 1000$.

However, during preliminary data reduction it became clear that the 1.5″ slit was too wide compared to the good seeing conditions on Cerro Tololo during southern summer; the position of the stellar image in the center of the slit could not be consistently reproduced from night to night, resulting in slightly different positions and hence larger RV scatter. This turned out to be particularly a problem for crowded stars, where variable seeing conditions impaired even more the identical centering of the target in the slit. Therefore, during the last campaign (2003/04, only at CTIO), the slit width was reduced to 1″ with the effect of reducing the RV scatter by almost a factor of two. We will come back to this problem later in this paper.

Exposure times were chosen to provide a signal-to-noise ratio (S/N) of ∼50-70 per pixel in the blue continuum around 4500 Å, and were adapted to the respective telescope efficiencies and weather conditions. For our faintest stars, exposures were broken into two or three parts to facilitate cosmic-ray rejection.

Even under best conditions, not more than two thirds to three quarters of our sample ("sequence A") could be observed in one night. The remaining stars ("sequence B") were then observed the following night before sequence A was restarted again, and so forth. To further break integer-day sampling (∼2-day sampling in particular), we also employed a scheme to re-observe the stars of a given sequence the following night before resuming observations of the other sequence, thereby obtaining a ∼1-day sampling (i.e. observations were carried out like ABBAABAB etc.). At CTIO, where we had relatively long runs of clear contiguous nights so that we could sufficiently plan ahead, this was particularly successfully employed. Moreover, some stars were observed more frequently (i.e. once or twice per every night) by default because they were of particular interest, e.g. they had been reported to be short-period

TABLE 2.1 – Journal of observations.

Run#	Observatory	Start (UT)	End (UT)	Clear nights	Epoch
1	CASLEO	02 Nov 2001	09 Nov 2001	6	1
2	MSO	09 Nov 2001	06 Dec 2001	14	1
3	CTIO	26 Dec 2001	31 Dec 2001	6	1
4	CTIO	23 Jan 2002	27 Jan 2002	4	1
5	SAAO	05 Nov 2002	12 Nov 2002	7	2
6	CTIO	19 Nov 2002	27 Nov 2002	8	2
7	CTIO	16 Dec 2002	24 Dec 2002	8	2
8	MSO	03 Jan 2003	18 Jan 2003	10	2
9	SSO	27 Jan 2003	31 Jan 2003	3	2
10	LCO	27 Jan 2003	02 Feb 2003	6	2
11	CTIO	19 Dec 2003	29 Dec 2003	10	3
12	CTIO	02 Jan 2004	06 Jan 2004	4	3
13	CTIO	07 Jan 2004	09 Jan 2004	2	3

TABLE 2.2 – List of observatories and instruments used.

Observatory	CASLEO	MSO	CTIO	SAAO	SSO	LCO
Telescope	2.15m	74in.	1.5m	74in.	2.3m	2.5m
Spectrograph	REOSC	CassSpec	RCSpec	GratingSpec	DBS[a]	WFCCD
Grating [l/mm]	600	600	600	600	600	600
Dispersion [Å/pix]	1.64	1.35	1.48	1.10	0.65	1.38
Spectral range [Å]	3970-5645	3885-5515	3980-5730	3485-5415	3905-4875	3775-5600
Comparison lamp	HeNeAr	FeAr	HeNeAr	CuAr	CuHeAr	HeH
Overscan	no	no	yes	yes	yes	yes

Notes: [a]Blue arm only.

and supposedly very massive binaries (e.g. BAT99-32) or, more often, a suspected binary, e.g. BAT99-118, the intrinsically most luminous WR star known in the Local Group, and therefore of particular interest (Crowther & Dessart 1998).

At the beginning of each night, bias frames and high-S/N, internal (Quartz lamp) flatfield frames were taken. For reliable RVs, a comparison-arc exposure was taken before and after each science exposure, the exception to this rule being the stars in the periphery of R136, because telescope slews were only very minor ($\lesssim 1'$) and differential flexure of the Cassegrain spectrographs not an issue. Neither dark nor twilight-flatfield frames were taken.

The observation journal is summarized in Table 2.1, while the instrumental properties are summarized in Table 2.2.

TABLE 2.3 – Program stars for which publicly available MACHO photometry was retrieved. J2000.0 coordinates and v band magnitudes are taken from BAT99. The selected MACHO objects are quoted with their MACHO B and R band magnitude, their angular distance D from the entered coordinates, and their MACHO ID, respectively. See text for more details.

BAT99 Name	RA (hh:mm:ss)	DEC (dd:mm:ss)	D ($''$)	v (mag)	MACHO B (mag)	MACHO R (mag)	MACHO-ID
012	04:57:27.4	-67:39:02.2	1.85	13.72	13.27	13.83	24.2741.10
016	05:03:08.8	-66:40:57.3	1.39	12.73	11.57	12.52	53.3724.12
030	05:21:57.6	-65:48:59.3	1.37	13.40	13.43	13.15	63.6762.13
032	05:22:22.5	-71:35:57.9	0.86	12.72	11.38	12.17	21.6796.10
054	05:31:18.0	-69:08:44.6	1.27	14.32	14.32	13.98	82.8285.10
055	05:31:25.5	-69:05:37.9	0.72	11.99	10.92	10.87	82.8286.1110
076	05:35:54.4	-68:59:07.1	1.6	13.46	14.30	13.12	82.9013.15
079	05:35:59.9	-68:11:21.4	1.66	13.58	13.53	13.49	82.9010.22

2.3.2 Photometric Data

In order to obtain repeated, high-quality photometry of our program stars, we browsed through the public archives of the Massive Compact Halo Object (MACHO; see Alcock et al. 1996) experiment, and the Optical Gravitational Lensing Experiment (OGLE; see Udalski et al. 2000). To search the databases[7], J2000.0 coordinates as given in BAT99 were entered, and a search radius of $10''$ was applied in both cases. While OGLE did not observe our programme stars (most WNL stars in the LMC were not even in the observed fields), MACHO yielded photometry of some of our targets. From the returned objects, we selected those stars with the smallest angular distance D to the entered coordinates *and* which had calibrated MACHO B and R band magnitudes comparable to the v magnitudes of our program stars as given in BAT99. A list of the thus identified stars is given in Table 2.3.

2.3.3 X-ray Data

We also made use of public archives to retrieve X-ray data for our program stars. The *Chandra* Archive[8] available from October 2004 and the entire *ROSAT* Archive[9] have been

[7]Web interfaces for lightcurve retrieval from the respective databases are accessible at `http://www.macho.macmaster.ca/` for MACHO, and at `http://bulge.princeton.edu/~ogle/` for OGLE

[8]The *Chandra* Archive is available using the *Chandra* Search and Retrieval Interface (Chaser) at the *Chandra* X-ray Observatory site; see at `http://cxc.harvard.edu`.

[9]The *ROSAT* Archive is supported by the High Energy Astrophysics Science Archive Research Center (HEASARC) of Goddard Space Flight Center, NASA. It can be accessed at the site `http://heasarc.gsfc.nasa.gov/W3Browse`.

searched for all *Chandra* ACIS and *ROSAT* PSPC and HRI observations including any of the 41 WNL stars studied in this paper. This search found *Chandra* ACIS observations for 25 WNL stars, and *ROSAT* PSPC and HRI observations for 13 and 3 WNL stars, respectively. A summarizing table of these observations is provided in Section 2.5.12. Further details of the selection and reduction of these observations are provided by Guerrero & Chu (2006a).

2.4 Data Reduction

Some of our observation runs, notably these at the Cerro Tololo Inter-American Observatory (CTIO), were interrupted by other, time-critical observations, and thus split into several runs. Since the spectrograph had to be set up again each time, we treated each such run individually to allow for effects of different grating positions, angles, alignments, etc. Thus, a total of 13 individual runs were processed.

Data reduction was carried out in the usual way using the NOAO-IRAF software package[10]. For each night, both an average bias frame and an average flatfield frame were created and used in the reduction process. Object spectra were optimally extracted using APALL with the 2D trace-fit option enabled. Sky background was fitted and subtracted from the stellar spectrum for all stars with the exception of those in the periphery of R136, where the emission spectrum of the 30 Dor nebula is strong and spatially highly variable. We could have employed the sky-subtraction method developed by Selman & Melnick (2005), but since the continuum background is very weak and does not dramatically decrease our final S/N, and since the strategic WNL emission line HeIIλ4686 is not affected by nebular emission, we abandoned sky subtraction for these stars. The major drawback is that the (intrinsic) Balmer lines of these WNL stars are affected, which renders the determination of the hydrogen content in the star highly uncertain. This has consequences which will be examined later.

Arc frames taken before and after each science exposure were averaged and then extracted.

[10]IRAF is distributed by the National Optical Astronomy Observatories, which are operated by the Association of Universities for Research in Astronomy, Inc., under cooperative agreement with the National Science Foundation.

For all observatories, dispersion correction was carried out by fitting a fourth-order Legendre polynomial. Unfortunately, due to the lack of good comparison lines at the blue edge of our spectra, the dispersion solution is less reliable in the region bluewards of 4400 Å. This has consequences that will be discussed later. Science spectra were then rebinned to uniform step-width, corrected for heliocentric velocities, and rectified by defining points in the continuum, roughly separated by ~250 Å, fitting a low-order cubic spline and dividing the spectra by the fit.

The spectra were then cleaned of cosmic rays and bad pixels as far as possible; where applicable, spectra from split exposures were combined. If a cosmic ray or bad pixel fell onto a strategic emission line, great care was taken not to significantly alter the original line profile. If this was not properly possible, the spectrum was discarded. The final stellar spectra were then rebinned to a uniform step-width of 1.65 Å/pixel. The achieved S/N ratios per rebinned pixel, calculated for the spectral region from 5050 to 5350 Å, are plotted in Figure 2.1 and 2.2, and range from 20 to 260, with a mean of 85.

2.5 Data Analysis and Results

2.5.1 Radial-Velocity Measurements

In all of our analyses, we made use of the ESO-MIDAS software package. Two different methods were employed to measure the radial velocities (RVs) of our program stars, *i*) cross-correlation (CC), using the task XCORR/IMA, and *ii*) emission-line fitting (ELF), using the task FIT/IMA to fit Gaussian profiles to emission lines.

In most of our WNL stars, the spectrum is dominated by the HeIIλ4686 emission, which is the strongest line by a wide margin. Thus, we concentrated our RV measurements on this emission line, although it is known to not always fully reflect the true orbital motion; excess emission due to wind-wind collisions (WWC) deforms HeIIλ4686 and thereby more or less

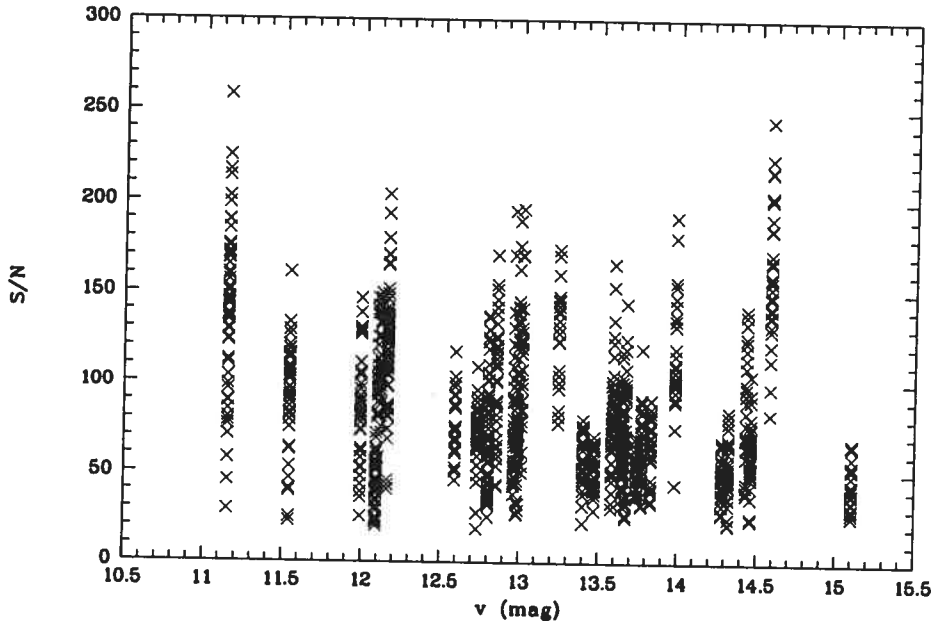

FIGURE 2.1 – S/N ratios as measured in the continuum between 5030 Å and 5300 Å of the reduced spectra. As can be seen, there is no magnitude-dependence of the achieved S/N because exposure times of fainter stars were increased accordingly.

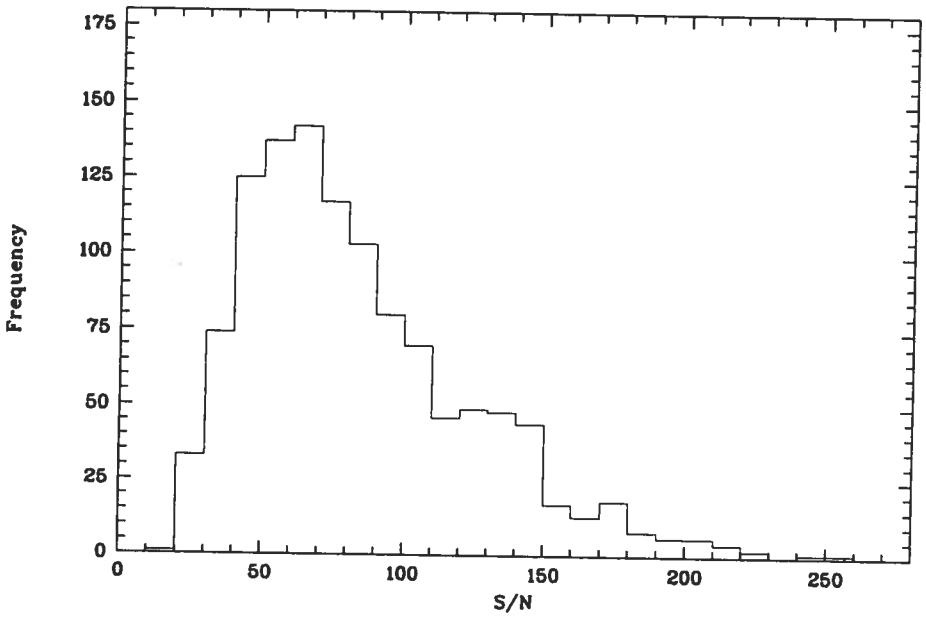

FIGURE 2.2 – The same data as in Figure 1, but in histogram form as a function of S/N. Bin-size is 10 S/N units. In total, 1145 good spectra were retained for this study. The mean S/N is ~ 85.

strongly affects both its phase and amplitude fidelity. In order to not dilute the RV signal obtained from HeIIλ4686 by that obtained from spectral lines which *do* reflect the true orbital motion, CC was restricted to the spectral region from 4600 to 4800 Å which almost exclusively contains HeIIλ4686.

CC can only measure relative RVs, i.e. shifts, with respect to a given template spectrum; thus, results obtained by CC obviously depend on the choice of the template. In order to render our CC method more robust against the unlucky choice of a poor template, we used an iterative approach. For a first CC pass, a real, high-S/N spectrum from the data set of a given star was chosen as template; usually, *but not always*, the template spectrum came from the 2003 CTIO campaign. This template was cross-correlated with all other spectra, using modified scripts which were originally developed by Kaufer (1996) around the ESO-MIDAS task XCORR/IMA. RV shifts were measured by fitting a Gaussian plus a (linear, rarely parabolic) continuum function to the CC profile. Thanks to the CC profile's symmetry, the fit was very good. Resulting RVs were then used to shift all spectra into the template's frame of reference. Then, a S/N-weighted average spectrum was computed using all shifted spectra, and used as new template for a second CC pass. Again, all spectra were shifted and added, and with this "supertemplate", a final CC pass was made.

The advantage of this approach is that the resulting supertemplate has a higher S/N than a single spectrum, and that both stochastic and cyclical LPVs are mostly averaged out. The same is true for the potentially present spectral signature of a companion, which is maximally smeared out, because it moves in anti-phase to the WNL star[11]. While there were noticeable differences in RVs between the first and the second CC iteration, in most cases the third CC pass did not improve the RVs; still, it was carried out in all cases for the sake of uniformity.

In order to measure absolute RVs, ELF was carried out using the HeIIλ4686 line as well,

[11] This is particularly the case if the WN star is the more massive component of the binary system, as might not be unexpected in luminous WNL systems. The O star then shows the larger RV amplitude; its absorption lines are hence smeared out over a larger spectral region.

since other lines were too weak and thus too noisy to be used. In particular the narrow and clean NIVλ4058 emission, which is at the blue edge of our spectra, suffered from two problems: not only was the instrumental throughput (and hence the achieved S/N) very low, but the lack of useful comparison-arc lines effectively rendered impossible a reliable wavelength calibration (see Section 2). This introduced a RV scatter more than twice larger than what was obtained from the somewhat more asymmetric, but much stronger HeIIλ4686 line.

The profile of HeIIλ4686 was reasonably well reproduced by fitting a single Gauss function to the emission line and a polynomial (usually linear, in some few cases parabolic) to the continuum. While differences between RVs obtained from fits and from CC remained remarkably small, direct fitting yielded a slightly larger RV scatter than CC, most likely because of noise (in particular in weak-lined stars) and the line being slightly asymmetric. Potential intrinsic line-profile variability (e.g. due to WWC) might also add to the problem. Thus, whenever it was possible, we relied on RVs obtained by CC rather than on those obtained through line-fitting.

2.5.2 Standard Stars and Systematic Shifts Between Observatories

Most stars show a small to very small RV scatter around or below 20 kms^{-1} (obtained by CC). However, before identifying the binary stars in our sample, another potential problem had first to be taken care of. Foellmi et al. (2003a,b) reported systematic shifts between CASLEO and SAAO. Both observatories together with others were also used for our study; therefore, we had to make sure that any RV variation is of stellar origin and not a consequence of different (and possibly variable) instrumental zero points. In order to compute systematic shifts among the respective runs, we proceeded as follows: Of our 41 program stars, we selected those *i*) which are well isolated (no composite spectrum due to crowding), *ii*) for which RVs could be measured using CC, *iii*) which displayed very small RV scatter, and *iv*) for which a preliminary period search in the period range from 1 d $\leq P \leq$ 200 d did not yield cyclical RV variability (the period-search method is described more comprehensively be-

low). Stars meeting these criteria are most likely true single stars or binaries with sufficiently long periods, large eccentricities, and/or low inclination angles that they can serve effectively, within our detection limits, as constant-RV standard stars. By construction, the only shifts these stars display are then solely due to systematic shifts among different observatories.

Twenty-three reference stars were thus selected. For each star, mean RVs were computed *for each individual run*. As described above, during the 2003/2004 campaign at CTIO (i.e. runs 11 through 13), a 1″ slit width was used, hence the RV scatter is very small in these data sets, reaching a minimum during run 11 (see below). SSO displays a similarly small scatter (although the slit was 1.5″, the seeing disc was larger, and the spectrograph is installed in the Nasmyth focus, which renders it very stable), but there are many fewer points available. Thus, for better statistics, run 11 was chosen to provide the overall zero point. For each reference star, the mean RV of run 11, $\overline{RV}_{11}$, was subtracted from all RVs in order to normalize RVs to run 11. This was necessary because the CC method only yields *relative* RVs with respect to an *arbitrarily* chosen template, i.e. one that does not necessarily come from run 11. (Note that the shift-and-add method described above also suffers from this effect, because it starts out with one arbitrarily chosen spectrum, too.) Thus, for every individual star, $\overline{RV}_{11} = 0$, whereas for all other runs $j \neq 11$ in general $\overline{RV}_j \neq 0$. By construction, the respective values of these $\overline{RV}_j$ are purely due, and directly correspond, to the systematic shifts among run 11 and all other runs.

However, not every star will display the same shifts, but the shifts will be randomly distributed. By combining the 23 reference stars into one "super-reference", we obtained the respective *average* mean velocities $\overline{RV}_j$ per run – and thus directly the systematic shifts among run 11 and all other runs – as well as the standard deviations σ_j, which were adopted as empirical *a posteriori* measurement errors for the RVs of each individual run. Values range from 23.8 kms^{-1} at LCO (run 10) to 10.3 kms^{-1} at CTIO (run 11). To reject outliers, a soft sigma-clipping was applied: Points from a given run j deviating from $\overline{RV}_j$ by more than $\pm 3\sigma_j$ were rejected. (This sigma-clipping on a per-run basis could not be done per individual star,

because there are not enough data points per run for meaningful statistics.) Both $\overline{RV}_j$ and σ_j were then re-calculated; final values are given in Table 2.4. Systematic shifts could now easily be removed in *all* program stars by simply subtracting the respective values from all RVs of a given star and run.

RVs obtained by XCORR and corrected for systematic shifts are shown, for each epoch separately, in Figures 2.3 through 2.43. The dashed line indicates the zero mean velocity to which all RVs were normalized.

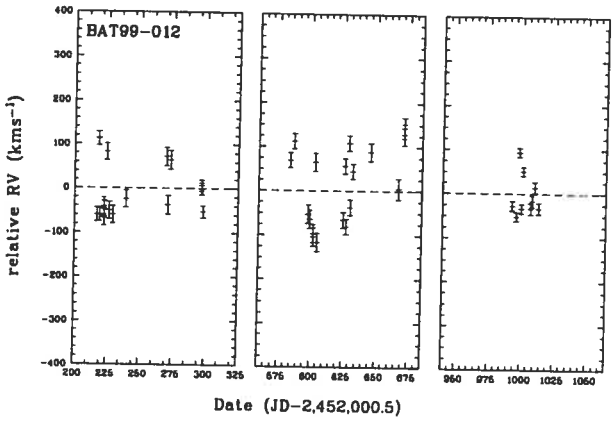

FIGURE 2.3 – RVs of BAT99-12 for all three epochs.

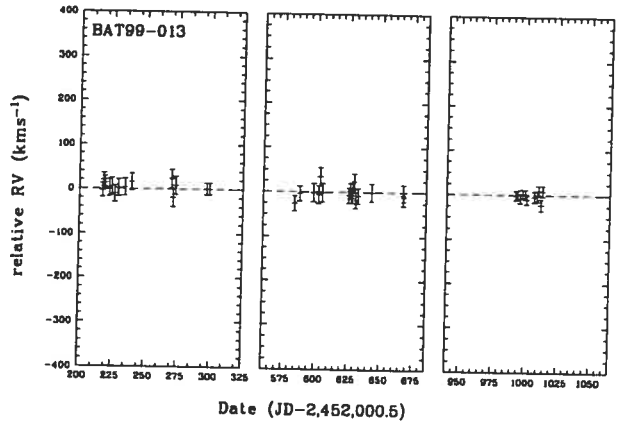

FIGURE 2.4 – RVs of BAT99-13 for all three epochs.

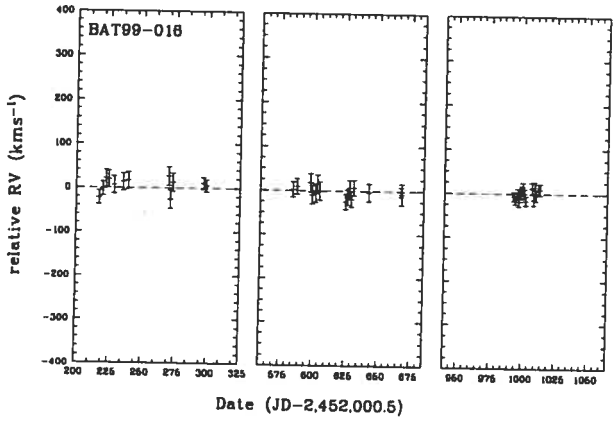

FIGURE 2.5 – RVs of BAT99-16 for all three epochs.

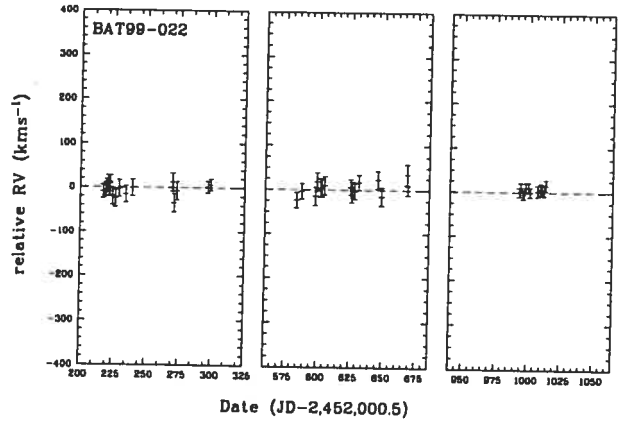

FIGURE 2.6 – RVs of BAT99-22 for all three epochs.

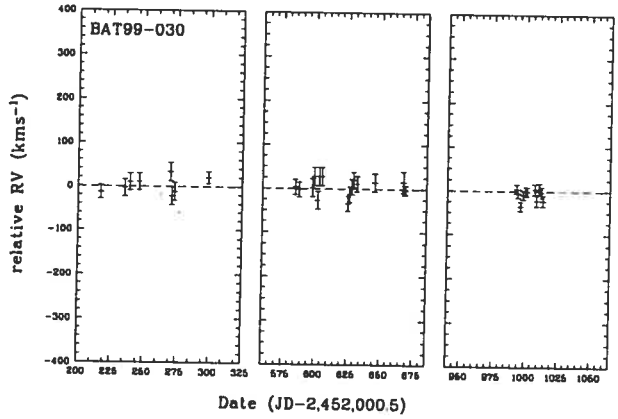

FIGURE 2.7 – RVs of BAT99-30 for all three epochs.

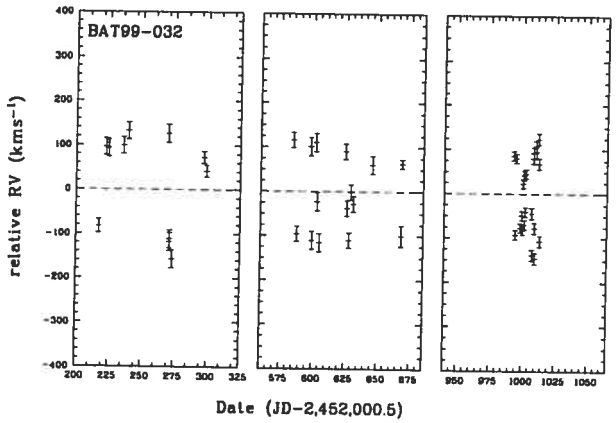

FIGURE 2.8 – RVs of BAT99-32 for all three epochs.

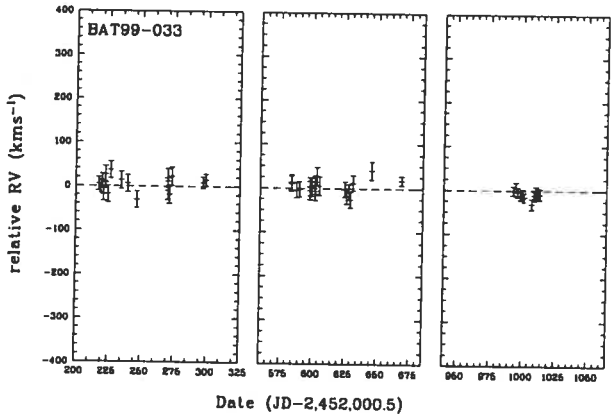

FIGURE 2.9 – RVs of BAT99-33 for all three epochs.

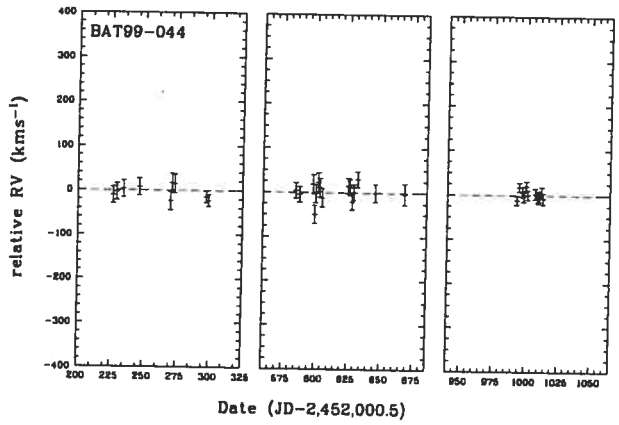

FIGURE 2.10 – RVs of BAT99-44 for all three epochs.

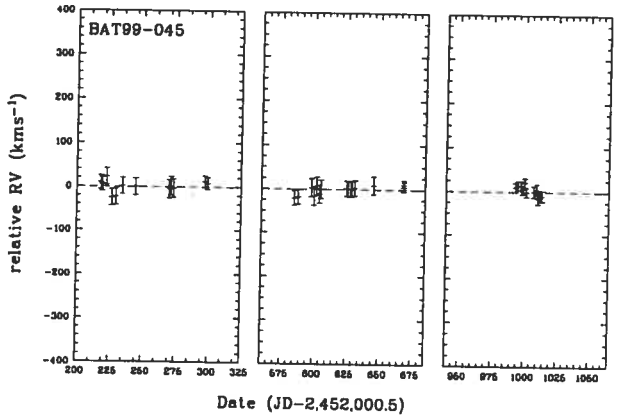

FIGURE 2.11 – RVs of BAT99-45 for all three epochs.

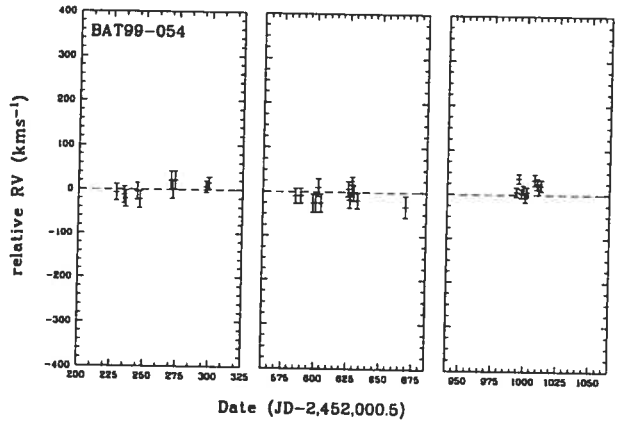

FIGURE 2.12 – RVs of BAT99-54 for all three epochs.

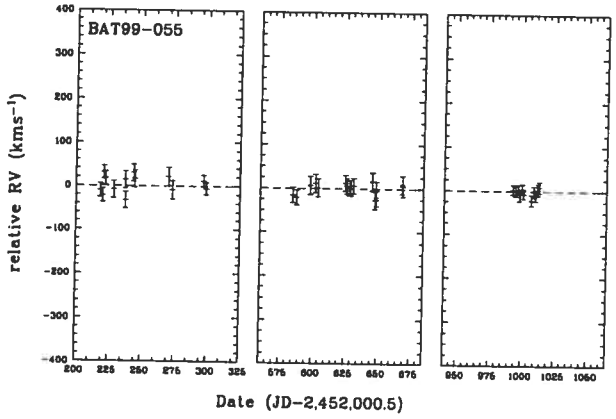

FIGURE 2.13 – RVs of BAT99-55 for all three epochs.

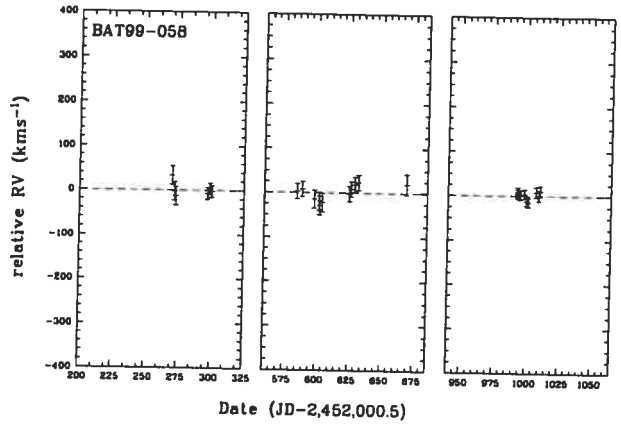

FIGURE 2.14 – RVs of BAT99-58 for all three epochs.

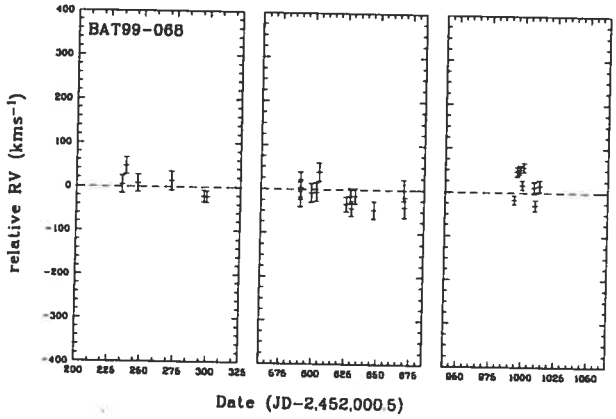

FIGURE 2.15 – RVs of BAT99-68 for all three epochs.

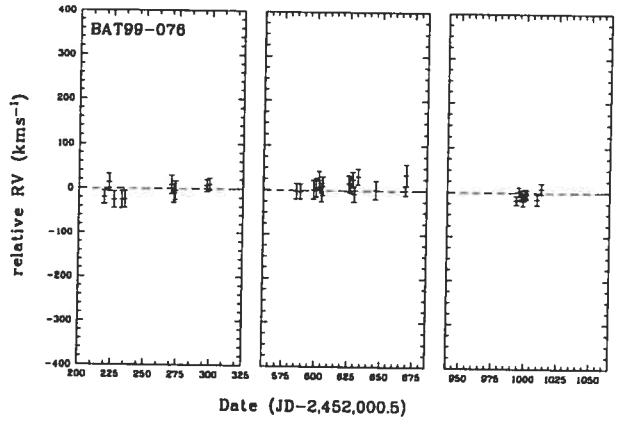

FIGURE 2.16 – RVs of BAT99-76 for all three epochs.

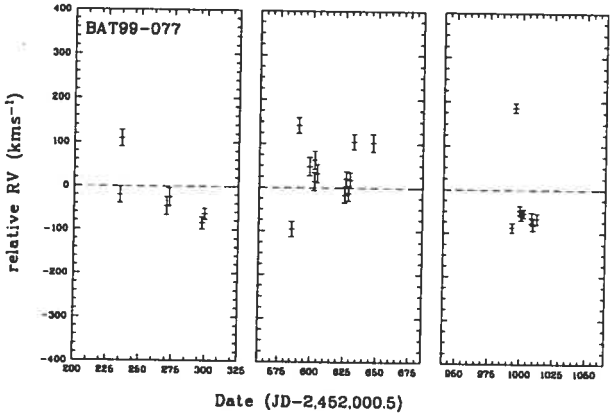

FIGURE 2.17 – RVs of BAT99-77 for all three epochs.

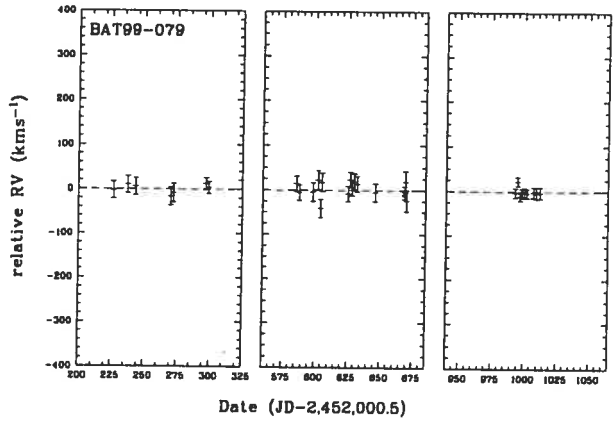

FIGURE 2.18 – RVs of BAT99-79 for all three epochs.

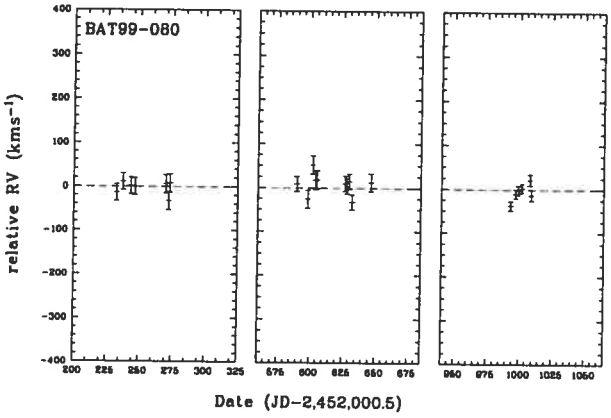

FIGURE 2.19 – RVs of BAT99-80 for all three epochs.

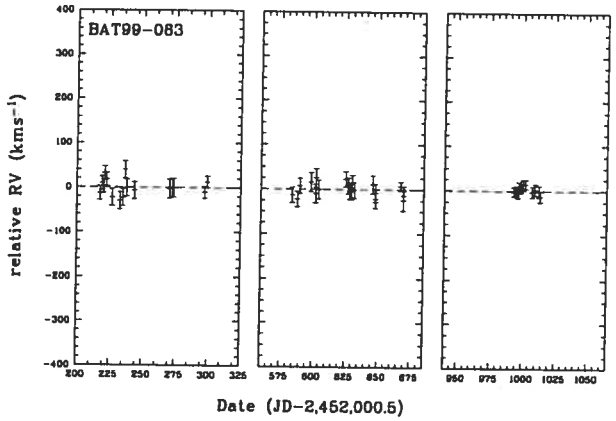

FIGURE 2.20 – RVs of BAT99-83 for all three epochs.

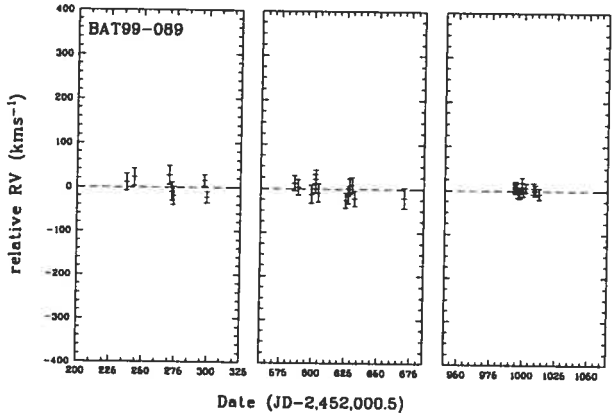

FIGURE 2.21 – RVs of BAT99-89 for all three epochs.

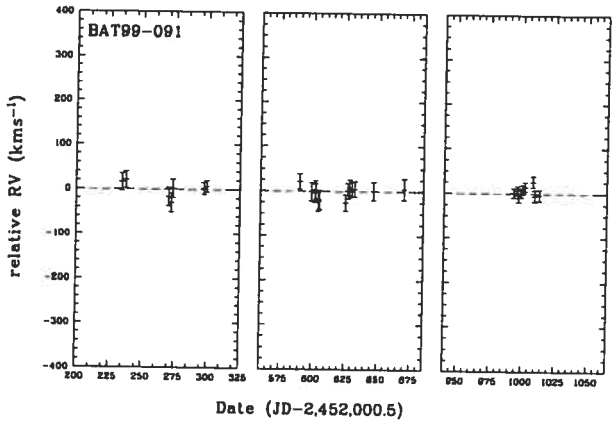

FIGURE 2.22 – RVs of BAT99-91 for all three epochs.

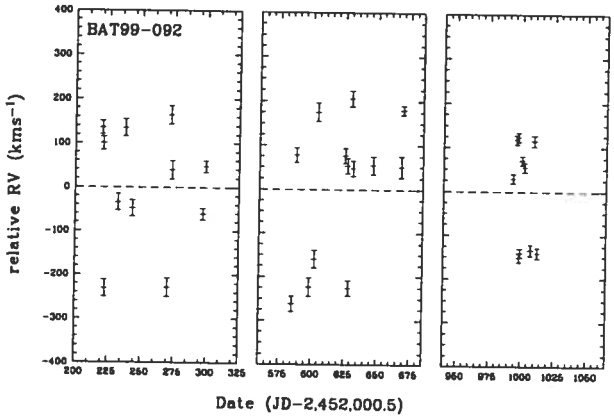

FIGURE 2.23 – RVs of BAT99-92 for all three epochs.

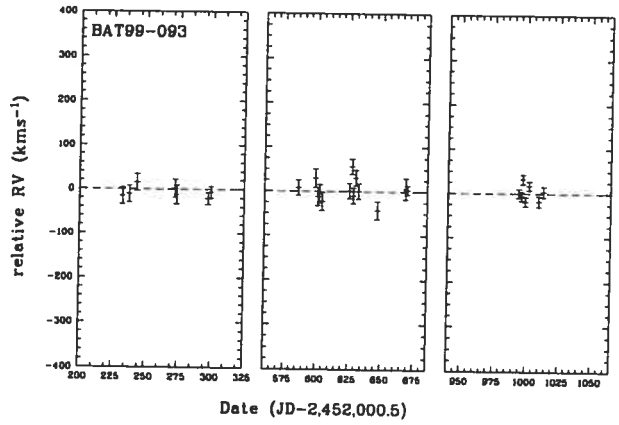

FIGURE 2.24 – RVs of BAT99-93 for all three epochs.

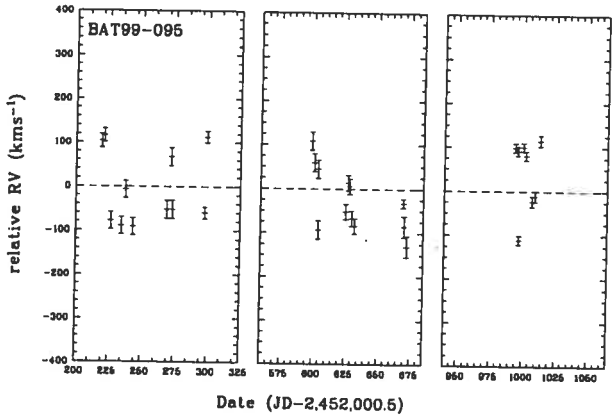

FIGURE 2.25 – RVs of BAT99-95 for all three epochs.

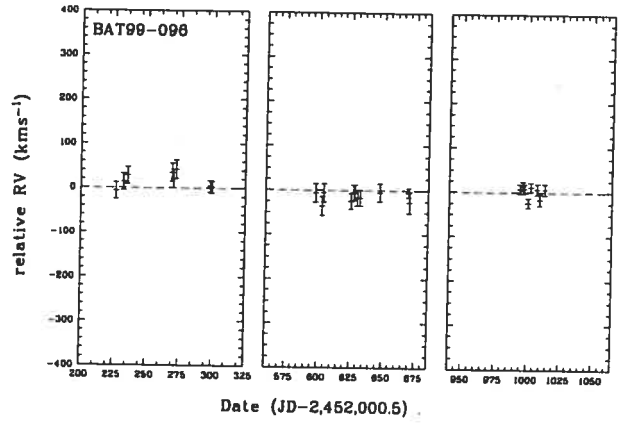

FIGURE 2.26 – RVs of BAT99-96 for all three epochs.

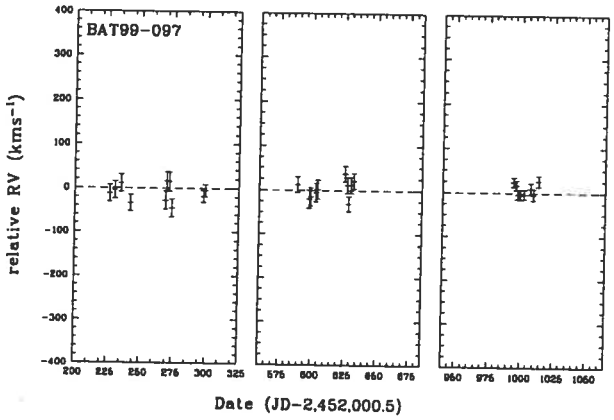

FIGURE 2.27 – RVs of BAT99-97 for all three epochs.

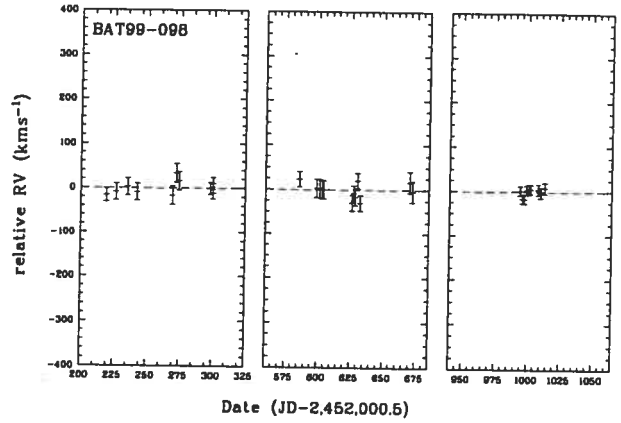

FIGURE 2.28 – RVs of BAT99-98 for all three epochs.

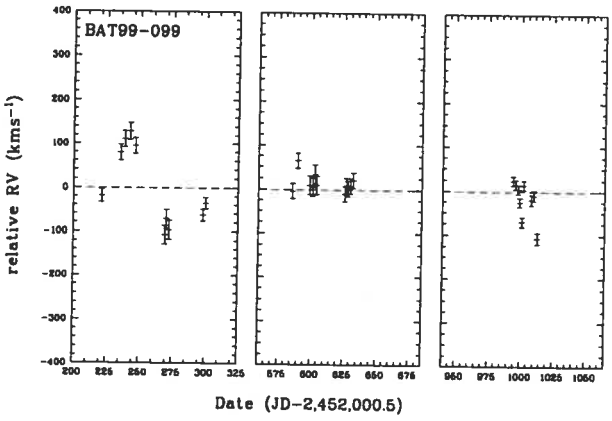

FIGURE 2.29 – RVs of BAT99-99 for all three epochs.

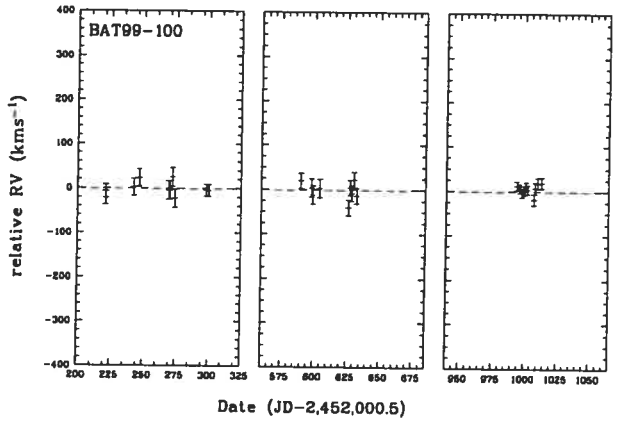

FIGURE 2.30 – RVs of BAT99-100 for all three epochs.

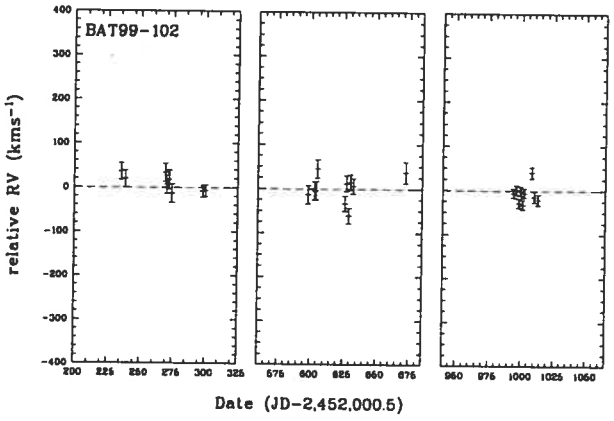

FIGURE 2.31 – RVs of BAT99-102 for all three epochs.

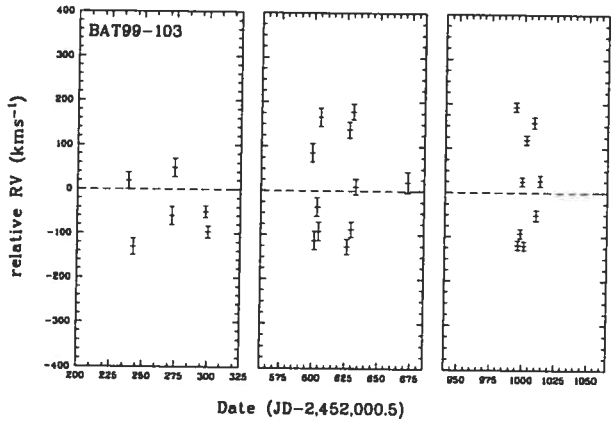

FIGURE 2.32 – RVs of BAT99-103 for all three epochs.

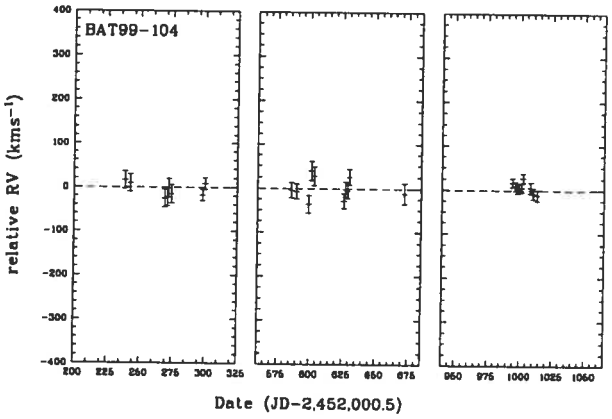

FIGURE 2.33 – RVs of BAT99-104 for all three epochs.

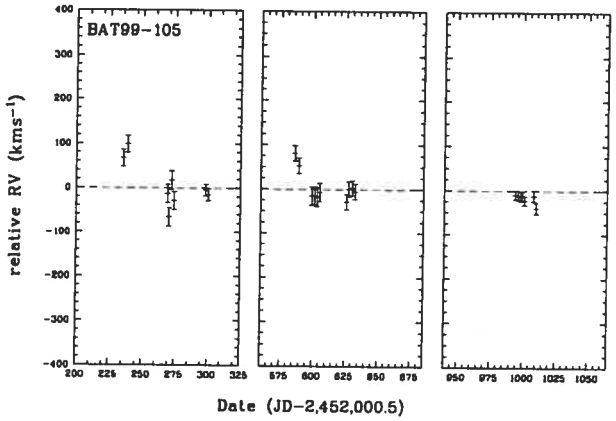

FIGURE 2.34 – RVs of BAT99-105 for all three epochs.

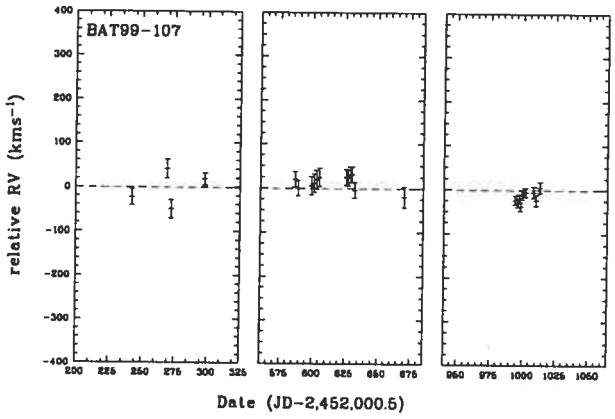

FIGURE 2.35 – RVs of BAT99-107 for all three epochs.

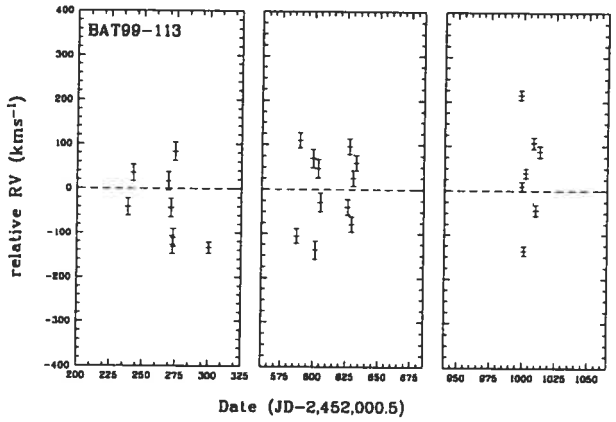

FIGURE 2.36 – RVs of BAT99-113 for all three epochs.

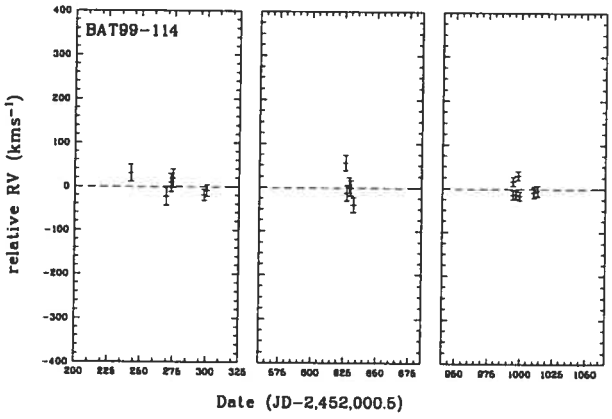

FIGURE 2.37 – RVs of BAT99-114 for all three epochs.

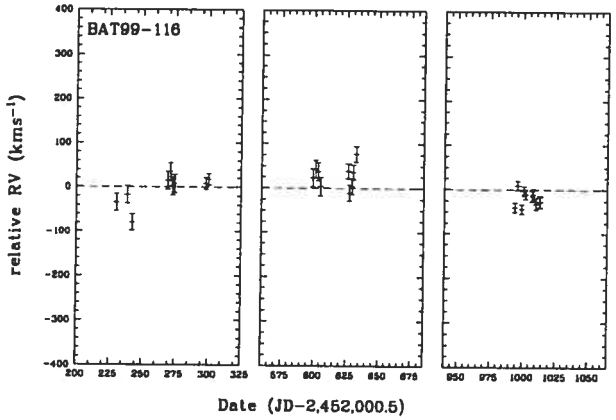

FIGURE 2.38 – RVs of BAT99-116 for all three epochs.

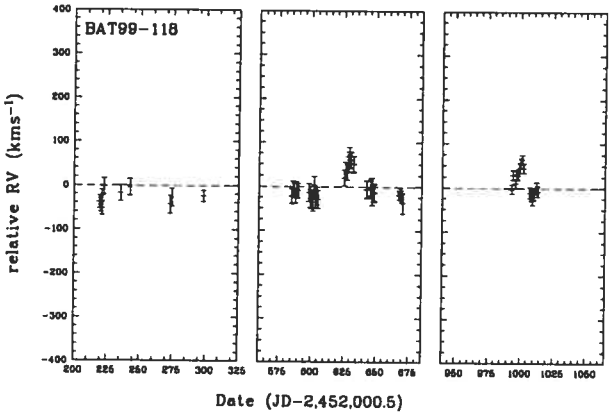

FIGURE 2.39 – RVs of BAT99-118 for all three epochs.

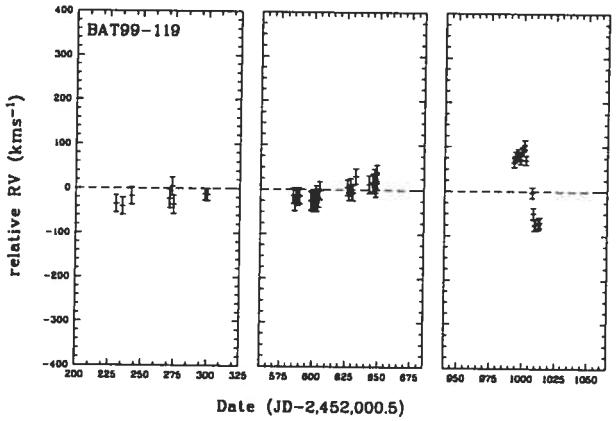

FIGURE 2.40 – RVs of BAT99-119 for all three epochs.

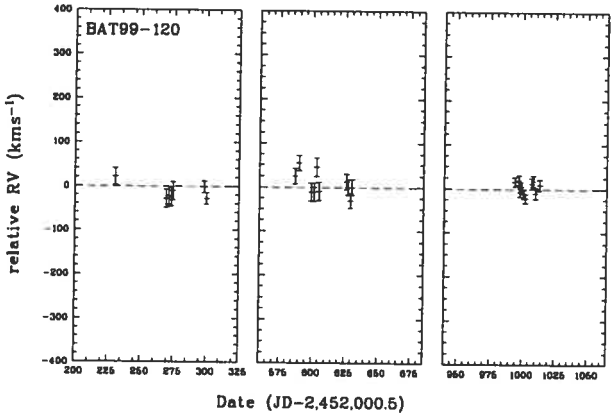

FIGURE 2.41 – RVs of BAT99-120 for all three epochs.

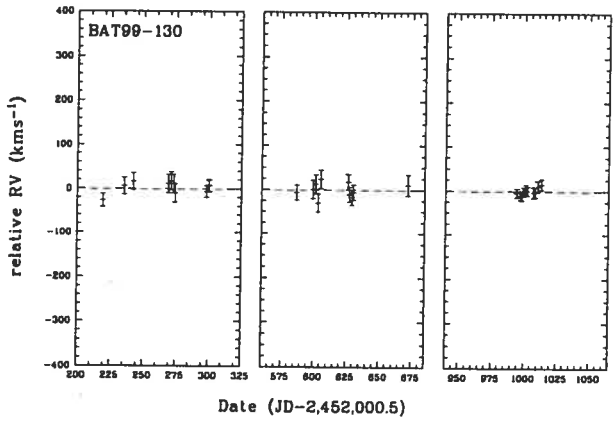

FIGURE 2.42 – RVs of BAT99-130 for all three epochs.

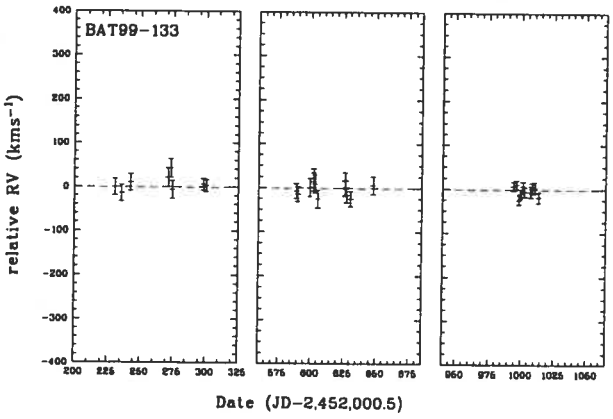

FIGURE 2.43 – RVs of BAT99-133 for all three epochs.

TABLE 2.4 – Systematic shifts between different runs and standard deviations of RV per run, used as *a posteriori* error bars. See text for details.

Run j	Observatory	RV shift kms^{-1}	σ_j kms^{-1}
1	CASLEO	-2.9	15.3
2	MSO	-16.1	19.0
3	CTIO	-3.0	20.9
4	CTIO	-10.7	13.3
5	SAAO	-8.7	17.2
6	CTIO	+0.2	20.7
7	CTIO	-1.9	17.4
8	MSO	+3.0	20.2
9	SSO	-24.9	10.4
10	LCO	-4.3	23.8
11	CTIO	0.0	10.3
12	CTIO	3.6	12.5
13	CTIO	-0.9	12.5

2.5.3 Scatter and Weights

Using the standard deviations σ_j of the respective runs, weights w_j were computed as the inverse variances of the respective run, i.e. $w_j = 1/\sigma_j^2$. Thus, after having corrected *all* program stars for systematic shifts among different runs, weighted mean RVs, $\overline{RV}_w$, and weighted standard deviations, σ_w^2, were computed for all stars according to the following equations:

$$\overline{RV}_w = \frac{\sum_{j=1}^{N} \frac{RV_j}{\sigma_j^2}}{\sum_{j=1}^{N} \frac{1}{\sigma_j^2}}$$

$$\sigma_w^2 = \frac{\sum_{j=1}^{N} \frac{(RV_j - \overline{RV}_w)^2}{\sigma_j^2}}{\sum_{i=1}^{N} \frac{1}{\sigma_j^2}},$$

Surprisingly, differences between weighted and unweighted values remained small and insignificant, so that in the following, unless stated otherwise, only *unweighted* data will be considered, which does not change the conclusions in any way.

2.5.4 Random Variability and Significance Levels

Since we are looking for binaries, the property we are initially most interested in is *variability*, i.e. the standard deviation around the mean RV. After all, we expect binaries to show larger RV scatter than constant stars. But how large a scatter is large enough for a given star to be identified as variable? To distinguish stars which are most likely variable from those which, within the measurement errors, are not, we applied the χ^2 test. The idea is the following: If *all* stars in our sample were truly constant, RV measurements would be scattered around a mean velocity *only due to random measurement errors*. We now define that a RV *amplitude* S is some span of RV such that a major fraction (say, 99.7%) of the measured RVs fall within this span. Obviously, the RV amplitude can then be related to the standard deviation of the RV distribution, since for the example here $S = 3\sigma_{\rm RV}$ (99.7%). For constant stars, RVs are now distributed such that the distribution of the *squared* RV amplitudes S^2 follows a χ^2 distribution with *df* degrees of freedom, where *df* is the number of RV measurements per star. If a star displays a value of S^2 *exceeding* the theoretically expected χ^2 distribution, its RV scatter is not consistent with the hypothesis that it is a constant star; hence it will be considered variable.

In Figure 2.44, the 770 RV measurements of the 23 combined reference stars (the "super reference") are shown in histogram form. By construction (see above), the distribution has $\overline{RV} = 0$ kms^{-1}. The unweighted standard deviation of this RV distribution is $\sigma = 16$ kms^{-1} (the weighted value differs only marginally: $\sigma_w = 15.5$ kms^{-1}; therefore we proceed with the unweighted value). The histogram looks very Gaussian; indeed, a Kolmogorov-Smirnov test yielded that the distribution of RVs in the "super reference" is, at a 99% confidence level, normal with $\overline{RV} = 0$ kms^{-1} and $\sigma = 16$ kms^{-1} at a 99% confidence level, a nice *a posteriori* confirmation to use those 23 stars as constant stars.

With this RV distribution function at hand, we proceeded to simulate an *artificial* sample of $41 \times 250 = 10{,}250$ constant stars. (The large number of artificial stars was merely chosen for better reliability.) For each star, 33 RV measurements were simulated, since this is on average

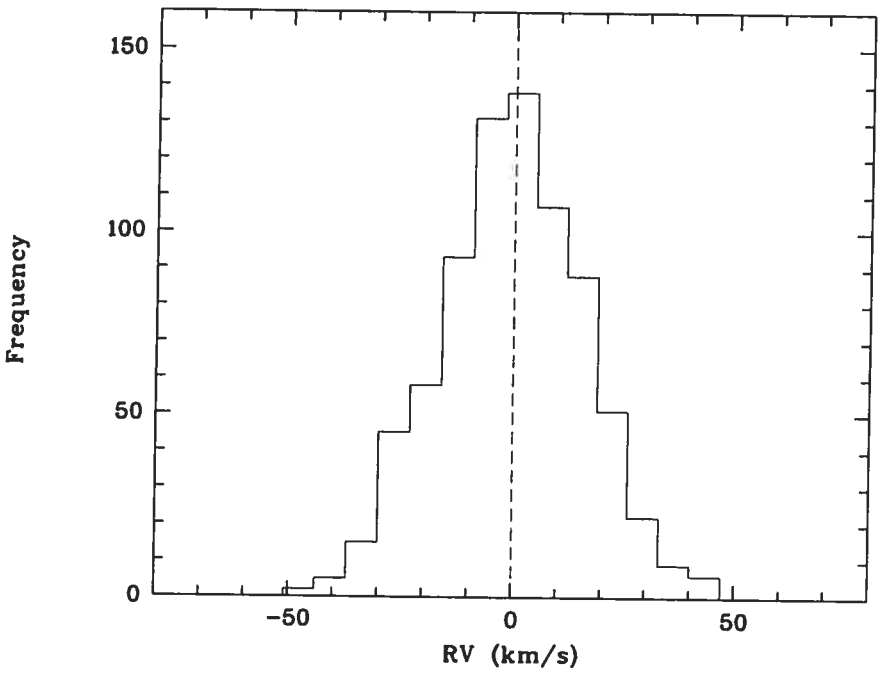

FIGURE 2.44 – Histogram of all corrected RVs of the 23 reference stars, obtained by cross-correlation, and after correction for systematic shifts. In total, 770 data points are used. Binsize is 7 kms^{-1}. The unweighted standard deviation around the mean is 16 kms^{-1}

the number of data points for each of our 41 program stars. RVs were randomly sampled from a normal distribution with $\overline{RV} = 0$ kms^{-1} and $\sigma = 16$ kms^{-1}. The underlying hypothesis here is that for all stars, the same statistical errors apply, and no other error sources exist for stars which are not reference stars. For the k^{th} star, the standard deviation σ_k, the peak-to-peak amplitude $S_k = 3.289 \times \sigma$ (i.e., the 99.9%ile), and the square-amplitude S_k^2 were computed. Values of S_k^2 were binned into a histogram, and number counts per bin (i.e. absolute frequencies) were integer-divided by 250 to obtain the (high-S/N) histogram of an artificial 41-star sample.

Next, a $\chi^2(x)$ function with $df = 33$ degrees of freedom was computed, where x is normalized; thus, a variable transform had to be done to compute values for physical S^2. The peak of the $\chi^2(S^2)$ function is adjusted with the help of the histogram of the simulated stars. Thus, by construction the $\chi^2(S^2)$ function is the envelope of the square-amplitudes *if* all 41

stars are constant and drawn from a normal distribution with $\sigma = 16$ kms^{-1}. Stars whose square-amplitudes lie outside this envelope ("exceed the χ^2") are inconsistent with the hypothesis of being constant, thus they are considered variable. This formal approach allows one to compute a threshold value for the square-amplitude above which the probability of a star still being consistent with the hypothesis "star is constant" is α. We chose $\alpha = 0.01\%$, so that in turn stars exceeding the χ^2 are variable at a 99.9% significance level. Since we reject stars exceeding the χ^2, we might be wrong; after all, there is the small, but non-zero probability that the star indeed is contant. Therefore, α is also called "error probability".

In order to compute the $\chi^2(x)$ function, we used values of the normalized x for $N = 30$ data points at a 99.9% level as tabulated in statistical textbooks (e.g. Kreyszig 1975); by linear interpolation to $N = 33$ (which is usually not tabulated), we obtained $x = 64.1$. This corresponds to a cut-off value $S^2 = 5380$ km^{2}s^{-2} and thus $\sigma_{\rm cut} = 22.6$ kms^{-1}. This means that stars with standard deviations above this value can be considered variable. Stars which have been found to exceed the χ^2 are shown in Table 2.5. As we shall see further below, most, however not all, of these variable stars also display periodicities in their RV curves, and are binaries. The theoretical $\chi^2(S^2)$ function plotted over the observed square-amplitudes of our 41 program stars is shown in Figure 2.45. Note that since the χ^2 distribution is a probability distribution, it has to be normalized to unity, i.e. the volume under the χ^2 function is 1. Since we are applying the χ^2 test to a population of 41 stars (and not 23, as might suggest the number of reference stars), the χ^2 function will be the envelope of the histogram of 41 stars, *only if these stars are all constant*. If, however, some of these 41 stars are variable, i.e. if they exceed the χ^2, they will lie outside and thus be "missing" under the χ^2 function.

At this point, we shall anticipate the comment that our chain of reasoning appears somewhat circular: First, we chose the 23 constant stars from our sample, and then, based on this "super reference" and some cumbersome statistics, find that the other stars are "not constant", indeed. This is something we already knew – after all, it is the reason in the first

TABLE 2.5 – Stars whose RV standard deviation σ_{RV} exceed the cut-off value of 22.6 kms^{-1} and which therefore are considered variable.

BAT99	σ_{RV} [kms^{-1}]	BAT99	σ_{RV} [kms^{-1}]
12	70.8	103	106.7
32	92.4	105	37.7
68	29.5	107	23.9
77	78.2	113	93.3
92	139.8	116	32.6
95	81.6	118	31.6
99	58.9	119	44.7
102	25.3	...	...

place why those variable stars were not chosen into the "super reference"! However, there are a couple of things to note here. First, recall that our choice of reference stars was *not* based on small RV scatter alone, but also on other criteria. This does of course not mean that stars which do not meet these criteria do not display small RV scatter as well. Second, one might obtain almost the same reference stars by applying an iterative "χ^2 clipping". The idea behind this term is that one can start out with all 41 program stars and compute the *overall* average RV scatter, use this σ_{all}, to compute the corresponding χ^2 function and plot it over the observed histogram, just as described above. Of course, binaries and other variable stars in the sample will pollute this value, therefore the χ^2 function will not fit the entire sample. Instead, it will be too broad and too shallow, and not peak at the right value of S^2. Then, this χ^2 function is evidently the wrong one. But still, some stars will exceed even this χ^2 at the 99.9% threshold, and can be considered variable. By discarding them, and recomputing a new overall σ and χ^2, one can gradually identify the variable stars in the sample and obtain a population of reasonably constant stars.

We applied this approach to our data and obtained, after the second iteration, a population of 28 constant stars, namely our 23 reference stars used above plus 5 stars which show equally small RV scatter, but did not obtain the reference status because they failed on the secondary criteria (crowdedness etc.). As was mentioned above, the χ^2 test is based on the hypothesis that the statistical errors are identical for all stars of our sample. By applying the filter with the secondary criteria, we explicitly negated this hypothesis, since we suspected other,

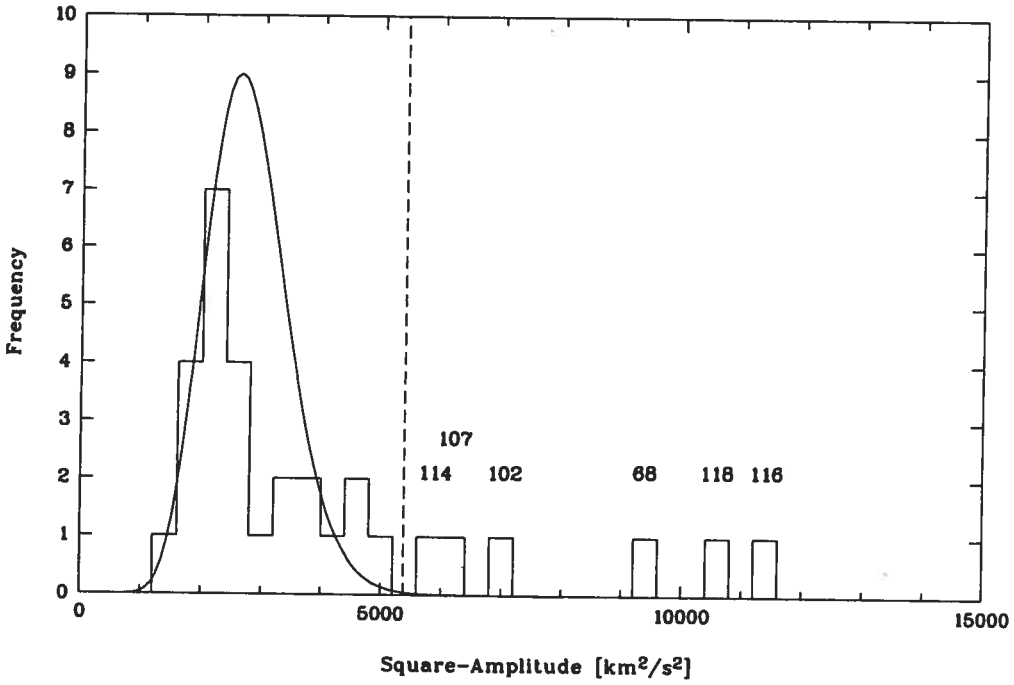

FIGURE 2.45 – Histogram of square-amplitudes S^2 of our program stars with the χ^2 distribution for $\sigma = 16$ kms^{-1} overplotted. Bin-size is 400 km^{2}s^{-2}. The dashed vertical line indicates the cut-off value corresponding to $\sigma_{RV} = 22.6$ kms^{-1}; stars to the right of this cut-off are considered variable at a 99.9% confidence level. They are named by their respective BAT99 number. Note that ten stars in our sample have square-amplitudes larger than 15,000 km^{2}s^{-2} (corresponding to RV scatters $\sigma_{RV} > 37.8$ kms^{-1}). For reasons of clarity, they are not shown in this diagram, but listed in Table 2.5.

external error sources to play a role. In retrospect and based solely on σ statistics, we could have indeed taken all the 28 stars with similar scatter for our super reference instead of only the 23 chosen stars. However, we have now stringently shown that we did not affect the quality of our results by the choices we made, and that our approach was a statistically viable one.

2.5.5 Cyclical Variability and Period Analysis

It has to be recalled that variability, i.e. significantly large RV scatter, is not a sufficient criterion for *cyclical* variability, let alone for binarity. There are stars which are erratically

variable, i.e. any measured RV scatter could be of stochastic nature. It is thus important to verify whether or not any star shows periodic RV variabilities.

Period-Search Algorithms

After having corrected all data sets for systematic shifts, we re-performed a period search on the unweighted RVs of *all* stars in the period range from 1 to 200 days, using a code by Kaufer et al. (1996). In each step of the iteration, this code computes CLEANed periodograms of unevenly distributed data points according to Deeming (1975; see also Schwarz 1978; Roberts et al. 1987). Significance levels are calculated for the found periods using Lomb-Scargle statistics (Lomb 1976; Scargle 1982) and applying equal weights to all data points. Periods exceeding the 3σ significance level are removed in each step of the iteration by fitting a sine wave with the corresponding period to the data points; the procedure is then re-applied on the residuals. For non-circular orbits, where significant power can be contained in the harmonics of the fundamental frequency, it is better to fit several (harmonic) sine waves simultaneously (i.e., higher terms of the Fourier expansion), even if the fundamental frequency will *always* be the highest peak in the periodogram. The problem is that if very non-circular orbits are to be considered, many higher-order terms of the Fourier expansions are required, rendering the fit more problematic (number of data points vs. degrees of freedom). We tested orders up to 3, without any significant changes in the found period; therefore, first-order sine waves (i.e., only the fundamental period) were used. For cross-verification, we also tested the analysis-of-variance (AOV) algorithm implemented in MIDAS by Schwarzenberg-Czerny (1989), with identical results. Thus, only results obtained with Lomb-Scargle statistics are quoted.

Stars Without Periodicities

For most stars with visibly small RV scatter, in particular the 23 RV reference stars, no periodicities at all were found (recall that we searched all RVs for periodicities prior to correcting for systematic shifts among observatories, and that the absence of any period in the

data was a selection criterion for the super-reference stars). Remarkably, the stars identified as variables above, BAT99-68, 102, 105, 107, 114, and 116, do not show any periodicity at all (i.e. not even a spurious one) in their RV curves, although Moffat (1989) reported a 52.7-day period in BAT99-107's RV curve.

For stars BAT99-68, 102, and 114, the result does not come unexpectedly; these stars are more or less severely crowded (see e.g. finding charts in BAT99), so that, depending on seeing conditions and the acquisition precision, their emission lines suffer from variable dilution and slit-position effects. These effects are stochastic and can easily account for the observed RV scatter without the need to resort to intrinsic stellar variability, or binarity. (Note however that BAT99-80 does not show this effect, although it is very crowded; its RV scatter is 20.5 kms^{-1}, i.e. slightly below the varibility limit.)

In contrast to this, stars BAT99-105, 107, and 116 are isolated enough to not suffer from this kind of effect. Also, their RV curves do not follow a trend, but are rather noisy (see Figures 2.34, 2.35, and 2.38). Note, however, that the CTIO 2003/2004 campaign with a $1''$ slit width yields considerably smaller RV scatter, 11, 13, and 17 kms^{-1} for BAT99-105, 107, and 116, respectively, consistent with our standard stars; moreover, the constancy over such short time intervals rules out short-period variability which would account for night-to-night scatter observed in other runs. While we can for none of these stars rule out long-period binarity ($P \gg 100$ d), it seems that at least in the case of BAT99-105 and 107, we are dealing with noise, and that these two stars are most likely not binaries with periods $\lesssim 150$ d, unless they have very low inclination angles. BAT99-116 and 118, however, seem to be peculiar objects that will be discussed in more detail further below.

Another particular case is BAT99-119 (Brey 90), a superluminous WN6ha star, whose tentative 25.4-day (assumed circular-orbit) period reported by Moffat (1989) could not be reproduced. It was only after combining with unpublished polarimetry that we were able to find the correct period of $P = 158.8$ days, and an orbital solution for BAT99-119. Since the

system has a long-period *and* a highly eccentric ($e \sim 0.7$) orbit, we are clearly limited by the phase coverage of our data; had it not been for the polarimetry, we would have missed the binarity of BAT99-119. We will discuss the limitations of our RV survey with respect to a detection threshold further below. Also, we will exclude BAT99-119 from further analyses; instead, this star will be discussed elsewhere (see Chapter 3).

However, it must be recalled that any star for which no coherent period was detected, is not necessarily single. It might simply be that the orbital period is too long, the orbital eccentricity too large, and/or the inclination angle too small for the binary system to display a RV amplitude large enough for our period-search algorithm to pick it up. We will discuss this issue later in more detail.

Stars With Periodicities

Almost all binary periods reported by previous studies (Moffat 1989; and references therein) were reproduced with remarkable similarity, and by combining our data with published data, we were able to further increase the accuracy of the periods even more (see Table 2.6). These revised periods were used in the further analysis. The confirmed binaries are (our periods quoted): BAT99-32 ($P = 1.9075$ d), BAT99-77 ($P = 3.0034$ d), and BAT99-92 ($P = 4.3111$ d). In one curious case, the 2.76-day period reported for BAT99-102 (R140a2) was clearly found, however in its *neighboring star*, BAT99-103 (R140b). Careful inspection of our logbooks did not reveal any possible confusion at the telescope, nor is there any indication of such a mishap in Moffat et al. (1987), who first detected the binary. BAT99-102 forms a visual pair with BAT99-101 (R140a1) which even under the best seeing conditions at CTIO could not be separated. Both stars lie very close to BAT99-103, and given our relatively large slit width, some cross-contamination of emission lines is not impossible, which could lead to a detection of the same periodicity in BAT99-102, too. While we cannot propose a solution to this issue, we will from here on consider BAT99-103 as the 2.76-day binary.

TABLE 2.6 – Periods (in days) found for our program stars in this work and previous studies. Newly identified, periodically variable stars are indicated. References are: (1) Moffat & Seggewiss (1986); (2) Moffat (1989); (3) Moffat et al. (1987; but see text for details).

BAT99	this work	previous studies	combined data	Ref.
12	3.2358 ± 0.0006	n/a	n/a	new
32	1.9075 ± 0.0002	1.9075 ± 0.0002	1.90756 ± 0.00005	1
77	3.0034 ± 0.0004	3.0032 ± 0.0002	3.00303 ± 0.00002	2
92	4.3111 ± 0.0004	4.3092 ± 0.004	4.31252 ± 0.00005	2
95	2.1110 ± 0.0002	n/a	n/a	new
99	92.60 ± 0.52	n/a	n/a	new
103	2.7597 ± 0.0003	2.7596 ± 0.0001	2.75975 ± 0.00003	3
113	4.699 ± 0.002	n/a	n/a	new

For four new stars, periodic RV variations were found which yielded a coherent RV curve when the data points were folded into the corresponding phases: BAT99-12 ($P = 3.2358$ d), BAT99-95 ($P = 2.1110$ d), BAT99-99 ($P = 92.60$ d), and BAT99-113 ($P = 4.699$ d). None of these four stars was included in the study of Moffat (1989), either because it was not listed as a WR star in previous Catalogue versions, or because it was too faint for Moffat's magnitude-limited sample ($V \leq 13$ mag). Interestingly, all new variables, with the exception of BAT99-95 (WN7ha), are listed as O3If/WN6 stars in the BAT99 catalogue, i.e. they can be considered as the most extreme Of stars. (However, their spectral types can also be assessed as genuine WR stars; see below).

At this point, it might be worth considering the problem of aliasing. Discrete sampling introduces artificial frequencies in the periodogram, and these so-called aliases particularly become problematic when the sampling frequency and the true frequency of the system under test (SUT) are similar or harmonically related. Also, if the sampling frequency is lower than the SUT's frequency (i.e. when the Nyquist criterion is not satisfied), beating of these two frequencies against each other introduces artificial, low frequencies in the power (i.e. Fourier) spectra. If an alias contains sufficient power, the algorithm will zero in on this artefact rather than identify the correct period of the SUT.

Given that our sampling frequency is not higher than once per day in practically all cases, the Nyquist criterion is not strictly satisfied for periods shorter than 2 days, and we should be

in trouble. However, an unlikely ally comes to our rescue: the effectively highly non-equidistant sampling of our data set. Unlikely because usually, uneven sampling is a nuisance; it complicates period analysis, because a simple Fourier transform is not sufficient, and an extra mathematical and computational effort has to be made. However, non-equidistant (and, more importantly, anharmonic) sampling, which leads to almost random sampling of the system phase, effectively "closes the phases". This term describes that, when sine waves are fitted to the data points (and nothing else does our algorithm to identify the period in the time series), the almost random distribution of the data points in the corresponding phase will very effectively rule out wrong frequencies because at least some of the data points, viz. those that do not fit into the phase, "will stand in the way" of the wrong sine wave, i.e. decrease the quality of the fit by increasing its χ^2, which directly corresponds to decreasing the power of the frequency in question.

Furthermore, the CLEAN algorithm should effectively remove all frequencies associated to the sampling of a given times series. To do so, this algorithm computes the power spectrum of the time series, the so-called dirty spectrum. Then, the value of each data point is set to unity, and the so-called window function (WF) is computed. This WF contains only frequencies which are related to the sampling process. Then, the dirty spectrum is deconvolved (*cleaned*, hence the name) with the WF, so that the resulting clean spectrum contains only frequencies which originate in the SUT. The caveat is that, should a SUT contain a frequency which coincides with one of the sampling-related frequencies, this very frequency is also removed, and lost for further analysis. It is clear that the more gaps there are in the time coverage, the more structured the WF will be; vice versa, the WF is pure white noise in the ideal case of perfectly random sampling. The behaviour of the WF is thus a perfect indicator of how much identified frequencies in the clean spectrum can be trusted.

Since our observations are fragmented into 13 runs of very different duration and typical sampling frequencies, and spread out over more than two years, there is no one, single sampling frequency, and it is to be expected that the WFs of our periodic stars are rather smooth

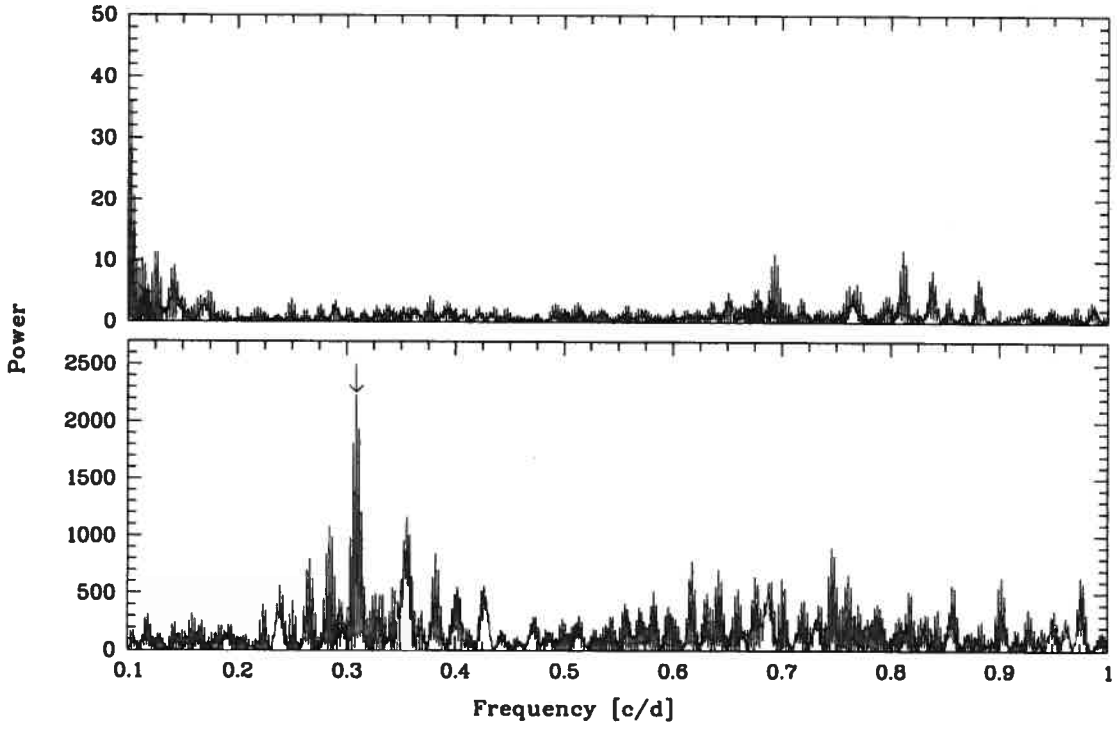

FIGURE 2.46 – Power spectrum (*lower*) and associated window function (*upper panel*) for BAT99-12. The frequency range plotted is 0.1 to 1 cycle per day (c/d), i.e. periods from 1 to 10 days are covered. The peak corresponding to the frequency quoted in this study in indicated by an arrow. Note the stark difference in y scale for the two panels.

and unstructured. This is even more so when combining our data with previously published data. For our data alone, the clean spectra of our periodic stars as well as their WFs are shown in Figures 2.46 through 2.53. In all cases, the WF is indeed very well-behaved and at a much lower power than the SUT's frequencies. This and the fact that we have very well reproduced the previously published periods (if any) for some of our systems, lend considerable weight to the quality of our period analysis (see also our discussion about binary detectability in Section 2.6.1).

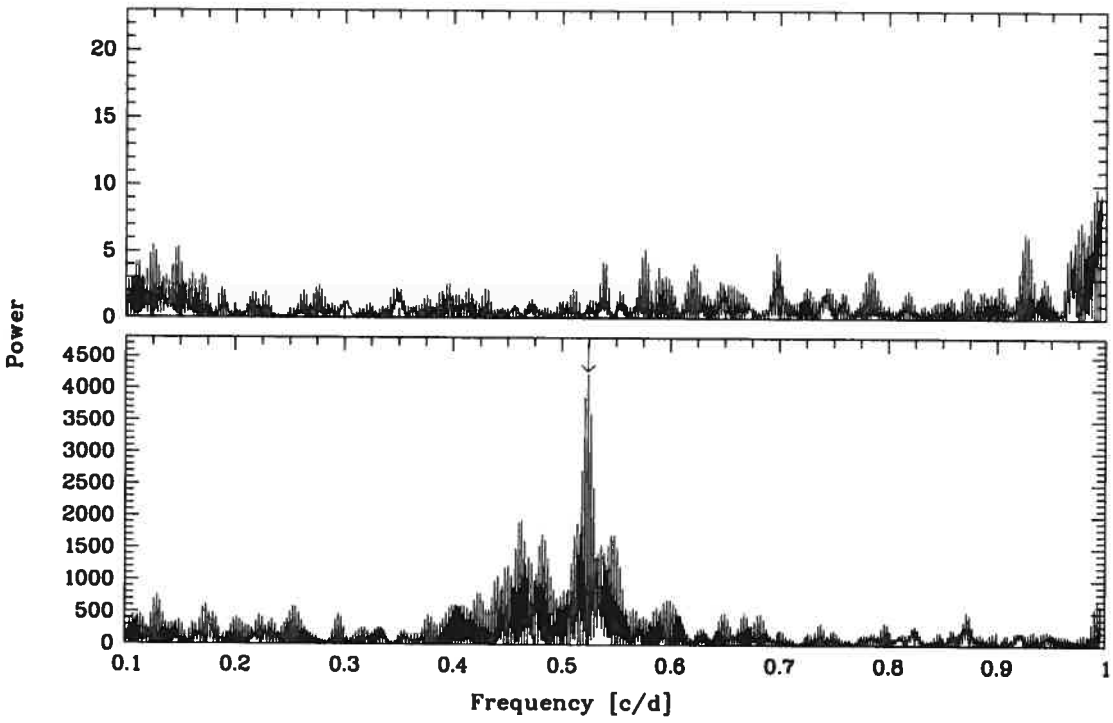

FIGURE 2.47 – As before, but for BAT99-32.

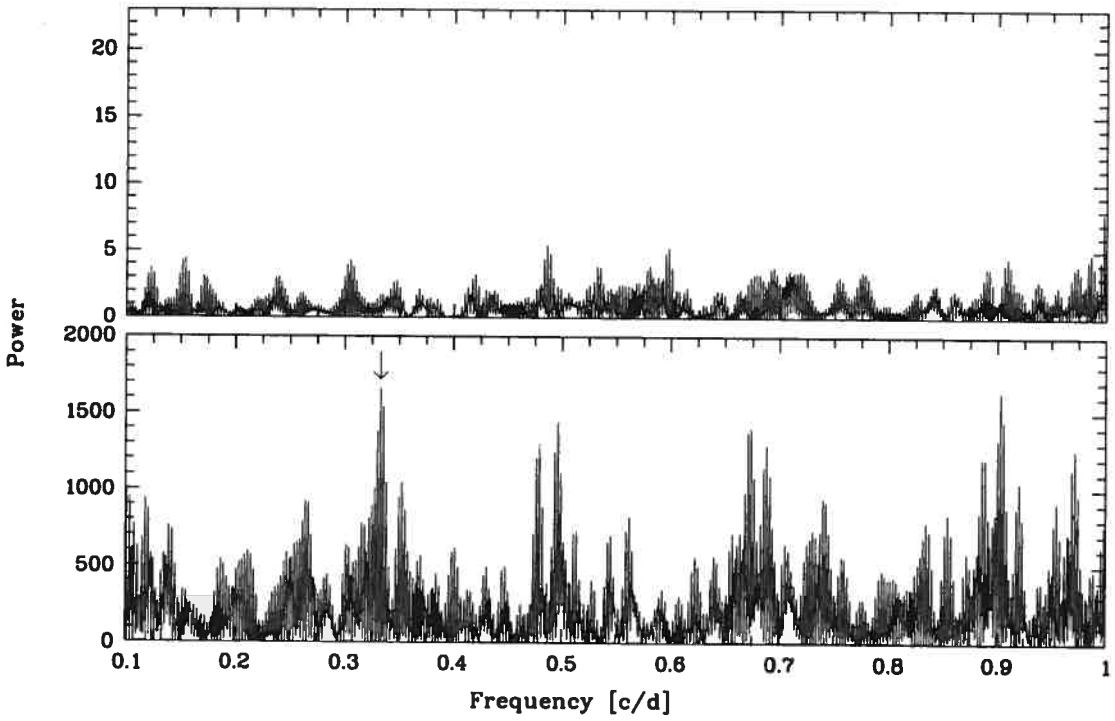

FIGURE 2.48 – As before, but for BAT99-77.

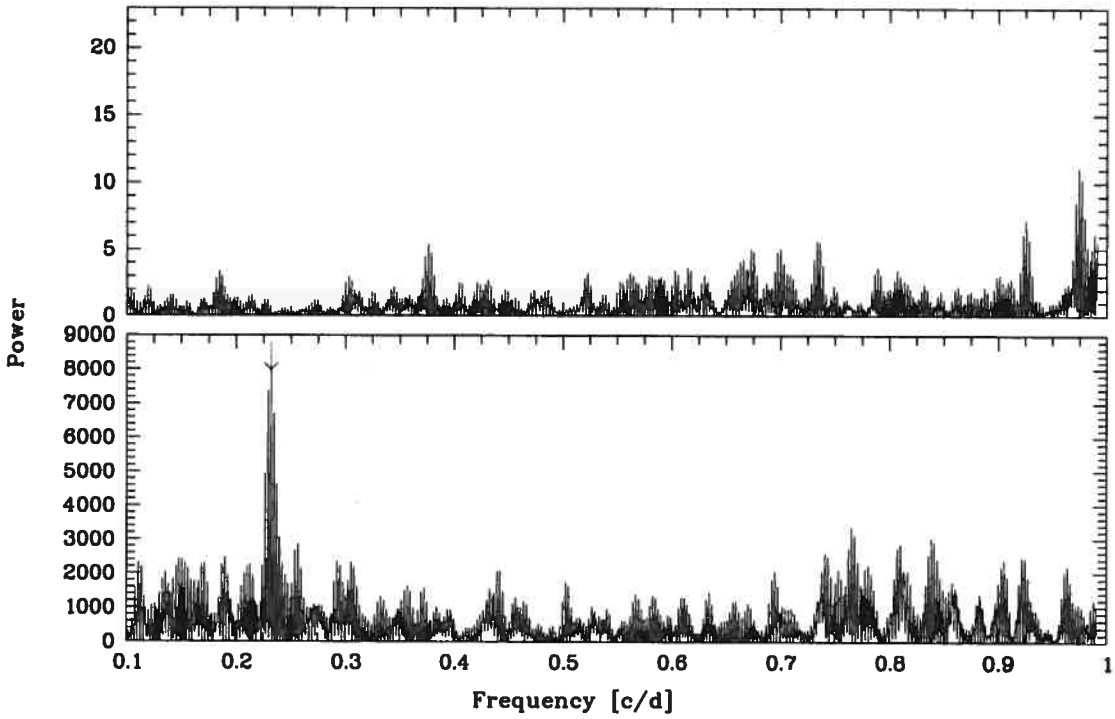

FIGURE 2.49 – As before, but for BAT99-92.

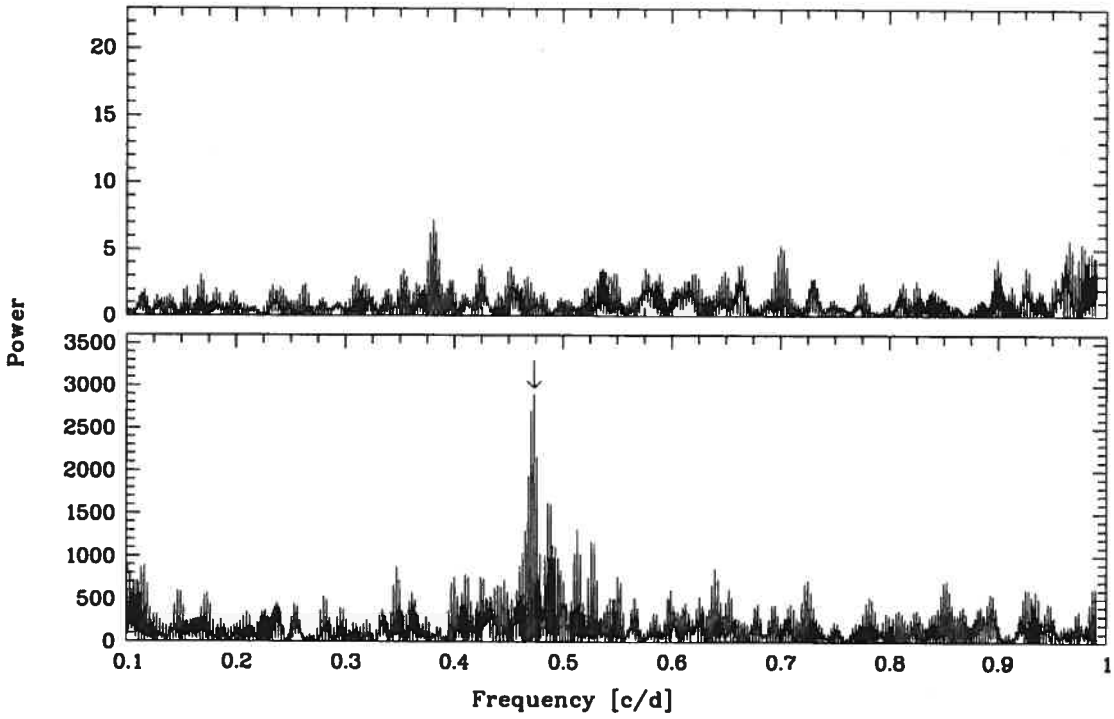

FIGURE 2.50 – As before, but for BAT99-95.

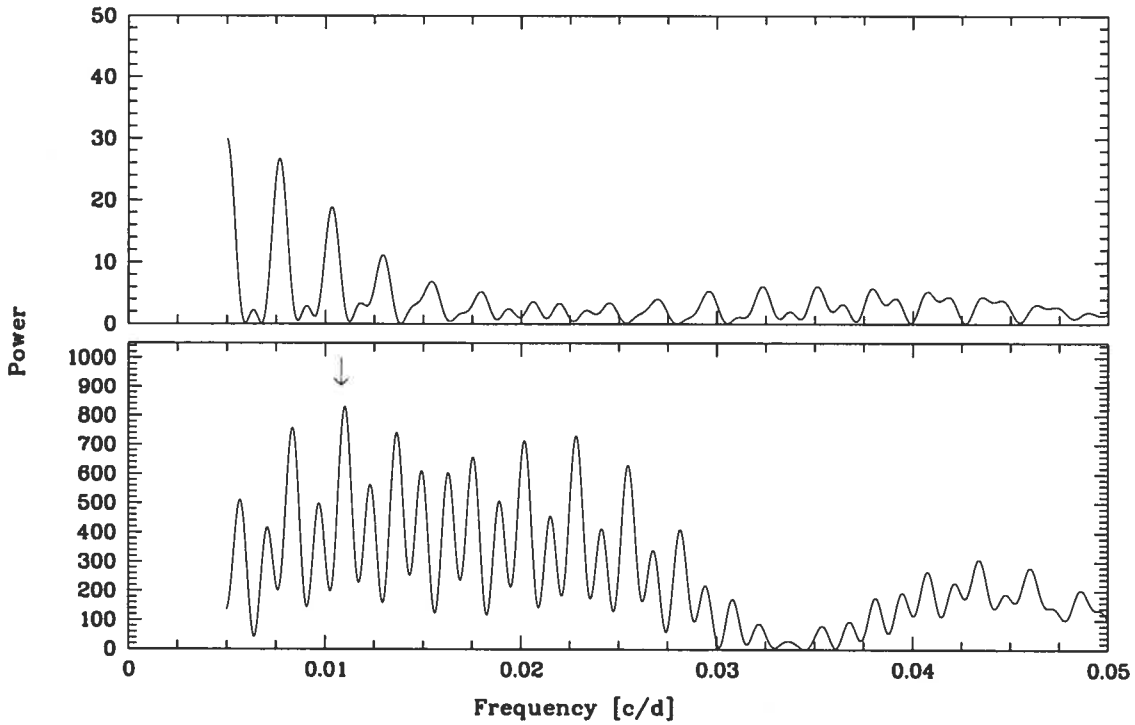

FIGURE 2.51 – Power spectrum (*lower*) and associated window function (*upper panel*) for BAT99-99. The frequency range plotted is 0.005 to 0.05 cycles per day (c/d), i.e. periods from 20 to 200 days are covered. While the window function is still reasonably well-behaved and the power in the periodogram sufficiently large, we are clearly approaching our detection limits. Again, the quoted period is indicated by an arrow.

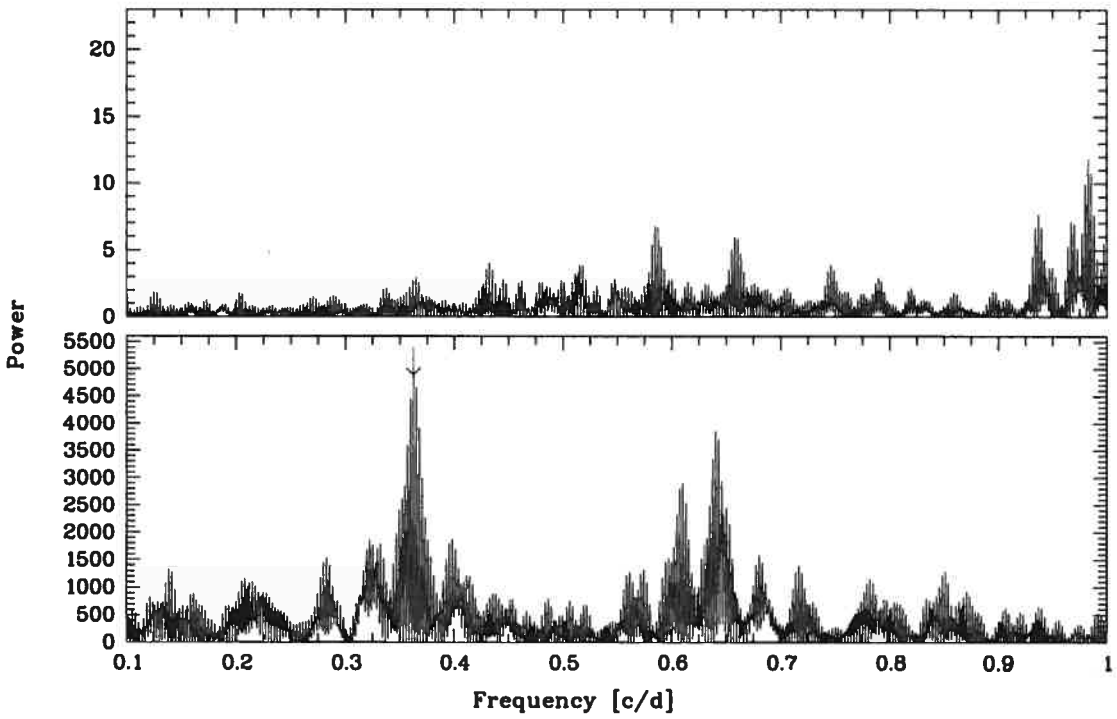

FIGURE 2.52 – As Figure 2.50, but for BAT99-103.

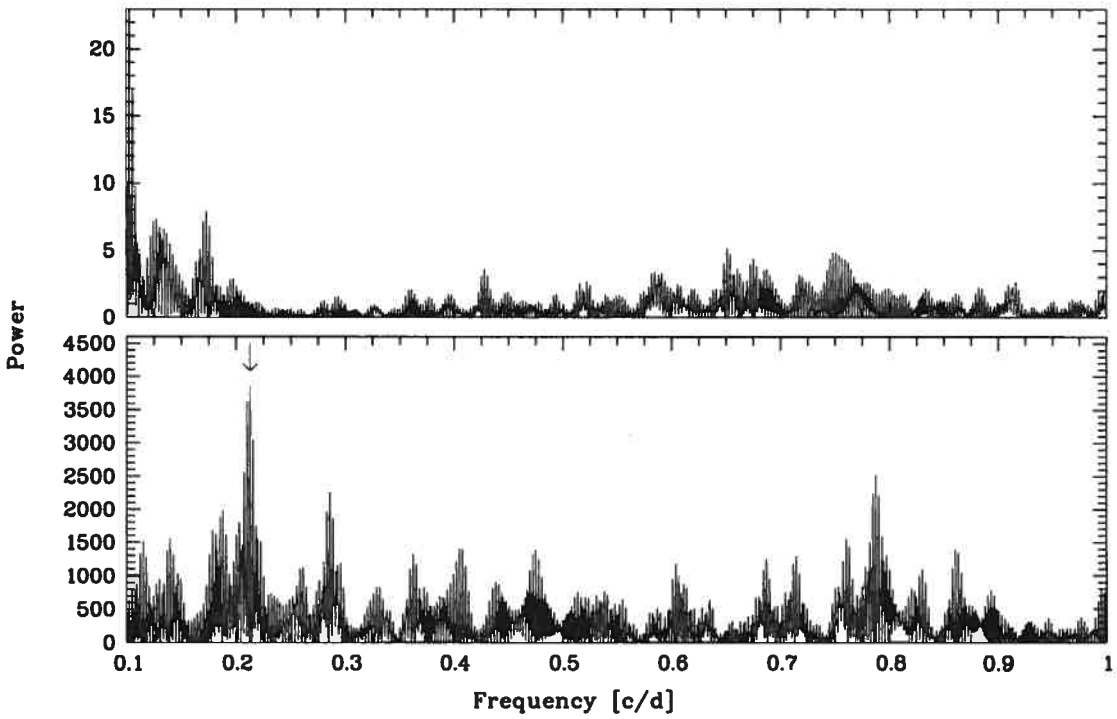

FIGURE 2.53 – As before, but for BAT99-113.

2.5.6 Binaries: The Remaining Orbital Parameters

For variable stars with identified, coherent periods, we attempted to compute orbital parameters using the program ELEMENTS (cf. Marchenko et al. 1994). This code fits an orbital solution to the RVs by χ^2 minimization, and computes the following orbital parameters and their respective errors: period P, eccentricity e, time of periastron passage T_0, angle between periastron and ascending node ω, the RV amplitude K, and systemic velocity γ. ELEMENTS also allows one to assign weights to each data point, with the particularity that the code expects weights between 0 and 1, where 1 is the highest weight. We thus normalized the weights to the variance of the best run (i.e. run 11 as above), obtaining the new weights $w_i^{(n)} = (\sigma_{11}/\sigma_i)^2$, so that $0 < w_i^{(n)} \leq 1$, which are mathematically equivalent to, but computationally more convenient than, the usual $1/\sigma^2$ weights[12].

As input guess for the orbital period, we used the value which was obtained from the CLEAN analysis of the *unweighted* data points, and where available, we use the periods obtained from the combined data sets (see above). Since we however did apply weights for the fit of the orbital solution, we did not fix the period but kept it as a free fitting parameter. In all cases, the periods found by ELEMENTS were, within the errors, identical to those obtained from our CLEAN analysis of either our or the combined data set. Fixing the value did thus not significantly change the orbital solution nor the errors. However, we again applied an iterative approach. For each data point j, ELEMENTS returns the value *observed minus computed*, $(o-c)_j$. After the first pass of ELEMENTS, we computed the overall mean $\overline{o-c}$ and the standard deviation from this mean, i.e. $\sigma(o-c)$. Any data point l with $|(o-c)_j| > 3\sigma(o-c)$ was removed from the data set, and the orbital solution was again fitted. This procedure was

[12]The reasons to treat weights in this rather odd way are purely historical. ELEMENTS is, by present-day standards, a very old code; it was written when available memory space in computers was small and high-precision floating-point arrays cumbersome to manipulate. In the case of very small values and even smaller associated errors, one would have had to handle very small values, in particular after the division by σ^2. If precision were to be conserved, longer-bit (i.e., larger) floating-point arrays had to be employed, dramatically affecting space and CPU time requirements. Re-normalizing the weights to the best σ leads to a division by a value which is rather close to unity. Also, for very small weights a cut-off could be applied, which is a reasonable thing to do, unless of course the overwhelming majority of data consist of rather bad data points and there are few, but excellent points. In such a case, of course, a user of ELEMENTS should reconsider the application of weights.

repeated until all data points were within $3\sigma(o-c)$ of the fitted orbital solution. Usually, this happened after the third iteration, which in turn means that only few data points had to be discarded. Naturally, the final orbital period no longer agreed with the initial guess, because the underlying data set had been modified. Yet, deviations remained very small.

In all cases where the algorithm converged, ELEMENTS returned an elliptical orbital solution, although e was small in most cases. Therefore, we repeated the fit and forced a circular solution by imposing $e = 0$, with $\phi = 0$ defined at the time E_0 of inferior conjunction, when the WR passes in front of its companion; thus, E_0 is different from the time of periastron passage, T_0, returned from the elliptical fit. Both sets of parameters are given in the respective Tables 2.7 through 2.14; parameters that were fixed for the circular fit are indicated by the symbol "@" after the value.

In all cases but for BAT99-77, the overall quality of the fit, expressed by $\sigma(o-c)$, did not significantly deteriorate. Thus, for the rest of this study the circular solution was adopted for all stars, with the said exception of BAT99-77. To illustrate the differences between the free, elliptical solution and the forced, circular one, both solutions are shown in Figures 2.54 though 2.61; overplotted are all data points which have been retained for the fit after having applied the iterative σ clipping described above. For the purpose of graphical comparison only, the circular solutions shown were computed using $E_0 = T_0$ of the given elliptical case, so that their zero phases coincide for better clarity. Note that in the tables, the dates for E_0 and T_0 are different.

In the following, we will discuss the binary status of individual stars which display cyclical RV variability.

— **BAT99-12:** This newly identified variable shows a clear periodicity of 3.2359 days in its RV curve obtained from the HeIIλ4686 emission lines. Although the RV curve is somewhat noisy when the RV points are folded into the corresponding phase, the orbital fit converges

TABLE 2.7 – Orbital parameters for BAT99-12

Parameter	Elliptical	Circular
P [days]	3.2359 ±0.0006	3.2359 ± 0.0006
K [kms^{-1}]	74 ± 5	68 ± 8
e	0.34 ± 0.06	0@
ω [degrees]	-29 ± 11	n/a
γ [kms^{-1}]	642 ± 13	650 ± 8
$\phi = 0$ at [JD-2,400,000.5]	[a]52269.84 ± 0.09	[b]52272.58 ± 0.10
σ_{o-c} [kms^{-1}]	24.8	27.1

[a]: Time of periastron passage T_0
[b]: Time of inferior conjunction E_0

(see Figure 2.54). The obtained eccentricity is surprisingly large for such a short-period orbit (see Table 2.7). This might be because the HeIIλ4686 emission is subject to severe distortions due to WWC. Forcing a circular fit deteriorates the overall error σ_{o-c} only slightly, so that a circular motion with slightly changed orbital parameters was adopted for the rest of the paper. The systemic velocity γ obtained from the orbital fit is very large, $\gamma = 650 \pm 8$ kms^{-1}, and qualifies this system for a fast runaway binary (see also Massey et al. 2005). This is very remarkable given the fact that such close and massive binary systems are very "hard" with respect to gravitational interactions with other cluster members. This object clearly deserves more attention; we have therefore obtained higher-quality, follow-up observations which are currently being reduced.

— **BAT99-32:** This star is a known binary with an orbital period of 1.9076 days. This makes BAT99-32 the shortest known binary system in the LMC, yet it does not display the largest RV amplitude (see BAT99-92). This might indicate that the system is seen under a low inclination angle. ELEMENTS converged easily. Note that within the errors, the system has a circular orbit, as might be expected for such short systems. Orbital parameters are given in Table 2.8 and the orbital fits (barely distinguishable) are shown in Figure 2.55.

— **BAT99-77:** This star is a known binary with an almost integer-day period which makes it hard to determine. However, we confirm Moffat's (1989) period. The orbital fit converged without problems (few points were exluded by σ clipping) and yielded quite a large eccen-

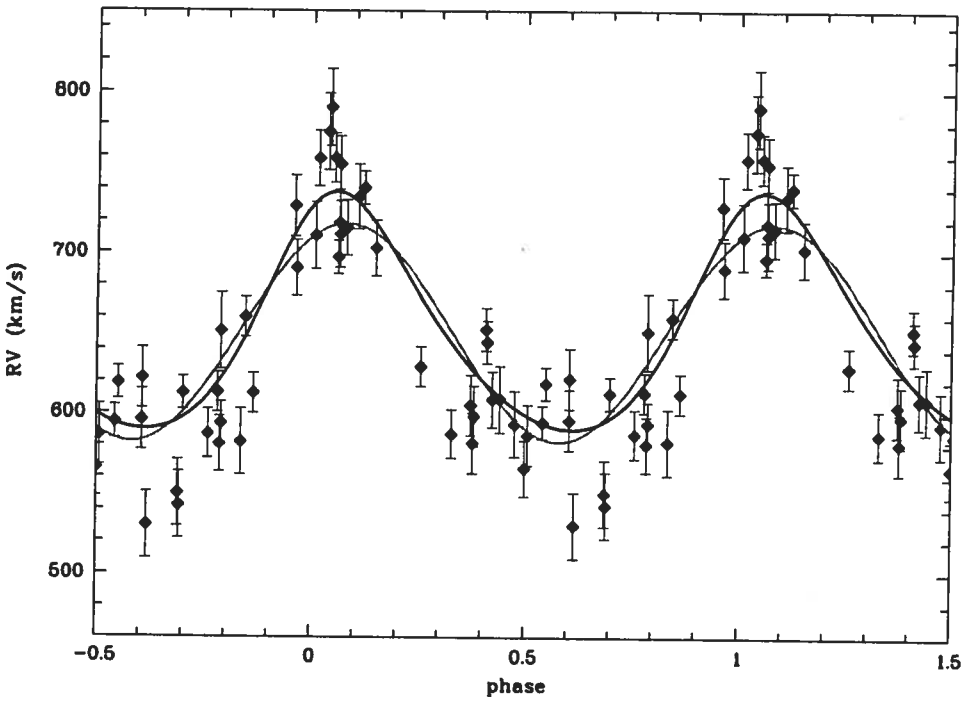

FIGURE 2.54 – Orbital solutions (elliptical in black, circular in grey) for BAT99-12, folded into the phase corresponding to the period of 3.2359 days.

TABLE 2.8 – Orbital parameters for BAT99-32

Parameter	Elliptical	Circular
P [days]	1.90756 ±0.00005	1.90756 ±0.00005
K [kms^{-1}]	120 ± 3	120 ± 3
e	0.06 ± 0.02	0@
ω [degrees]	250 ± 22	n/a
γ [kms^{-1}]	288 ± 6	288 ± 6
$\phi = 0$ at [JD-2,400,000.5]	[a]53011.57 ± 0.12	[b]53011.68 ± 0.12
σ_{o-c} [kms^{-1}]	13.5	14.2

[a]: Time of periastron passage T_0
[b]: Time of inferior conjunction E_0

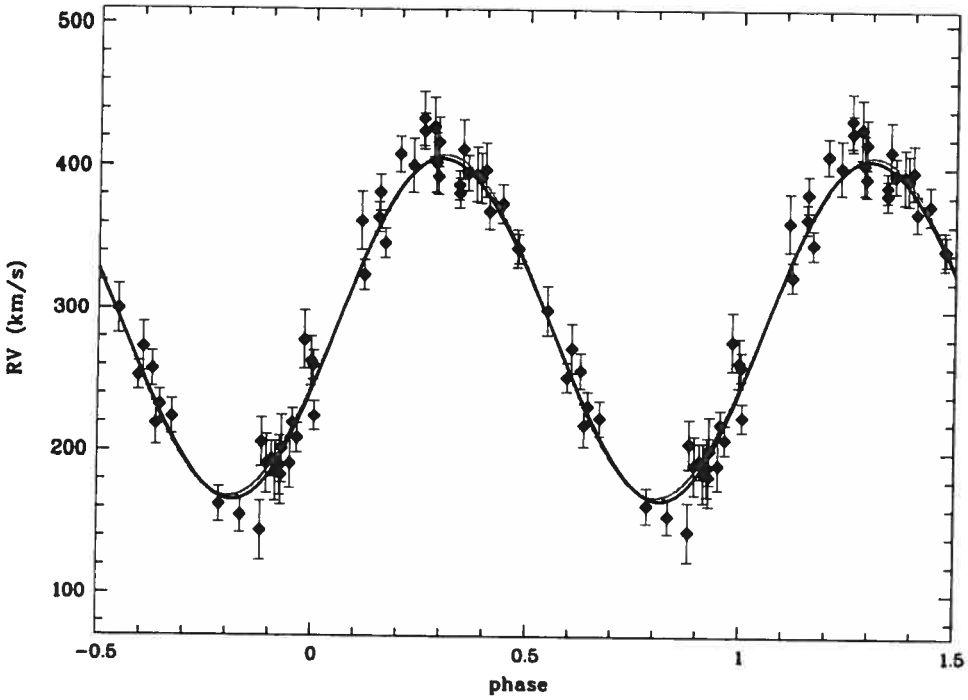

FIGURE 2.55 – Orbital solutions (elliptical in black, circular in grey) for BAT99-32, folded into the phase corresponding to the period of 1.9075 days. Note that the two solutions are almost identical.

tricity for such a short system. Consequently, the overall error increased significantly when a circular solution was imposed. Presently, we have not enough data to confirm whether this is due to WWC-induced distortions of the HeIIλ4686 emission or whether the orbit is indeed non-circular, but for the rest of this paper, we adopted the elliptical solution because of the smaller overall error. Orbital parameters are given in Table 2.9 and the orbital fits are shown in Figure 2.56.

— **BAT99-92:** This star is a known binary. The orbital fit went without any problems (σ clipping excluded a few points) and yielded a remarkably small eccentricity. The circular solution is virtually equal. This system shows the largest RV amplitude of our program stars, although it does not have the shortest period. This might indicate that it is seen under a large inclination angle, which renders BAT99-92 potentially interesting for a photometric campaign

TABLE 2.9 – Orbital parameters for BAT99-77

Parameter	Elliptical	Circular
P [days]	3.00303 ± 0.00002	3.00303 ± 0.00002
K [kms^{-1}]	144 ± 4	144 ± 15
e	0.32 ± 0.02	0@
ω [degrees]	7 ± 4	n/a
γ [kms^{-1}]	333 ± 8	346 ± 10
$\phi = 0$ at [JD-2,400,000.5]	[a]52631.87 ± 0.04	[b]52637.05 ± 0.06
σ_{o-c} [kms^{-1}]	10.9	16.9

[a]: Time of periastron passage T_0
[b]: Time of inferior conjunction E_0

TABLE 2.10 – Orbital parameters for BAT99-92

Parameter	Elliptical	Circular
P [days]	4.31252 ± 0.00005	4.31252 ± 0.00005
K [kms^{-1}]	204 ± 5	204 ± 5
e	0.02 ± 0.02	0@
ω [degrees]	109 ± 66	n/a
γ [kms^{-1}]	332 ± 7	332 ± 7
$\phi = 0$ at [JD-2,400,000.5]	[a]52998.03 ± 0.04	[b]52999.96 ± 0.04
σ_{o-c} [kms^{-1}]	16.8	17.0

[a]: Time of periastron passage T_0
[b]: Time of inferior conjunction E_0

to obtain the inclination angle from a light curve. Orbital parameters are given in Table 2.10 and the orbital fits are shown in Figure 2.57.

— **BAT99-95:** This is a newly discovered binary system in the 30 Dor region. Despite its short orbital period of 2.1113 days, is has a remarkably small RV amplitude. ELEMENTS converged without problems after the exclusion of only few data points by our σ clipping process, and the circular solution with essentially unchanged parameters is almost identical. Orbital parameters are given in Table 2.11 and the orbital fits are shown in Figure 2.58.

— **BAT99-99:** This is a newly discovered binary system located in the periphery of the R136 cluster in the center of the 30 Dor region. Massey et al. (2005) reported this star to be a binary, but did not quote an orbital period. From our analysis, we find a rather long period of 92.2 days (see above). Unfortunately, folding the data points into the corresponding phase yields a rather noisy RV curve. As a consequence, and because we are reaching the limits of

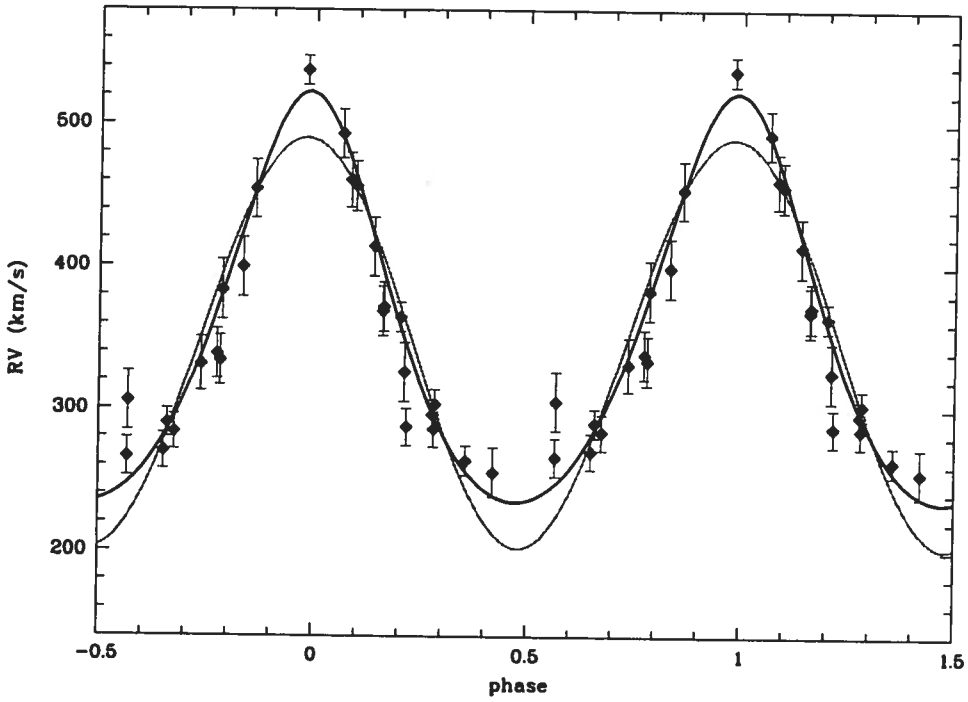

FIGURE 2.56 – Orbital solutions (elliptical in black, circular in grey) for BAT99-77, folded into the phase corresponding to the period of 3.0033 days. The differences are large enough to prefer the eccentric solution.

our data in terms of phase coverage, ELEMENTS did not converge. We therefore estimated an orbital solution by adopting a circular orbital motion (as our period-search algorithm does) and minimising the *unweighted* $\sigma(o-c)$. $\sigma(o-c)$ remains however uncomfortably large, probably because the true orbit is elliptical rather than circular as was assumed for the fit. We here report, for the first time, a tentative set of orbital parameters for BAT99-99 in Table 2.12. Errors on individual parameters are not stated, rather we quote the *unweighted* $\sigma(o-c)$ of the total solution. Note that $\phi = 0$ was set to be the time when the WR star passes in front of the O star. The orbital fit is shown in Figure 2.59.

— **BAT99-103:** This star is a known binary system, located in the periphery of the R136 cluster. Again, we are unable to verify whether or not the non-zero, albeit mild eccentricity yielded by the orbital fit is real, but the circular fit is only moderately worse. Since the RV

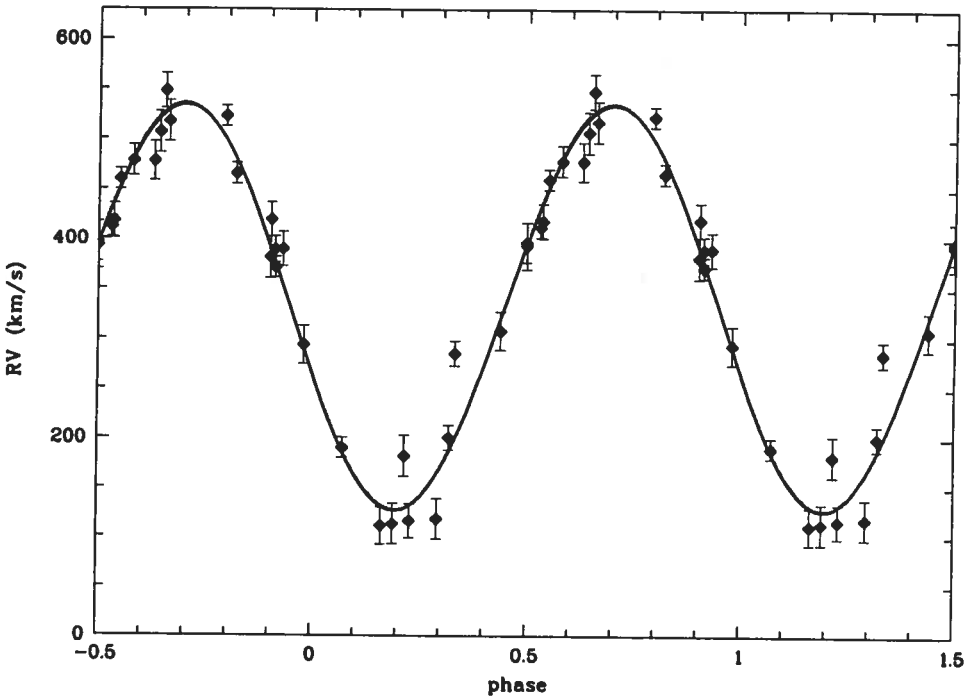

FIGURE 2.57 – Orbital solutions (elliptical in black, circular in grey) for BAT99-92, folded into the phase corresponding to the period of 4.3111 days. Note that the two solutions are almost identical.

curve is not very clean, both WWC-induced distortions and the weakness of the HeIIλ4686 emission line are the most likely causes for this result. Orbital parameters are given in Table 2.13 and the orbital fits are shown in Figure 2.60.

— **BAT99-113:** This is a newly discovered binary system in the periphery of R136. Regarding the non-zero eccentricity, the same remarks apply as for the previous system. Orbital parameters are given in Table 2.14 and the orbital fits are shown in Figure 2.61.

2.5.7 Mass Functions

Since in principle, we are only interested here in the identification of binaries, it is not necessary to assess the binary status beyond SB1, i.e. a binary with only one component (in

TABLE 2.11 – Orbital parameters for BAT99-95

Parameter	Elliptical	Circular
P [days]	2.1113 ± 0.0002	2.1113 ± 0.0002
K [kms^{-1}]	107 ± 3	107 ± 3
e	0.07 ± 0.03	0@
ω [degrees]	285 ± 18	n/a
γ [kms^{-1}]	274 ± 9	274 ± 9
$\phi = 0$ at [JD-2,400,000.5]	[a]52999.87 ± 0.10	[b]52999.78 ± 0.09
σ_{o-c} [kms^{-1}]	10.6	10.9

[a]: Time of periastron passage T_0
[b]: Time of inferior conjunction E_0

TABLE 2.12 – Orbital parameters for BAT99-99

Parameter	Circular
P [days]	92.60 ± 0.52
K [kms^{-1}]	91 ± 19
e	0@
ω [degrees]	n/a
γ [kms^{-1}]	337 ± 16
E_0 [JD-2,400,000.5]	53045.9 ± 1.3
$\sigma(o-c)$ [kms^{-1}]	30.5

TABLE 2.13 – Orbital parameters for BAT99-103

Parameter	Elliptical	Circular
P [days]	2.75975 ± 0.00003	2.75975 ± 0.00003
K [kms^{-1}]	158 ± 4	156 ± 10
e	0.23 ± 0.03	0@
ω [degrees]	-41 ± 7	270@
γ [kms^{-1}]	388 ± 8	388 ± 8
$\phi = 0$ at [JD-2,400,000.5]	[a]53007.80 ± 0.05	[b]53010.22 ± 0.05
σ_{o-c} [kms^{-1}]	19.9	23.8

[a]: Time of periastron passage T_0
[b]: Time of inferior conjunction E_0

TABLE 2.14 – Orbital parameters for BAT99-113

Parameter	Elliptical	Circular
P [days]	4.6988 ± 0.002	4.6988 ± 0.002
K [kms^{-1}]	130 ± 8	125 ± 15
e	0.20 ± 0.05	0@
ω [degrees]	308 ± 16	n/a
γ [kms^{-1}]	390 ± 10	397 ± 11
$\phi = 0$ at [JD-2,400,000.5]	[a]52993.07 ± 0.13	[b]52992.53 ± 0.14
σ_{o-c} [kms^{-1}]	18.1	

[a]: Time of periastron passage T_0
[b]: Time of inferior conjunction E_0

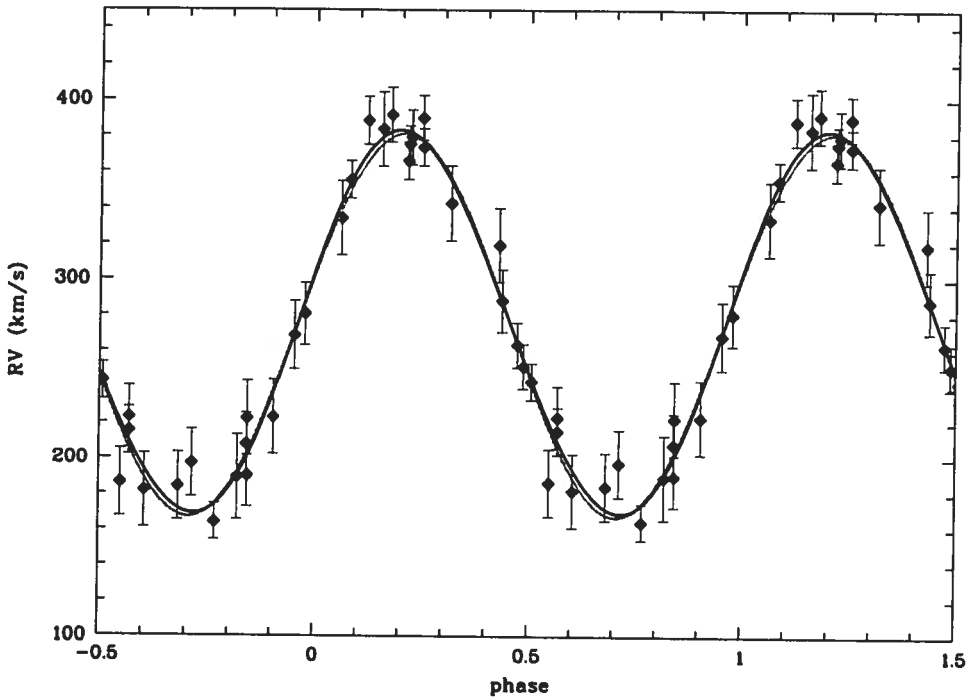

FIGURE 2.58 – Orbital solution (elliptical in black, circular in grey) for BAT99-95, folded into the phase corresponding to the period of 2.1113 days.

our case, the WR star) visible. Thus, a more detailed analysis of the binaries, together with new and better data, will be published in a forthcoming paper.

Remarkably, despite the fact that we have better (higher S/N, CCD) data than Moffat (1989), none of our binaries displayed a readily visible, spectral signature of the companion, just as Moffat had already reported. This can be explained by the fact that, with the exception of BAT99-32, all binaries contain H-rich WN stars or extreme Of stars. These are almost certainly H-burning objects, which in turn means that in order to drive WN-like winds, they have to be very luminous and hence extremely massive. It might thus be that the WNL star is the more massive component of the binary (see e.g. the case of WR22; Schweickhardt et al. 1999). Thus, given the comparable bolometric corrections for this kind of WN star and the (typically) O-type companion, the O star is most likely the fainter partner. BAT99-32, in

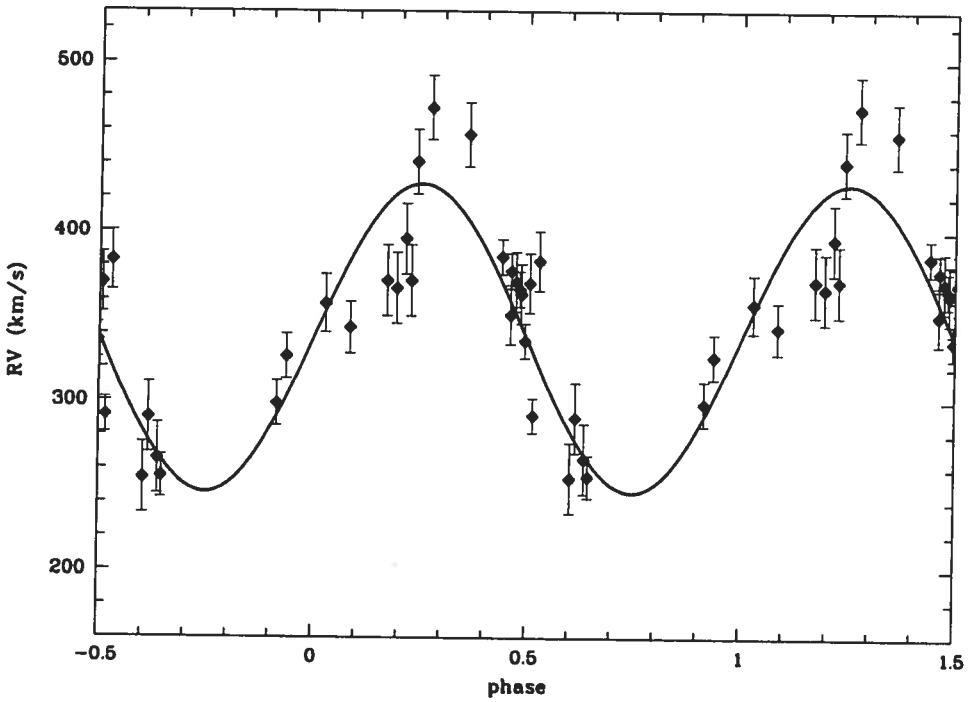

FIGURE 2.59 – Preliminary orbital solution for BAT99-99, folded into the phase corresponding to the period of 92.6 days.

turn, contains a visual companion of type B1Ia that is not the true companion to the WR star; the light of this visually very bright supergiant dominates the optical absorption spectrum, so that here, too, the true, close binary companion could not be detected. Follow-up spectroscopy has already been secured and is currently being reduced. Results will be published elsewhere, together with the results of a more sophisticated analysis.

Using the values for the visible components in the usual units (period P in days, RV amplitude K in kms^{-1}, M in solar masses), one has for the mass function

$$f_1(M) = 1.035 \times 10^{-7} K_1^3 P (1-e^2)^{\frac{3}{2}} M_\odot \equiv \frac{M_2 \sin^3 i}{(1+M_1/M_2)^2}.$$

With the exception of BAT99-77, whose eccentric orbit yields a much better fit to the

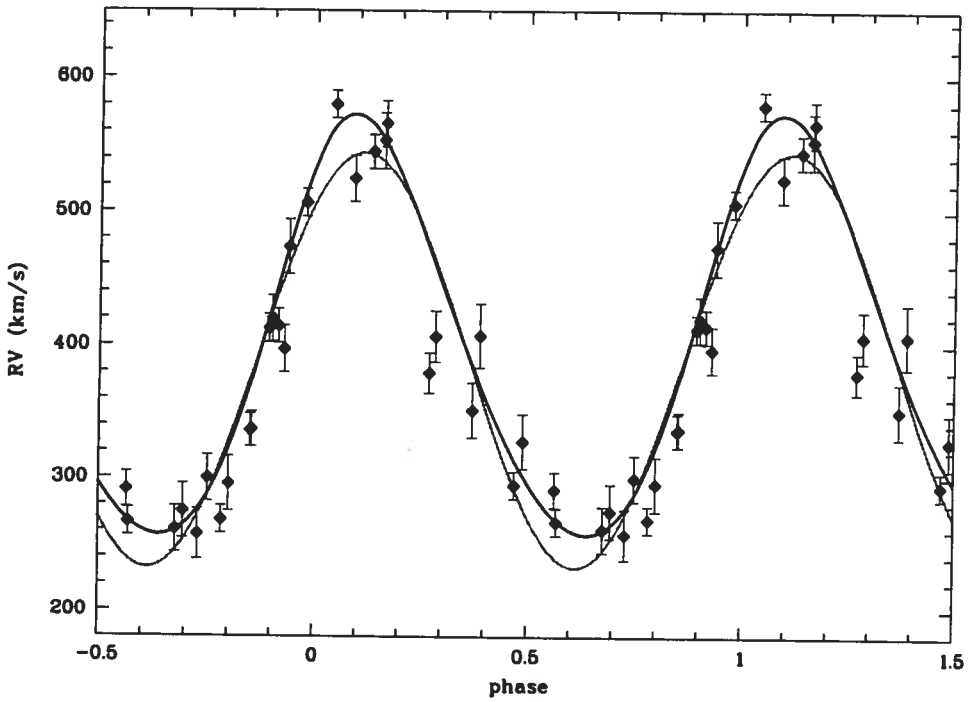

FIGURE 2.60 – Orbital solution for BAT99-103, folded into the phase corresponding to the period of 2.7597 days.

data, we have used the orbital parameters of the circular solution, i.e. $e = 0$, to calculate the respective mass functions. The results are given in Table 2.15.

The fact that only one binary component is visible in the spectrum, and that it most likely is the (much) more massive partner in the system, is reflected by the relatively low values of the mass function for the binaries; moreover, the systems might be seen under particularly low inclination angles. An exception to this is BAT99-92, which displays a relatively larger mass

TABLE 2.15 – Mass functions $f_1(M)$ for our binary systems.

BAT99	$f_1(M)$ $[M_\odot]$	BAT99	$f_1(M)$
12	0.14	95	0.27
32	0.34	99	7.22
77	0.79	103	1.08
92	3.79	113	0.95

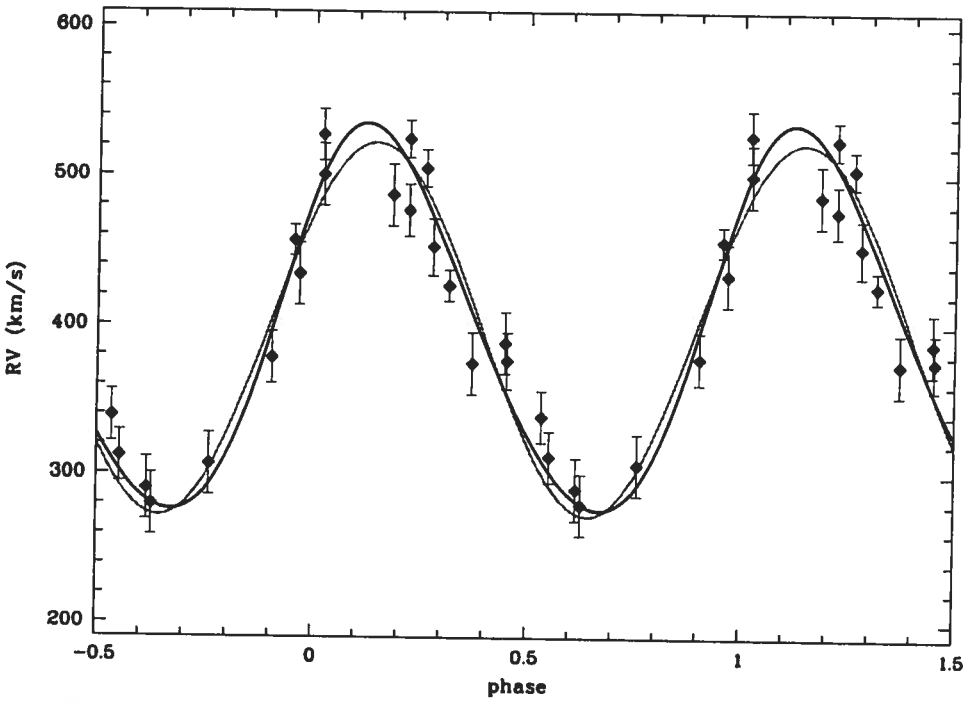

FIGURE 2.61 – Orbital solutions (elliptical in black, circular in grey) for BAT99-113, folded into the phase corresponding to the period of 4.6988 days.

function; while we have argued above that star BAT99-92 might be seen under a very high inclination angle, the large value of the mass function is perfectly consistent with BAT99-92 being a more evolved (and hence less massive), helium-burning WN3b star. BAT99-99, on the other hand, displays a comparatively large mass function. We currently have no explanation for this, but it might be that this star, too, is seen under a very high inclination angle, or that the RV amplitude has been (greatly) overestimated by forcing a circular fit of the orbital solution.

2.5.8 Wind-Wind Collisions and Line-Profile Variations

It is well known that in WR+O binaries, where both stars have strong winds, WWCs occur, and a shock cone is formed as the contact discontinuity between the two winds wraps around the star with the weaker wind, which is usually the O star. (More precisely, the wind

momentum of the O star is smaller than that of the WR star, since both winds are ~equally fast, but the WR wind is an order of magnitude denser than the O star's wind.) As the shocked matter flows with high velocities along the contact discontinuity, it cools, giving rise to excess emissions which can be seen atop some optical emission lines of the WR star. Since the flow velocity seen by an observer depends on the orientation of the flow, the position of the excess bumps atop the emission lines depends on the orbital phase. The shock-cone acts like a beacon of a lighthouse: if it is pointing towards the observer, the excess emission will be blue-shifted, and if the matter flows away from the observer, the excess emission will be red-shifted. From geometrical considerations, one can derive properties of the shock cone and even the inclination angle of the binary system, with a surprisingly good precision. (For a detailed discussion of this approach, see e.g. Luehrs 1997; Hill et al. 2002.) However, since these excess emissions will deform the line profile, WWCs might lead to a more or less severely reduced amplitude and phase fidelity of the RV curve with respect to the true orbit of the star, when an affected emission line is used.

Excess emissions are particularly strong in emission lines which sensitively react to density variations; the best known example is CIIIλ5696 in WC stars, which unperturbed is an almost rectangular, flat-topped emission line, thus allowing one to identify fairly easily any excess emission. In WN stars, the HeIIλ4686 emission line is prone to such excess emissions due to WWC, i.e. our strategic line we used to derive RV for our program stars. Thus, we certainly expect to find evidence of WWC when inspecting the HeIIλ4686 emission line in our binaries more closely. Contrary to the CIIIλ5696 in WC stars, however, the HeIIλ4686 line in WN stars is round and not flat-topped. Thus, it is not quite as easy as in the case of WC stars to isolate the excess emissions; one has to have a good idea what the unperturbed emission-line profile looks like. Hence, we content ourselves here to simply describe line-profile variations (LPV) in identified binary systems.

To do so, we have shifted all spectra of a given star into the rest frame of the WR star, computed a minimum spectrum of the time series, and subtracted it from all spectra of the

series to obtain residuals. The idea is that this minimum spectrum resembles the unperturbed spectrum most closely. Some deviations are introduced by imperfect knowledge of both the RVs (i.e., the true orbital motion), and the continuum, which in WR stars is notoriously difficult to properly fit during the rectification process, but for the illustrative purposes we have here, this approximation will be sufficient.

We constructed a minimum spectrum by calculating a simple pixel-by-pixel minimum of the time series. This approach, however, understimates the true minimum spectrum because each pixel suffers from noise. Thus, the simple pixel-by-pixel minimum will yield a spectrum with average intensity $I - \Delta$, and any residual (thus, excess) emission will be overestimated by the same amount. This can be particularly important in the extended emission-line wings, where the line intensity slowly reaches continuum level.

In zeroeth-order approximation, this effect can be corrected for by multiplying the minimum spectrum with a factor $f = I/(I - \Delta)$. If Poisson noise is the only noise source, then Δ is directly related to $\sigma = \sqrt{I}$: The larger the intensity of this pixel, the better the true minimum value of a given pixel p_i of a time series will be estimated. Thus, to a first-order approximation, the total correction factor f modifies with the square-root of the pixel intensity, and we obtain

$$f = \frac{1}{1 - \Delta/\sqrt{I}}$$

One has to bear in mind, though, that this correction factor in all cases remains very small compared to the expected, WWC-related LPVs, because the S/N of each individual spectrum is good enough for Δ to be small (namely of the order of 1/(S/N)). At this noise level, the precision of the RVs by which the respective spectra are shifted into the WR star's frame of reference, i.e. the relative position of the minumum spectrum and the spectrum of the series, becomes the dominant source of error, so that no further correction was deemed necessary.

Since we work on rectified spectra, the correction procdure was very straightforward. We calculated the average value $cont(min)$ of the continuum region between 4950 and 5300 Å in the uncorrected minimum; since the continuum by definition should be unity, $\Delta = 1 - cont(min)$. The average intensity $\overline{I(p_i)}$ for each p_i of the spectrum was obtained from a S/N-weighted average spectrum of the times series. The minimum was then corrected accordingly, slightly smoothed, and subtracted from all spectra of the time series for a given star. We then shifted the residuals back into the observer's frame of reference and constructed a phased "dynamic spectrum" in the region around HeIIλ4686, i.e., a plot of the residual spectra with their intensities coded in greyscales (white being the strongest emission), and folded into the corresponding phase of the binary period (10 phase-bins were used throughout). Dynamic spectra are shown in Figures 2.62 to 2.69. Also shown are the overplotted original spectra (in light grey) and the minimum spectrum of the respective time series that was subtracted to obtain the residuals (in thick black), in the WR star's frame of reference, respectively. The point in phase where the WR is in front of its companion (inferior conjunction) is indicated by an arrow on the right hand side of the plot. At this time, because the WR wind is stronger (denser) than that of the (supposed) O star, the shock cone points ~away from the observer; the excess emission arising in the matter that flows along the cone will thus display its highest redshifted velocities. Any delays (i.e. phase shifts) between the time of conjunction and the maximum redshift is thus related to cone distortions due to e.g. Coriolis force and other effects, i.e. this information can be used to constrain the geometry of the shock zone, etc. This will be done in a forthcoming paper.

In circular orbits, the WR star is in front at $\phi = 0$ by definition; in elliptical orbits, however, the situation is more intricate, because the moment in time (and thus in phase) depends on the spatial orientation of the ellipse, i.e. on the argument of the periastron, ω. From simple geometrical considerations, one can derive that the WR is in front of its companion, which is located in the focus of the orbital ellipse, when $v + \omega = 90°$ with v the true anomaly of the orbit. Using the eccentric anomaly E and the transcendent Kepler equation, v can be

computed from the time (phase) elapsed since periastron passage (which occurs at T_0):

$$E - e \sin E = \frac{2\pi}{P}(t - T_0).$$

After numerically solving this equation using a simple Newton-Raphson iteration scheme, E can then be used in the following equation to isolate v:

$$\tan \frac{E}{2} = \sqrt{\frac{1-e}{1+e}} \tan \frac{v}{2}$$

The time (phase) at which $v = 90° - \omega$ was then graphically obtained for the v vs. ϕ plot of each binary. Note that only for star BAT99-77 was an elliptical orbit assumed, while for the other binaries the circular solution was used.

Most binary systems show phase-dependent excess emissions to some degree. A notable exception is BAT99-12; not only is the HeIIλ4686 emission line much less variable than in other binary systems, but no structure whatsoever can be seen in the greyscale of the residuals. It could thus be that BAT99-12 either is not a binary or has a companion which displays no noticeable wind, so that WWC does not occur in this system. In this context it might be worth noting that BAT99-12 bears a striking resemblance with the Galactic O4Inf star ζ Pup, which also displays cyclic LPV (for details see Eversberg et al. 1998, and references therein); also, both stars are runaways (see Section 2.5.9). These LPV could introduce RV variations that mimic a binary motion. While we have not sufficiently good data to doubt the binary nature or to firmly conclude on this issue, this star clearly deserves more attention. Data from follow-up observations are currently being reduced and will be published elsewhere.

Results are further discussed in the captions of Figures 2.62 though 2.69.

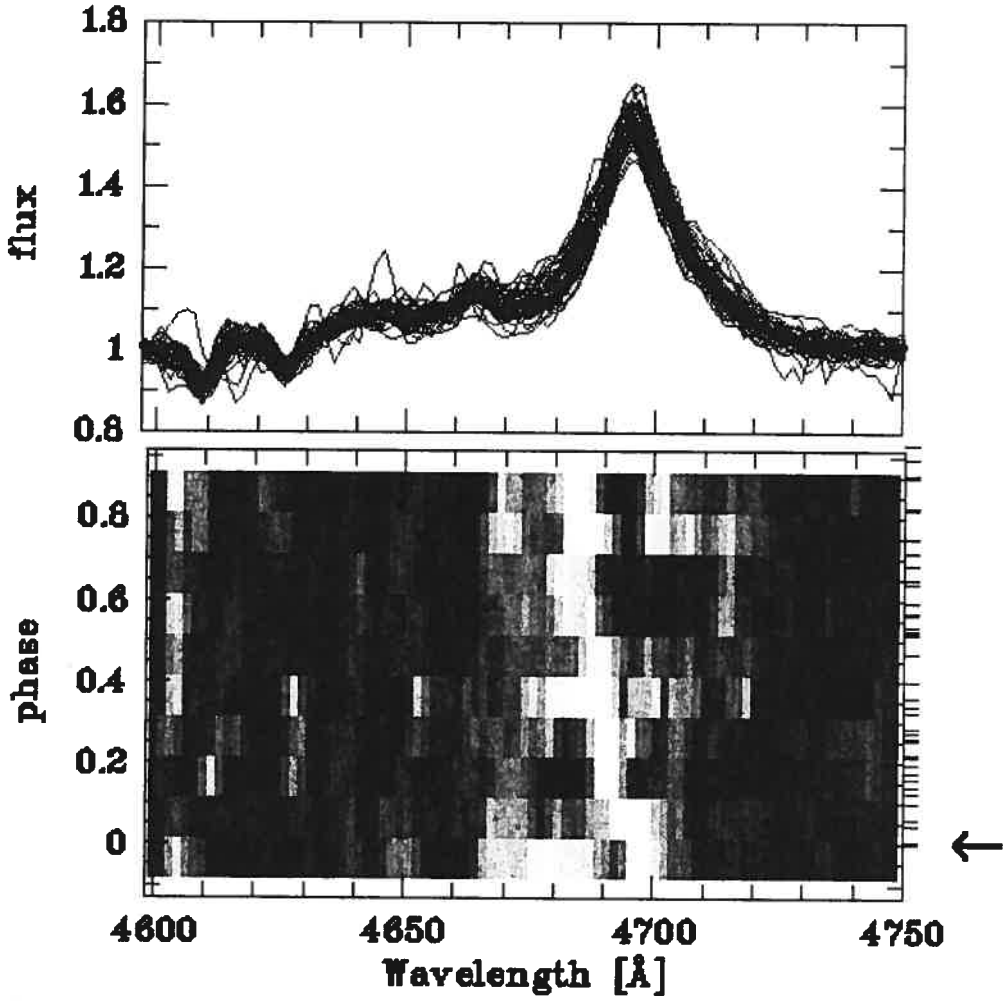

FIGURE 2.62 – BAT99-12: *Upper panel:*: Overplot of the original spectra (grey) and the minimum spectrum (thick black), both in the WR star's frame of reference. *Lower panel:* Dynamic spectrum of the residuals after subtraction of the minimum shifted back into the observer's frame of reference and folded into the corresponding orbital phase. The arrow indicates the orbital phase $\phi = 0$ at which the WR star passes in front of the companion (circular orbit assumed). As can be seen, the line is much less variable than in other binaries, and shows no presence of WWC excess emission at all.

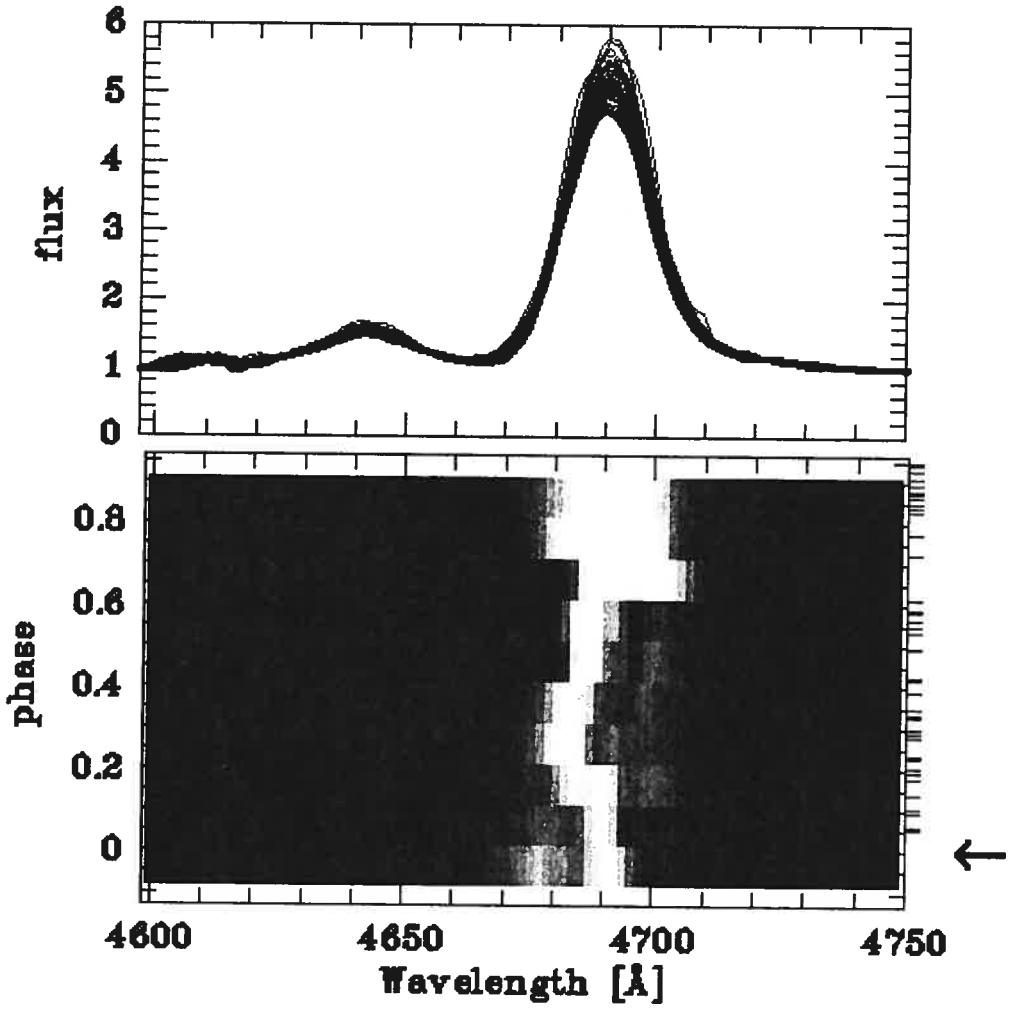

FIGURE 2.63 – Same as Figure 2.62, but for BAT99-32. The WR star passes in front of the O star at $\phi = 0$ (circular orbit). Although the strong WWC excess emission is clearly visible in the overplot (*upper panel*), it is not too well defined in the dynamic spectrum. Remarkable is the apparent increase in excess emissions between phases 0.6 and 0.8; even if an elliptical orbit is assumed, this increase does not coincide with periastron passage. We curently have no explanation for this behaviour. Given the very short orbital period of 1.9075 days, one might expect continuum-variation effects due to photometric eclipses of the stars; however, the system does not display strong enough eclipses to account for the large line variations (see Section 2.5.11).

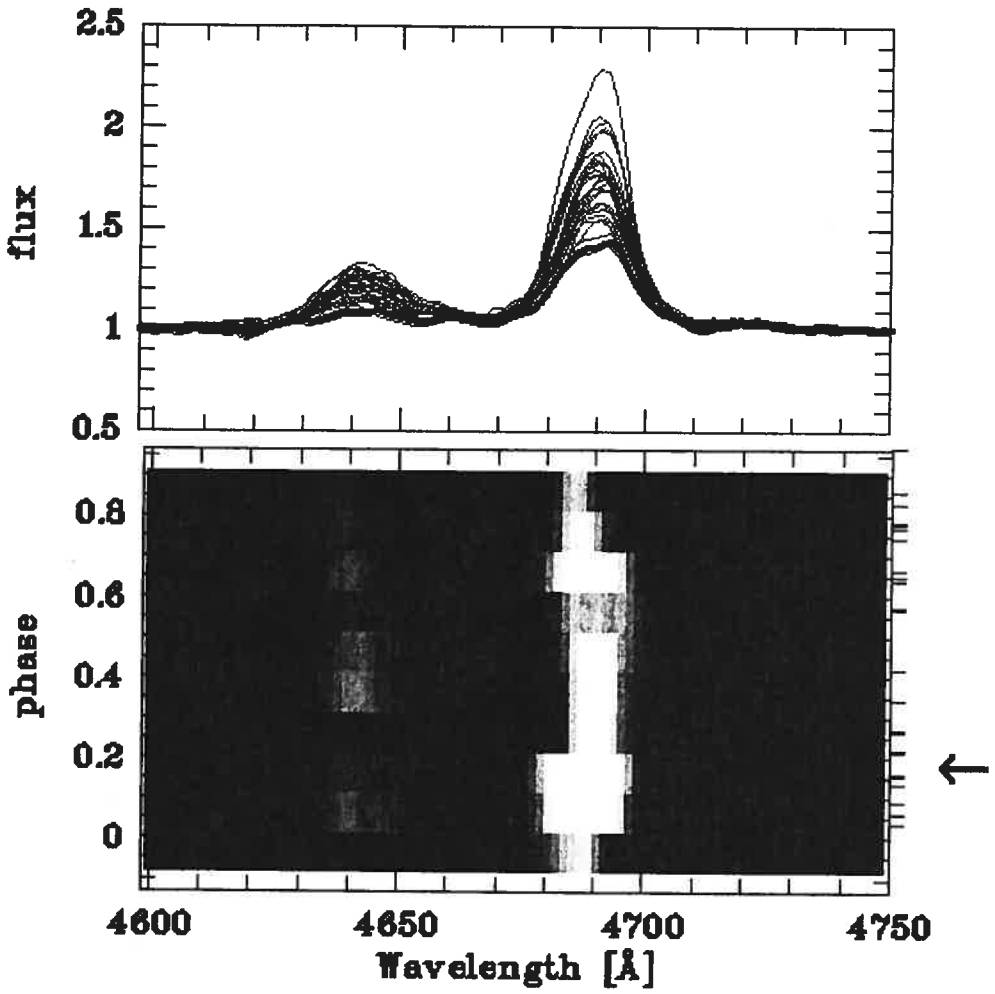

FIGURE 2.64 – Same as Figure 2.62, but for BAT99-77. Unfortunately, due to crowding, the spectrum of this star is randomly diluted, which accounts for the largely imperfect subtraction and the resulting emissions in the grescales. The highest redshift of the (excess?) emission occurs when the WR star is in front ($\phi \sim 0.18$; an elliptical orbit was used), as indicated by the arrow. While this result is in agreement with the theory, it needs to be taken with care, for the said reasons.

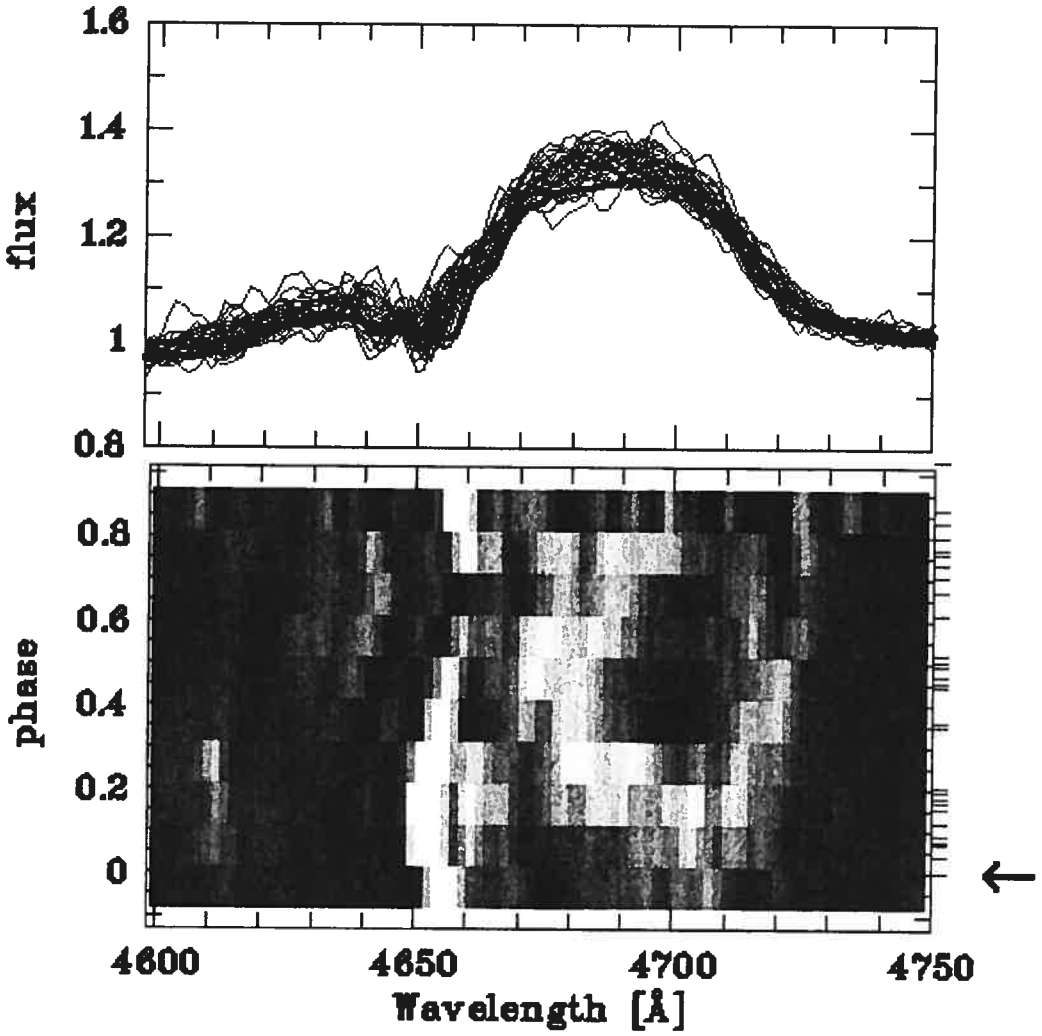

FIGURE 2.65 – Same as Figure 2.62, but for BAT99-92. Given the strong dilution of the HeIIλ4686 line due to the presence of an extremly bright B supergiant, any WWC excess emission is most likely diluted as well, and thus drowned in the noise of our spectra. Absorption features visible in the dynamic spectrum (*lower panel*) are artefacts of the lines of the stationary supergiant, because the minimum spectrum has been subtracted in the rest frame of the WR star, not the B star.

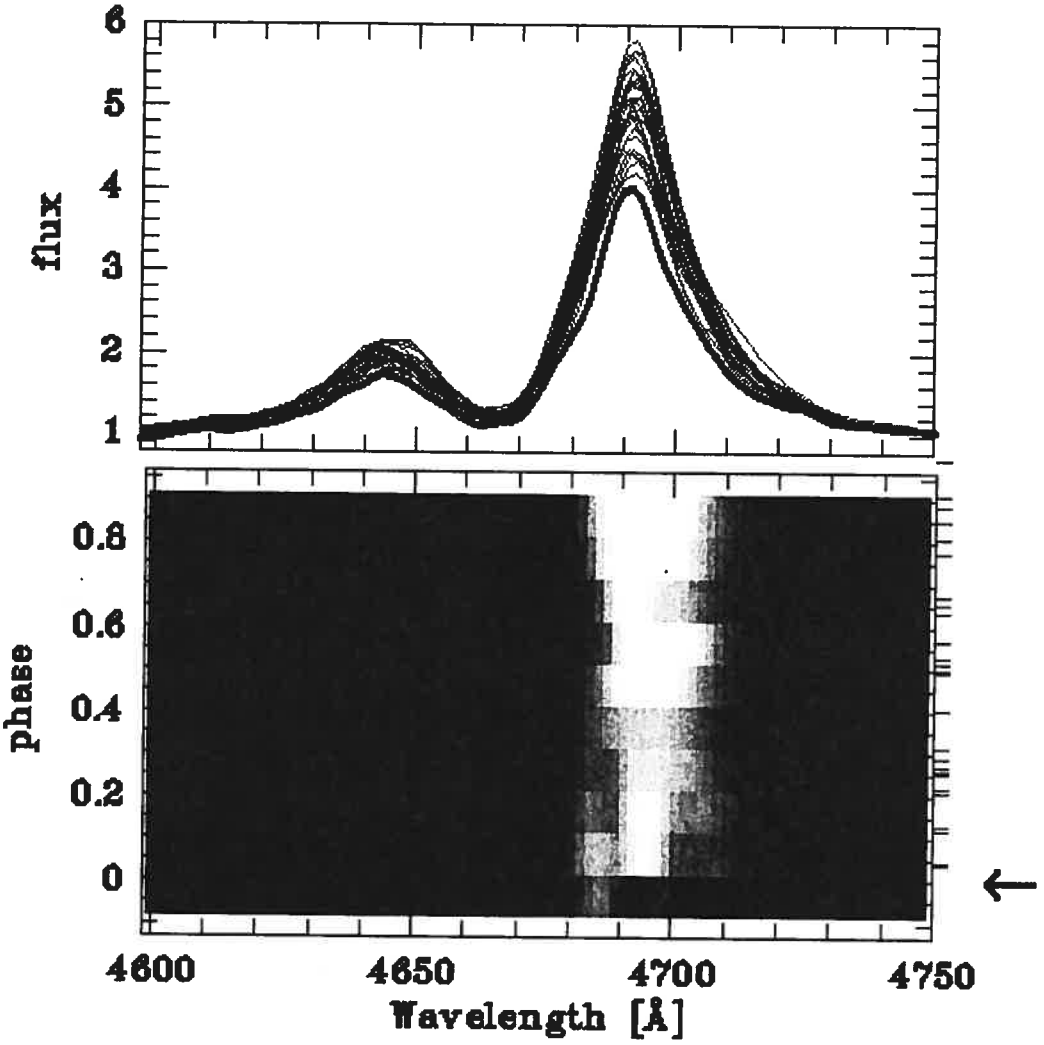

FIGURE 2.66 – Same as Figure 2.62, but for BAT99-95. As indicated by the arrow, the WR star is in front at $\phi = 0$ (circular orbit). Remarkably it seems that the excess emission is strongest around inferior conjunction, which might be an indication for the WR star eclipsing the O star.

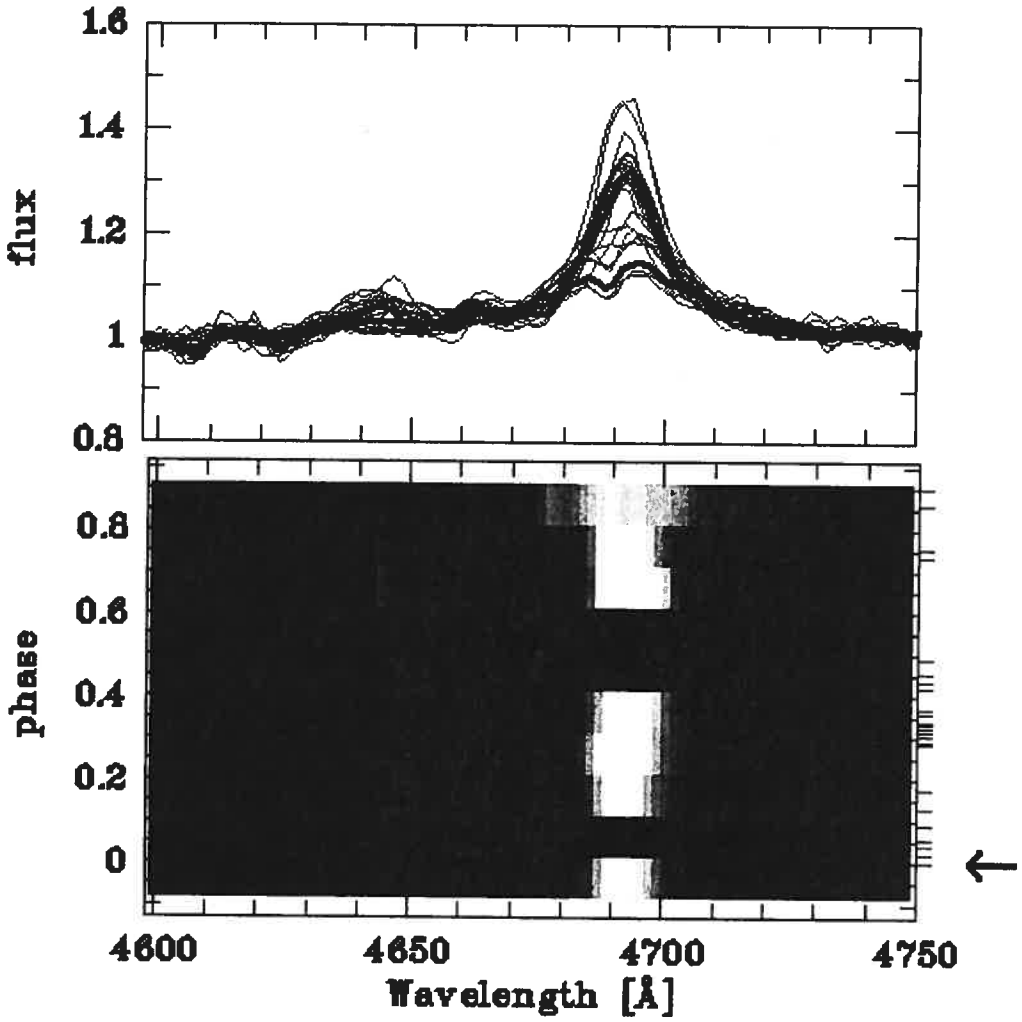

FIGURE 2.67 – Same as Figure 2.62, but for BAT99-99. The strong line variability (*upper panel*) suggests that this binary either has a non-circular orbit, displays photometric eclipses, or suffers from some other kind of continuum variability. Note that a circular orbit was assumed, hence the phase at which the WR is in front is set to $\phi = 0$, but most likely this is an incorrect assumption. The dynamic spectrum (*lower panel*) remains inconclusive; the black area indicates two empty phase-bins due to insufficient time coverage of the data.

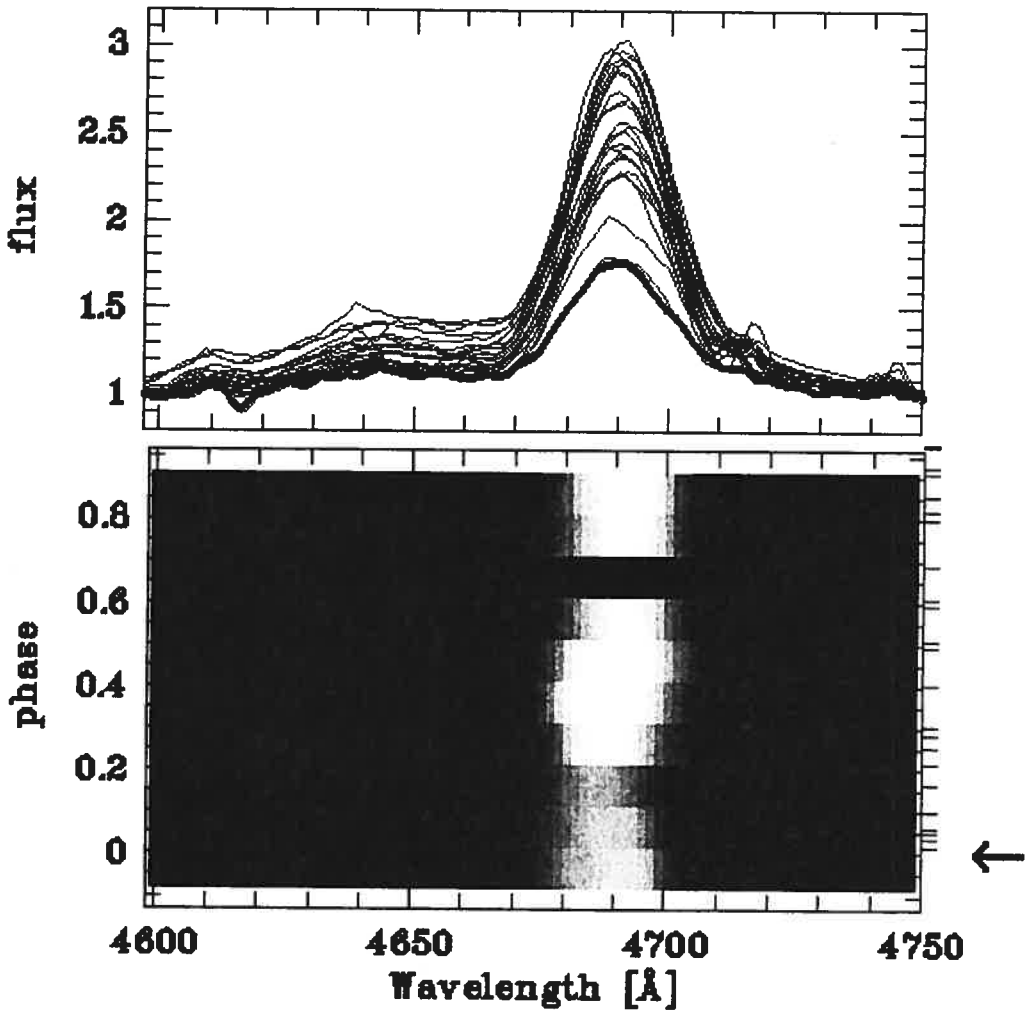

FIGURE 2.68 – Same as Figure 2.62, but for BAT99-103. As can be seen from the emission feature at 4650 Å in the overplotted spectra (*upper panel*), BAT99-103 suffers from variable light contribution of the WC star in BAT99-101/102: The residual emission traces remarkably well the WR star's circular orbit which renders its dynamic spectrum (*lower panel*) inconclusive.

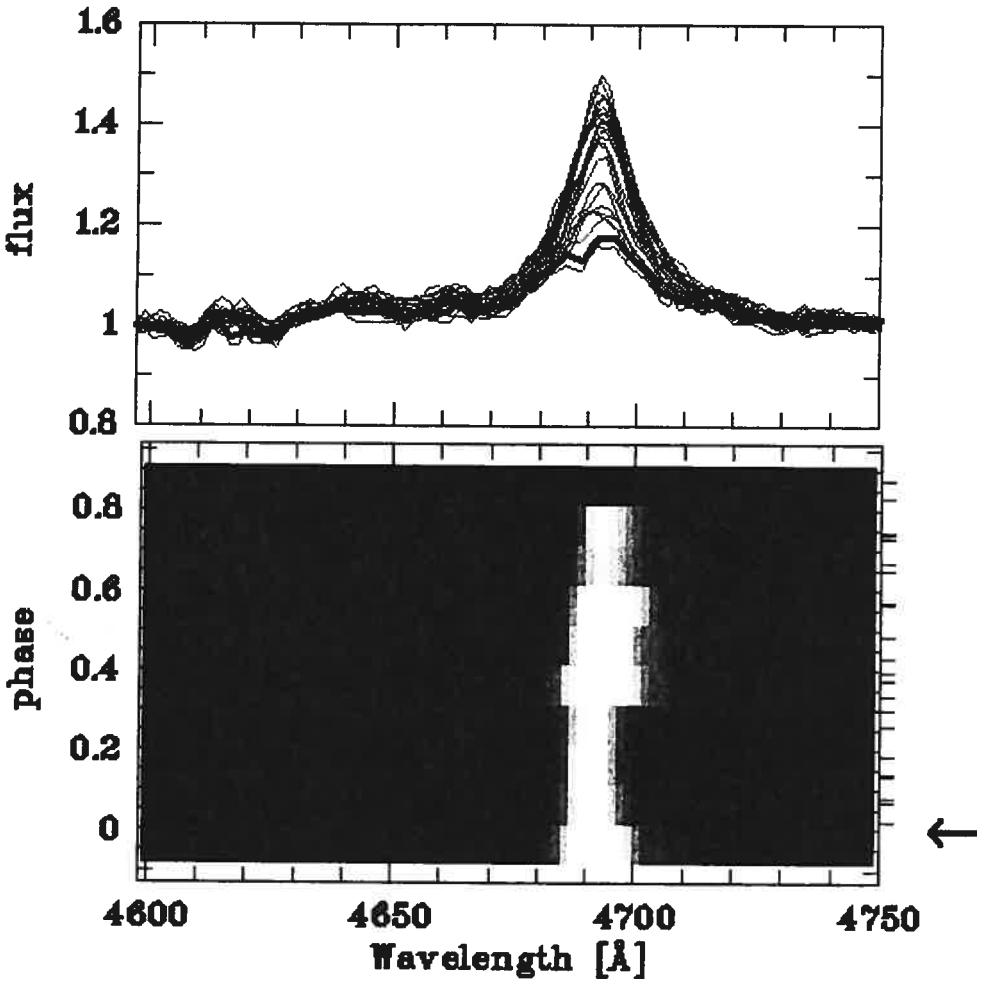

FIGURE 2.69 – Same as Figure 2.62, but for BAT99-113. As can be seen from the overplotted spectra (*upper panel*), the HeIIλ4686 emission line is highly variable. The WR star is in front at $\phi = 0$ (circular motion assumed), but the largest redshift of the excess emission occurs ~half a phase later, when the WR star is *behind* the O star (*lower panel*). This would mean that the invisible companion displays the stronger wind, which is unlikely. Possible error sources are once more the uncertain RVs, given the fact that HeIIλ4686 is visibly strongly affected by WWC.

Two Peculiar Cases: BAT99-116 and BAT99-118

Two program stars of our sample, BAT99-116 and BAT99-118, display line-strength variations as well (see Figure 2.70). These LPV result or at least coincide with significantly large RV scatter, $\sigma_{\rm RV}$, 33 kms^{-1} and 32 kms^{-1} (unweighted), respectively (compare to the cut-off value of 22.6 kms^{-1}). However, no periodicity was found in their RV curves (see above). Interestingly, Massey et al. (2002) report significant photometric variability for BAT99-116 (their star R136-08) over a time scale of $\sim$3 weeks. The line-strength variability we observed is indeed consistent with continuum variability through an eclipse. Both stars have in common that they are relatively well isolated, so that they are easy to acquire; hence, there are no obvious sources for variable light pollution that could account for the time-dependent dilution of the emission lines. We therefore suggest that these LPVs are real, and that they merit further investigation.

If both WR stars were members of an elliptical binary system, one would expect that the LPV is linked to the orbital separation, i.e. that the system suffers from much stronger WWC excess emissions around periastron passage than during the rest of the orbital phase, and the more so, the more eccentric the orbit is. In turn, periastron passage is linked to a swift change in RV, so that a spike in the RV curve should more or less coincide with a sudden increase in equivalent width (EW) of the emission lines most susceptible to WWC effects. We verified whether BAT99-116 and BAT99-118 displayed this kind of behaviour in Figures 2.71 and 2.72 by plotting the measured equivalent widths of the HeIIλ4686 emission lines together with the measured RVs *versus* the Julian dates. Unfortunately, however, for neither BAT99-116 nor for BAT99-118, could a coherent or coincident behaviour be observed. Thus, much better spectroscopic and photometric data are required in order to assess the binary status of these two stars.

2.5.9 Systemic Velocities and Runaway Stars

In order to compute the *systemic* velocities $\overline{RV}_{sys}$ of our program stars, we used RVs obtained through Gauss fits to the HeIIλ4686 emission line. For each program star, both weighted mean RVs and standard deviations were computed, using the same weights as des-

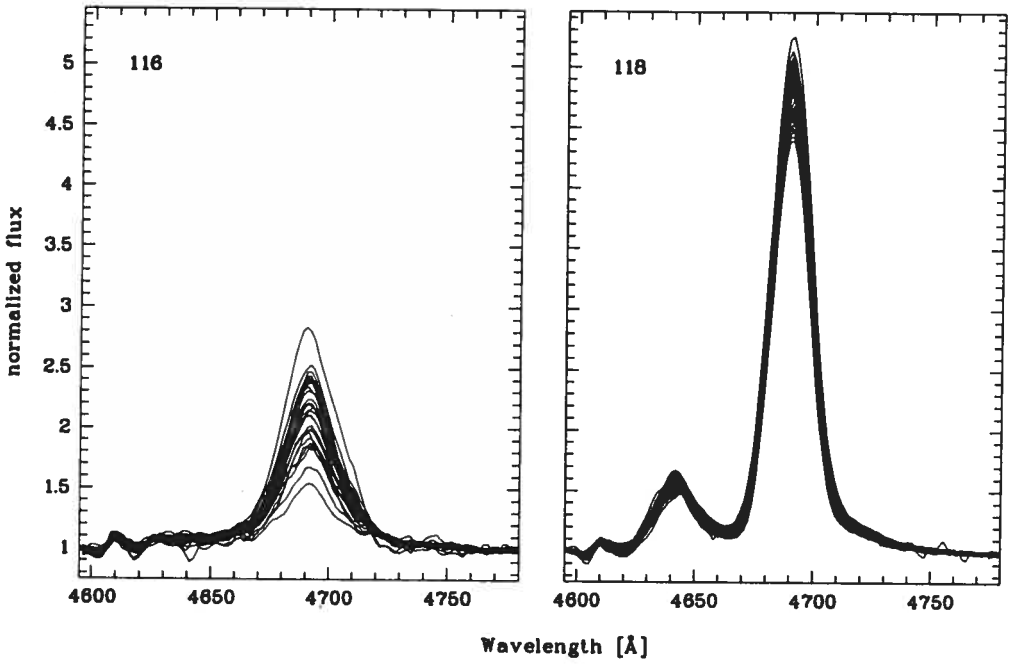

FIGURE 2.70 – Overplot of the HeIIλ4686 emission lines of the stars BAT99-116 (*left*) and BAT99-118 (*right panel*). One can clearly see the variability of the line strength, particularly strong in BAT99-116.

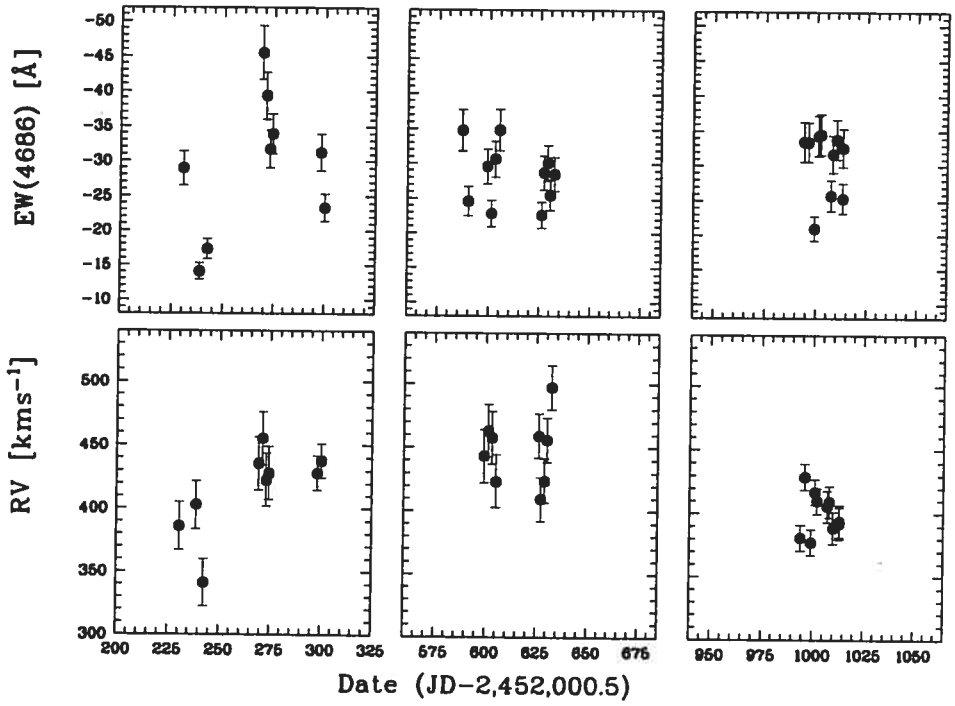

FIGURE 2.71 – Equivalent widths (*upper*) and RVs (*lower panel*) measured from HeIIλ4686 for BAT99-116. No obviously periodic or related behaviour is visible.

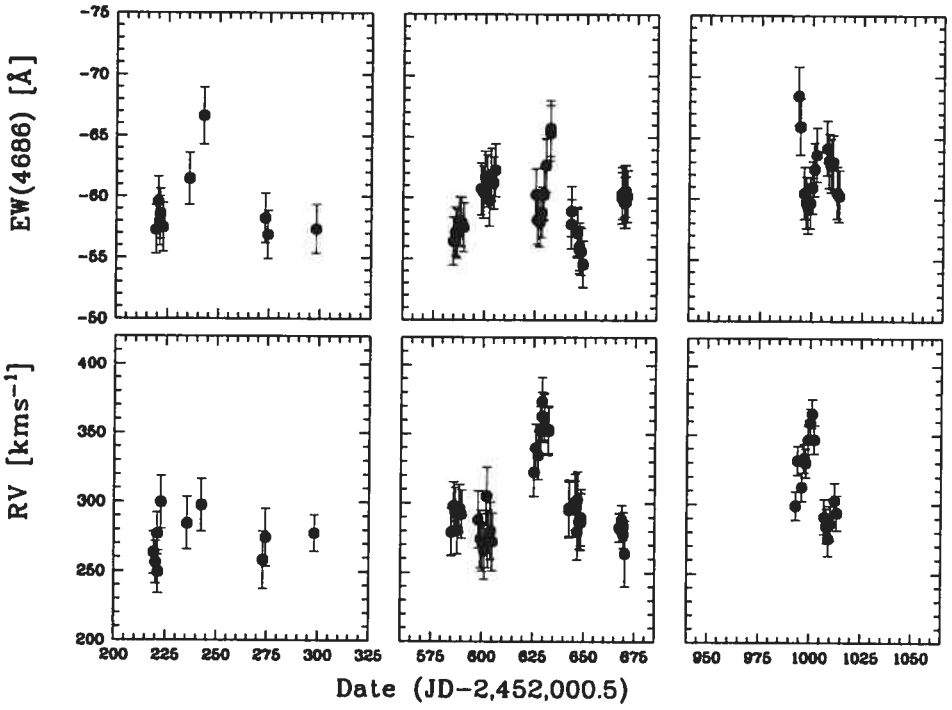

FIGURE 2.72 – As Figure 2.72, but for BAT99-118.

cribed above. For binary stars, the systemic velocities, γ, obtained from ELEMENTS by fitting the orbital solution to the weighted RV data points, were used. Resulting $\overline{RV}_{sys}$ are shown in histogram form in Figure 2.73.

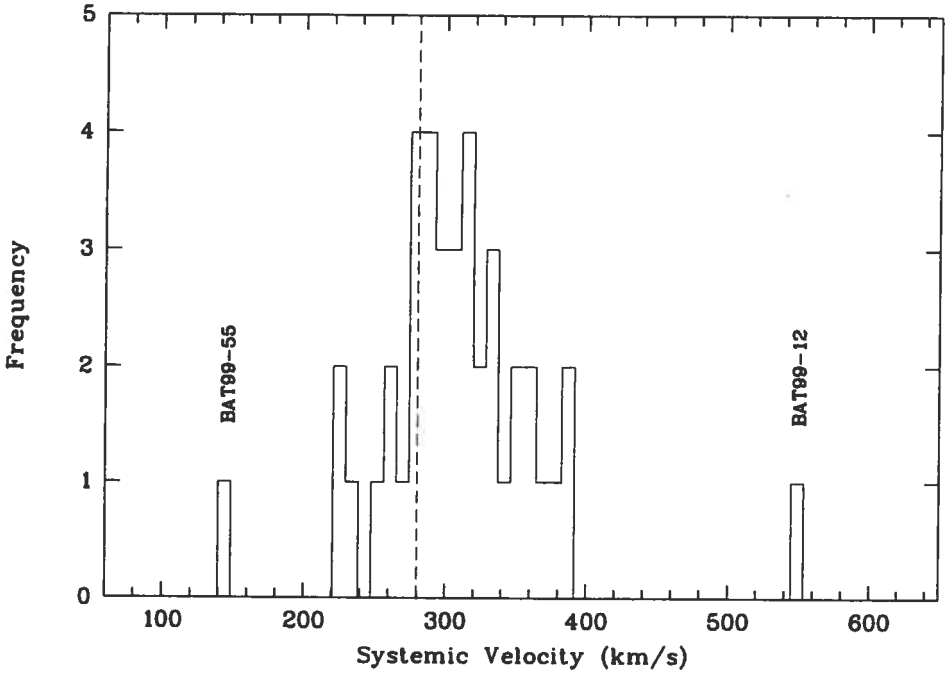

FIGURE 2.73 – Histogram of mean systemic velocities of our program stars as measured by Gauss fits to the HeIIλ4686 emission line. The dashed vertical line indicates the expected systemic velocity of the LMC, 280 kms^{-1}. Note the two outliers, BAT99-12 and BAT99-55; these are most likely runaway stars. See text for more details.

Two interesting cases, BAT99-55, a constant star, and BAT99-12, a periodic RV variable star, are marked in Figure 2.73 with their names. These stars have systemic velocities which are quite different from the systemic velocity of the LMC, 146 kms^{-1} (BAT99-55) and 650 kms^{-1} (BAT99-12; circular orbit assumed), respectively. Thus, these stars are excellent runaway candidates (for a definition of runaway stars, see Blauuw 1961). Moreover, Massey et al. (2005) report a systemic velocity of 430 kms^{-1} for BAT99-12, obtained from absoption lines in their better-resolved spectra, confirming its high systemic velocity; our much larger velocity

is most likely an artefact due to the mentioned P Cygni absorption in the blue flank of the HeIIλ4686 emission line. The runaway nature is another property that BAT99-12 shares with its Galactic counterpart, the O4Inf star ζ Pup.

On average, we expected our stars to reflect the systemic velocity of the LMC, which is 280 ± 20 kms^{-1} (e.g. Kim et al. 1998). The measured mean of the weighted systemic velocities of our program stars is 314 ± 10 kms^{-1} (error of the mean, $eom = \sigma_{\rm RV}/\sqrt{N}$), i.e. higher than the expected value but still consistent with it, if one adopts the $3eom$ confidence level. Our mean velocity is also consistent with the value that Foellmi et al. (2003b) reported for their WNE stars, $\overline{RV}_{\rm sys} = 324 \pm 6$ kms^{-1}. However, we have re-examined the Foellmi et al. (2003b) data (see below), and measured a significantly larger average systemic velocity for the WNE stars, 345 ± 6 kms^{-1}, which is neither consistent with the WNL measurement nor with the expected LMC value of 280 kms^{-1}. The origin of this difference is not known, but it is not impossible that different zero-point wavelengths λ_0 were used for the HeIIλ4686 line; throughout this paper, we used $\lambda_0 = 4685.682$ Å. In order to compare the measurements, we have used our values for both the WNE and WNL stars in the following discussion.

If the two suspected runaway stars, BAT99-12 and 55 (see below), are excluded from our WNL sample, the mean systemic velocity changes only slightly to 312 ± 7 kms^{-1}, compared to 300 ± 9 kms^{-1} if the 9 binaries in our sample are omitted. Leaving out both the binaries and the runaways (BAT99-12 belongs to both groups) results in an average systemic velocity of 305 ± 7 kms^{-1}. Although these values are consistent with the expected value, they are systematically higher than the systemic velocity of the LMC. Leaving out the binaries from the WNE sample yields a slightly higher mean systemic velocity, 353 ± 6 kms^{-1}. Taking the average of the whole WN population (i.e. WNE+WNL), we obtain an overall mean systemic velocity of 334 ± 5 kms^{-1}. Without the binaries, the value changes to 338 ± 5 kms^{-1}, which clearly shows that binaries do not significantly affect the overall velocity of a WR population as long as repeated spectroscopy is obtained to insure good phase coverage; furthermore, runways are rare enough that their very large deviations from the mean velocity are reliably

diluted by the bulk of the given population.

That WR stars display systematically red-shifted, systemic velocities that are obtained from their emission lines, is well known, and has also been reported by e.g. Bartzakos et al. (2001; for WC stars) and by e.g. Foellmi et al. (2003a,b; for WNE stars). Both studies attributed this phenomenon to the fact that WR emission lines contain a non-negligible P-Cygni absorption component. This absorption is more or less blue-shifted with respect to the center of the emission line, thereby diminishing the blue flank of the latter so that the resulting composite line profile peaks at red-shifted wavelengths with respect to the emission-line center (see Figure 8 in Bartzakos et al. 2001). It was theorized that narrow emission lines (i.e. from optically thin winds) are particularly sensitive to this effect, while broad emission lines (i.e. from dense winds) are supposed to better reflect the true systemic velocity; indeed, both Foellmi et al. (2003b; Figure 8) and Bartzakos et al. (2001; Figure 8) reported a negative correlation between the line width (FWHM) and the measured systemic velocities, showing that broader lines better reflected the true systemic (i.e. LMC) velocity. However, neither did we detect an asymmetry in the emission-line profile that one can expect to find if the blue flank was indeed strongly diminshed, nor did we find this relation in our narrow-lined WNL stars. To the contrary, from very symmetric lines we found a *positive* correlation between the linewidth and the measured systemic velocities. Surprised by these findings, we re-examined the LMC WNE data of Foellmi et al. (2003b) and combined their data with ours; the combined data are shown in Figure 2.74.

Indeed it seems that *only* the most narrow-lined WNL stars do correctly reflect the systemic velocity of the LMC, whereas broader-lined stars *on average* yield redder systemic velocities. In order to verify this perception statistically, we have binned stars to certain FWHM ranges, and calculated the bin mean systemic velocity and its error. The results are listed in Table 2.16.

The first FWHM bin (from 0 to 500 kms^{-1}) comprises the very narrow WN9-11 stars (see

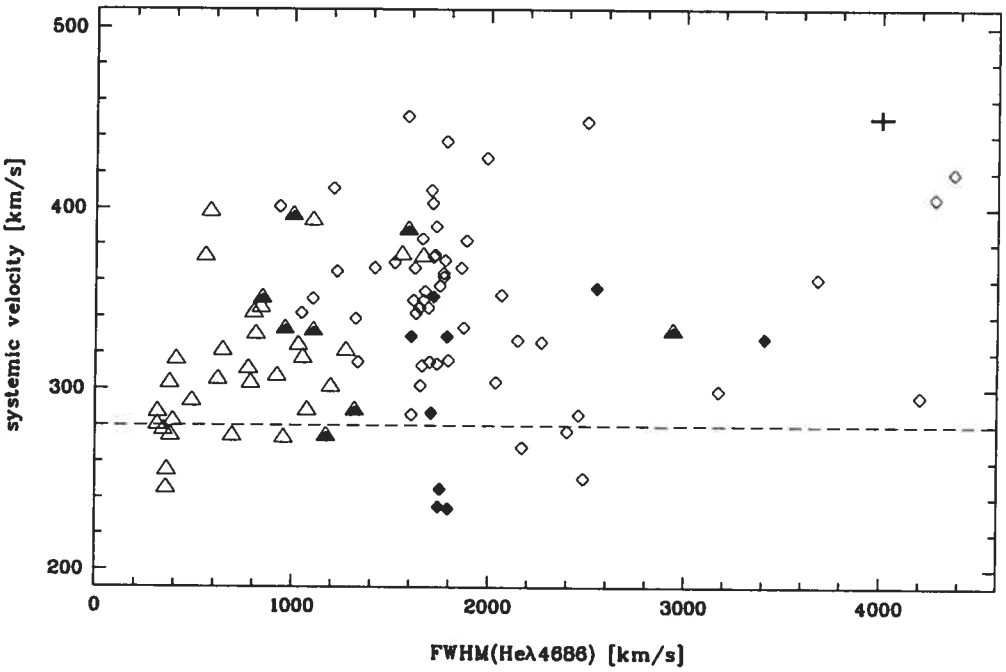

FIGURE 2.74 – Mean systemic velocities plotted against the FWHM (in velocity units) of HeIIλ4686 emission line. Triangles denote our 41 WNL stars, lozenges denote the 61 WNE stars studied by Foellmi et al. (2003b). Filled symbols are identified binaries. The dashed line indicates the systemic velocity of the LMC ($\sim$280 kms^{-1}). For clarity, error crosses have been omitted, but a typical error cross ($\pm eom = \sigma/\sqrt{N}$) is shown in the upper right-hand corner. Most stars have larger systemic velocities than the LMC, and the star-to-star scatter is significant. Note that the two runaway candidates, BAT99-12 and 55, have been omitted for this graph so that the y axis is not unduly compressed. See text for more details.

Section 2.5.10) which reflect the true systemic velocity of the LMC with both a remarkable accuracy and a small scatter. However, as soon as the lines become slightly larger, the measured mean systemic velocities are significantly shifted to the red, and the scatter becomes larger, up to more than twice the value for narrow-lined WNL stars. Note that contrary to what Foellmi et al. (2003b) reported, the measured systemic velocities do not seem to converge again towards the true LMC value; rather the systematic redshift remains essentially constant at $\sim$ 55 kms^{-1} for all FWHM ranges above 500 kms^{-1}.

Obviously, the details of this behaviour are very intricate, since they depend on the phy-

TABLE 2.16 – Mean systemic velocities of stars binned into different FWHM ranges. N is the number of stars per FWHM bin, $\overline{RV}$ the mean systemic velocity, σ the RV scatter, and $eom = \sigma/\sqrt{N}$ the error of the mean systemic velocity in the respective bin.

FWHM [kms^{-1}]	0-500	500-1000	1000-1500	1500-2000	2000+
N	10	16	16	40	17
$\overline{RV}$ [kms^{-1}]	281	335	333	335	332
σ [kms^{-1}]	21	41	38	49	55
eom [kms^{-1}]	6.6	10.3	9.5	7.7	13.3

sical properties of the wind (velocity and opacity structure of the wind, position of both the line-forming and the absorbing region in the wind, etc.). The observed effect, however, is real, since it has been found in several independent data sets, e.g. also in that of Crowther & Smith (1997; and private communication). Thus, the main conclusion that can be drawn here is that, despite their broad lines and thus contrary to what one might have expected from Bartzakos et al.'s (2001) and Foellmi et al's (2003b) findings, broader-lined WNE stars are *not* better tracers for the systemic velocity of their host environment than narrow-lined WNL stars; as a matter of fact, one should rely on *only* very narrow-lined WNL (i.e. WN9-11) stars if a high degree of accuracy is desired. This is particularly true given the surprisingly small RV scatter that such stars display. Moreover, the mechanism orginally proposed by Bartzakos et al. (2001) to explain this effect should lead to a strong line asymmetry, which, at least in HeIIλ4686, is not generally observed; this in turn casts considerable doubt on Bartzakos et al.'s scenario.

The observed lack of line asymmetry also rules out another possible explanation for the redshifted emission lines, namely that electron-scattering wings greatly affect the red flank of emission lines (e.g. Auer & van Blerkom 1972), leading to an effectively redshifted, total profile even in absence of a P-Cygni absorption component. However, such strong electron-scattering wings are never observed – emission lines *are* relatively symmetric after all –, and thus the effect remains negligible. Hence, we presently have no viable explanation for the measured redshifts in HeIIλ4686 to offer.

2.5.10 Mean Spectra and Spectral Re-Classification

Given our large and very homogeneous spectroscopic data set, we proceeded to verify the spectral types of most of our program stars, the exception being the Ofpe/WN9 or "cool slash-stars"; most of them have already been re-classified into WN10-11 by Crowther & Smith (1997). Thus, only the WN5-9 stars were considered. The classification criteria of Smith et al. (1996; hereafter SSM96) were applied, so that our way of assigning spectral types is consistent with Foellmi et al. (2003a,b), and direct comparisons can be made.

Remarkably, all O3If/WN6 or "hot slash-stars" (Walborn 1986) were re-classified as WN5-7 *solely based on the relative strength of their emission lines*; we feel that the WN spectral class is more appropriate because the strongest emission lines were always stronger than the strongest absorption lines. Note, however, that for some of these stars, Massey et al. (2004, 2005) proposed the O2If classification, applying the critera of Walborn et al. (2002). At this point it becomes evident that the borderline between the most extreme Of stars and the least extreme WN stars is too fuzzy, and too often depends on the personal opinion of the classifying person rather than on objective and blindly applicable criteria. We therefore recommend that efforts be undertaken to homogenize the hot end of the MK classification, and that mass-loss, which renders those stars WN-like, be taken into account more systematically.

Spectral classification was carried out using averaged and thus fairly high-S/N spectra. This method to obtain a mean spectrum is closely related to that described above regarding the construction of a "supertemplate" for cross-correlation. Individual spectra were shifted into the reference frame of the template by the RV obtained from CC. Then, a S/N-weighted mean was computed. This had to be carried out individually per observatory, since each observatory does not cover the same spectral range. The observatory mean spectra were then concatenated to obtain an average spectrum covering the full spectral domain. Of course, the region in common, i.e. from 4000 to 5000 Å, has the highest S/N. A montage of the (re-)classified, mean spectra of each one of our program stars is given in Figures 2.75 to 2.81. Note that for stars in 30 Dor, no sky subtraction was performed (see Section 2.4); rather,

nebular lines were simply clipped in the final spectra. Thus, in some spectra, the Hβ and Hγ lines appear truncated, because the nebular contribution was clipped.

Since our program stars encompass all WNL types, many of them still contain residual hydrogen. Some of them are even expected to be still in the CHB phase. Depending on the H content, WN stars are further classified into the subgroups WNha (H in emission and absorption), WNh (H emission present), WN(h) (H emission weakly present, and WNo (for "zero"; H not visible, but may be present), according to SSM96. Broad-lined WN stars obtain the suffix "b". It has been shown by Smith & Maeder (1998) that the suffix "b" strongly correlates with the total absence of H in the star, i.e. that WNb stars are the truly H-depleted (and thus, CHeB) WN stars.

The main indicator for the presence of H in the WR spectrum is the alternating HeII Pickering decrement. However, some stars, in particular those in the 30 Dor region, have spectra too polluted by nebular emissions (see Section 2.4), so that hydrogen lines are severely compromised. In those cases, the alternating Pickering decrement of helium lines also suffers considerably, and the determination of the H content remained (very) uncertain; such subtypes feature a ":" (or even "::") to indicate this uncertainty. If not stated otherwise, nebular lines did not hamper the spectral classification.

— **BAT99-12**: Listed as O3If*/WN6-A in the BAT99 catalogue, we reclassify this star as WN5ha from its emission-line spectrum, because the emission lines are stronger than the absorption lines; thus, a WR classification applies. There seems to be a distinct emission feature at $\lambda \sim$4650 Å which could either be a real emission line due to CIII or the blue emission edge of a P Cygni profile with nearly central absorption. Given the variability of the line (cf that of ζ Pup; Moffat & Michaud 1981), we favor the second possibility.

— **BAT99-13**: WN10. Not reclassified.

— **BAT99-16**: This star is listed as WN8h in BAT99; however, we reclassify it as WN7h.

— **BAT99-22**: This star is listed as WN9h. We confirm this classification.

— **BAT99-30**: Both BAT99 and SSM96 classify this star as WN6h. We concur.

— **BAT99-32**: This star is listed as WN6(h), whereas SSM96 classified this as WN6(h)+abs?. It has very strong emission lines; we find WN6(h).

— **BAT99-33**: This star is listed as Ofpe/WN9. There are very weak nebular lines, but the hydrogen dominates over HeII. We change the spectral type to WN8ha.

— **BAT99-44**: This star is listed as WN8h. Because of subtle, yet visible, blue-shifted absorption components in the Balmer lines, we assign WN8ha.

— **BAT99-45**: WN10h. Not reclassified, but it looks very much like BAT99-13; however we note that He3-519 in Walborn & Fitzpatrick (2000) closely resembles BAT99-45, but is clasified as WN11h.

— **BAT99-54**: This star is listed as WN9h. We classify it as WN8ha, with very clear, blue-shifted absorption components in the Balmer lines.

— **BAT99-55**: WN11h. Not reclassified.

— **BAT99-58**: Both BAT99 and SSM96 assign WN6h. It has strong, narrow emission lines. We find WN7h.

— **BAT99-68**: This star is listed as WN5-6, while SSM96 find Of. We find WN7ha:. It has only relatively weak emission lines, which might come from the heavy crowding (dilution).

For the same reasons, "a" is uncertain. A CIIIλ4650 emission feature is present.

— **BAT99-76**: This star is listed as WN9h. Because of blue-shifted absorption components in the Balmer lines, we reclassify it to WN9ha.

— **BAT99-77**: This star is listed as WN7. We find WN7ha; although this star is heavily crowded, absorptions in the lower Balmer lines *are* blue-shifted and not just superimposed from an OB companion, hence the "a".

— **BAT99-79**: This star is listed as WN7h+OB. We confirm this, and find central absorption features superimposed on the Balmer emission lines which might come from imperfect (over)subtraction of nebular emission lines.

— **BAT99-80**: This star is listed as O4If/WN6. While there are no nebular lines, the star is crowded. There is no clear feature at λ ~4650 Å. We classify it as WN5ha:. Because of heavy crowding, the "a" feature is uncertain.

— **BAT99-83**: This ex-LBV R127 is listed as Ofpe/WN9 in the BAT99 catalogue. However, it now is much cooler than WN9; the spectrum resembles the spectrum of η Car (Walborn & Fitzpatrick 2000), and contains many forbidden iron lines.

— **BAT99-89**: This star is listed as WN7h. We concur.

— **BAT99-91**: This star is listed as WN7. We reclassify it as WN6h:a:. There are weak nebular lines, which render "h" uncertain; furthermore, the star is heavily crowded, which renders the "a" feature uncertain.

— **BAT99-92**: This star is listed as WN6, as quoted from Moffat & Seggewiss (1986). However, a closer inspection of the spectrum reveals that the dip at λ ~4650 Å is strong

and probably a photospheric absorption line of the B1Ia component. I.e., NIII is not seen; rather HeIIλ4686 is very broad, like HeIIλ5411. Hence, BAT99-92 is hotter, although very difficult to determine because of the dominating B supergiant spectrum. We tentatively assign a WN3:b(+O)+B1Ia type to this system. The presence of the narrow emission component in Hβ has three possible origins: *i*) nebular, *ii*) emission from the B1Ia star, or *iii*) wind-wind collision (WWC) excess. A narrow emission does not fit coming from the WN star, because the latter has broad lines, and "b" and "h" are incompatible (Smith & Maeder 1998). Conclusion: it is not a WNL but a WNE star.

— **BAT99-93**: This star is listed as O3If/WN6. The star shows a hint of the CIIIλ4650 emission feature. Relatively weak and narrow emission lines make for WN6h:a. There are moderate nebular emissions.

— **BAT99-95**: This star is listed as WN7h. It has very strong emission lines, and we find WN7. Strong nebular lines prevent determination of the H content.

— **BAT99-96**: This star is listed as WN8h. We confirm WN8, but the strong nebular lines render the determination of H impossible.

— **BAT99-97**: This star is listed as O3If/WN7-A. We reclassify it as WN7h::a, while the H content remains very uncertain because of strong nebular lines and the Pickering lines clearly show slightly blue-shifted absorption components. The star also weakly shows the CIIIλ4650 emission feature.

— **BAT99-98**: This star is listed as WN6(h). It has very strong emission lines; however, because of the very strong nebular lines, we cannot determine the H content. Here, we have just WN6.

— **BAT99-99**: This star is listed as O3If/WN6. From the emission-line spectrum, we

derive WN5h:a (but see Massey et al. 2005), where the H content is uncertain because of strong nebular lines. The star is very similar to other hot "slash stars", including the peak at $\lambda \sim$4650 Å.

— **BAT99-100**: This star is listed as WN6h. We find WN7. There are strong nebular lines, making the H content impossible to determine.

— **BAT99-102**: This star is listed as WN6+O. We find WN6. There are very strong nebular lines. This star is more contaminated by the neighboring WC star than BAT99-103; the broad base of HeIIλ4686 stems from the CIIIλ4650 complex originating in the WC star.

— **BAT99-103**: This star is listed as WN6, which we confirm. The spectrum is less contaminated by the WC star (BAT99-101) than BAT99-102. Again, there are very strong nebular lines.

— **BAT99-104**: This star is listed as O3If/WN6. From the emission line spectrum, which is stronger than the absorption spectrum, we find WN7. Because of the relatively strong nebular lines, we are unable to determine the H content. The star shows the CIIIλ4650 emission feature.

— **BAT99-105**: This star is listed as O3If/WN6-A. However, it looks more like a genuine WR star. From the emission-line spectrum, we reclassify it as WN7. It has strong nebular lines.

— **BAT99-107**: This star is listed as WNL/Of. We reclassify it to WN9h::a, where because of the strong nebular lines, the H content is very uncertain. Blue-shifted absorptions in the pure Pickering lines indicate "a".

— **BAT99-113**: This star is listed as O3If/WN6. Strong emission lines make for a very uncertain hydrogen content, although pure Pickering lines are weaker than the H-inflicted

Balmer-Pickering blends, which indicates the presence of H. We reclassified it as WN5h::a, i.e. absorption lines are intrinsic to the WN star. This star also shows a CIIIλ4650 emission feature.

— **BAT99-114**: This star is listed as O3If/WN6. It is somewhat crowded and shows fairly strong nebular lines. From the emission line spectrum, we assign the new spectral type of WN5h:a. Same comments as for BAT99-116 (next entry) apply. BAT99-114 also shows an emission peak at 4650 Å (see BAT99-12).

— **BAT99-116**: SSM96 classified this star as WN5o, compared to BAT99, where the star is WN5h. Very strong nebular emission lines prevent a detailed analysis, but we tentatively assign WN5h:a to this star. The presence of H has been derived from the fact that the Balmer lines have broad bases with the very much narrower nebular emission lines superimposed. These bases are stronger than in the case of the pure Pickering lines. Thus, from the alternating Pickering decrement, the presence of H is deduced. The "a" comes from the blue-shifted absorption lines superimposed on the HeII Pickering lines ($\lambda\lambda$5411, 4542, 4200). This star does *not* show the CIIIλ4650 feature!

— **BAT99-118**: This star is listed as WN6h. We find WN6h, too, with a clear H content.

— **BAT99-119**: This star is listed as WN6(h). The star has strong emission lines; we find WN6h from the Pickering decrement, but it just makes it to h.

— **BAT99-120**: This star is listed as WN9h. Since the H is obvious, we concur.

— **BAT99-130**: WN11h. Not reclassified.

— **BAT99-133**: WN11h. Not reclassified.

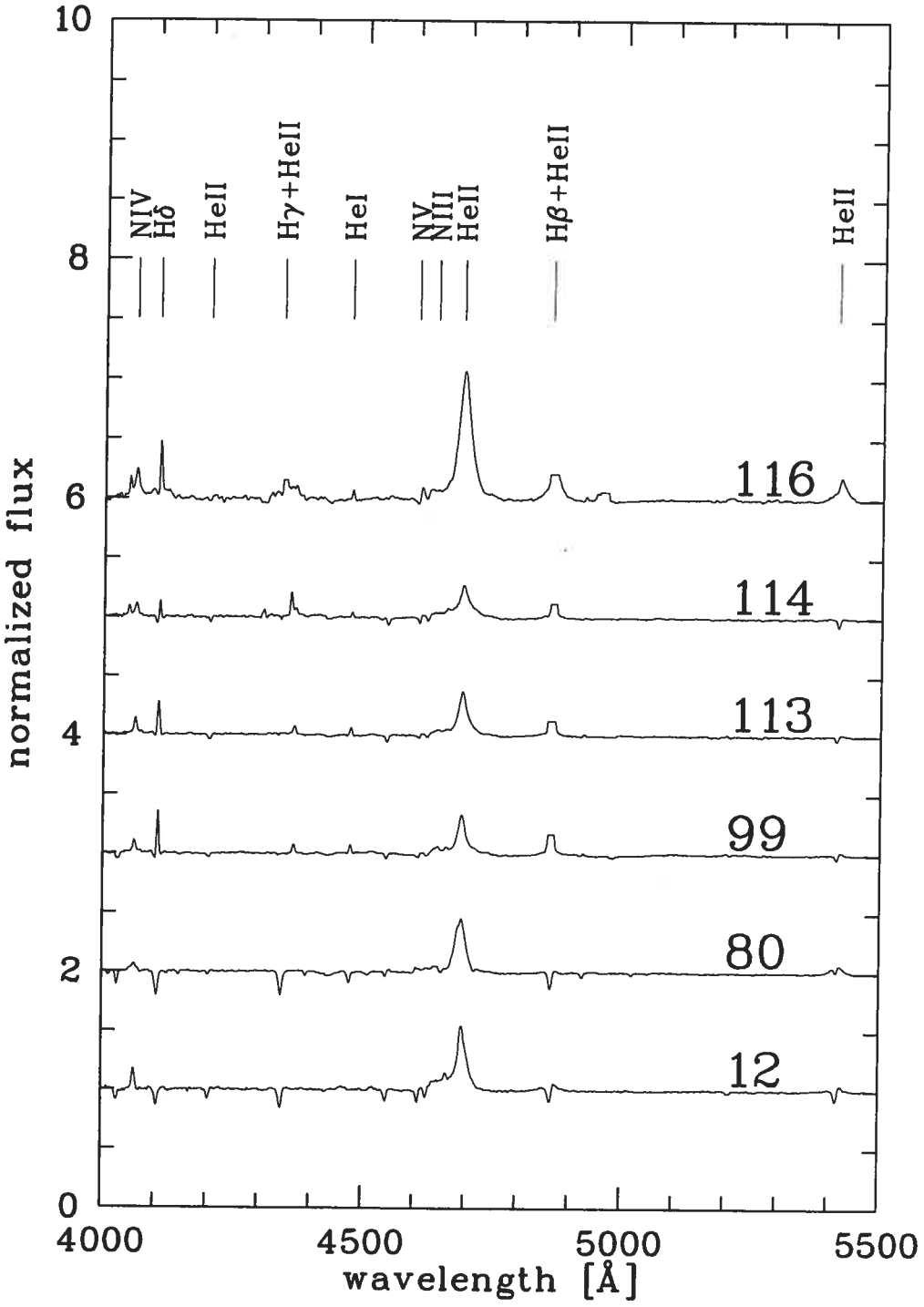

FIGURE 2.75 – Montage of mean spectra for all WN5 stars in our sample in order of BAT99 number. For clarity, each spectrum except the bottom one has been shifted in flux (units are given on the y-axis).

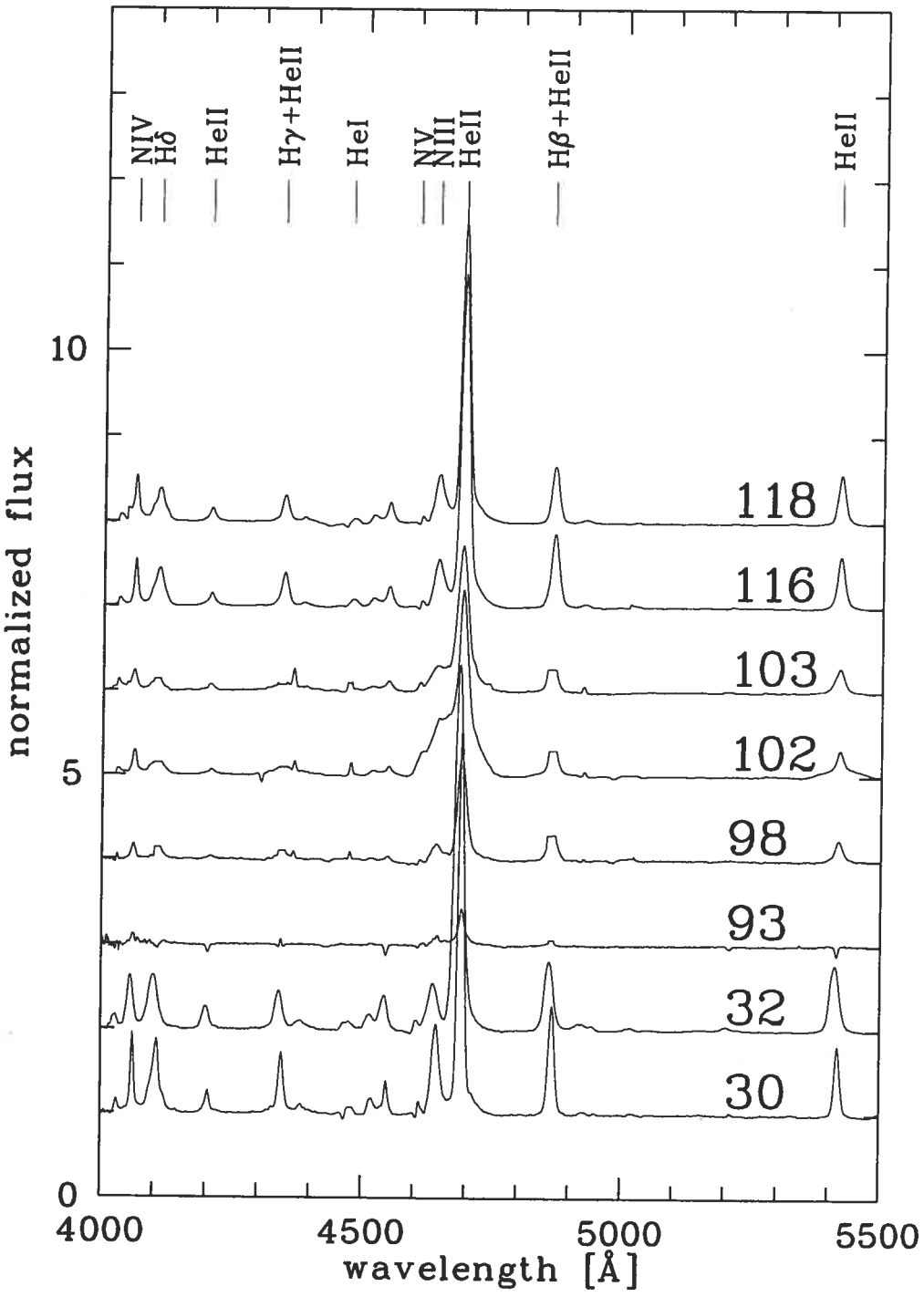

FIGURE 2.76 – Same as Figure 2.75, but for the WN6 stars in our sample.

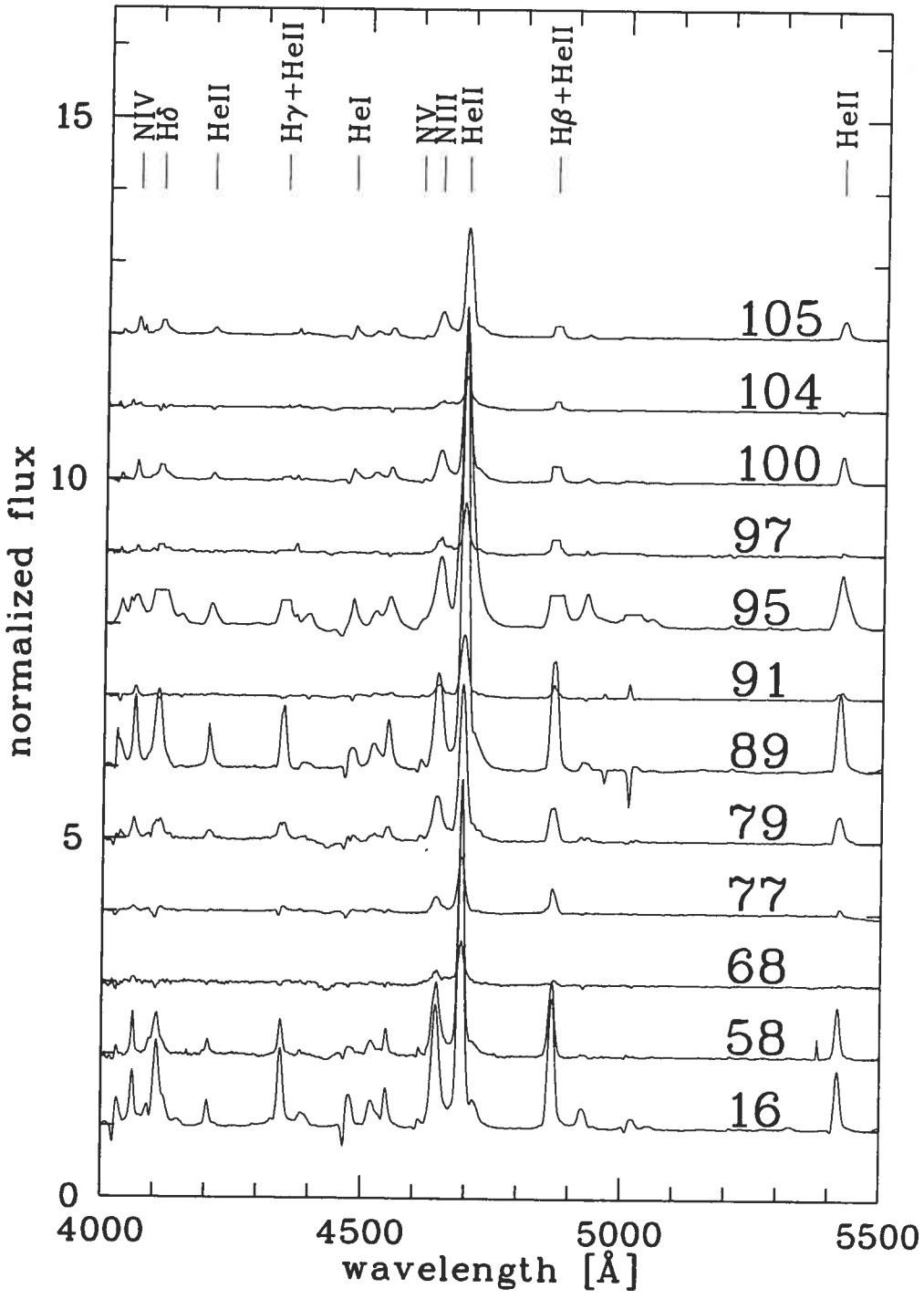

FIGURE 2.77 – Same as Figure 2.75, but for the WN7 stars in our sample.

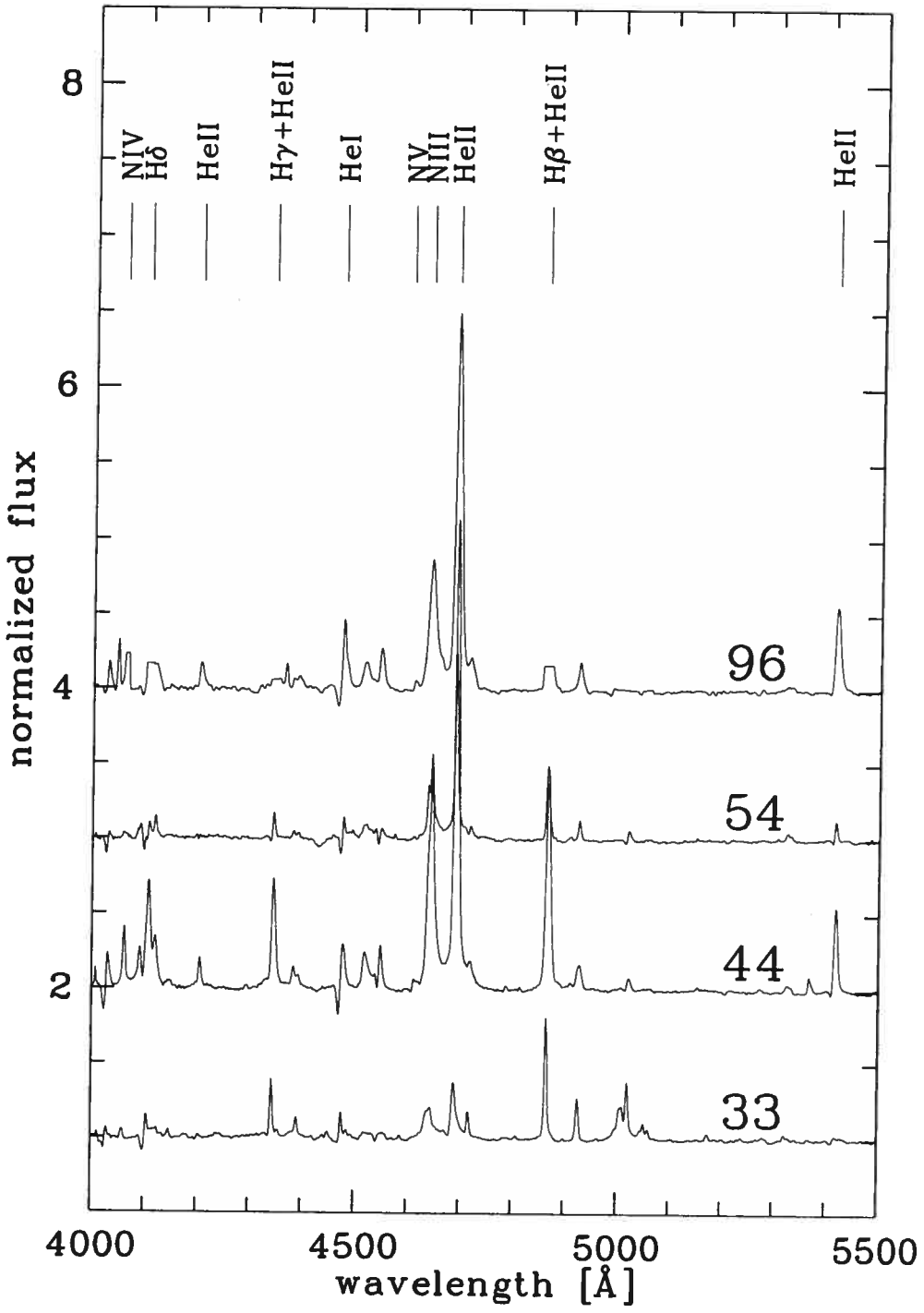

FIGURE 2.78 – Same as Figure 2.75, but for the WN8 stars in our sample.

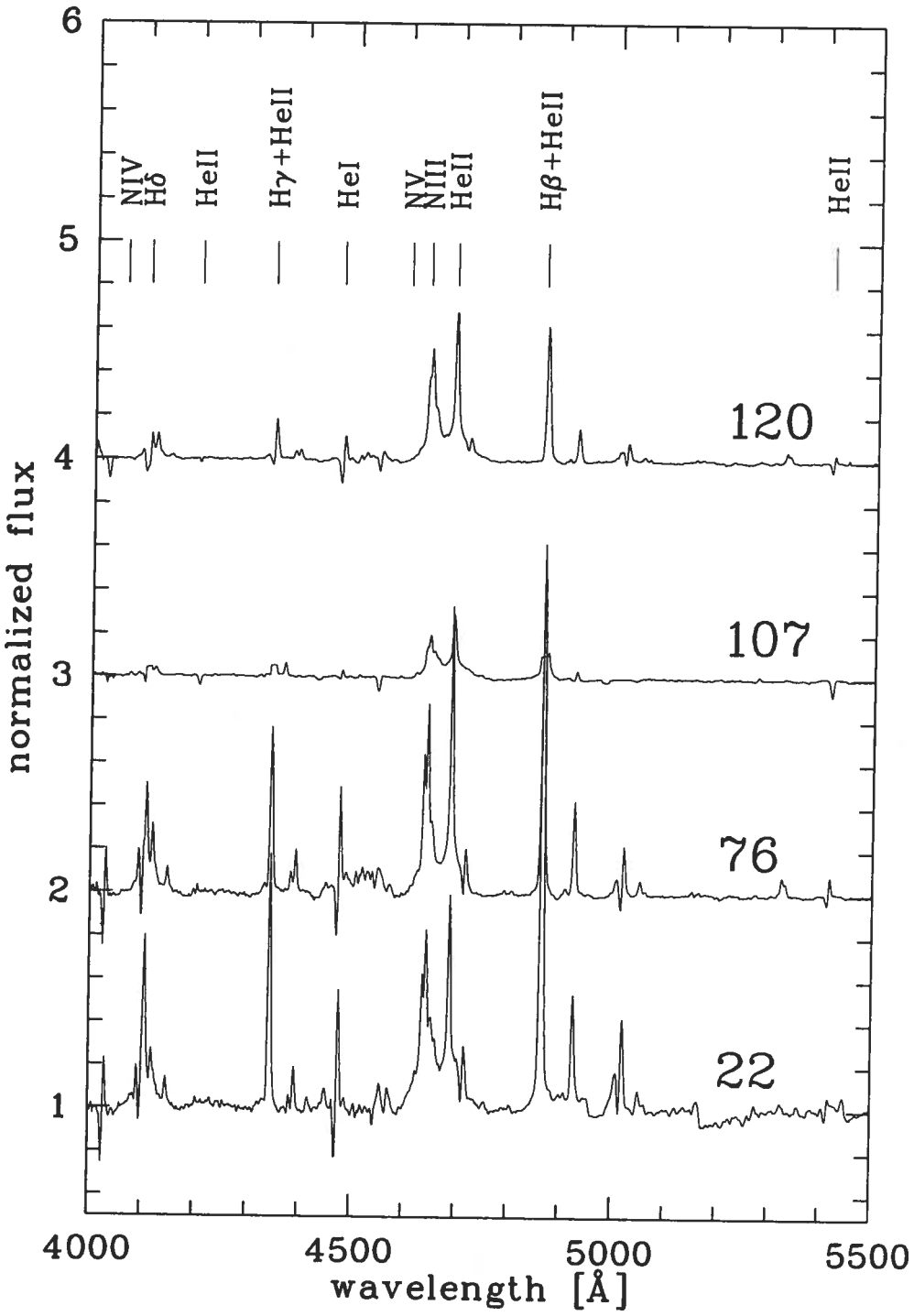

FIGURE 2.79 – Same as Figure 2.75, but for the WN9 stars in our sample.

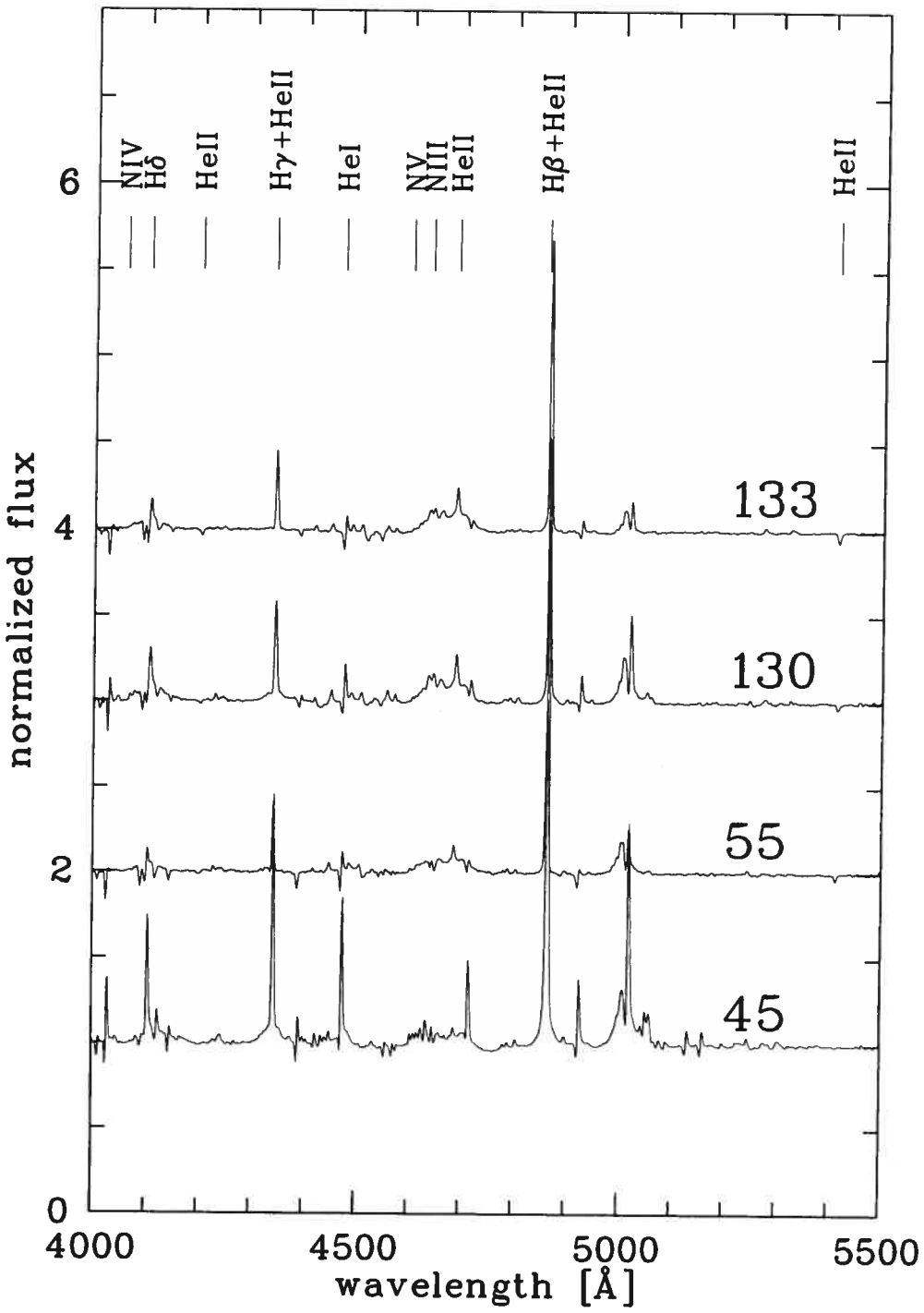

FIGURE 2.80 – Same as Figure 2.75, but for the WN11 stars in our sample.

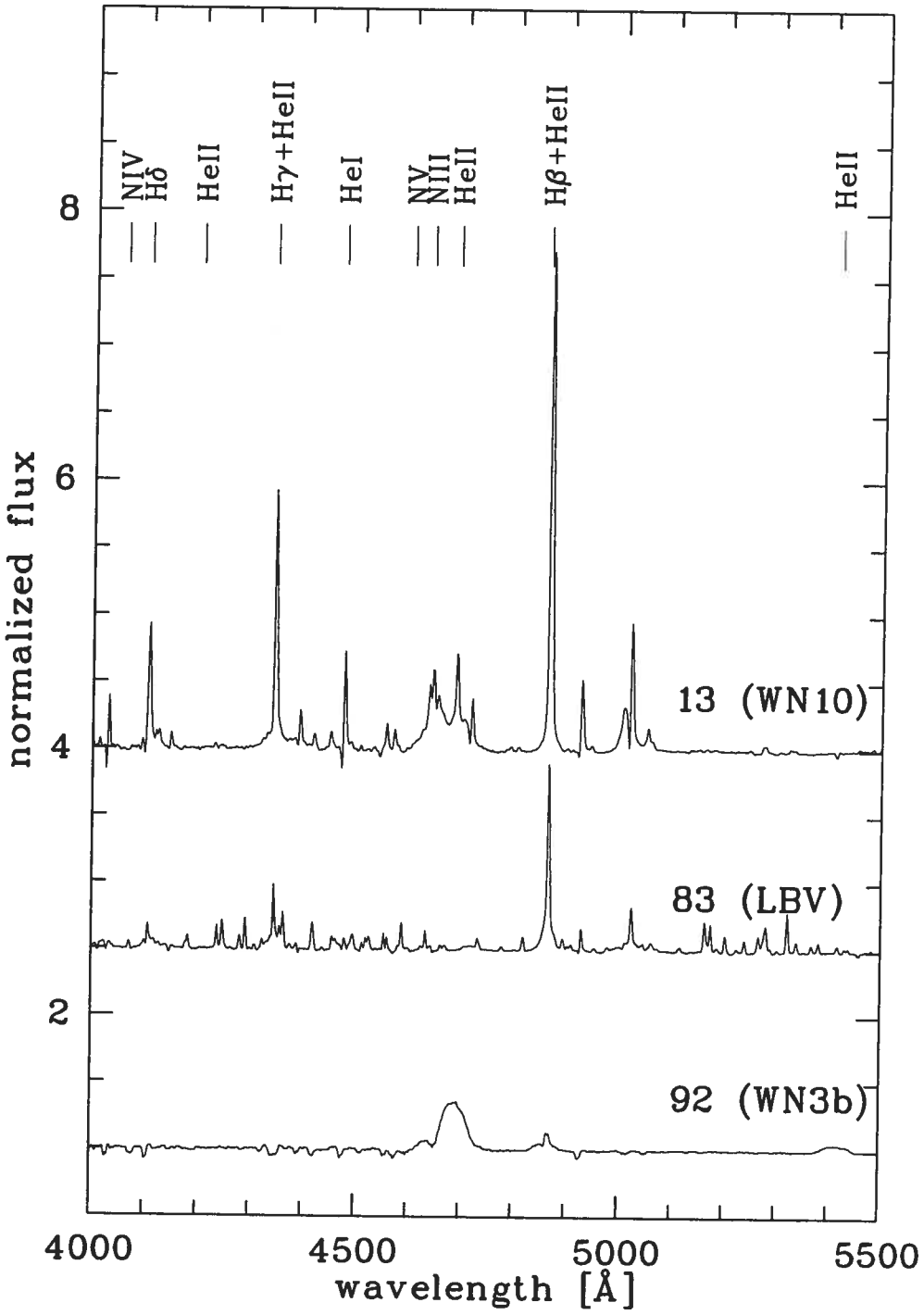

FIGURE 2.81 – Same as Figure 2.75, but, *from bottom to top*, for the stars BAT99-92 (WN3b), BAT99-83 (R127, LBV), and BAT99-13 (WN10).

2.5.11 Analysis of the Photometric Data

MACHO photometry is available for eight of our program stars, two of which are binaries (BAT99-12 and 32). While the quoted measurement error of the individual data points is very small (a few thousandths of a magnitude), it can clearly be seen that the lightcurves are much noisier than that. Typical standard deviations range from a few hundredths to a few tenths of a magnitude in the worst cases. Furthermore, the very brightness of our stars – the general reason why photometry of only a few of our interesting objects was extracted from the MACHO observations (D. Welch 2003, private communication) – might easily push CCDs into their non-linearity regime. Crowding is another serious problem for the extraction of clean photometry from CCD images.

As in the case of our RVs, we applied a very soft, $\pm 3\sigma$ clipping to the photometric data. Unweighted, average b and r magnitudes were calculated and adjusted to simply match the v band magnitudes published by BAT99. Thus, no colour correction $(b-r)$ was applied. Routinely, a search for sinusoidal variations using our Scargle/CLEAN algorithm from 1 to 200 days was carried out, without any success. Two stars, BAT99-54 and BAT99-76, seem to show a structured light curve on scales of a tenth of a magnitude over several hundred days (see Figures 2.86 and 2.88). We therefore repeated our search for sinusoidal variations in the range from 200 to 2000 days, but were unable to pick up any periodic signal. BAT99-76 is a WN9ha star, and its classification remains unchanged, but BAT99-54, which was listed by BAT99 as WN9h, too, has been reclassified by us as WN8ha. BAT99-54's variability therefore does not entirely come as a surprise, since WN8 stars are known to be the most variable WR type (Marchenko et al. 1998); however, it is notoriously difficult to identify stable periods in these stars. However, given the generally poor quality of the data, we did not attempt further analyses. In Table 2.17, we list the standard deviations σ_b and σ_r obtained in the respective bands.

To the best of our knowledge, no repeated photometry has been previously published for BAT99-12. Remarkably, the data of this star show no cyclical variability, nor are there eclipse-like variations over the orbital phase. The phased data points are shown in Figure 2.82. If the

TABLE 2.17 – Photometric variability of program stars for which MACHO b and r band data could be retrieved. Standard deviations after 3σ-clipping are given. See text for details.

BAT99	σ_b [mag]	σ_r [mag]	Comments
12	0.048	0.125	binary
16	0.290	0.290	
30	0.235	0.085	
32	0.490	0.022	binary
54	0.033	0.038	
55	0.552	0.438	
76	0.246	0.043	
79	0.064	0.087	

star displays any kind of periodic light variations, much better data are required to find them.

For BAT99-32, Seggewiss et al. (1991) published Walraven V and Johnson B photometry. They found in their lightcurves that BAT99-32 shows two, $\sim$ 0.04 mag deep eclipses (their Figure 3a). Our MACHO photometry for BAT99-32 (Figure 2.83) has $\sigma_b \sim 0.49$ mag and $\sigma_r \sim 0.022$ mag in the blue and red band, respectively. While the blue band is obviously useless, we should in principle be able to see the eclipses in the red band, given the fact that we are folding with the period and thereby effectively increasing the S/N of the data. Yet, we see no such event in the phased r band data. BAT99-32's magnitude is $v = 12.72$ mag, which is relatively bright even by the standards of our sample of luminous stars. It is well possible that with such bright stars, MACHO is operating at the instrumental and software limits (saturation, aperture size, etc.). Since the MACHO data have been acquired over a relatively long time interval ($\sim$2500 days), another possibility is that the orbital period is not known precisely enough to allow for a reliable folding of the photometric data into the corresponding phase. Of course, it can also be that, as Seggewiss et al. (1991) noted themselves, the eclipses are false detections. At this time, we cannot conclude this issue, but it is clear that the slightest possibility that BAT99-32 might show *double-eclipses* makes the effort worthwhile to obtain better CCD photometry.

For the remaining stars in our sample for which MACHO photometry is available, there is not much information to be gained. Therefore, we show the data without any further com-

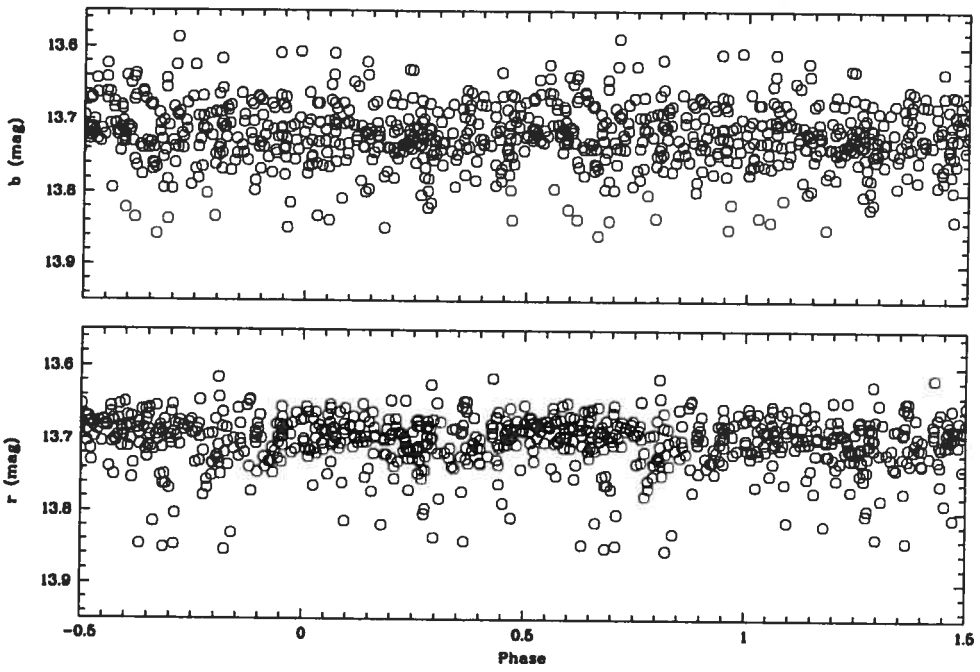

FIGURE 2.82 – MACHO lightcurves in blue (*upper*) and red band (*lower panel*) for the binary star BAT99-12, folded into the orbital phase derived from spectroscopy.

ments in Figures 2.84 to 2.89.

2.5.12 Analysis of the X-Ray Data

Chandra and *ROSAT* observations were searched for X-ray emission from the WNL stars in the LMC. We first extracted *Chandra* ACIS X-ray images in the 0.3–7.0 keV energy band, and *ROSAT* PSPC and HRI images in the full energy range of these instruments, i.e., 0.1–2.4 keV for the PSPC and 0.1–2.0 keV for the HRI. We then compared these X-ray images with optical images extracted from the Digitized Sky Survey[13] (DSS). We identified each WR star

[13]The Digitized Sky Survey (DSS) is based on photographic data obtained using the UK Schmidt Telescope and the Oschin Schmidt Telescope on Palomar Mountain. The UK Schmidt was operated by the Royal Observatory of Edinburgh, with funding from the UK Science and Engineering Research Council, until 1988 June, and thereafter by the Anglo-Australian Observatory. The Palomar Observatory Sky Survey was funded by the National Geographic Society. The Oschin Schmidt Telescope is operated by the California Institute of Technology and Palomar Observatory. The plates were processed into the present compressed digital form with the permission of these institutes. The Digitized Sky Survey was produced at the Space Telescope Science

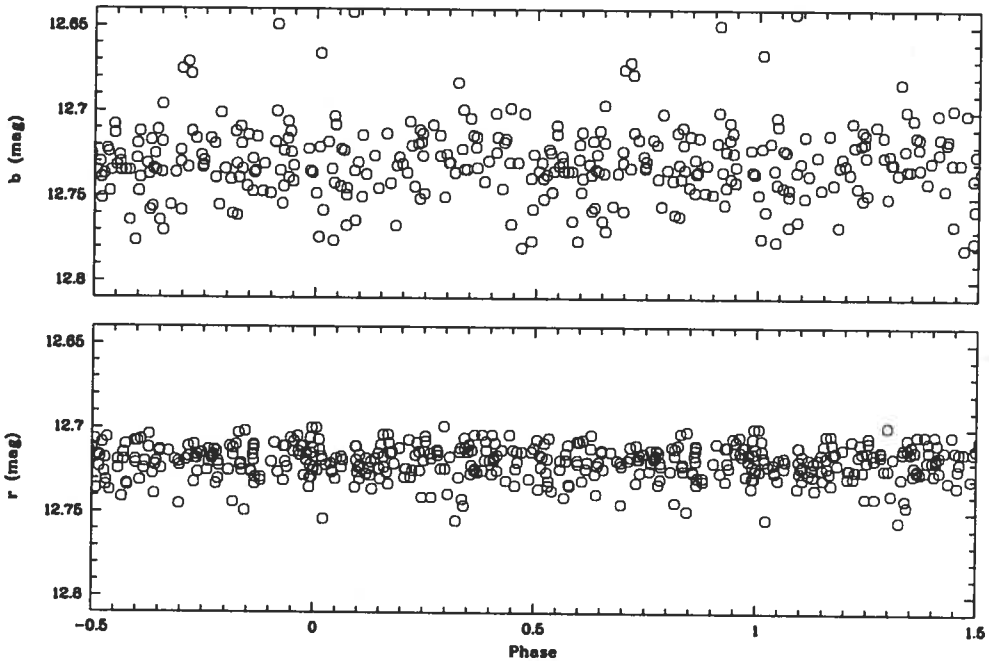

FIGURE 2.83 – Same as Figure 2.82, but for BAT99-32.

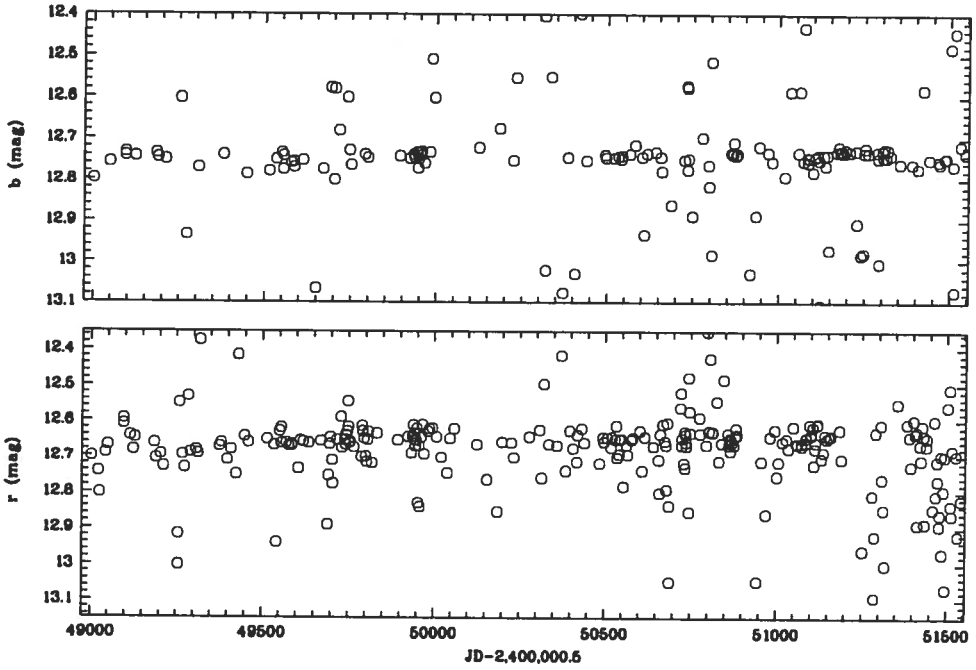

FIGURE 2.84 – MACHO lightcurves in blue (*upper*) and red band (*lower panel*) for the single star BAT99-16, plotted *versus* Julian date.

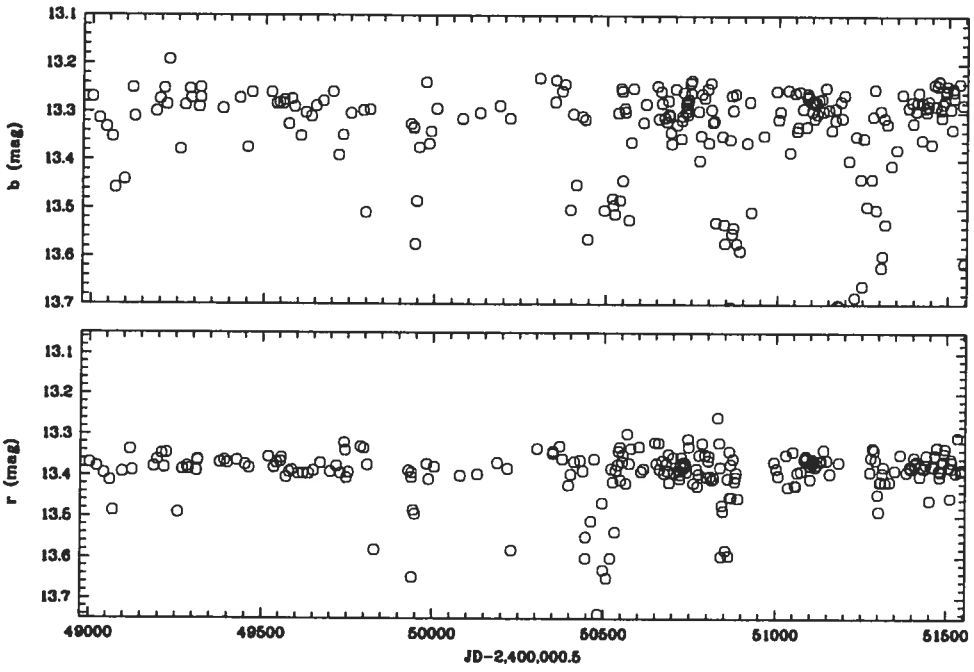

FIGURE 2.85 – Same as Figure 2.84, but for BAT99-30.

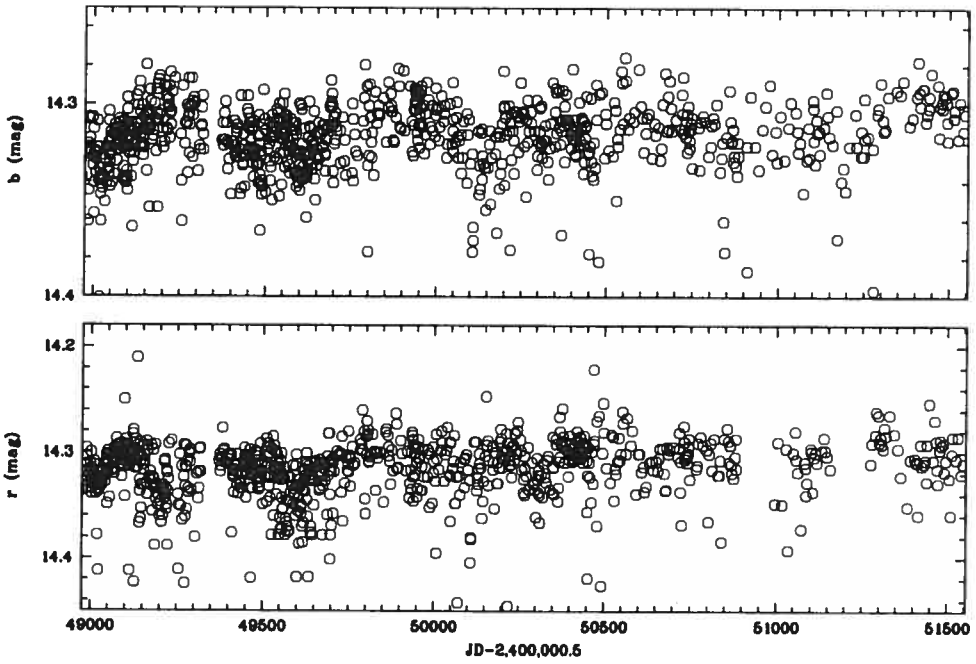

FIGURE 2.86 – Same as Figure 2.84, but for BAT99-54.

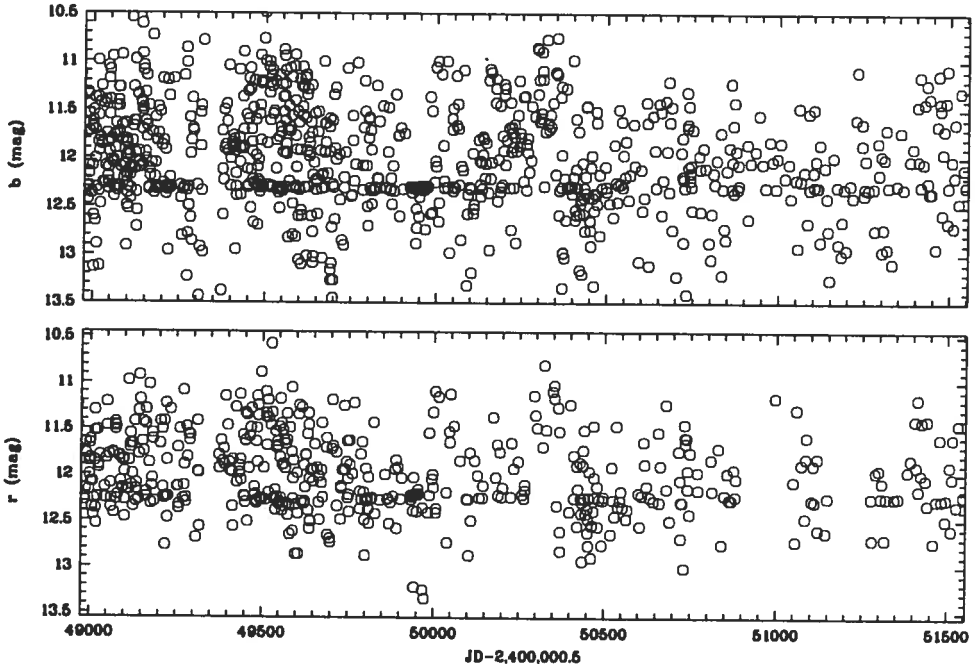

FIGURE 2.87 – Same as Figure 2.84, but for BAT99-55.

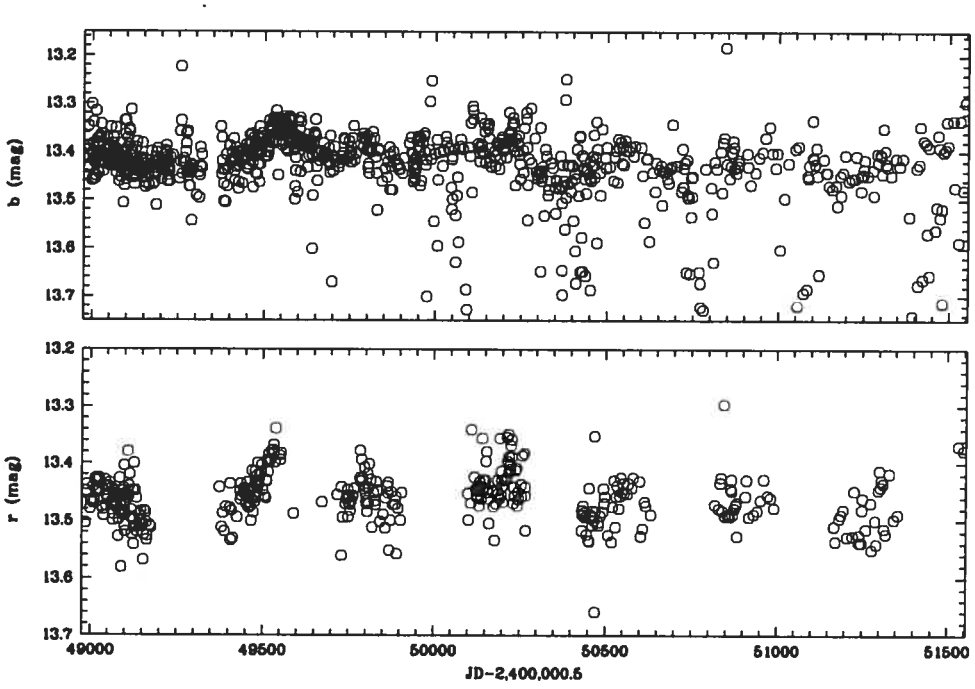

FIGURE 2.88 – Same as Figure 2.84, but for BAT99-76.

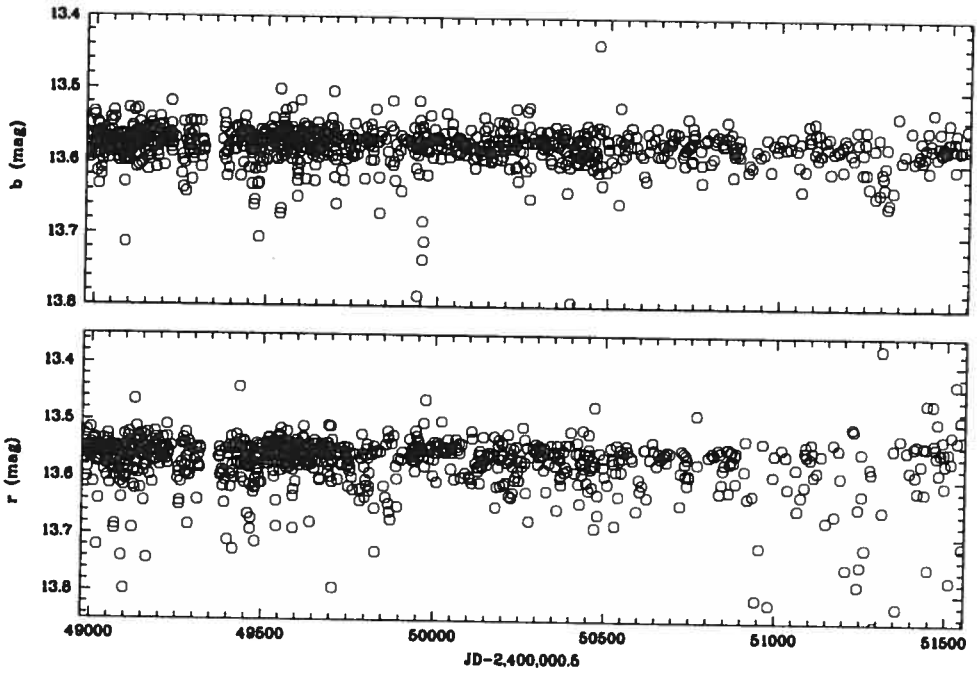

FIGURE 2.89 – Same as Figure 2.84, but for BAT99-79.

in the optical images using the coordinates listed by BAT99, and then searched for X-ray emission at the location of the WR star.

X-ray emission is detected in 15 WNL stars in the LMC, as indicated in Table 2.18. To confirm these detections, we defined source regions encompassing the X-ray sources at the location of the WR stars and appropriate background regions. The background-subtracted count number and count rates are also listed in Table 2.18. For two stars, BAT99-101/102 and BAT99-116, the background-subtracted count number is large enough to render possible the analysis of their X-ray spectra. The spectral analysis has been performed adopting a single-temperature MEKAL optically thin plasma emission model (Kaastra & Mewe 1993; Liedahl et al. 1995), and the photoelectric absorption model of Balucinska-Church & McCammon (1992) for the absorption along the line of sight. The chemical abundances of the X-ray-emitting gas and for the absorbing material have been set to 0.33 $Z_{\odot}$. The best spectral fits indicate plasma temperatures of 0.9±0.2 and $5.0^{+1.5}_{-1.0}$ keV and hydrogen column densities of $(9\pm2)\times10^{21}$ and $(9\pm2)\times10^{21}$ cm^{-2} for BAT99-101/102 and BAT99-116, respectively. Further details of these spectral fits are provided by Guerrero & Chu (2006a). The X-ray luminosities in the 0.5–7.0 keV energy band of BAT99-101/102 and BAT99-116 derived from these spectral fits are listed in Table 2.18. For the other 13 WNL stars detected in X-rays, their X-ray luminosities listed in Table 2.18 have been derived from their count rate, assuming that their X-ray emission follows a single-temperature MEKAL optically thin plasma emission model with a temperature of 1.6 keV and a hydrogen column density of 3×10^{21} cm^{-2} (Guerrero & Chu, 2006a).

For the WNL stars undetected by *Chandra* and *ROSAT* observations, we have derived count rate 3σ upper limits (see Table 2.18) using source regions with radii matching the PSF of each observation. These limits assume the same single-temperature MEKAL optically thin plasma emission model as above.

Institute under US government grant NAGW-2166.

TABLE 2.18 – List of our program stars for which X-ray data are available from public archives.

BAT99	Instrument	Detection?	Count Number [cnts]	Count rate or 3σ upper limit [cnts/s]	L_x or 3σ upper limit [ergs/s]
12	ROSAT PSPC	No		$< 1.1 \times 10^{-3}$	$< 6.0 \times 10^{33}$
13	ROSAT PSPC	No		$< 4.0 \times 10^{-4}$	$< 2.2 \times 10^{33}$
16	ROSAT PSPC	No		$< 1.2 \times 10^{-3}$	$< 6.6 \times 10^{33}$
22	ROSAT PSPC	No		$< 6.8 \times 10^{-4}$	$< 3.7 \times 10^{33}$
30	ROSAT PSPC	No		$< 3.5 \times 10^{-4}$	$< 1.9 \times 10^{33}$
32	ROSAT PSPC	No		$< 5.5 \times 10^{-4}$	$< 3.0 \times 10^{33}$
33	ROSAT HRI	No		$< 3.2 \times 10^{-4}$	$< 4.5 \times 10^{33}$
44	ROSAT PSPC	No		$< 4.3 \times 10^{-4}$	$< 1.6 \times 10^{33}$
45	ROSAT PSPC	No		$< 3.3 \times 10^{-4}$	$< 1.8 \times 10^{33}$
54	ROSAT PSPC	No		$< 2.7 \times 10^{-4}$	$< 1.5 \times 10^{33}$
55	ROSAT PSPC	No		$< 2.8 \times 10^{-4}$	$< 1.5 \times 10^{33}$
58	ROSAT PSPC	No		$< 1.0 \times 10^{-3}$	$< 5.5 \times 10^{33}$
68	ROSAT HRI	No		$< 1.9 \times 10^{-4}$	$< 2.7 \times 10^{33}$
76	ROSAT PSPC	No		$< 2.9 \times 10^{-4}$	$< 1.6 \times 10^{33}$
77	Chandra ACIS	Yes	18 ± 7	3.1×10^{-4}	$(5 \pm 2) \times 10^{32}$
79	Chandra ACIS	Yes	19 ± 7	3.1×10^{-4}	$(5 \pm 2) \times 10^{32}$
80	Chandra ACIS	Yes	45 ± 9	4.9×10^{-4}	$(1.0 \pm 0.2) \times 10^{33}$
83	Chandra ACIS	No		$< 1.3 \times 10^{-4}$	$< 2.6 \times 10^{32}$
89	Chandra ACIS	No		$< 3.7 \times 10^{-4}$	$< 7.4 \times 10^{32}$
91	Chandra ACIS	No		$< 5.0 \times 10^{-4}$	$< 7.9 \times 10^{32}$
92	Chandra ACIS	Yes	12 ± 4	6.7×10^{-4}	$(1.3 \pm 0.4) \times 10^{33}$
93	Chandra ACIS	Yes	24 ± 9	5.0×10^{-4}	$(8 \pm 3) \times 10^{32}$
95	Chandra ACIS	No		$< 3.2 \times 10^{-4}$	$< 6.4 \times 10^{32}$
96	Chandra ACIS	No		$< 3.5 \times 10^{-4}$	$< 7.0 \times 10^{32}$
97	Chandra ACIS	No		$< 3.1 \times 10^{-4}$	$< 6.2 \times 10^{32}$
98	Chandra ACIS	No		$< 3.6 \times 10^{-4}$	$< 7.2 \times 10^{32}$
99	Chandra ACIS	Yes	77 ± 9	4.4×10^{-3}	$(1.3 \pm 0.2) \times 10^{34}$
100	Chandra ACIS	Yes	8 ± 3	4.1×10^{-4}	$(8 \pm 3) \times 10^{32}$
101,102	Chandra ACIS	Yes	330 ± 20	1.9×10^{-2}	$(1.5 \pm 0.1) \times 10^{35}$
103	Chandra ACIS	Yes	7 ± 3	3.8×10^{-4}	$(8 \pm 3) \times 10^{32}$
104	Chandra ACIS	No		$< 5.1 \times 10^{-4}$	$< 1.0 \times 10^{33}$
105	Chandra ACIS	Yes	21 ± 5	1.2×10^{-3}	$(2.4 \pm 0.6) \times 10^{33}$
107	Chandra ACIS	Yes	16 ± 4	9.2×10^{-4}	$(1.8 \pm 0.5) \times 10^{33}$
113	Chandra ACIS	No		$< 6.4 \times 10^{-4}$	$< 1.3 \times 10^{33}$
114	Chandra ACIS	Yes	9 ± 3	5.1×10^{-4}	$(1.0 \pm 0.3) \times 10^{33}$
116	Chandra ACIS	Yes	860 ± 30	4.9×10^{-2}	$(1.8 \pm 0.1) \times 10^{35}$
118	Chandra ACIS	Yes	13 ± 4	7.5×10^{-4}	$(1.5 \pm 0.5) \times 10^{33}$
119	Chandra ACIS	Yes	11 ± 4	6.1×10^{-4}	$(1.2 \pm 0.4) \times 10^{33}$
120	Chandra ACIS	No		$< 3.6 \times 10^{-3}$	$< 5.7 \times 10^{33}$
130	ROSAT HRI	No		$< 7.0 \times 10^{-4}$	$< 1.0 \times 10^{34}$
133	ROSAT PSPC	No		$< 7.1 \times 10^{-3}$	$< 3.9 \times 10^{34}$

X-Rays and Binarity

As can be seen from Table 2.18, *Chandra* ACIS is more sensitive than *ROSAT*'s instruments; the latter does not yield a single detection of our program stars. We will therefore concentrate on the *Chandra* data for most of our discussion.

Chandra observed 25 of our 41 program stars, detecting 15 sources. WR+O binaries are expected to be bright X-ray sources because of the high-energy WWCs occurring in such systems (e.g. Prilutskii & Usov 1976). However, of the seven binaries observed, only five are detected, two of which, BAT99-99 and 119, are long-period binaries. Two binary systems, BAT99-95 and 113, were missed, with BAT99-95 apparently being a particularly faint X-ray source. One might now suspect that short-period, close binary systems produce fewer observable X-rays, because *i*) the two winds have not yet reached their respective terminal velocities, and *ii*) the self-absorption in the wind of generated X-ray photons might decrease the observable flux (see e.g. Owocki & Cohen 2001; Ignace & Gayley 2002). On the other hand, binaries with longer periods have larger orbital separations, so that their winds are geometrically thinned. This might lead to a decreased self-absorption of the X-rays produced in the WWC, so that these systems show larger observed X-ray fluxes compared to shorter-period, closer systems.

In order to test these speculations, we combined our data with those of Foellmi et al. (2003b) and plotted the observed X-ray flux *versus* the orbital period, expecting longer-period systems to show larger X-ray luminosities. The result is shown in Figure 2.90. Non-detections of both *Chandra* and *ROSAT* are given with their upper limit and by downward-pointing arrows. One might have expected that binaries containing hydrogen-depleted WNb stars generate more X-rays due to their higher mass-loss rates and faster winds (i.e. there is more wind momentum available), but this is not supported by the observations. Also, there is no apparent trend in the data which indicates that longer-period binaries indeed do display larger X-ray fluxes than shorter-period systems

Interestingly, BAT99-99 is much X-ray brighter than BAT99-119, but this could in part

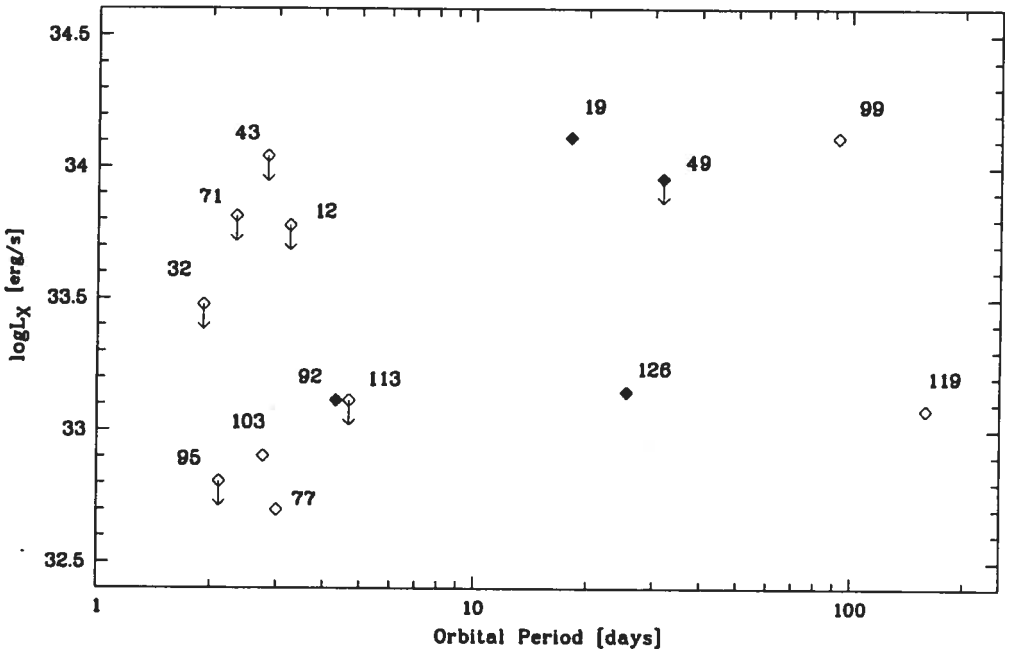

FIGURE 2.90 – X-ray luminosities of identified WN binaries in the LMC as a function of their orbital period. Filled symbols denote broad-lined, hydrogen-depleted WNb stars; empty symbols denote H-containing WN stars. Upper limits are indicated by downward-pointing arrows, and stars are named by their BAT99 numbers. As can be seen, WNb binaries do not show higher X-ray luminosities as might have been expected from the stronger winds of WNb stars.

be due to the large eccentricity ($e \sim 0.69$; see Chapter 3) of BAT99-119. It is thus not unlikely that *Chandra* missed the moment of maximum X-ray luminosity for BAT99-119 during periastron passage. Note however that the circular orbit which was assumed for BAT99-99 might be incorrect, and that this binary might be (highly) eccentric, too. In fact, both systems merit a closer look for orbit-related X-ray variability.

X-Rays in Apparently Single Stars

Although some of the remaining 10 program stars detected by *Chandra* have X-ray luminosities which are comparable to those of the confirmed binaries, we have found no evidence

for RV variability due to binarity in these objects. While we cannot rule out that they are long-period ($P > 200$ days) binaries or binaries with very low inclination angles, there is the possibility that the X rays are emitted by single WR stars due to radiatively-induced instabilities in their winds (Lucy & White 1980; Willis & Stevens 1996).

Two X-ray sources detected by *Chandra*, BAT99-101/102 and 116, are extremely luminous. BAT99-101/102 are two visually very close stars which can only be resolved using HST or AO-assisted NIR imaging, and thus *Chandra*'s aperture integrated the combined flux. BAT99-101 is a WC5 star (Moffat et al. 1987) and potentially a binary (Bartzakos et al. 2001), while for BAT99-102, there is some confusion: As detailed above, we find that BAT99-103 is the 2.76-day binary, not BAT99-102. There might be sufficient wind momentum confined in a very small volume to account for the large X-ray flux, even if 102 is single, but if both 102 and 101 are binaries, there certainly is more wind momentum available. Presently, there is not enough data available to verify this interesting issue.

BAT99-116, on the other hand, is visually isolated enough not to be subject to such ambiguities. BAT99-116 is even more luminous than the combined BAT99-101/102 system; in fact, it exceeds the X-ray brightest WR stars known, the Galactic WN6ha stars NGC3603-C (Moffat et al. 2002) and WR25 (Seward & Chlebowski 1982). Both NGC3603-C (Schnurr et al., in prep.) and WR25 (Gamen et al. 2006) have been readily identified as binaries, and they both contain two of the most luminous WN stars known, so that there is an explanation why these objects are so X-ray bright. However, unless the photometry published by BAT99 is wrong, BAT99-116 is not particularly optically bright. With $v = 13.65$ mag, it is $\sim$1.5 mag fainter than BAT99-119, which is a confirmed binary (no reddening considered, but it is low and probably $\sim$similar for the two stars anyway). Since both stars are similar enough (WN5ha for 116, and WN6ha for 119; see below) to have the $\sim$same bolometric correction, this makes for a considerably less luminous and hence less massive system for BAT99-116. Thus, if BAT99-116 is indeed single, its ratio L_x/L_{bol} is abnormally high, but if X-rays originate from WWC in a binary, the question remains how such visually faint objects (the total mass has now to be

split between two stars) can provide the required wind momenta. Thus, one might be inclined to believe that BAT99-116 is not an ordinary WR+O binary, but rather some exotic, WR+cc object, where cc stands for compact companion, denominating a black hole or a neutron star which accretes matter from the WR wind. This very intriguing system merits a closer look.

As for BAT99-118, the sheer luminosity of the object renders a two-star scenario more likely. Not only does it closely resemble BAT99-119 in terms of spectral type, but its X-ray luminosity is also comparable to that of BAT99-119 (in fact, it is equal within the errors). It is thus possible that BAT99-118 turns out to be a long-period binary as well, especially given the fact that it also shows a significantly large RV scatter. Both BAT99-118 and 119 will be discussed in more detail in a forthcoming paper (see Chapter 3).

2.5.13 Stellar Properties and Correlations Among the Data

The salient properties of our program stars are summarized in Table 2.19.

Now that we have determined the binary status of each of our program stars, we can use measured quantities and stellar properties to search for correlations among the data which would allow us to tie down more firmly the binary (or single) nature of a given star. To do so, in most cases we combined our data with those published by Foellmi et al. (2003b); where required, we re-analysed their data.

From an observational point of view, the most important property of a star is its spectral appearance. Since our spectral classification method is consistent with that of Foellmi et al. (2003b), we used both data sets to see which observable properties of WN stars in the LMC change with spectral type, and how.

Magnitudes and Spectral Types

For a large fraction of the WN stars in the BAT99 catalogue, no colour information $b-v$ is provided, hence we did not attempt to de-redden the apparent v magnitudes; rather, we used

TABLE 2.19 – Summary of the properties of the observed program stars.

BAT99	Spectral Type	$\overline{RV}$ [kms^{-1}]	σ_{RV} [kms^{-1}]	EW 4686 [Å]	FWHM 4686 [Å]	Bin?	P [days]	remarks
12	WN5ha	650	70.8	-7.38	17.9	yes	3.24	runaway
13	WN10	277	12.5	-2.32	5.4	...	...	
16	WN7h	330	13.3	-54.90	12.7	...	...	
22	WN9h	255	13.3	-3.86	5.7	...	...	
30	WN6h	345	17.3	-56.90	13.1	...	...	
32	WN6(h)	288	92.4	-94.24	20.6	yes	1.91	
33	WN8ha	293	16.2	-2.05	7.6	...	...	
44	WN8ha	398	15.8	-25.69	9.0	...	...	
45	WN10h	245	11.4	-1.40	5.6	...	...	LBV?
54	WN8ha	316	18.2	-6.80	6.4	...	...	
55	WN11h	140	14.6	-0.38	4.7	...	...	runaway?
58	WN7ha	311	14.7	-42.94	12.1	...	...	
68	WN7ha:	321	29.5	-4.63	10.0	...	...	
76	WN9ha	274	15.5	-6.41	6.0	...	...	
77	WN7ha	333	78.2	-10.77	15.0	yes	3.00	
79	WN7ha+OB	288	14.3	-39.54	16.8	...	...	
80	WN5ha:	374	20.5	-10.51	24.3	...	...	
83	LBV	...	14.9	...	...	...	...	LBV
89	WN7h	303	14.3	-59.65	12.3	...	...	
91	WN6h:a:	324	13.7	-13.02	16.1	...	...	
92	WN3:b(+O)+B1Ia	332	139.8	-15.03	46.0	yes	4.31	
93	WN6h:a	373	20.5	-2.61	8.6	...	...	
95	WN7	274	81.6	-51.71	18.4	yes	2.11	
96	WN8	274	18.7	-21.17	10.8	...	...	
97	WN7h::a	305	19.6	-4.85	9.7	...	...	
98	WN6	321	14.7	-24.72	19.9	...	...	
99	WN5h:a	337	58.9	-3.20	13.2	yes	92.6	
100	WN7	307	15.4	-26.50	14.4	...	...	
102	WN6	317	25.3	-24.31	16.4	?	...	strong X-rays
103	WN6	388	106.7	-39.83	24.8	yes	2.76	
104	WN7	342	18.4	-4.10	12.5	...	...	
105	WN7	273	37.7	-19.01	14.9	...	...	
107	WN9h::a	303	23.9	-1.24	5.9	...	...	
113	WN5h::a	397	93.3	-4.36	15.6	yes	4.70	
114	WN5h:a	393	23.2	-3.67	17.2	...	...	
116	WN5h:a	373	32.6	-27.36	26.0	...	...	strong X-rays
118	WN6h	301	31.6	-70.92	18.7	?	...	
119	WN6(h)	332	44.7	-57.35	17.3	yes	158.8	
120	WN9h	282	21.8	-3.73	6.1	...	...	
130	WN11h	287	13.2	-0.93	4.9	...	...	
133	WN11h	280	15.4	-0.78	4.9	...	...	

them as given in BAT99. Absolute magnitudes M_v were calculated using the v magnitudes listed in BAT99 and the relation $v - M_v = DM + A_v$, where $DM = 18.5$ mag the distance modulus to the LMC, and A_v the extinction towards the LMC, estimated to be ~uniform and ~0.5 mag for all stars. We thus obtain $M_v = v - 19$ mag. In Figure 2.91, we have plotted M_v *versus* the spectral type. As was to be expected, earlier types are in general visually fainter than later-type stars, since more evolved WNE stars are hotter and more compact than cool and extended, less evolved WNL stars (e.g. Hamann et al. 2006). This is particularly true for those WN5-7ha stars which are still in in their CHB phase; their slightly lower "surface" temperatures are compensated by much bigger radii. However, this does not necessarily mean that WNE stars have significantly lower luminosities; due to their high temperatures, they have larger bolometric corrections than cooler WNL stars. Note that qualitatively, Figure 2.91 closely resembles Figure 4 in van der Hucht (2001), which is the same but for Galactic WR stars.

As was also to be expected, binaries tend to be, on average, brighter than their single counterparts of the same spectral type. This is of course due to the light contribution of the companion, which, for fainter, early-type stars, can be quite substantial. Single stars which, in Figure 2.91 appear to be visually very bright are very often simply subject to crowding; thus, their magnitudes suffer from light contribution of nearby stars. A prominent exception is the well isolated star BAT99-118, the brightest of all WN6h stars in the diagram, which turns out to be also the most luminous WR star known; however, it might turn out to be a binary as well.

One might be tempted to draw the conclusion that the assessment of the binary nature of a given star can be carried out with a relatively high degree of confidence by simply comparing its magnitudes to a sufficiently large peer group of known single counterparts with reliable photometry. This is, however, not necessarily true, because the flux contribution from the companion (and hence the total brightness of the system) can span a large range, not only due to the cosmic scatter of the WR star's magnitude, but also depending on the properties of the companion (i.e., its mass, evolutionary state, and luminosity class). As can be seen in

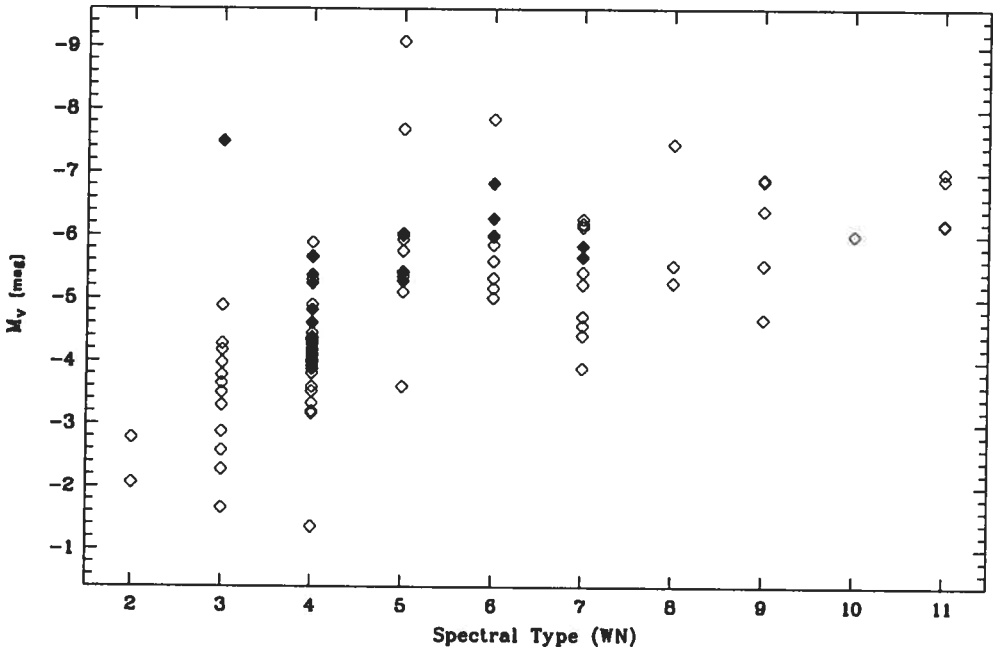

FIGURE 2.91 – Absolute magnitude M_v of our program stars and those of Foellmi et al. (2003b) as a function of spectral type. Confirmed binaries, uncorrected for companions, are indicated by filled symbols.

Figure 2.91, binaries seem to be brighter on average, but the difference is visibly not pronounced enough to rely on it. Also, since it is not *a priori* known which stars are binaries, their inclusion will affect the value of the average magnitude of a given WR spectral type, possibly to an extent that might render the approach entirely useless.

Emission-Line Properties and Spectral Types

In Figure 2.92, we have measured the FWHM of the HeIIλ4686 emission line as a function of the WN spectral type. Using $\Delta\lambda/\lambda_0 = \Delta v/c$, where $\lambda_0 = 4686$ Å, we have transformed them into velocity-FWHM (VFWHM) and plotted the values *versus* the respective spectral types.

As can be seen, there is a global trend that the VFWHM increases as the WR types become earlier. In this respect, our Figure 2.92 resembles van der Hucht's (2001) Figure 5 remarkably well; van der Hucht used values of v_∞ that were obtained from much more reliable P Cygni absorption profile measurements in the UV. However, one has to bear in mind that unless the lines form in a region where the wind has already reached its terminal velocity, which for HeIIλ4686 never is the case, one cannot derive the terminal speed of the wind (or vice versa) from the width of optical emission lines. The reason for this is that the FWHMs first and foremost depend on the velocity, opacity, and ionization structure of the wind. Comparisons of line widths between different subtypes therefore have to be drawn with extreme care.

Even within a given subtype, the wind structure can (and does) significantly differ, as is evidenced by the large scatter in Figure 2.92. This is of course because the wind structure of a star cannot be concluded from its spectral type alone; an evolved, He-burning WN star and an unevolved, H-burning WN star might share the same spectral type, say WN6, based on morpholgy alone, yet they have entirely different wind (and internal) structures. Conversely, WR stars of sufficiently similar evolutionary stage and internal structure will, everything else being equal, not only display the same spectral type, but also very similar wind parameters, i.e. FWHM of optical lines and v_∞ will related pretty closely. However, as soon as the ionization structure of the wind is modified, e.g. by changes in metallicity, the spectral properties will be affected, and nothing can be said anymore about the FWHM-v_∞ relation.

For obvious reasons, the measurement of the FWHM depends on the spectral resolution of the data, even if in our case, the broad lines are well sampled. Therefore, we have also measured the equivalent widths (EW) of the HeIIλ4686 emission line and plotted them *versus* the respective spectral types (Figure 2.93). Again it can be seen that |EW| increases as the WN types become earlier. This has two reasons: The stars become increasingly hotter and more compact; thus the optical continuum flux decreases, while the line flux itself increases due to increasingly stronger winds. As net effect, the EW increases.

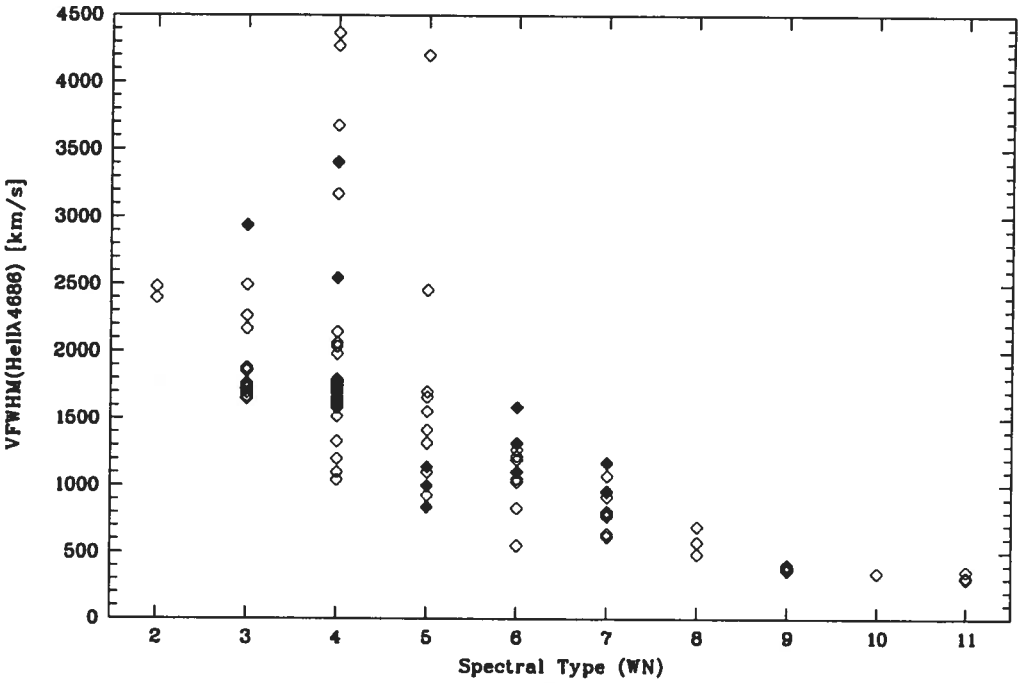

FIGURE 2.92 – Velocity-FWHM of the HeIIλ4686 emission line as a function of the spectral WN subtype. Earlier, more compact stars have faster winds. Binaries are indicated by filled symbols. See text for more details.

Since the EW is thus sensitive to continuum variations, one expects to find strong effects in binaries, where the (usually cooler) companion contributes a more or less substantial part of the continuum flux; also, one expects that the earlier the WR star (i.e., the weaker its continuum), the more the EW is affected. It can clearly be seen in Figure 2.93 that WN4 binaries tend to have diluted emission lines; the same is true for the WN3 binary and the WN5 binaries. Note that most of the WN5 stars are re-classified O3f/WN6 stars, i.e. extreme Of stars which have, compared to classical WN stars, a relatively weak HeIIλ4686 emission. Very interestingly, though, the situation seems reversed when it comes to WN6 binaries. This is most likely due to the fact that *i*) the WN6 components are more luminous than their companions (as stated before, we did not find any spectral signatures of the companions), so that depending on the luminosity ratio, the dilution effect is less or not at all pronounced; and *ii*) the three weakest-lined single WN6 stars in our sample show diluted spectra because of crowding. From our diagrams it can be clearly seen that diluted emission lines are neither a necessary nor a sufficient condition for binarity. It is thus very risky to rely on diluted emission lines as a means to assess the binary status of a WR star.

Radial-Velocity Precision and Spectral Types

In Section 2.5.4, we have relied on our reference stars irrespectively of their spectral types. However, there might be reasons to suspect that narrow-lined WN stars provide a better measurement of the RV than broader-lined WN stars. In Figure 2.94, we have therefore plotted the RV scatter (unweighted $\sigma_{\rm RV}$) *versus* the spectral type in order to find any correlations. Since Foellmi et al. (2003b) did not publish their $\sigma_{\rm RV}$ values, we have restricted this analysis to our own, WNL program stars. As was to be expected, binaries clearly stand out, well above the cut-off value of 22.6 kms^{-1} obtained from our χ^2 analysis (dashed line in the diagram). Below this threshold, there seems to be a very slight advantage for later-type stars, in particular for spectral types later than WN7. This is mainly because these stars not only have narrower, but also more lines in the spectral range, increasing the inherent advantage of the cross-correlation to condense RV information into a "super-line" (Penny 1996). However, given the rather co-

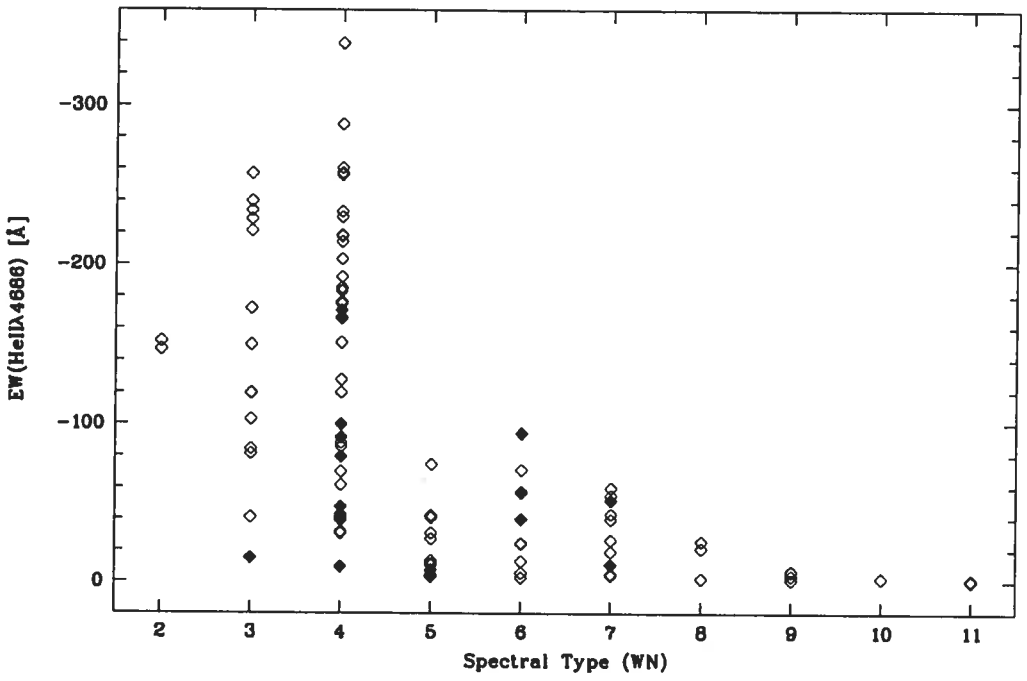

FIGURE 2.93 – Equivalent widths of the HeIIλ4686 emission line as a function of the spectral type. Earlier types show stronger lines. See text for more details. Binaries are indicated by filled symbols.

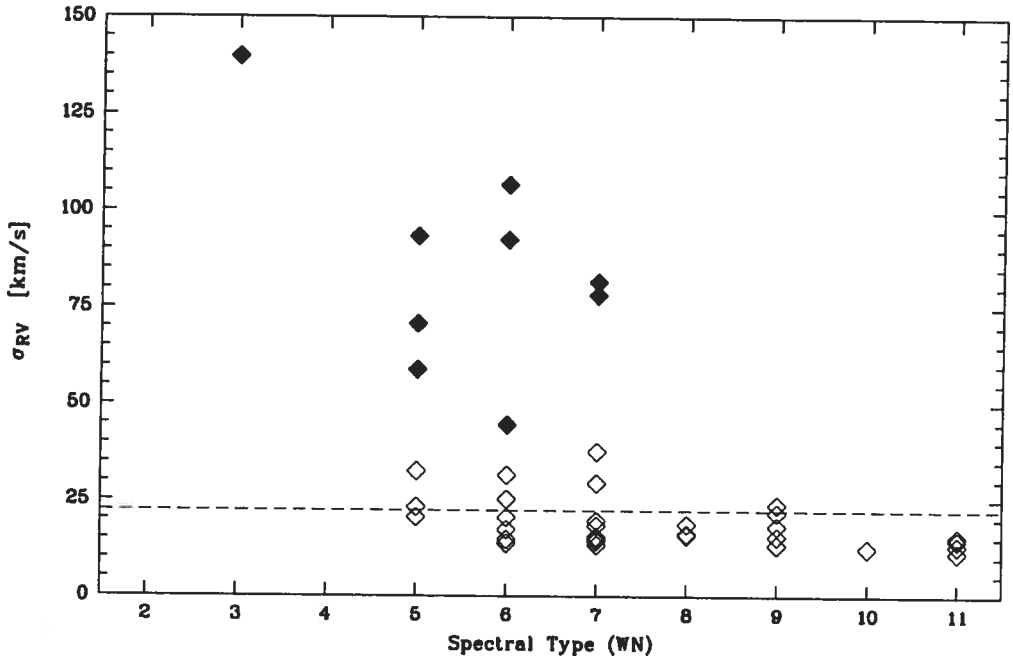

FIGURE 2.94 – RV scatter as a function of spectral types. Binaries are indicated by filled symbols, and show the largest scatter. The dashed line represents the cut-off value of 22.6 kms^{-1} above which stars are considered variable. See text for more details.

arse spectral resolution of our data, it is very likely that we do not fully exploit this potential advantage in RV precision, simply because the emission lines are not well enough sampled. However, together with what was shown in Section 2.5.9, narrow-lined WNL stars prove to be excellent targets to determine the systemic velocity of a given environment.

X-Ray Luminosities and Spectral Types

For 21 WN stars, 15 of our WNL stars plus 6 WNE stars of the Foellmi et al. (2003b) sample, X-ray luminosities L_x were measured by either *Chandra* (18 stars) or *ROSAT* (3 stars; see Foellmi et al. 2003b for details). For the remaining 67 Magellanic Cloud WN stars that have been observed with either satellite, only upper limits can be given. For reasons of clarity, we shall discuss these two populations separately.

For those stars which have been detected, we have plotted L_x *versus* the respective WN spectral types in Figure 2.95. As can be seen, most stars have X-ray luminosities below $\log L_x \sim 33.7$, independent of their (short-period, i.e. $P < 200$ days) binary nature. Five stars are X-ray brighter than $\log L_x \sim 34$, of which only two are confirmed binaries. As has been discussed above, at least one of the two superluminous X-ray sources seems to be a peculiar object rather than a binary. The first preliminary conclusion that can be drawn here is thus that not every binary is a bright X-ray source (due to WWCs, for instance). This is important to note because sometimes, the binary nature of a given WR star is concluded from its X-ray brightness; hence, a significant fraction of binaries might be missed if one relies only on the X-ray luminosity. The second conclusion is that there seems to be no readily visible trend of the X-ray luminosity with the spectral type.

Three of our apparently single WN5 stars are detected X-ray sources, one of them being BAT99-116. (Note that there are reclassified O3f/WN6 stars among the WN5h/ha sample.) Foellmi et al. (2003b) reported two apparently single WN5 stars with *ROSAT* detections and one apparently single WN4 star with a *Chandra* detection. This is in contradiction with the findings of Guerrero & Chu (2006b) who reported that there are *no* single WN4 or WN5 stars with X-ray emissions.

As to the non-detections, we have 67 WN stars (both WNL and WNE combined) for which (mostly *ROSAT*) observations yielded only upper limits. For clarity, these values are shown separately in Figure 2.96. It can be seen that six confirmed binaries are too faint X-ray sources to be detected by *ROSAT*, despite the fact that *Chandra* confirmed that some WN4 binaries can have X-ray fluxes which should well fall into *ROSAT*'s detection limits. Furthermore, since *Chandra* does not find significantly lower X-ray fluxes than *ROSAT*'s upper limits, it also seems that WN stars later than WN7 indeed have only marginal X-ray luminosities, hence that this is not a bias due to deficiencies of *ROSAT*. This is in line with the findings of Oskinova (2005) that single Galactic WN8 stars do not show X-ray emissions, most likely

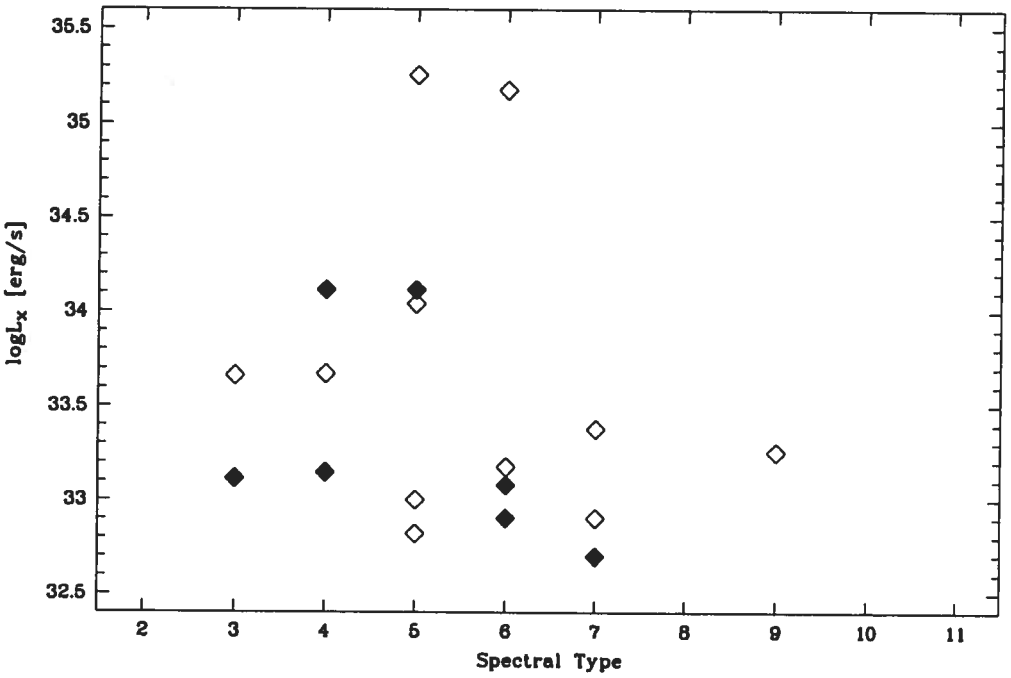

FIGURE 2.95 – X-ray luminosities of detected program stars as a function of their WN spectral types. Binaries are indicated by filled symbols. See text for more details.

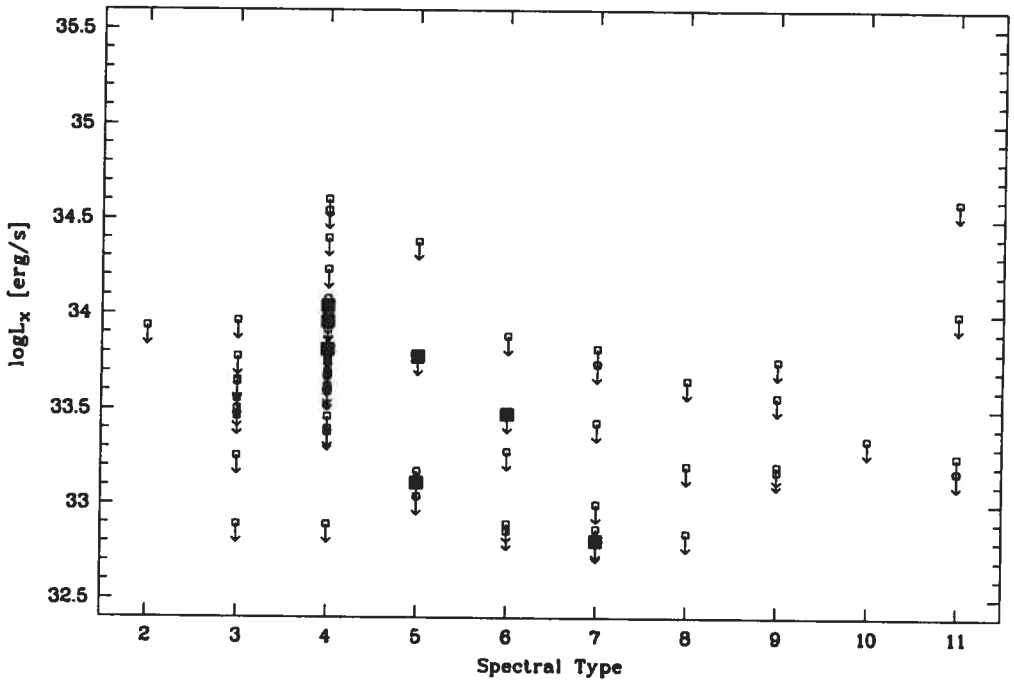

FIGURE 2.96 – Upper limits of X-ray fluxes vs. their WN spectral types for program stars which were non-detections. Binaries are indicated by filled symbols. See text for more details.

because their winds are too opaque. Interestingly, the only exception to this, the detected WN9 star, is none other than BAT99-107, for which Moffat (1989) found a clear long-term RV variability, a finding that we did not confirm. Either this star is indeed in a (long-period) binary, or, in contrast with its Galactic and Magellanic Cloud counterparts, some mechanisms in its wind generate detectable X-ray flux. We presently have no explanation for that.

2.6 Discussion

2.6.1 Binary Detectability and Statistical Corrections

Before we can discuss the evolutionary implications of the binary frequency, we have to discuss the completeness of our survey. A *detected* binary is a star for which a viable orbital solution could be obtained from the RV curve of the star. From this naturally follows that

the observed RV variability is cyclical (after all, a periodicity was found). However, it does *not necessarily* follow that the observed RV variability is significant (although this is often the case in real data). This statement will become clearer further below.

Most proposed solutions dealing with how to detect a binary through RV variations are based on statistical tests which compare the observed RV scatter $\sigma_{\rm RV}$ of a binary candidate to the (Gaussian) scatter of an observed, constant comparison star (our χ^2 method), or to the RV scatter of a simulated binary through the F-test (Foellmi et al. 2003b; see also Duquennoy et al. 1991). The obvious weakness of these "σ statistics" is that the standard deviation is a statistical quantity which is *independent of the number N of data points*: whether one has a hundred or ten thousand data points, this does not affect the numerical value of $\sigma_{\rm RV}$ in any systematic way. The statistical quantity that, however, is affected, is the *error of the mean.* In the case of a constant star, this error of the mean will be $\sigma/\sqrt{N}$, i.e. it will diminish as the number of points increases. If some function with df degrees of freedom is fitted, the error of the mean will be $\sigma/\sqrt{N-df-1}$; thus the number of data points is obviously relevant for the quality of the orbital solution.

If the Discrete Fourier Transform (DFT) of the RV data is calculated (and this is essentially what our period-search algorithm does), the situation becomes more complicated, because the total time span T covered by observations compared to the systemic periods P becomes important, as well as the distribution of data points in phase *and* time. Detection limits do not directly depend on the ratio of the RV ampitude K of the binary (the signal) to the measurement error σ (the noise) in data space, but on the S/N ratio achieved *in the frequency domain.* Thus, short periods which have a large T/P and better "phase-filling", therefore have a larger detection probability than longer periods which suffer from holes in the phase coverage and a lower S/N per frequency unit. Vice versa, the same detection probability as for longer periods can be obtained for shorter periods but lower RV amplitudes, which means that low-K (low-inclination) binaries with a given K tend to be detected more easily if they are short-period. Clearly, data that have not been acquired in one continous run

but in several runs distributed in time, suffer from fairly large phase-gaps when it comes to longer periods.

So far, we have only considered circular orbits with sinusoidal RV curves. But as soon as non-circular orbits enter the stage, the eccentricity e, the orientation of the orbital ellipse (characterised by the argument of the periastron ω), and the time of periastron passage T_0 start to seriously affect the detection probability of periods for two reasons. First, the orbital RV curve becomes distorted in a way that generates harmonics in the DFT spectrum. Power is transferred from the fundamental to the harmonic spectrum, thereby lowering the peak of the fundamental frequency. If the orbit is highly eccentric, the fundamental peak might be pushed into the noise floor, and the period will not be detected. Second, the distribution of the data points over the orbital phase is even more critical, because the star spends most of the time near apastron; if the passage of periastron, where the RVs change rapidly, is missed, the RV curve will look flatter than it really is. This is obviously not only a problem for the DFT, but also for any σ-based statistics

From a more practical point of view, the question we are interested in here is not "What are the detection limits?" but rather "How many binaries have been missed?" The standard approach to this problem is a "simulation of observed simulations" (SOS). A population of artificial binaries is simulated whose orbital parameters are drawn randomly, but following a distribution function. Then, observations of these artificial binaries are simulated by applying some random sampling of the orbit, and adding noise to the "measured" RVs. The data can then be subjected to either simple σ statistics (i.e. χ^2 testing) or to much more demanding DFT analyses (for reasons of convenience, usually the former is done). From the detected fraction of artificial binaries, one can reconstruct the true binary frequency among the artificial sample by statistical means. (For an excellent description of this approach and all related problems, see Kouwenhoven 2006).

The main problem of course is to determine reasonable distribution functions for the res-

pective orbital parameters, because the results of the SOS will obviously depend strongly on what initial assumptions were made for the underlying, true binary population. For their WNE stars in the LMC, Foellmi et al. (2003b) used distribution functions for Galactic O stars (based on statistics published by Mason et al. 1998; also see references therein); they found that 35% of the binaries in their sample were missed. For our study, the most relevant assumption Foellmi et al. used was that the orbital periods P are distributed flat in log$P$, i.e. there are as many binaries between 1 and 10 days as there are between 10 and 100 days, etc. In our WNL sample, we have found eight binaries with periods shorter than 100 days. Of these eight binaries, only one, BAT99-99, has a period between 10 and 100 days; the remaining seven binaries have periods ranging between 1 and 10 days. Thus, without any sophisticated Monte Carlo simulation, we can immediately determine that we have missed six binaries in the period range from 10 to 100 days, of course only under the condition that we set the initial period distribution to be flat in log$P$ and that we believe that we are complete in the period range from 1 to 10 days.

However, any other choice of the period distribution function (among other orbital parameters) would produce a different result, and of course one must not forget that we operate with small numbers here. From the fact that we have not discovered the binary nature of BAT99-119 through our RV data alone, we can reasonably assume that we start to miss systems with periods above $\sim$100 days. It is however not impossible that we have indeed found all the binaries from 10 to 100 days, because there is a surprising lack of binaries between 5 and 50 days. Given the fact that we have identified BAT99-99, which has a period of 92.4 days, there is no obvious reason why we should have missed a binary with half or a quarter that period. From our χ^2 analysis in Section 4.4, we cannot even propose a good binary candidate, with the exception of BAT99-118 which is also bright enough and shows X-ray emission, thus which satisfies secondary criteria of binarity. While it is not impossible that in some cases, we have erroneously attributed significant RV variability to effects of crowding rather than recognizing the true binary nature of the star, the missed periods are too short to produce such low K values, and low orbital inclination angles that could explain the observations are very unlikely.

Thus, there is no reasonable way we can conclude how many binaries we have missed. In fact, any statistical correction is subject to small-number statistics: even if we had a way to obtain the true number of binaries from the number of observed binaries, we would have to show first that the observed number is statistically not consistent with the expected value; otherwise, the correction could not be justified. Thus, instead of applying a correction factor based purely on statistical considerations of detection thresholds, we will proceed with our discussion using the *uncorrected binary frequency*, assuming that, whatever the detection bias is, Bartzakos et al. (2001), Foellmi et al. (2003a,b), and this study suffer from it in roughly the same way, given that we have carried out more or less the same kind of observations. In regard to the achieved RV precision, one can argue that the somewhat better precision obtained in this study is compensated by the fact that WNL stars are, on average, more massive than WNE stars, because they had less time to shed their mass by stellar winds; thus, RV amplitudes of WNL binaries will, on average, be somewhat smaller than those of WNE and WC/WO binaries. Since neither of the three studies used a more sophisticated detection threshold than the RV scatter of (presumably) constant, reference stars, we feel that all three studies have the ∼same detection probability to periods up to ∼100 days.

2.6.2 Binary Frequencies at Different Metallicities

WR Samples in LMC, SMC, and Milky Way

Before we can proceed to compare the binary frequencies among the respective WR subtypes in the different environments, we have to establish viable and comparable samples of WR populations. In the LMC, this task is straightforward, since the studies of Bartzakos et al. (2001, WC/WO), Foellmi et al. (2003b; WNE) and the present one (WNL) used the BAT99 catalogue to establish the program samples.

The present survey encompassed all 41 WNL stars listed in the BAT99 catalogue outside R136. The remaining 6 WNL stars in the core of R136 required adaptive-optics assisted spectroscopy with VLT/SINFONI; the work is in progress and results will be published elsewhere

(Schnurr et al., in prep.). Recall that Foellmi et al. (2003b) reclassified one of their program stars, BAT99-78, to WN6 (i.e. to WNL). In turn, one of our stars, BAT99-92, was recognized to be an early-type WN3b star (cf. Section 2.5.10). Thus, the respective numbers of WNE and WNL stars which have been studied remain unchanged: 61 WNE and 41 WNL. The number of WC/WO stars in the LMC is 24.

In the SMC, there are only 12 WR stars, which most likely constitute the complete population (Massey, priv. comm.) and which have all been studied (Bartzakos et al. 2001; Foellmi et al. 2003a; Foellmi 2004; and references therein). Thus, we now only need to establish a viable comparison sample in the Milky Way.

Binary frequencies among the Galactic WR stars have been quoted by many different authors. van der Hucht et al. (1988) derived a WR binary frequency of 37% among the WR stars in a limited volume of $d < 2.5$ kpc around the Sun. In contrast to this, Moffat (1989) counted 42% binaries among the Galactic WR population. In order to compare the binary frequency in the Galaxy to that in the Magellanic Clouds obtained here and by Bartzakos et al. (2001) and Foellmi et al. (2003a,b), one must be careful not to count binaries with periods above $\sim$ 160 days. Moreover, due to the metallicity gradient in the Milky Way, a volume-limited sample is required.

We have therefore constructed a Galactic WR sample at $\sim$solar metallicity. To take into account the metallicity gradient in the Galaxy, only those stars from van der Hucht's (2001) catalogue were selected which are located in the Galactocentric distance interval of R = [6.5kpc;9.5kpc] (the solar circle is taken at $R_{\odot} = 8.0$ kpc), and at a distance $d \leq 4$ kpc from Earth. In total 68 WR stars, 38 WC and 30 WN stars, were thus selected. Among the Galactic WN stars, there are 15 WNE and 15 WNL stars, when one applies the usual classification (WNE = WN2 to WN5, and WNL = WN6 to WN11).

Of course, the Galactic numbers can be but a gross estimate, since the precision of the

TABLE 2.20 – WR populations and population ratios for our three comparison samples. Note that the LMC sample does not include the 6 WNL stars in the core of R136, and that no distinction was made between WC and WO stars.

Group	Galaxy	LMC	SMC
WR total	68	126	12
WN total	30	102	11
WC total	38	24	1
WNE	15	61	9
WNL	15	41	2
WC/WN	38/30	24/102	1/11
WNE/WNL	15/15	61/ 41	9/ 2

distances does not allow one to apply firm limits, so completion issues remain. Also, not every star in this sample is equally well studied to firmly establish its binary status, nor have all stars been studied using homogeneous data sets, which of course raises the concern of bias. However, Galactic WR stars have, for obvious reasons, been studied much longer than extra-galactic WR stars, and since we are here only interested in relatively short-period binaries, it is not unreasonable to believe that overall, the constructed Galactic WR population is well enough studied to serve as a viable comparison sample.

The resulting comparison samples for the three differerent galaxies are listed in Table 2.20.

For reasons of simplicity, we shall refer to both WC and WO stars as "WC stars". It can immediately be seen from Table 2.20 that the WC/WN ratio is indeed strongly Z-dependent: At $Z_{\odot}$, there are more WC than WN stars (WC/WN=38/30=1.27), whereas in the LMC, the WN stars constitute more than three quarters of the WR population (WC/WN=24/102=0.24). In the SMC, the fraction WC/WN is even lower (WC/WN=1/11$\sim$0.1).

As was reported by Crowther (2000), spectral types of WR stars tend to be earlier at lower metallicities, since the wind is less opaque so that deeper, hotter layers of the atmosphere can be seen. Furthermore, higher contents of residual hydrogen due to lower mass-loss rates at lower Z decrease the wind opacity as well, to the same effect. This tendency is well observed among the respective WN populations, where the WNE/WNL ratio increases with decreasing

TABLE 2.21 – WR binary frequencies for three different environments.

Group	Galaxy	LMC	SMC
WN	9/30 = 0.30	16/102 = 0.15	4/11 = 0.36
WC	7/38 = 0.18	3/ 24 = 0.13	(1/ 1 = 1.00)
WR	16/68 = 0.24	19/126 = 0.15	5/12 = 0.42
WN8,9	0/ 4 = 0.00	0/ 8 = 0.00	not present

ambient Z.

2.6.3 Binary Frequencies Among the Different Samples

Before we proceed to discuss the binary frequencies in different galaxies, let us once more recall that the notion "binary" refers only to stars whose orbital period is shorter than ~ 160 days (i.e. we have included BAT99-119 with a period of 158.8 days, but see previous section). Thus, all stars referred to as "single" might very well be in a longer binary system, but neither do we have sufficiently good data to identify these systems, nor are they relevant for the scope of this study.

The binary frequencies among the samples in the three different environments are listed in Table 2.21. Note that any quoted binary frequency can only be regarded as a lower limit. While any true errors on the binary frequency can thus not be symmetric, they are very difficult to compute correctly. For an approach solely based on statistics (i.e. not taking into account any systematic errors), see Burgasser et al. (2003).

Moffat (1989) reported 6 binaries among the 14 WNL stars he had studied. Our study has added four previously unknown WNL binary systems to that list, and confirmed four known binaries and their orbital periods, one of which, BAT99-92, has been reclassified as WN3b. One star, BAT99-119, was already suspected to be a binary by Moffat (1989), but we were unable to determine the orbital period for the spectroscopic data alone. However, in a forthcoming paper (see Chapter 3), Schnurr et al. (2007) were able to use additional polarimetric data to find that BAT99-119 is indeed a binary with a 158.8 day period. Another of Moffat's

(1989) binaries, BAT99-107, was found to be a single star. One star newly classified as binary here, BAT99-12, might actually not be one but rather a rapid rotator that diplays cyclical LPVs, but currently we do not have enough data to rule out its binarity; hence, we will count BAT99-12 as binary. From significantly large RV scatter, its visual brightness, and its high X-ray luminosity, only one additional star, BAT99-118, qualifies as binary candidate. Thus, the total number of certain WNL binaries is 8, with one possible candidate (BAT99-118). This brings the confirmed WNL binary frequency to $8/41 = 20\%$.

Among the 61 WNE stars in the LMC, Foellmi et al. (2003b) reported only five certain binaries, two systems with unreliable orbital solutions (which we count as identified), and two potential binaries; we have added to this one of our binaries, BAT99-92, so that the confirmed binary frequency among the WNE stars in the LMC is now $8/61 = 13\%$. If one combines the results for WNE and WNL stars, one obtains 102 WN stars studied among which $8 + 8 = 16$ are confirmed binaries; thus, the confirmed binary frequency is $16/102 = 15\%$. Note that statistically, the binary frequencies among WNE and WNL stars are consistent with each other.

Among the 24 WC/WO stars, Bartzakos et al. (2001) studied 23 and reported three confirmed binaries. The 24^{th} star is very faint and thus likely single. While they also reported 5 potential binaries, even the one with the largest RV scatter, MG6, failed to be significantly (99% confidence level) variable; therefore, we consider their remaining binary candidates to be constant as well. This brings the binary frequency among 24 WC/WO stars in the LMC to 3; thus, the binary frequency is $3/24 = 13\%$. This value is fully consistent with the combined WN-binary frequency of 15% as well as with the binary frequencies of the respective subtypes WNE and WNL.

Foellmi et al. (2003a; see also Foellmi 2004) report 4 confirmed binaries and one binary candidate among the WN population in the SMC. The WN binary frequency is thus $4/12 = 33\%$. Bartzakos et al. (2001) reported the sole WC/WO star in the SMC, AB8, to be a confirmed binary. Thus, the binary frequency among the WC/WO "population" in the SMC is 100%.

Due to small-number statistics, we shall exclude the SMC WR population from further discussion, but it should be remembered that in principle, the binary frequency among SMC WR stars is consistent with that in the LMC and in the Milky Way (see below).

Among the Galactic WR stars, we considered binary systems with a confirmed orbital period up to 160 days as quoted by van der Hucht (2001); secondary criteria such as diluted emission lines and X-ray luminosities were however *not* considered, as they have proven to be misleading. Among the 38 WC stars are 7 confirmed binaries ($7/38 = 18\%$), and among the 30 WN stars are 9 confirmed binaries ($9/30 = 30\%$), which are practically evenly distributed: 4 (44%) contain WNL stars, and 5 (56%) contain WNE stars. In total, the binary frequency among Galactic WR stars is $16/68 = 24\%$.

Interestingly, it seems that in the Galaxy there are more binaries among the WN stars than among the WC stars. While one could suspect that this reflects an observational bias (WNL stars are brighter than WC stars, thereby easier to observe; however, WC stars have stronger lines), one has to guard oneself against small-number statistics. Indeed, a Pearson χ^2 test (e.g. Kreyszig 1975; see also Miller et al. 1990) shows that despite the large differences, the two binary frequencies among WC and WN stars are statistically consistent with each other (i.e., drawn form the same underlying distribution) at a 99% level. The same is true for the WN and WC populations in the LMC, which display remarkably similar binary frequencies.

Furthermore, it can be seen that in neither the Galactic nor the LMC sample, short-period ($P < 200$ days) binaries can be found among the WN8,9 stars – as a matter of fact, they yield the smallest RV scatter of our sample stars –, whereas WN6,7 stars do show binaries among them. This seems to confirm the findings of Moffat (1989), who suspected that this dichotomy reflected more deeper-going differences between WN6,7 and WN8,9 stars. He argued that Galactic WN8,9 stars tend to be runaway stars (an observation that we cannot confirm from the systemic velocities measured for our WN8,9 stars in our sample), and that in the LMC, WN8,9 stars tend to avoid clusters, very much unlike WN6,7 star. However, this

only reflects a tendency *in our Galactic sample* and not in the whole Milky Way: There are known binaries among the Galactic WN8 stars, like e.g. WR12[14] (Rauw et al. 1996), that do not appear in our comparison sample because they fall outside our applied distance limits.

Another striking feature is the apparent lack of binaries among the WN3 population of the LMC; among the 13 known WN3 stars, ony one, BAT99-92, is in a binary system, whereas 9 out of 39 known WN4 stars have been reported binary or binary candidate by Foellmi et al. (2003b), and the binary frequency among the WN5-7 stars is higher as well. However, a Pearson χ^2 test reveals that the binary frequency among the WN3 stars is consistent with that among the WN4 stars at a 99% level. This is mainly because of the small numbers of WN3 stars, which constrains only poorly the binary frequency among these stars. It is thus not impossible that this trend becomes statistically significant if the considered number of stars becomes larger.

Are the respective, total WR binary frequencies of the Galaxy and the LMC consistent with each other? A Pearson χ^2 test reveals that they are, at a 99.7% confidence level; the same is true when one considers the WN population in the SMC. This means that *there is no statistically significant difference between the WR binary frequency in the Magellanic Clouds and in the Galaxy.* This is in line with the conclusions published by Foellmi et al. (2003b).

2.6.4 Implications for Stellar Evolution

Bartzakos et al. (2001; updated by Foellmi et al. 2003a) computed the expected frequencies for interacting (RLOF) binaries among the WR populations at three different metallicities – Galaxy, LMC, and SMC – to be $20 \pm 6\%$, $52 \pm 14\%$, and $98 \pm 32\%$, respectively. A Pearson χ^2 test reveals that the binary frequency among our Galactic comparison sample is consistent with the predicted value; however, the observed binary frequencies in both the LMC and the

[14] At the time Moffat (1989) drew his conclusion about the lack of WN8,9 binaries, WR12 was classified as WN7 (see van der Hucht et al. 1981). WR12's spectral type was revised to WN8 only later, by Smith et al. (1996).

SMC rule out the predictions at a 99.9% confidence level. Thus, in the context of the old, non-rotating models by Maeder & Meynet (1994), RLOF in interacting binaries cannot be a viable solution to make the models match the observations.

The question remains whether the WR stars in binaries did become WR stars *because* their progenitors are members of a binary system, i.e. whether or not RLOF really occurred at some time in their evolution. Foellmi et al. (2003a) used prescriptions by Vanbeveren et al. (1998) to verify whether or not the WR progenitors had gone through a RLOF phase. Through considerations of the present-day periods and the required pre-RLOF period, they found that if RLOF occured in the SMC binaries, it most likely did not occur in all of them. A strong indication against the occurrence of RLOF in the binaries was, however, that many of them contain a significant fraction of residual H which should have been fully removed by RLOF and the subsequent onset of strong WR winds. However, the main problem is that there are no detailed model calculations available to better constrain the initial conditions, the mass-loss rates during RLOF, and the accretion rate onto the secondary star. The latter is of extreme importance because depending on whether the transferred mass leaves the system or is accreted by the secondary, the period of the binary system decreases or increases.

Petrovic et al. (2005) carried out these sorts of detailed studies on three Galactic WR binaries. They found that stellar rotation, which was included in their stellar-evolution models, dramatically decreases the mass-accretion rate onto the secondary, because the transfer of angular momentum quickly spins up the secondary to critical rotation; hence, it cannot further accrete more mass, and the mass is lost to the system. In that case, the system widens, which means that initial periods had to be shorter than the observed, present-day periods. This in turn means that RLOF took place early in the evolution, while the primary was still in its CHB phase, and again when the star expanded its envelope during SHB (so-called Case AB RLOF). If the system went through a common-envelope (CE) phase, however, the expulsion of the CE would tighten the binary; this scenario might be the only possibility to produce very-short period (below $\sim$10 days) WR+O binaries, even if the primary turns into a compact

LBV rather than into an extended RSG. One can conclude that for all practical purposes the question of RLOF cannot be answered in a general way, but has to be considered for different cases individually.

Thus, if RLOF in interacting binaries cannot account for the majority of WR stars in the Magellanic Clouds, what could be their formation history? Since 1994, theoretical modelling of stellar evolution has made considerable progress. Most of the advances are due to the inclusion of stellar rotation in the models, which previously was believed to generate second-order effects only. Maeder & Meynet (2000) found that rotationally-induced mixing during the CHB phase could enhance WR formation for the following reasons: *i*) The mixing-down of H into the H-burning core makes the core grow, thereby increasing its luminosity and thus, the mass-loss rates; moreover, mass-loss rates can be rotationally enhanced (see also Maeder 1999); *ii*) because the core is supplied with more fuel, the duration of the CHB phase is extended, and the star has more time to lose mass; *iii*) the mixing-up of CNO-cycle elements (He and N) enables the stars to reach the WN phase earlier; for instance, at solar Z, the most massive stars ($M_{\rm ini} \geq 60 M_{\odot}$) will reach the WN phase while still in the CHB phase.

With these new models, Meynet & Maeder (2005) were able to much better reproduce the observed WR populations in nearby galaxies without the need to resort to higher frequencies of interacting binaries. Also, rotation is able to somewhat alleviate the problem of the BSG/RSG ratio at different Z in that rotating models produce more RSGs at low Z than do non-rotating models (Maeder & Meynet 2000), and therefore better match the observations, something that other proposed solutions cannot explain.

However, while rotation certainly is a very important ingredient for stellar-evolution models, because after all, most O stars do rotate, there are still many open issues. To begin with, there are problems purely linked to the models: even the updated models lack important input physics. For instance, the inclusion of magnetic fields and the effects they have on the transport of angular momentum within the star is still in its infancy (Maeder & Meynet 2003, 2004).

First calculations show that magnetic fields produced by dynamos in differentially-rotating stars (Spruit 1999, 2002) lead to almost rigid-body rotation of the star, since the magnetic fields couple different layers together, thereby inhibiting the differential rotation that is their source. Obviously, a delicate equilibrium will arise, but the exact consequences are not yet fully understood (Maeder & Meynet 2004).

Then, mass-loss rates are, as they always have been, another important ingredient for evolutionary models, in particular those with rotation, since mass loss leads to loss of angular momentum of the outer layers of a star, thereby affecting the internal angular-momentum distribution, which in turn is crucial for the occurrence of mixing processes. The potential presence of magnetic fields increases the importance of knowing well the mass-loss rates in different evolutionary phases of massive stars. However, recent findings have upset the cart once again. Mass-loss rates of WR stars have recently been found to be Z dependent (Crowther et al. 2002; Vink & de Koter 2005), which has implications for the evolution of WR stars, while mass-loss rates of O stars are still debated. Bouret et al. (2005), Martins et al. (2005), and Fullerton et al. (2006) reported results of studies of Galactic O stars which indicate that mass-loss rates at least of some O stars are overestimated by factors of 10 to 100. The consequence of these findings, if they are confirmed, is that assumptions about the loss of angular momentum in rotating models have to be revised, because most stars do not lose enough mass to considerably spin down during their MS lifetime. Thus, initial rotation rates of massive O stars will not significantly differ from the observed, present-day rotation rates, which has consequences for the evolution of angular momentum in the stellar models. So far, Maeder & Meynet (2000) and Meynet & Maeder (2005) have used relatively high initial rotation rates (300 kms^{-1}); this value is not often observed in Galactic O stars, and it certainly does not represent the *average* rotation rate.

The general expection is that at lower Z, rotation rates are initially higher (due to the decreased opacity, the stars are more compact) and remain high for a longer time than in high-Z environments, because the Z-dependent, reduced mass loss also reduces the loss of

angular momentum. The results of Maeder et al. (1999) indicate that at lower Z, there is a higher ratio of Be/B stars; if the Be phenomenon is indeed directly caused by rapid rotation, than these findings suggest that rotation rates increase with decreasing Z, at least in the case of B stars. Penny et al. (2004) from UV spectroscopy of early LMC and SMC stars find that O-type stars do not appear to rotate faster than their Galactic counterparts. However, they studied a relatively small sample ($\sim$ 20 stars per galaxy), which might lead to uncertain small-number statistics. A more comprehensive study of 100 early B-type MS stars in the LMC was carried out by Keller (2004). He finds that the stars in the LMC are indeed more rapid rotators than in the Galaxy. Recently, the VLT-FLAMES Survey of Massive Stars (Evans et al. 2005) was completed, and first results were published by Mokiem et al. (2006). While these authors observed only 31 O- and early B-type stars, of which 21 are located in only one SMC cluster, NGC 346, their results lead to the tentative conclusion that rotation rates of unevolved SMC stars are significantly different from those observed in unevolved Galactic stars. However, one must again bear in mind that all these studies suffer from small-number statistics, and Mokiem et al.'s (2006) study focusses on only one cluster. That it is dangerous to generalize from one cluster to the properties of all stars in the host galaxy, is well illustrated by the Galactic cluster NGC 7419, which, although at $\sim Z_{\odot}$, shows a large fraction Be/B as well, contrary to what one might expect (see Caron et al. 2003). Comparison of rotation rates in NGC 7419 and NGC 346 *alone* would thus reveal that there are no significant differences between the Galaxy and the SMC, something which might be refuted by a larger-scale study.

Hence, much more systematic and comprehensive, large-scale studies of rotation rates at different Z are required to obtain firm observational results as input for evolution models. While the VLT-Flames survey will certainly greatly extend our knowledge on this topic, one has to bear in mind that even in our Galaxy, stars do rotate. Thus, any effects introduced by rotation can only be *differential* and thus possibly small enough to be swamped by "noise" in the form of cosmic scatter. However, the Geneva group repeatedly points out (e.g. Meynet & Maeder 2005), that the comparison between observed and theoretically predicted rotation rates for stars with large masses ($M \gtrsim 30 M_{\odot}$) is really much more a test bearing on the mass-

loss rates than a test of the internal coupling and evolution of rotation. It might therefore be that this question cannot be settled by brute-force, large-number statistical approaches alone.

Recently, Hamann et al. (2006) published new grids of model atmospheres for Galactic WN stars that include the latest input physics. From the stellar parameters obtained by these calculations, they constructed a Hertzsprung-Russell diagramm (HRD), and compared it with a theroretical HRD obtained from both rotating and non-rotating, stellar-evolution models of the Geneva group. The results were surpringly disappointing in that there was no preference for evolution tracks that account for stellar rotation. In particular, the evolution models produce low-luminosity WN stars which show substantial amounts of residual H in their atmospheres, whereas the atmosphere analyses reveal that most such stars are fully H-depleted.

2.6.5 Comments on Foellmi et al.'s (2003b) Classification

In this context, we also revisit the idea of Foellmi et al. (2003b) who, based on a study by Smith & Maeder (1998), developed their concept of new "evolutionary" WR classes, proposing that only WNb stars from Smith et al.'s (1996) classification system were the true, fully-hydrogen depleted WNE stars. Thus, Foellmi et al. (2003b) called them eWNE ("e" stands for evolutionary). Traditionally, theoreticians regard WNE stars as fully H-depleted, while WNL stars are those which contain residual H (e.g. Vanbeveren & Conti 1980). This purely chemical distinction has led to a lot of confusion between observers and theoreticians, since it renders very difficult the comparison of observational results and theoretical predictions. So, it seemed very attractive that only WNb stars were fully H-depleted eWNE stars, because then, more meaningful comparisons could be made. Indeed, Meynet & Maeder (e.g. 2005) apply this classification scheme. However, Foellmi et al.'s (2003b) approach is flawed in several ways.

First, it has to be recalled that the suffix "b" was introduced by Smith et al. (1996) based purely on grounds of obtaining a clearer WR classification, but not on stellar physics. This

is a viable and justified approach in terms of morphological classification since of course, any stellar-classification scheme is naturally based on morphology. However, one has to bear in mind that Smith et al.'s classification worked fine for *Galactic* WN stars, but there is no physical reason why fully H-depleted WN stars at different (in particular, lower) Z should have emission lines that qualify as "broad" in Smith et al.'s sense (they used a cut-off value of 30 and 40 Å, respectively, for the FWHM of the HeIIλ4686 emission and for the EW of the HeIIλ5412 emission.). Moreover, Hamann et al. (2006) have shown that spectra of some WNo stars, i.e. WN stars which do not show broad emission lines nor detectable H, can be best fit by fully H-depleted model atmospheres. Thus, if one bases eWNE number statistics purely on the b criterion, as was proposed by Foellmi et al. (2003b), one misses *a substantial and* a priori *unkown fraction of truly H-depleted WN stars.*

Furthermore, Foellmi et al. (2003b) defined all WN6-7ha stars to be non-classical WR stars, i.e. extreme O stars in the CHB phase. Some of the O3f/WN6 stars, i.e. certainly H-burning objects, have been reclassified into WN5ha, thereby diluting the fraction of classical, He-burning WN5 stars. Again, this cannot be known *a priori*, as cannot be known how this changes with Z. However, Crowther (2000) has shown that at lower Z, stars will display earlier types (due to the reduced wind opacity, one sees deeper, hotter layers of the star). Also, a mere change in Z will affect the emission-line strengths (Crowther & Hadfield 2006), which in turn affects the spectral classification (which relies on line-strength ratios).

Foellmi et al. (2003b), based on their new classification, re-calculated number ratios. Most strikingly, the new ratio fitted very well the model predictions of Maeder & Meynet (1994), i.e. those models with too high mass-loss rates and without rotation, without having to resort to a larger frequency of interacting binaries. Furthermore, Foellmi et al. speculated that the presence of residual H in the atmospheres of even the earliest WN stars in the SMC and of a large fraction of LMC WN stars not only were an indication against the occurrence of RLOF (see above), but also an indication that rotationally-induced down-mixing of H into deeper layers had taken place, just as Maeder & Meynet (2000) had predicted. In turn, it is expected

that in the Galaxy, where rotation is expected to have a smaller influence on stellar evolution due to rapid loss of angular momentum, there are more fully H-depleted, eWNE stars.

However, a quick number count among both the LMC and the Galactic comparison sample constructed above reveals that this is not so, if one takes the eWNE class at face value. While in the LMC, we count 32 WNb out of 102 WN stars, i.e. a fraction of $32/102 = 31\%$, we find 8 WNb stars among the 31 WN stars in our Galactic sample, i.e. a fraction of only $8/31 = 26\%$. Omitting small-number statistics for the moment, one could get the impression that there are indeed *more* fully H-depleted WN stars at *lower* metallicity, just the contrary to what is expected if rotation really is the deciding factor. However, this result is of course affected by small-number statistics, so that we find that these WNb frequencies are statistically constistent with each other. Most remarkably, though, none of the Galactic WNb stars resides in a binary system, thus the H-rich envelope had to be removed through some single-star mechanism. This is even more in contradiction to what is expected from rotation; thus, it is very difficult to establish useful tests for the influence of rotation.

As was noted above, the number of truly H-depleted WN stars will be underestimated if some WNo stars are excluded from the eWNE class. A formally correct treatment of this issue would thus require that one obtains H contents of all WN stars by means of atmosphere modelling (and relying entirely on the quality of the models) to perform the correct number count for either the eWNE, eWNL, or eO class. The obvious consequence is that one cannot rely on the spectral appearance of a WN star to derive its internal structure. One has to bear in mind that this is a principal problem that cannot be solved by large-scale statistical approaches, e.g. by simply increasing the numbers of observed WR stars. This issue will most likely not be solved before there are fully self-consistent models of both internal structure and atmosphere.

2.6.6 Rotation and Binarity

Before we summarize and conclude this study, we shall comment on the effects that the inclusion of rotation in stellar models has on the potential occurrence of Case B RLOF in O+O binaries, i.e. mass transfer during the SHB phase. We have already mentioned that for RLOF to happen, the primary has to expand its envelope beyond its Roche limit. However, if the primary is initially too massive (the canonical mass limit is $M_{\rm i} \gtrsim 40 M_{\odot}$), it cannot reach the RSG phase but rather experiences the LBV stage at a much smaller stellar radius. Only if the binary system is very close, the stars might be sufficiently close so that the primary exceeds its Roche lobe before reaching its Eddington or Γ instability limit. In this case, RLOF is in competition with the huge, episodic mass loss experienced in LBV outbursts. It is clear, however, that the occurrence of RLOF in somewhat wider binaries, where the Roche lobe is larger than the radius of the potential LBV, critically depends on whether the primary is capable (as a single star) of turning into an extended RSG or not. Presently, the canonical initial-mass range for an O star to become a RSG is 25 to 40 $M_{\odot}$ (but see Massey et al. 2007).

Model calculations with rotation (e.g. Maeder & Meynet 2000) show that lower-mass massive stars do not lose enough mass (and thus, angular momentum) to significantly slow down during their MS evolution. This means that when the star experiences a brief, overall contraction at the end of its CHB phase, the star might spin up to over-critical rotation rates, i.e. experience its so-called Ω limit. This over-critical rotation might dramatically enhance mass-loss rates and be responsible for the bipolar shape of LBV nebulae as e.g. in the case of the Galactic LBV η Carinae (Maeder 2002). This is particularly the case if the star is already close to its Γ limit, which is why the combination of those two limits has been coined $\Gamma\Omega$ limit (Langer 1998; see also Maeder & Meynet 2000b and references therein). Indeed, there is direct evidence that one of the lower-luminosity LBVs, AG Carinae, displays rapid rotation at a significant fraction of its break-up velocity (Groh et al. 2006).

In very close binaries, tidal interaction between the two stars quickly leads to co-rotation, i.e. the stellar spin and the orbital rotation couple. This might mean that even if the primary

loses considerable amounts of angular momentum, it can be replenished from the reservoir of angular momentum which is stored in the orbital motion. To the best of our knowledge, the evolution of rotation in tidally coupled binaries has not yet been subject of detailed analysis. However, one might theorize that the effects of stellar rotation are more pronounced in close massive binaries, because such systems are able to maintain their spin rates for a longer time than in wider binaries (tidal interaction is a strong function of the distance, and $\propto r^{-3}$; see e.g. Zahn 1977). Thus, close binaries will not evolve as single stars of the same mass even while still in the CHB phase (see also Massey et al. 2002).

On the other hand, rotation might inhibit the formation of RSGs. As can be derived from the Geneva evolution tracks (e.g. Maeder & Meynet 2000), lower-mass, rotating O stars evolve to higher luminosities than non-rotating O stars. Given the fact that canonical mass-loss rates of O stars are on the constant decrease because of clumping etc. (see above), so are the rates of loss of angular momentum. It might therefore very well be that rotating O stars do indeed *not* turn into RSG even below the canonical $40M_{\odot}$ limit, but possibly only for very much lower initial masses. This is in line with empirical evidence that, with the possible exception of Westerlund 1 (Clark et al. 2005; Crowther et al. 2006), there seems to be no known coeval cluster which contains both RSGs and classical WR stars, be the latter binary or not (Mermillod, private communication; Massey, private communication). This might indicate that WR stars are not post-RLOF descendents of RSGs because even O stars in the mass range of, say, $25M_{\odot} \lesssim M_{\rm i} \lesssim 40M_{\odot}$ do not reach the RSG phase, but go through the LBV stage instead. Obviously, in this case, the required conditions for the occurrence of RLOF would then be dramatically changed in that only the very closest O+O binaries can undergo mass-transfer events. Thus, number ratios computed by Bartzakos et al. (2001), which are affected by old-model deficiencies (Maeder & Meynet 1994), have to be recalculated based on more sophisticated models for different Z which include rotation and up-to-date mass-loss rates, along with detailed hydrodynamical computations of the RLOF process itself. It is only after having obtained a clear, theoretical picture of stellar evolution in interacting binaries that one can construct meaningful observational tests. Thus, in this context, from the fact that we did

not confirm the prediction by Bartzakos et al. (2001), it cannot be concluded irrefutably that RLOF does not play a role in WR formation when it comes to very low ambient metallicities, although it seems that RLOF can be excluded for all but the initially closest O+O systems.

2.7 Summary and Conclusion

We have carried out spectroscopic monitoring of all 41 (actually 40, after eliminating BAT99-92 which is now WNE) WNL stars in the LMC that could be reached by conventional, ground-based observations. We also used publicly available b and r band photometry from the MACHO project, and analysed archival X-ray data from the *ROSAT* and *Chandra* missions.

Measured RV curves were subjected to a period analysis to identify the binaries among our sample with orbital periods up to $\sim$ 200 days. In this period range, we found four new binaries, confirmed the previously known 5 binaries, and identified one previously suspected binary as single (i.e., not a binary with an orbital period in the quoted range). One binary candidate was identified from its RV scatter, but no period could be established. Remarkably, all but one binary contain hydrogen-rich WN5-7ha stars, which most likely are extreme, superluminous, and hence very massive super-Of stars, and possibly even the most massive stars known. These binaries offer the tremendous opportunity to directly weigh these extreme stars using model-independent, Keplerian orbits. Follow-up observations have partly been obtained and are currently reduced, or are under way. The results of these observations will be published elsewhere.

We combined our results with those obtained in earlier studies of other WR subtypes in the Magellanic Clouds (WC/WO: Bartzakos et al., 2001; WNE: Foellmi et al. 2003a,b; Foellmi 2004) and were able to draw, for the first time, a complete and homogeneous picture of the WR population in the Magellanic Clouds. We also constructed a Galactic comparison sample at $\sim$solar metallicity to study the influence of binarity on WR-star formation at different Z.

Our findings indicate, as was already concluded by the ealier studies, that the contribution of Roche-lobe overflow (RLOF) in O+O binaries to the WR-star formation does not significantly increase as the ambient metallicity Z decreases. We find in fact that the binary frequencies observed in the LMC and the Galactic sample are statistically consistent with each other. Thereby we rule out that at lower Z, a larger fraction of interacting binaries is required to form WR stars, a mechanism that Maeder & Meynet (1994) had required to match the observed WR populations at different Z to their prediction obtained from non-rotating models.

We do point out, however, that our study might suffer from too-small population numbers to allow for the detection of the anticipated, small, differential effects between the Galaxy and the LMC. This is particularly true since new, updated models not only affect single-star evolution, but also the occurence of RLOF in close binaries by probably lowering the upper mass limits at which an O stars turns into a RSG rather than experiencing the LBV stage. Also, we have not found any direct evidence that supports the hypothesis that single WR stars have been formed because of a larger influence of rotation at lower Z. This, too, might indicate that the difference in Z between the Galaxy and the LMC is too small to allow for the significant detection of any anticipated effects rotation may have.

Our study has contributed to establish a well studied WR population in the LMC which can be used as a referenc sample. We therefore strongly promote the establishment and study of as complete a WR population as possible in environments with Z strongly different from that of the LMC, in order to assess, by comparison with the LMC sample, the influence of metallicity, rotation, and binarity on the evolution of massive stars.

Chapter 3

FIRST ORBITAL SOLUTION FOR THE MASSIVE BINARY R145 (≡ BAT99-119 ≡ Brey 90)

O.Schnurr[1] A.F.J. Moffat[1], A. Villar-Sbaffi[1], N. St-Louis[1]

N.I. Morrell[2]

In preparation for MNRAS

[1]Département de Physique, Université de Montréal, C.P. 6128, Succ. Centre-Ville, Montréal, Québec H3C 3J7, Canada; [redacted]

[2]Las Campanas Observatory, Observatories of the Carnegie Institution of Washington, Casilla 601, La Serena, Chile; [redacted]

3.1 Abstract

We report the results of a spectroscopic and polarimetric study of the massive, hydrogen-rich WN6h stars R144 (= HD 38282 = BAT99-118 = Brey 89) and R145 (HDE 269928 = BAT99-119 = Brey 90) in the LMC. Both stars have been suspected to be binaries by previous studies (R144: Schnurr et al. 2007; R145: Moffat 1989). We combined radial-velocity (RV) data from Chapter 2 and Moffat (1989), and previously unpublished polarimetric data. For R145, we were able to establish, for the first time, the orbital period of 158.8 days, along with the full set of orbital parameters, including the inclination angle i, which was found to be $i = 39° \pm 6°$. By applying a modified version of the shift-and-add method developed by Demers et al. (2002), we were able to isolate the spectral signature of the very faint companion star. Having found its RV amplitude, we were thus able to estimate the absolute masses of the two components in R145. We find $M_{WR} sin^3 i = 126 \pm 32 M_\odot$ and $M_O sin^3 i = 55 \pm 21 M_\odot$ for the WR and the O component, respectively. Given the low inclination of 39°, the true masses must be even higher. This makes R145 the most massive star weighed so far. As to R144, however, the combined data sets are not sufficient to find any periodicity. More and better data are required to firmly establish the nature of this potentially very massive and thus very important system.

3.2 Introduction

What are the most massive stars, and how massive are they? Recent models maintain that the primordial (Population III) stars are extremely massive, with masses from ~100 to $1000 M_\odot$ (Ostriker & Gnedin 1996; Nakamura & Umemura 2001; Schaerer 2002). However, even under present-day conditions, i.e. in the Local Group and at non-zero metallicity Z, massive stars remain poorly understood. Fundamental questions of stellar astrophysics suffer from an almost complete lack of truly empirical evidence when it comes to stars with the highest masses both on and evolved off the main sequence.

Herrero et al. (1992) were the first to note the sharp mismatch between stellar masses

obtained from spectroscopic analysis and those from stellar evolution models. While with updated models the *systematic* discrepancy is now reduced, there still remain significant differences in individual cases (Herrero et al. 2002). Also, with new evolution models including stellar rotation (Maeder & Meynet 2000), which are once again upsetting the apple cart, one wonders how far we are from having a self-consistent, overall picture of the upper MS, i.e. at masses above $100M_{\odot}$. With respect to the IMF, it is thus still uncertain at what mass an upper cut-off really occurs, if at all, although recent studies put forward both theoretical and observational arguments in favor of a cut-off in the Galaxy around $\sim 150M_{\odot}$ (Weidner & Kroupa 2004; Figer 2005).

Clearly, calibration of the models is urgently required. The only model-independent way to directly measure stellar masses is by Keplerian orbits in binary systems. So far, however, only three very massive-star systems have been reliably "weighed": the two Galactic Wolf-Rayet (WR) stars WR22 ($55M_{\odot}$ for the WN6ha component; Rauw et al., 1996; Schweickhardt et al. 1999) and WR20a (83 and $82M_{\odot}$ for both WN6ha components; Rauw et al. 2004; Bonanos et al. 2004), and R136-38, containing an O3V star just outside R136 in the LMC ($57M_{\odot}$; Massey et al. 2002). Thus, it can be stated that the most massive stars are not found among main-sequence O stars, but more likely among a superluminous subtype of WR stars, the so-called WN5-7ha stars. At least some of these WN5-7ha are young, unevolved, hydrogen-rich stars on the main sequence (de Koter et al. 1997; Crowther & Dessart 1998) above O2-3 stars rather than "classical" WR stars, which are usually identified with evolved, massive stars with compact, helium-burning cores. WN5-7ha stars mimic WR stars since their tremendous luminosity, a result of their extremely high masses, drives a dense and fast wind which gives rise to WR-like emission lines. The very massive WN components in both WR22 and WR20a belong to the WN5-7ha class, which lends additional weight to this idea.

In a recent, intense survey of *all* WNL stars in the LMC, Schnurr et al. (2007; hereafter referred to as S07; see also Chapter 2) used 2m-class telescopes to obtain repeated, intermediate-quality (R=1000, S/N$\sim$80) spectra in order to assess the binary status of the 41 targets from

radial-velocity (RV) variations. Schnurr et al. (2007) identified four new binaries containing WN5-7ha stars, bringing the total number of known WNLha binaries in the LMC to nine. However, for one of the known binaries, R145 (= HDE 269928 = BAT99-119 = Brey 90), the preliminary 25.4-day period reported by Moffat (1989) could not be confirmed, but neither could a coherent period be established from the RV data of this study alone. Therefore, we combined S07's RVs with those published by Moffat (1989), and with previously unpublished polarimetry. It was only after the combination that we were able to find the true orbital period of this system as well as other orbital parameters.

From both its RV and EW variations and its high X-ray luminosity, S07 identified another WN6ha star, R144 (= HD 38282 = BAT99-118 = Brey 89), to be a binary candidate, although Moffat (1989) had identified this star as probably single. In terms of spectral type, R144 is almost a perfect clone of R145; however, at the ~same bolometric correction and after allowing for differential interstellar extinction, R144 is ~ 0.5 mag brighter than R145. Indeed, Crowther & Dessart (1998), using old atmosphere models, derived a spectroscopic mass in excess of $100 M_{\odot}$, and a luminosity of $\log L/L_{\odot} = 6.34$ for R144, which makes this star the most luminous WR star known in the Local Group. New, updated models most likely would yield an even higher mass and luminosity for this extreme object. Since there is also unpublished polarimetry for R144, we have revisited this object as well, using the spectroscopic data obtained by S07.

In the present paper, we will report the results of this study. In Section 3.3, we will briefly describe the observations and the data reduction. In Section 3.4, we will describe the analysis of our data and present the results. The paper is then summarized in Section 3.5.

3.3 Observations and Data Reduction

3.3.1 Spectroscopy

The spectroscopic observations are described in detail in S07. We briefly recapitulate here that long-slit spectrographs attached to ground-based, southern, 2m-class telescopes were used. Data were obtained in three campaigns or "epochs" between 2001 and 2003 to maximize the time coverage, and were carried out during 13 runs at 6 different telescopes. The spectral coverage varied from one instrument to another, but all spectrographs had the region from 4000 to 5000 Å in common, thereby comprising the strategic emission lines HeIIλ4686 and NIVλ4058.

Data were reduced in the standard manner using NOAO-IRAF[3], and corrected for systematic shifts among different observatories (see S07 for more details). The achieved linear dispersion varied from 0.65 Å/pixel to 1.64 Å/pixel, but all data were uniformly rebinned to 1.65 Å/pixel, thereby yielding a conservative 3-pixel resolving power of $R \sim 1000$. The achieved signal-to-noise (S/N) ratio was ~ 120 per resolution element for both stars, as measured in the continuum region between 5050 and 5350 Å.

Additional RV data for R144 and R145 were taken from Moffat (1989; hereafter M89), to which we refer for more details on the data acquisition and reduction.

3.3.2 Polarimetry

Linear polarimetry in white light was obtained during a total of six observing runs between October 1988 and May 1990 at the 2.2m telescope of the Complejo Astronómico El Leoncito (CASLEO) near San Juan, Argentina, with VATPOL (Magalhães et al. 1984), and at the ESO/MPG-2.2m telescope at La Silla, Chile, with PISCO (Stahl et al. 1986). RCA GaAs

[3]IRAF is distributed by the National Optical Astronomy Observatories, which are operated by the Association of Universities for Research in Astronomy, Inc., under cooperative agreement with the National Science Foundation.

phototubes were employed in both cases. Exposure times were typically 15 minutes per data point. Appropriate standard stars were taken to calibrate the polarization angle and the zero level, and exposures of the adjacent sky were obtained to correct for the background count rates.

The polarimetric data were calibrated the ususal way (e.g. Villar-Sbaffi et al. 2006). Since Thompson scattering is wavelength-independent (i.e. grey), and the differences between the sensitivity curves of the respective detectors are small, no correction for the different passbands was deemed necessary. However, a small instrumental offset between PISCO and VATPOL was found in polarization; we therefore have added $\Delta Q = +0.10\%$ and $\Delta U = 0.10\%$ to the PISCO data to match the VATPOL data, on average. The final data for R144 and R145 are listed in Tables 3.1 and 3.2, respectively.

Taken at face value, statistics reveal that R144 displays a rather small scatter (standard deviation) in both Stokes parameters, 0.052% and 0.063% in Q and U, respectively; by comparison, the quoted error per data point is only ~half this. However, one can clearly see that over the observation period of ~15 days, the polarization in Stokes-U increases constantly by ~0.2% (i.e. almost ten times the quoted error per data point), which is a strong indication that some coherent process is involved, e.g. a (longer-period) binary motion. R145, on the other hand, is much more variable; the scatter is 0.26% and 0.20%, respectively, in Q and U, with well defined and coherent variability episodes. The data are shown in Figures 3.1 and 3.2.

3.4 Data Analysis and Results

3.4.1 Spectroscopic Data

We here only briefly describe the methods employed to extract radial velocities (RVs) from the spectra (for details we refer the reader to S07 and references therein): Cross-correlation (CC) and emission-line fitting (ELF), using routines programmed around the ESO-MIDAS

TABLE 3.1 – Linear polarimetry for R144, obtained with VATPOL at CASLEO over a two-week period in January 1990.

JD	Q	U	Δ
2447907.783	-0.292	0.175	0.022
2447908.819	-0.213	0.112	0.031
2447909.813	-0.103	0.099	0.028
2447910.681	-0.136	0.206	0.020
2447911.754	-0.131	0.204	0.026
2447912.754	-0.084	0.160	0.025
2447913.566	-0.162	0.188	0.020
2447914.628	-0.134	0.213	0.035
2447915.762	-0.138	0.220	0.021
2447916.758	-0.103	0.232	0.028
2447917.803	-0.194	0.218	0.030
2447919.763	-0.179	0.308	0.031
2447920.753	-0.173	0.277	0.025
2447921.699	-0.180	0.279	0.025
2447923.789	-0.170	0.310	0.025

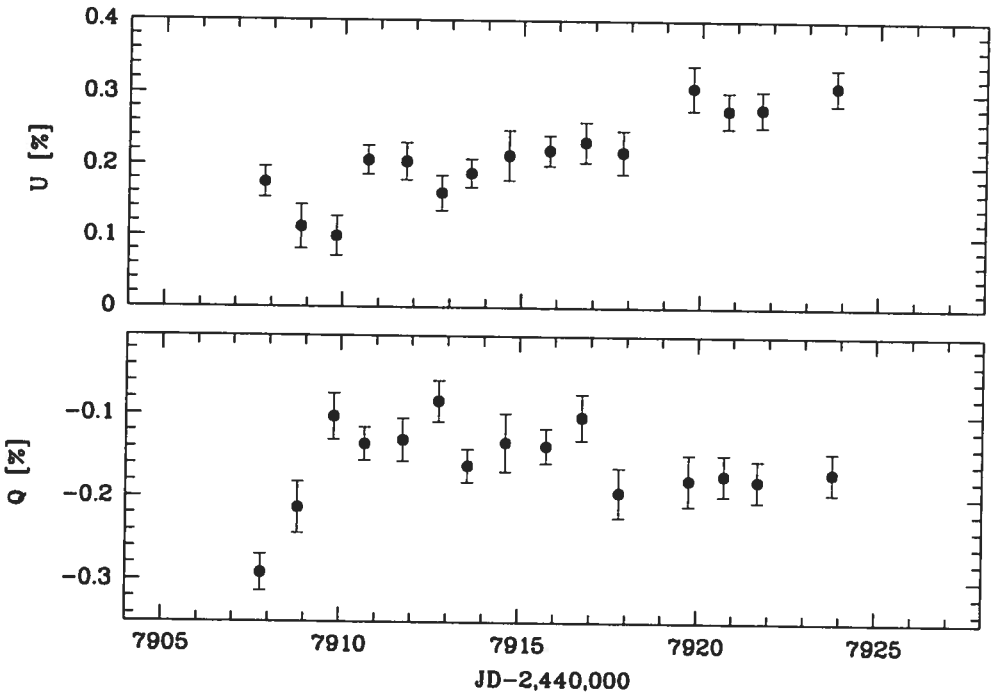

FIGURE 3.1 – Polarimetric data for R144 plotted versus Julian date.

tasks XCORR/IMA and FIT/IMA, respectively. Since the spectra of both R144 and R145 are largely dominated by the strong HeIIλ4686 emission line (see Figure 3.3), we initially

TABLE 3.2 – Linear polarimetry for R145, obtained with PISCO at ESO and VATPOL at CASLEO, between October 1988 and May 1990.

JD	Q	ΔQ	U	ΔU	Instrument
2447438.872	-2.244	0.028	0.552	0.028	PISCO
2447440.856	-1.746	0.020	0.551	0.020	PISCO
2447442.832	-1.517	0.020	0.447	0.020	PISCO
2447444.810	-1.386	0.022	0.811	0.022	PISCO
2447446.838	-1.718	0.024	1.119	0.024	PISCO
2447449.858	-2.626	0.027	0.822	0.027	PISCO
2447449.839	-2.542	0.025	0.573	0.025	PISCO
2447451.853	-2.029	0.024	0.457	0.024	PISCO
2447452.852	-1.771	0.025	0.408	0.025	PISCO
2447437.859	-2.048	0.032	0.473	0.032	VATPOL
2447438.849	-1.969	0.029	0.476	0.029	VATPOL
2447439.843	-1.926	0.027	0.502	0.027	VATPOL
2447440.856	-1.835	0.019	0.451	0.019	VATPOL
2447441.854	-1.839	0.027	0.472	0.027	VATPOL
2447442.873	-1.502	0.038	0.589	0.038	VATPOL
2447444.848	-1.586	0.023	0.843	0.023	VATPOL
2447445.858	-1.748	0.027	1.009	0.027	VATPOL
2447472.852	-2.202	0.029	0.388	0.029	VATPOL
2447473.810	-2.105	0.021	0.800	0.021	VATPOL
2447476.819	-2.198	0.021	0.714	0.021	VATPOL
2447477.812	-2.181	0.021	0.642	0.021	VATPOL
2447478.815	-2.211	0.023	0.676	0.023	VATPOL
2447479.803	-2.182	0.018	0.701	0.018	VATPOL
2447480.824	-2.162	0.020	0.736	0.020	VATPOL
2447481.819	-2.238	0.021	0.736	0.021	VATPOL
2447482.772	-2.131	0.019	0.693	0.019	VATPOL
2447860.775	-2.259	0.016	0.614	0.016	VATPOL
2447861.785	-2.236	0.017	0.591	0.017	VATPOL
2447862.779	-2.155	0.020	0.618	0.021	VATPOL
2447863.807	-2.258	0.019	0.682	0.019	VATPOL
2447864.793	-2.183	0.017	0.626	0.017	VATPOL
2447865.715	-2.218	0.018	0.569	0.018	VATPOL
2447866.733	-2.157	0.014	0.635	0.014	VATPOL
2447907.768	-2.301	0.019	0.567	0.019	VATPOL
2447908.808	-2.356	0.033	0.309	0.033	VATPOL
2447909.802	-2.261	0.029	0.150	0.029	VATPOL
2447910.671	-2.236	0.027	0.186	0.027	VATPOL
2447911.745	-2.061	0.029	0.329	0.029	VATPOL
2447912.742	-2.124	0.029	0.462	0.029	VATPOL
2447913.379	-2.024	0.025	0.430	0.025	VATPOL
2447915.774	-2.038	0.031	0.418	0.031	VATPOL
2447916.772	-1.884	0.021	0.496	0.021	VATPOL
2447917.792	-1.877	0.029	0.417	0.029	VATPOL
2447918.713	-1.921	0.025	0.518	0.025	VATPOL
2447919.751	-1.716	0.028	0.550	0.028	VATPOL
2447920.739	-1.732	0.027	0.644	0.027	VATPOL
2447921.690	-1.692	0.025	0.912	0.025	VATPOL
2447922.733	-1.849	0.027	1.040	0.027	VATPOL
2447923.772	-2.216	0.027	1.090	0.027	VATPOL
2447974.536	-2.186	0.024	0.719	0.024	VATPOL
2447975.531	-2.229	0.028	0.654	0.028	VATPOL
2447976.579	-2.239	0.032	0.648	0.032	VATPOL
2447977.559	-2.244	0.030	0.607	0.030	VATPOL

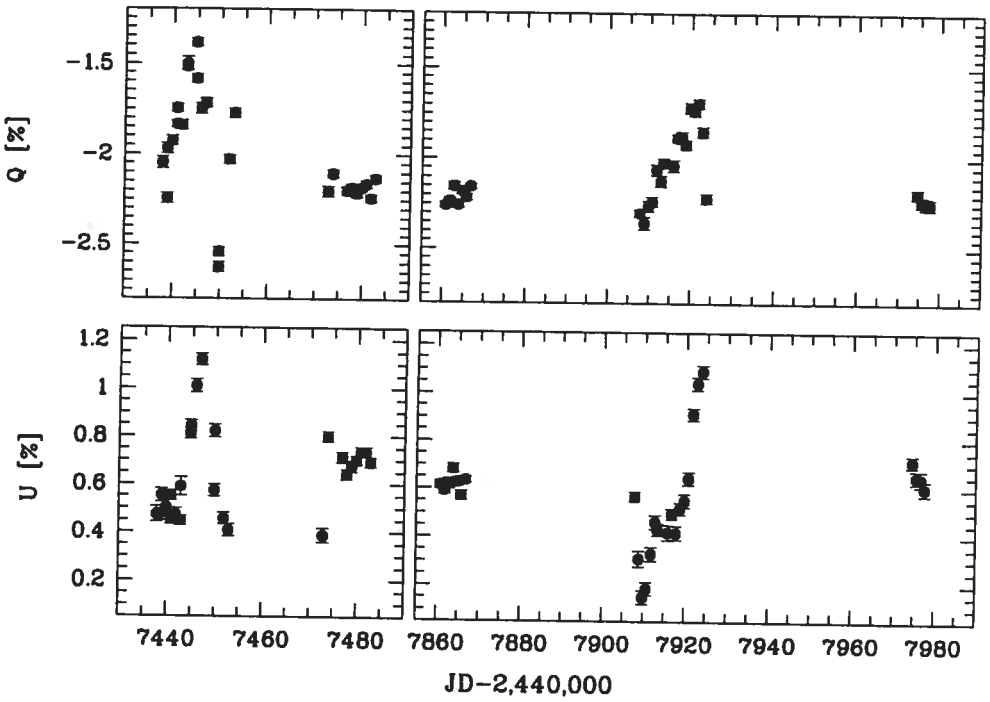

FIGURE 3.2 – Same as Figure 3.1, but for R145. Note the enormous amplitude of ∼1%, rarely seen so large in other WR+O systems.

confined the CC to the spectral region from 4600 to 4800 Å and used an iterative approach; contrary to S07, however, we also used the HeIIλ5412 line in order to derive RVs for R145. Unforntunately, the NIVλ4058 line yielded much worse results than HeIIλ5412 (see SO7 for a discussion), and was therefore not further considered in this study.

ELF was used to obtain independent measures of the RVs of our program stars. For both R144 and R145, ELF yielded a slightly larger RV scatter, therefore the results from XCORR will be used throughout this paper. However, ELF was used to obtain absolute, systemic velocities. These were used to correct the relative RVs obtained by XCORR. Also, M89 used ELF of the HeIIλ4686 emission line to extract RVs from his spectra; hence, RVs obtained from ELF of our data were used to combine both data sets. The combined RV data are shown in Figure 3.4 and Figure 3.5.

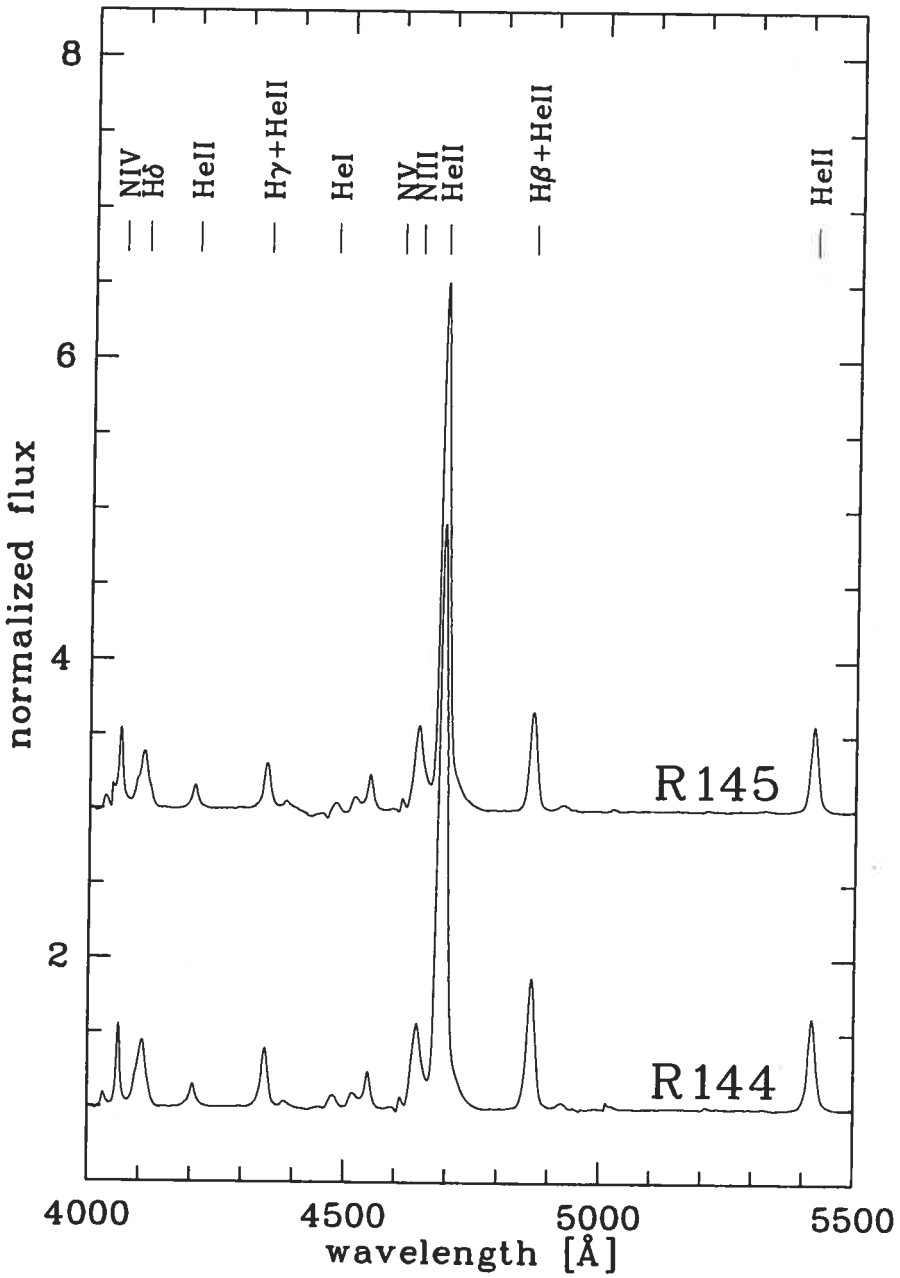

FIGURE 3.3 – Mean spectra of R144 (*bottom*) and R145 (*top*). For clarity, the upper spectrum has been shifted by 2 flux units.

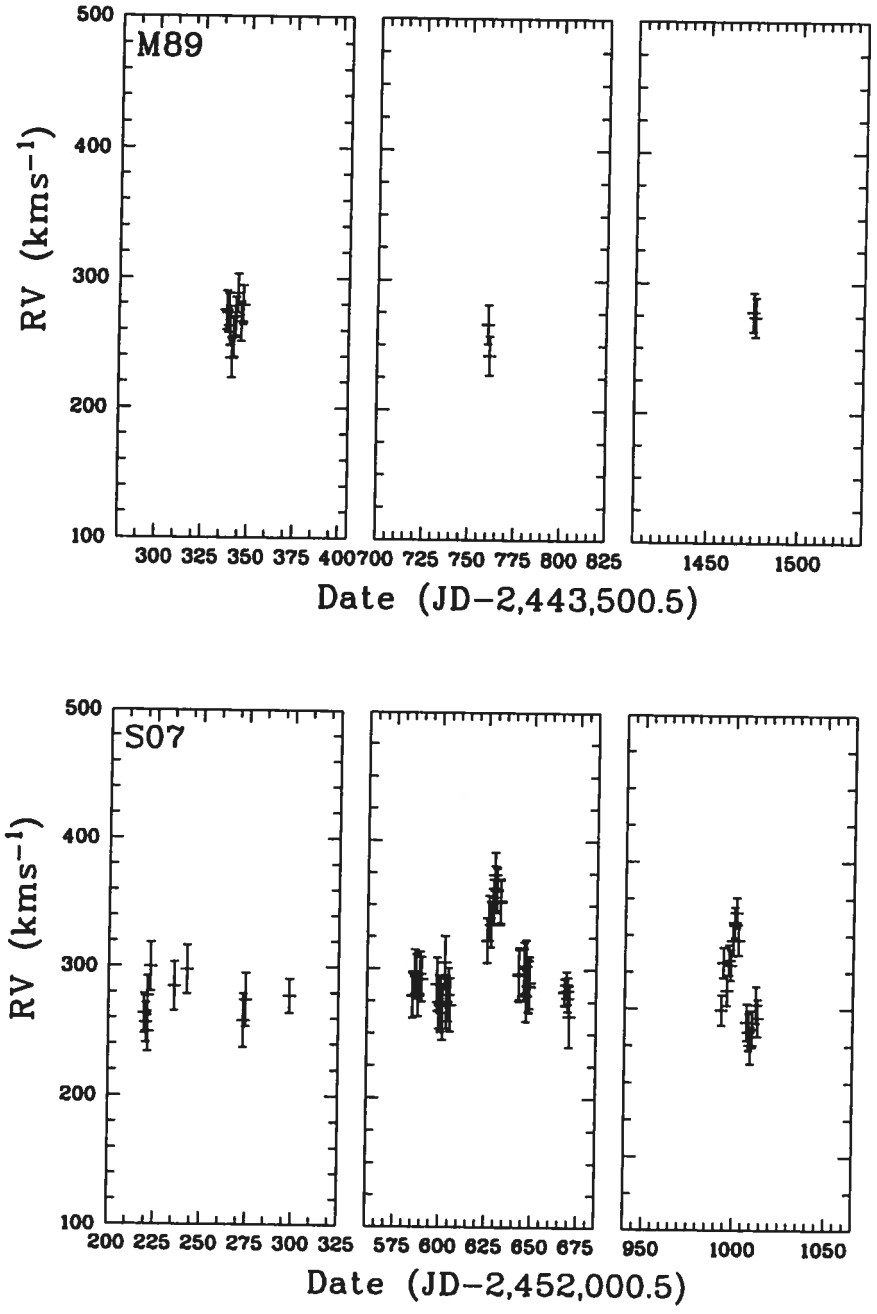

FIGURE 3.4 – RV data of R144 from M89 (*upper panel*) and S07 (*lower panel*) for the respective epochs.

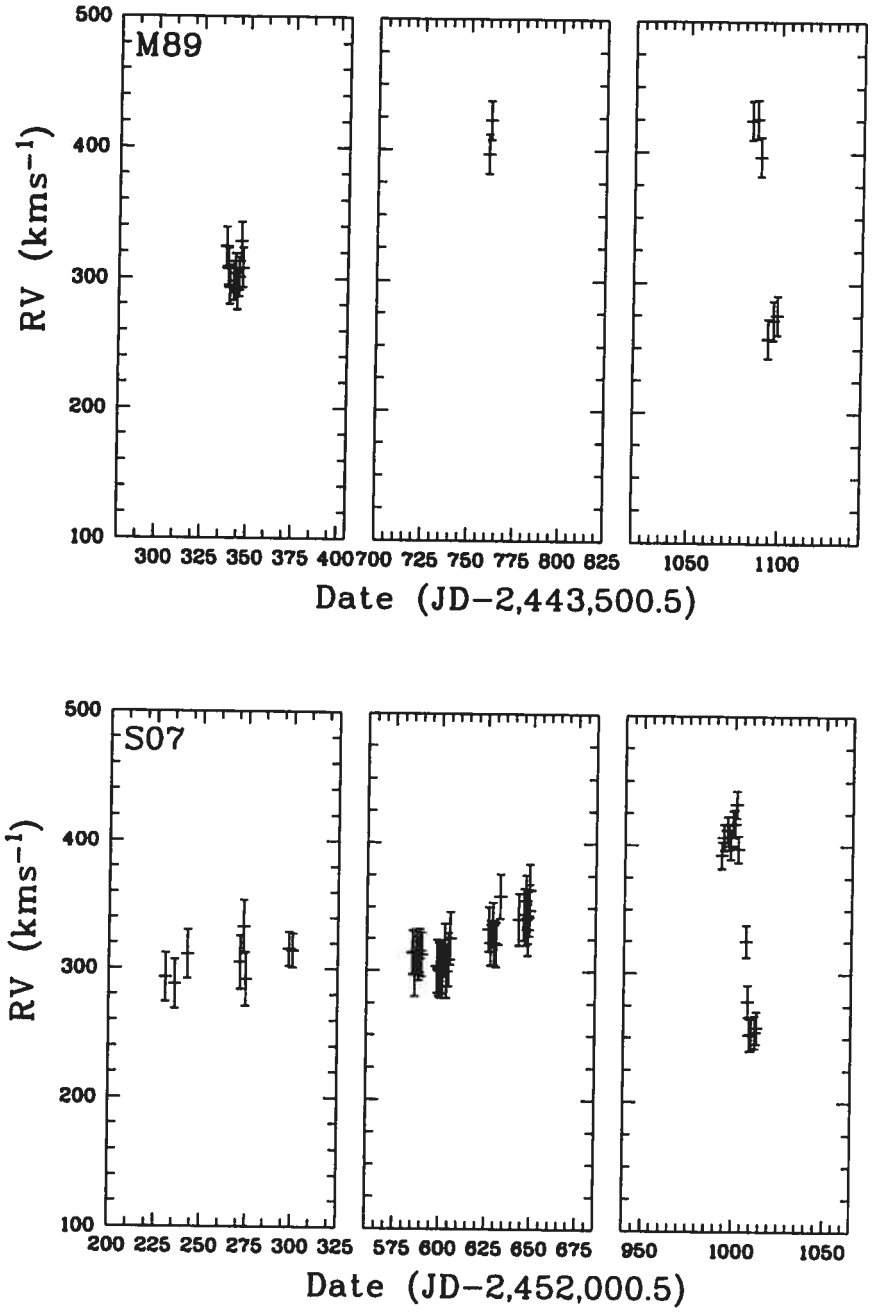

FIGURE 3.5 – RV data of R145 from M89 (*upper panel*) and S07 (*lower panel*) for the respective epochs.

3.4.2 Search For Periodicities in the RV Curves

As S07 reported, a comprehensive period analysis using different methods of their RV data in the range from 1 to 200 days yielded no coherent period for either R144 or R145. We repeated this analysis on the combined S07+M89 data set, also without success. Additionally, we tried to employ the phase-dispersion minimization (PDM) method (Stellingwerf 1978), which is very reliable because it does not rely on some assumed wave form (e.g. sinusoids) and which is very useful for strongly eccentric binaries with highly distorted RV curves. Unfortunately however, the data are too dispersed for periods much longer than 100 days, so that the PDM suffers from many severely depleted or downright empty phase bins. Thus, a different approach was used.

R144

On close inspection, R144 does not show any clearly repeating pattern in S07's RV data – the reason why S07 were not able establish a period in the first place –, and there certainly is no pattern at all visible in the M89 data set. We therefore have to conclude that better data are required for R144, if any periodicity is to be found. Long-term monitoring is currently under way.

R145

Close inspection of R145's RV curves in Figure 3.5 reveals a repeating pattern: In both M89's and S07's last epoch, the RV curve drops from its highest to its lowest value within a very short interval of time. This event can consistently be interpreted as the periastron passage (PP) of a highly eccentric, long-period binary. But what is its period? We are lucky, because we have three such PP events recorded: two in the M89 data set (called PP1 and PP2), and one in the S07 data set (PP3). We further distinguish the highest and the lowest RVs during the respective event; thus, we find that the combined RV data set covers the following events: PP1 high, PP2 high and low, PP3 high and low. Julian Dates and RVs for

TABLE 3.3 – Measured dates and RVs for the presumed periastron-passage (PP) events PP1 through PP3 in the data sets of M89 and S07, respectively. "High" and "low" refer to maximum and minimum RVs measured just before and after the supposed PP, respectively. See text for more details.

Data set	Event	MJD[a]	RV[b]
M89	PP1 high	44261.4	423
M89	PP2 high	44584.4	424
M89	PP2 low	44599.5	276
S07	PP3 high	53001.8	432
S07	PP3 low	53012.4	252

[a] MJD = JD-2,400,000.5; all values ±3 days (estimated error)
[b] in kms^{-1}; errors ±15 kms^{-1} (estimated)

each event are given in Table 3.3.

From Table 3.3, one can also immediately derive the systematic shifts between the two data sets M89 and S07. Since by construction, the PP-high events coincide both in orbital phase and RV, we find that the systematic shift $\Delta RV(S07 - M89)_{hi} \sim 10$ kms^{-1}. Note the two PP-low events are less good indicators of a systematic shift, for the following reason: It seems that the duration of the PP2 event is somewhat longer than that of the PP3 event, $\sim$ 15 versus $\sim$ 10 days. However, the observed RV amplitude during PP2 is smaller than that observed during PP3. It is thus likely that the true minimum RV was missed during the observations of the PP2 event, thus the full RV peak-to-valley swing of the WR star (i.e., $2K$) might be closer to the value obtained from PP3, $\Delta RV(PP3) = 180$ kms^{-1}.

Measuring the elapsed time between corresponding events will yield an integer multiple of the period, if, of course, there is one. Thus, we obtain the following time intervals:

$$\Delta T_{31,hi} = MJD(PP3_{hi} - PP1_{hi}) = 8740.4 \pm 4 \text{ days}$$
$$\Delta T_{32,hi} = MJD(PP3_{hi} - PP2_{hi}) = 8417.4 \pm 4 \text{ days}$$
$$\Delta T_{21,hi} = MJD(PP2_{hi} - PP1_{hi}) = 323.0 \pm 4 \text{ days}$$
$$\Delta T_{32,lo} = MJD(PP3_{lo} - PP2_{lo}) = 8412.9 \pm 4 \text{ days},$$

TABLE 3.4 – Possible orbital periods of R145 as computed from the condition that the true period has to be an integer fraction n of the respective time interval between the observed "high" or "low" events.

ΔT	n	P [days]
21,hi	1	323.0 ± 4
	2	161.5 ± 2
	3	107.7 ± 1.3
	4	80.8 ± 1.1
	5	64.6 ± 0.8
31,hi	27	323.72 ± 0.15
	53	164.91 ± 0.80
	54	161.86 ± 0.07
	55	158.92 ± 0.07
32,hi	26	323.75 ± 0.15
	51	165.05 ± 0.08
	52	161.87 ± 0.08
	53	158.82 ± 0.08
32,lo	26	323.57 ± 0.15
	51	164.96 ± 0.08
	52	161.78 ± 0.08
	53	158.73 ± 0.08

where the overall, quadratic error has been obtained from $\sqrt{3^2+3^2} \sim 4$. From $\Delta T_{21,hi}$ follows that the longest possible period is 323 ± 4 days; otherwise, two high events would occur during one phase. The true period is thus 323 days or an integer fraction n thereof. Using appropriate values for n, we have computed the possible periods $P = \Delta T/n$ and listed them in Table 3.4. Note that any period shorter than $\sim$ 60 days is ruled out by S07's observations, even if it satisfied the integer condition.

Given that the data are too sparse to rely on an automated PDM method, the only way to discriminate the true period is to fold the data into the respectively corresponding phases and to choose the most coherent-looking curve. We have shown this for five periods between $\sim$ 323 and and $\sim$ 64 days in Figure 3.6. As can be nicely seen, the longest possible period, $\sim$ 323 days, fits the data, but of course it does so by construction, and it leads to a gap of almost exactly half a phase, which is suspicious. The period around $\sim$ 160 days also yields a coherent, albeit somewhat less clean RV curve, but the phase coverage is much better and it does yield a less eccentric orbit, as can already be seen by eye. The other periods yield an increasingly incoherent RV pattern, which is why they can be dismissed as wrong.

Unforntunately, from the RV curve alone we cannot firmly rule out the long, 323-day period. Therefore, from the RV data alone, we opt for the shortest possible orbital period that yields a coherent RV pattern, i.e. ~ 160 days.

Note that while we have chosen to show only five discrete periods, differences between e.g. 158 and 161 days were very small compared to the stark differences between ~ 160 days and an altogether different period, such as e.g. ~ 80 days.

3.4.3 Polarimetric Data

With these results from the spectroscopy, we proceeded to analyze the polarimetric data. To derive the orbital parameters, we used the elliptical orbit model by Brown et al. (1982; with the correction by Simmons & Boyle 1984), modified for an extended source of scatterers (cf. Robert et al. 1992), i.e. assuming an ensemble of optically thin, free electrons that follow the wind density around one of the stars spherically symmetrically (for details, see Moffat et al. 1998).

For R144, the fit did not converge, and since there is no orbital solution from the spectroscopy, we were unable to constrain the fit. This does not entirely come as a surprise, given the small number of data points ($N = 15$) spread over only ~ 2 weeks, and the rather small level of variability. Thus, we abandon the study of R144 based on the current data. For R145, however, the fit of the polarization data alone yielded a coherent solution with a period of $P \sim 159$ days. Encouraged by this result, we then proceded to combine the spectroscopic (i.e., M89+S07) and polarimetric data sets and force a simultaneous fit. We also obtained RVs from the slightly weaker, but less perturbed, HeIIλ5411 emission line, so that we had two spectroscopic data sets, one for HeIIλ4686 and one for HeIIλ5411.

Note that the fits to the respective data sets do not have all orbital parameters in common. For instance, spectroscopy cannot yield the inclination angle i and the orientation of the line

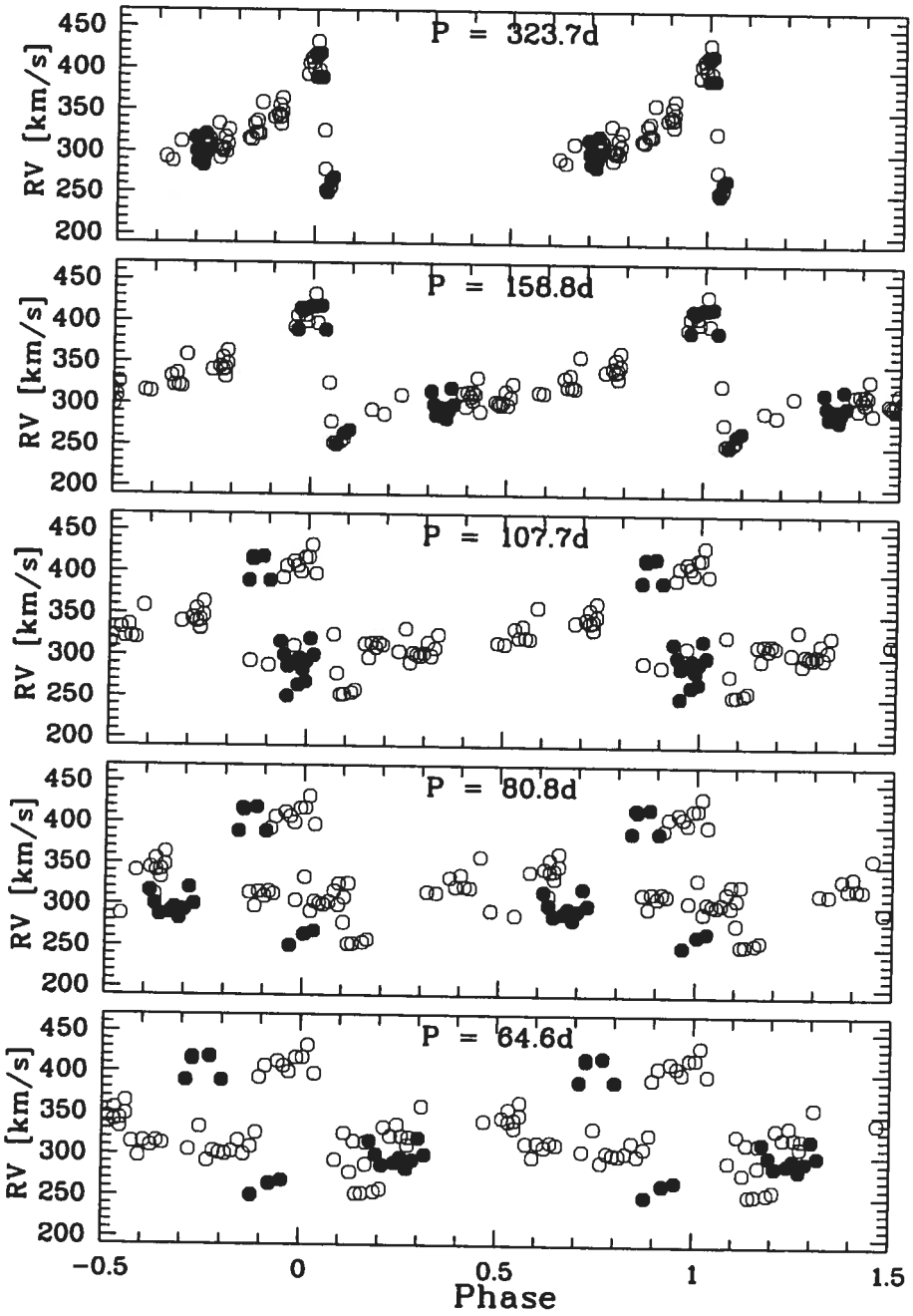

FIGURE 3.6 – Combined RV data of R145 (M89: filled; S07: empty symbols) folded into the corresponding phases of five different, possible periods.

of nodes Ω[4], which both are calculated from the polarimetry.

The following parameters were obtained from the fit of the combined RV and polarimetric data: Interstellar polarizations Q_0 and U_0 of the Stokes parameters; Ω (see above); the inclination angle i; the orbital longitude of the centroid of the scattering region at periastron passage λ_p (linked to the argument of the periastron by the relation $\lambda_p = \omega - 90°$); the orbital period P; the RV amplitude $K_{\rm WR}$ of the WR component; the systemic velocity V_0; the systematic RV shift between the M89 and S07 data sets ΔV; the orbital eccentricity e; the time of periastron passage T_0; the total electron scattering optical depth τ (assuming Thompson scattering to be the only source of opacity); the exponent γ in the power law describing how the electron density falls off from the WR stars (e.g., $\gamma = 2$ for an inverse square law around a scattering point source).

In order to facilitate its convergence, the fit was carried out for three parameter groups which are, to first order, independent of each other: 1. (K, V_0, ΔV); 2. (Q_0, U_0, τ, γ); 3. (i, Ω, λ_p, e). One group was fitted while the two others were kept constant. For each permutation χ^2 was computed, and the procedure was repeated until the fit yielded a constant χ^2 for all permutations. In order to estimate the errors on individual fit parameters, we explored the sensitivity of the fit (i.e., its χ^2) by varying one parameter around its best-fit value (obtained from the overall fit) while keeping all other parameters constant. Those variations of each individual parameter which resulted in a 5% deterioration of the χ^2 compared to its minimum value from the overall fit, were used as error levels of the respective parameter. Results of the fits for both HeIIλ4686 and HeIIλ5411 are shown in Table 3.5. The resulting orbital solutions together with the polarimetric data folded into the corresponding phase is shown in Figures 3.7 and 3.8.

Note the difference in the systemic velocities obtained from the two respective lines, which

[4]We here follow the definition of Harries & Howarth (1996) that Ω is the angle of the ascending node measured from north through east with the constraint that $\Omega < 180°$, i.e. an ambiguity of 180° exists in the determination of Ω since it is impossible from polarimetry to discern the ascending from the descending node. However, this can be done using the spectroscopic orbit of the binary.

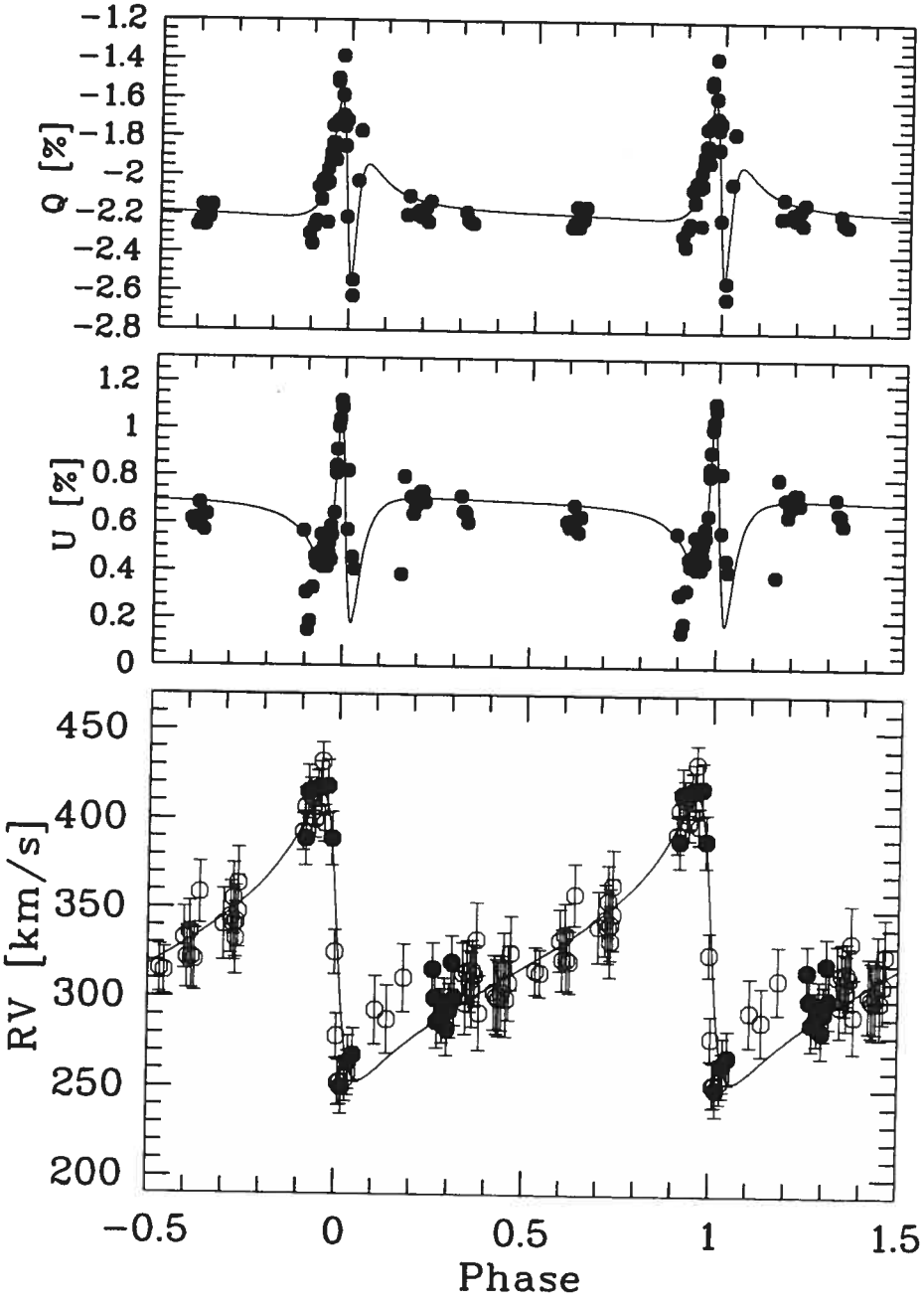

FIGURE 3.7 – Orbital solution for R145 obtained from the Stokes Q (*upper panel*) and Stokes U (*middle panel*) parameters, and the combined M89+S07 RV data sets (*lower panel*) for the HeIIλ4686 emission line. S07 data are shown in empty symbols, and M89 data are shown in full symbols.

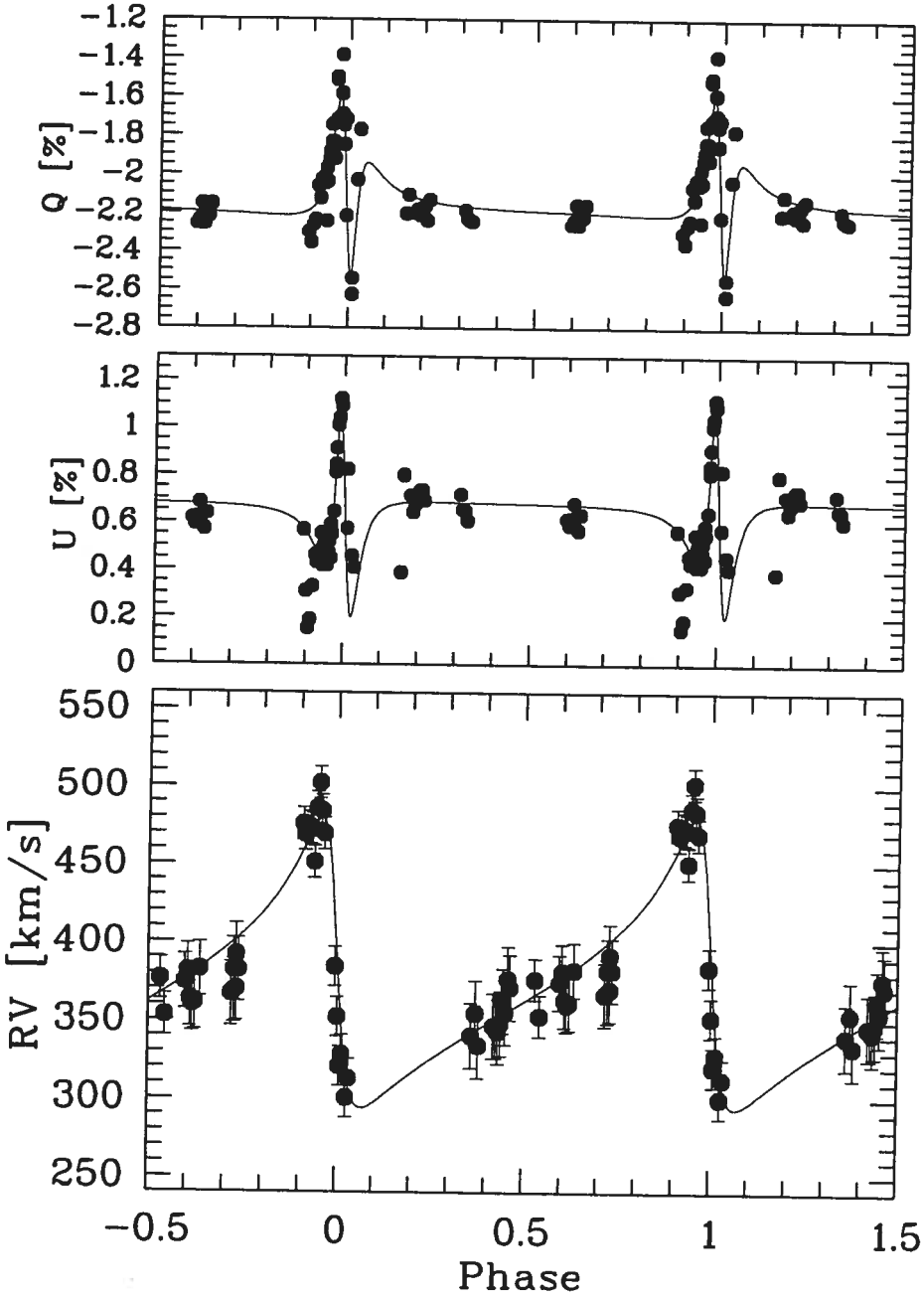

FIGURE 3.8 – Orbital solution for R145 obtained from the Stokes Q (*upper panel*) and Stokes U (*middle panel*) parameters, and RVs of the HeIIλ5411 emission line (*lower panel*; S07 data only). Note that since not all spectra in the S07 data set cover HeIIλ5411, there are fewer points than in Figure 3.7.

TABLE 3.5 – Orbital parameters from the combined fit of both the spectroscopic and the polarimetric data sets.

Parameter	HeIIλ4686	HeIIλ5411
τ [%]	0.048 ± 0.006	0.049 ± 0.006
Q_0 [%]	-2.17 ± 0.04	-2.18 ± 0.04
U_0 [%]	0.67 ± 0.04	0.68 ± 0.04
Ω [°]	-40 ± 7	-42 ± 7
i [°]	37 ± 7	39 ± 6
$\omega = \lambda_p + 90$[°]	85.0 ± 6.7	83.4 ± 6.6
P [days]	158.8 ± 0.1	158.8 ± 0.1
K_{WR} [kms^{-1}]	81 ± 21	93 ± 21
ΔV^a [kms^{-1}]	10 ± 29	n/a
e	0.70 ± 0.02	0.69 ± 0.02
V_0 [kms^{-1}]	328 ± 14	382 ± 13
T_0 [JD-2,400,000.5]	53007.763 ± 0.25	53007.763 ± 0.25
γ	1.70 ± 0.15	1.75 ± 0.14

[a]: ΔV =M89-S07

amounts to ~ 55 kms^{-1}. S07 reported that in some of their stars, the systemic velocity obtained from fitting HeIIλ4686 was larger than the systemic velocity of the LMC; this was also reported by other studies (e.g. Foellmi et al. 2003). All authors attributed this effect to the fact that most WR emission lines display more or less pronounced P Cygni profiles. Thus, the possible presence of a P Cygni type absorption line diminishes the blue flank of the emission line so that the resulting profile peaks at a more redshifted velocity. If this explanation is correct, our findings here suggest that in R145, HeIIλ4686 is less affected by its absorption component than HeIIλ5411, in line with what is expected from the wind structure (Crowther, private communication). Cross-verification with R144 yielded the very same effect with roughly the same shift (~ 50 kms^{-1}) between the systemic velocities obtained from the two respective He lines.

As was mentioned above, errors on the individual parameters were estimated by a 5% deterioration of the overall χ^2. This kind of tolerance analysis is frequently used in cases where the solution is complex and parameters are not independent from (i.e., in terms of solution space, not perpendicular to) each other, and yields a good estimate of which parameter dominates in the quality of the overall fit. Based on this approach, the resulting error for the inclination angle i was found to be 6°. Choosing a higher cut-off value than 5% will of course lead to a larger error on i (and all other parameters), but the χ^2 deteriorates very quickly,

when the inclination angle varies by much more than 10 to 15°, and the discrepancies between the fit and the data become notably large.

However, it is well known among polarimetrists that there is a bias of the polarimetric determination of the inclination angle towards higher values than the true value of i; this bias is more pronounced, the lower the true inclination angle and the lower the data quality is (in terms of both the number of available data points and their respective individual errors); see e.g. Aspin et al. (1981), Simmons et al. (1982) or, more recently, Wolinski & Dolan (1994) for a comprehensive discussion of this issue. This bias can readily be seen when one compares inclination angles derived from photometric *atmospheric* (i.e. wind) eclipses with those derived from polarimetry (e.g. Lamontagne et al. 1996, their Table 10), although these authors state that comparison yielded "reasonably good consistency in the most reliable cases". Using *core*-eclipsing binaries, on the other hand, shows that the differences to i-values derived from polarimetry remain small, simply because eclipsing binaries are seen under high inclination angles, so that the polarimetric bias remains small as well. As soon as the inclination angle under which a system is seen becomes smaller, so that the polarimetric bias would play a more important role, the system is no longer eclipsing, and it is very difficult to assess the true amount by which i is overestimated. Thus, while is is to expected that our polarimetric approach overestimates the true value of the inclination angle, it is very difficult to assess by how much it does so.

Unfortunately, the inclination angle is the crucial factor for determining the absolute masses of the binary components, because it has such a low value and the orbital eccentricity is rather well-constrained by the RV curve (compare e.g. with the case of WR 22; Schweickhardt et al. 1999). Interestingly, from a pure bias-related point of view, our analysis is bound to *over*estimate the true value of i, which means that the true inclination angle is lower than 39°, rendering the resulting masses even higher. If on the other hand we were to force a fit with the inclination angle fixed at 90°, the resulting χ^2 would more than double compared to the best-fit value. Unless the orbital period is wrong altogether, it is thus unlikely that the

inclination angle is that high. This is most unfortunate, since this result rules out the possibility of R145 being an eclipsing system, so that photometry does not seem to be a viable alternative to reveal core eclipses, although atmospheric eclipses may still be possible. On the other hand, we are not aware of any existing or published photometry of R145, so that we have no possibility to verify the polarimetric result. We will therefore adopt the value of $i = 39 \pm 6°$ for the rest of the paper. However, given the great importance of an accurate determination of the inclination angle, we strongly encourage that more high-quality data be collected.

3.4.4 Search for the Companion in R145

While we have obtained the orbital solution for the WN component in R145, including the inclination angle of the orbital plane, we have so far not isolated the spectral signature of the companion star which is presumed to be an O star (if it were also an emission-line star, this would have been fairly obvious, as e.g. in WR20a). As both S07 and M89 reported, no trace of the companion's absorption lines could be found in the individual spectra.

In a first attempt to isolate the spectrum of the companion, we shifted all spectra of R145 into the frame of reference of the super-template. This super-template was obtained from XCORR by shifting all spectra into the frame of reference of the WR star and co-adding them, using their respective S/N values as weights (see S07 or Section 2.5 for more details). By subtracting the super-template from each spectrum, we obtained residuals in which the WR spectrum was, by construction, removed. Thus, if any O-star absorptions were visible, we expected to find them in the individual residual spectra. However, there was no obvious trace; any absorption-like structure was essentially lost in the noise.

We therefore adopted a modified version of the method developed by Demers et al. (2002), the so-called "shift-and-add" method. Originally it consists of shifting all spectra into the frame of reference of the WR star and subtracting the mean (which we have done), shifting

the residual spectra back into the frame of reference of the O star, and co-adding all shifted residuals to obtain a cleaner mean spectrum of the O star. While this method can be used iteratively to obtain ever better disentangled spectra of the WR and the O components, respectively, its caveat is obvious: one has to know the orbit of the O star, otherwise one cannot shift the residuals into its frame of reference.

Since we had neither the companion's orbit nor any, even weak, spectral signatures of absoption lines, we proceeded as follows: Assuming that the companion is indeed an O star and not another emission-line star (as suggested by the orbital behaviour of the emission-line profiles), and knowing that the companion has to move in perfect anti-phase (i.e. phase shift of $\Delta\phi = 180°$) to the WR orbit (which we obtained above), we simply "mirrored" the WR star's RV values to obtain the corresponding RV values for the O star. Since the RV amplitude $K_{\rm O}$ of the O star is simply given by $qK_{\rm WR}$, where $q = K_{\rm O}/K_{\rm WR} = M_{\rm WR}/M_O$ the mass ratio, one can, by adopting values for q, use the $RV_{\rm WR}(t)$ values to compute the corresponding $RV_{\rm O}(t)$ values. That is, one considers differential motions ΔRV_{ij} of the WR star as measured at two dates i, j (this is the information we do have from our RV curve of the WR star), and multiply this value by $-q$ to obtain the assumed motion of the O star. For instance, if the WR star changes its RV by 50 kms^{-1}, and if, say, $q = 2$, then the O star's RV has to change by -100 kms^{-1} in the same time interval $[i; j]$. This approach is independent of the systemic velocity $\gamma_{\rm O}$ of the O star which in WR+O binaries is known to not necessarily equal to the WR star's $\gamma_{\rm WR}$ value, but which is not at all required for the mass determination of both components of the binary system.

With this tentative $RV(t)$ curve for the O star, the individual residual spectra (i.e., after WR subtraction) can now be shifted by their respective RVs into the tentative frame of reference of the O star. Co-adding of the so shifted residuals should make the O star's absorption spectrum appear with greater clarity, *if one has the correct value for* q, because the co-added average spectrum has a S/N$\sim$ 800.

How can one know that a chosen q is the right one? If the residual spectra are shifted by exactly their correct $RV_{\rm O}(t)$ value, the co-added absorption lines will have maximum intensity (i.e., depths), because they are co-added while in perfect superposition. If, however, a wrong mass ratio was assumed (too large or too small), then the co-added absorption lines will be shallower, because the individual spectra are not shifted into the correct frame of reference in which they stand still over time. Thus, when using different tentative values for q (or $K_{\rm O}$, which is immediately given by $qK_{\rm WR}$) and measuring the depth of a given, co-added absorption line, the depth of the line will go through a maximum when plotted versus q (or KO). The only challenge is to wisely choose the O-star absorption lines one measures, given that the WN6h star in R145 shows strong emissions in most hydrogen and helium lines.

We opted for the two lines HeIIλ4200 and λ4542, because WN emissions at this positions are relatively weak and because these are the strongest He lines in a hot, early-type O star, the anticipated companion. We carried out the "shift-and-add" exercise scanning through values of q so that the (intuitively more easily understandable) $-qK_{\rm O}$ values range from -100 kms^{-1} (i.e., the O star is less massive than the WR star and moves *in phase* with it, which is of course unphysical, but it gives a strong constraint on the zero level of the measured absorption-line depth) to $+600$ kms^{-1} (i.e., the O star is ~ 8 times less massive than the WR star and moves in *anti-phase* with it, just as it should if it was its true companion), depending on the line. Thus, we also considered the case were the O star is actually more massive than the WR star, i.e. it moves with a smaller RV amplitude than the WR star.

The residual spectra were thus shifted by their individual, tentative $RV_{\rm O}(t)$, and co-added, and absorption-line strengths were obtained from the mean spectrum using the ESO-MIDAS task GET/GCUR. Absorption-line depths were measured by obtaining continuum values on either side of the absorption, averaged, and subtracted from the peak value such as to obtain positive values for the line strength, with deeper lines yielding larger values. Results are shown in Figures 3.9 and 3.10 for the HeIIλ4200 and the HeIIλ4542 absorptions, respectively, where measured line intensities versus the respective $K_{\rm O}$ value are plotted. The asymmetry of the

curve might be caused by *i*) an intrinsic absorption-line asymmetry due to a modest P Cygni profile in the O star spectrum, or *ii*) a residual emission of the WR star due to imperfect subtraction. Both effects will distort the curve because the intensity is not the same on both sides of the absorption-line center. Asymmetry is particularly visible in the data for the HeIIλ4200 line; however, whether this comes from an intrinsic asymmetry in the O-star absorption or is related to imperfect WR subtraction, cannot be determined.

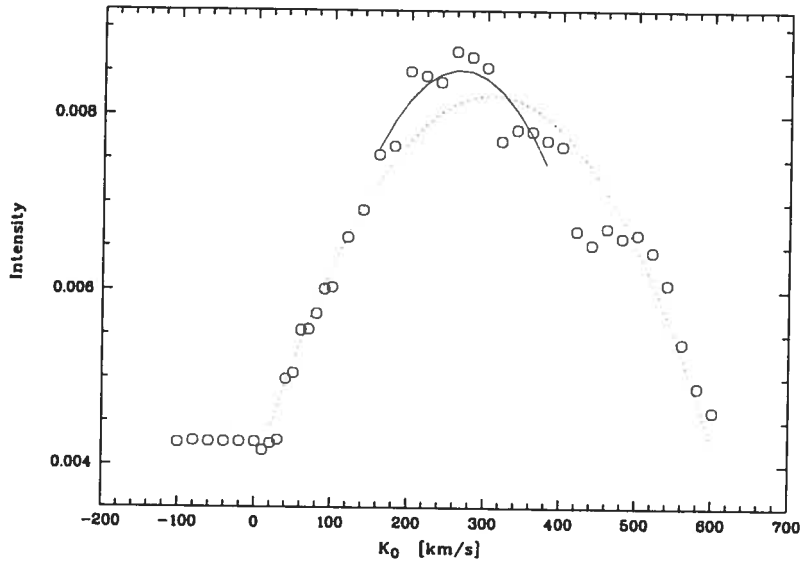

FIGURE 3.9 – Measured intensities of the HeIIλ4200 absorption line in the co-added spectra versus the assumed value for K_O. Note the strong asymmetry. The parabolic fit is shown considering all data (*dotted line*) or only the central cusp (*solid line*). See text for more details.

In order to determine the value for K_O (and thus q) at which the absorption-line depth was maximal, i.e., at which the true rest frame of the O star had been found, we fitted a parabola to the data (see Figures 3.9 and 3.10). Comparing HeIIλ4200 and HeIIλ4542 immediately reveals that the strong asymmetry in HeIIλ4200 leads to a position of the global maximum which is greatly different to the value obtained from HeIIλ4542, 306 ± 69 versus 217 ± 24 kms^{-1}. While technically, these two values are constistent with each other within their respective errors, we re-fitted both sets of points considering only the central cusp (fit shown in solid line). We

now obtained 265 ± 67 and 214 ± 19 kms^{-1} for HeIIλ4200 and HeIIλ4542, respectively. Since the error on the result for HeIIλ4200 is ~ 3.5 times larger than for HeIIλ4542, this leads to a very small weight ($\sim 1/12$), if one were to calculate a σ-weighted average. Also recall that S07 reported that due to the lack of arc-comparison lines towards the blue end of their spectra, RV scatter was found to be larger than in the central region of the spectra (i.e., around HeIIλ4686).

Therefore, we did not calculate a weighted mean shift but rather entirely relied on the value obtain from the HeIIλ4542 absorption. In Figures 3.11 and 3.12, respectively, the resulting mean spectra for the O star (i.e., co-added in the frame of reference of the O star) are shown. Downward arrows indicate the position of the respective absorption. Note that it seems that the subtraction of the WR spectrum was not perfect; the HeIIλ4542 absorption is superposed on a broad (pseudo?) emission, which might just be the residual WR emission line. Furthermore, in both resulting mean spectra, there can be found two little absorption features bluewards of both identified HeII absorptions, around $\sim \lambda$4177/4183 and $\sim \lambda$4513/4521, respectively. We presently do not know whether these features are artifacts in the data (i.e., improper sky or nebular subtraction – R145 is located in the 30 Dor region and thus surrounded by nebular emission –, bad CCD cosmetics, etc.) or whether these are real spectral features of the O type companion (if they belonged to the WR star, they would have been smeared out by the "shift-and-add" process). However, none of the feature share the same wavelength or velocity distance to the respective HeII absorptions, so at least we can rule out that they are somehow related to each other, and since we have in both cases applied the same $K_{\rm O}$ value, it is unlikely that these features are an artifact from the "shift-and-add" procedure itself.

Also note that the y axes have the same scale in both figures, and that the absorption lines are very weak, of the order of 1% of the continuum flux. However, given the extremely high S/N obtained in the co-added spectra (S/N$\sim$800), we are confident that these are the real lines. Comparing with the depth of the absorption lines HeIIλ4200 and λ4542 in single, early-type O stars, which are 0.12 and 0.16 in continuum units, respectivly (e.g., Walborn &

Fitzpatrick 1990), we find that the companion is diluted by a factor of $\sim 10 - 15$. Thus, the WN6h component is brighter by at least 2.5 mag than the O star, very similar to the Galactic binary WR22 ($\Delta m_v \sim 2.65$ mag; Schweickhardt et al. 1999).

3.4.5 Masses of the Binary Components

We have obtained all those orbital parameters of R145 which are required to determine the absolute masses of both components in R145. The critical values are the RV amplitude $K_{\rm O}$ of the companion, and the orbital inclination i, obtained from polarimetry. With the usual relation:

$$M_1 \sin^3 i = 1.035 \times 10^{-7} (K_1 + K_2)^2 K_2 P (1 - e^2)^{3/2} M_\odot$$

and

$$M_2 \sin^3 i = 1.035 \times 10^{-7} (K_1 + K_2)^2 K_1 P (1 - e^2)^{3/2} M_\odot,$$

where P is in days, K in kms^{-1}, masses M in solar units, and taking the values $K_{\rm WR} = 93 \pm 21$ kms^{-1}, $e = 0.69 \pm 0.02$, $P = 158.8 \pm 0.1$ days from HeIIλ5411, and $K_{\rm O} = 214 \pm 19$ kms^{-1} from the HeIIλ4542 absorption (see above), we obtain masses $M_{\rm WR} \sin^3 i = 126 \pm 32 M_\odot$ for the primary and $M_{\rm O} \sin^3 i = 55 \pm 21 M_\odot$ for the secondary. Since $i = 39 \pm 6°$, $sin^3 i = 0.25 \pm 0.1$, the true masses are four times higher. Even if the correct inclination angle were closer to 60°, the factor would still be ~ 1.5, and if $i \sim 90°$, the primary mass is approaching the limit of 150 $M_\odot$ for star formation determined from the populous and young Arches cluster (Figer 2005). The much lower mass of the secondary compared to that of the primary is compatible with our deduction above, that the secondary is the much fainter component in R145.

It is clear that, as long as the absorptions of the companion have been correctly identified, R145 ranges among the most massive systems known. Even if it were seen edge-on (i.e. $i = 90°$

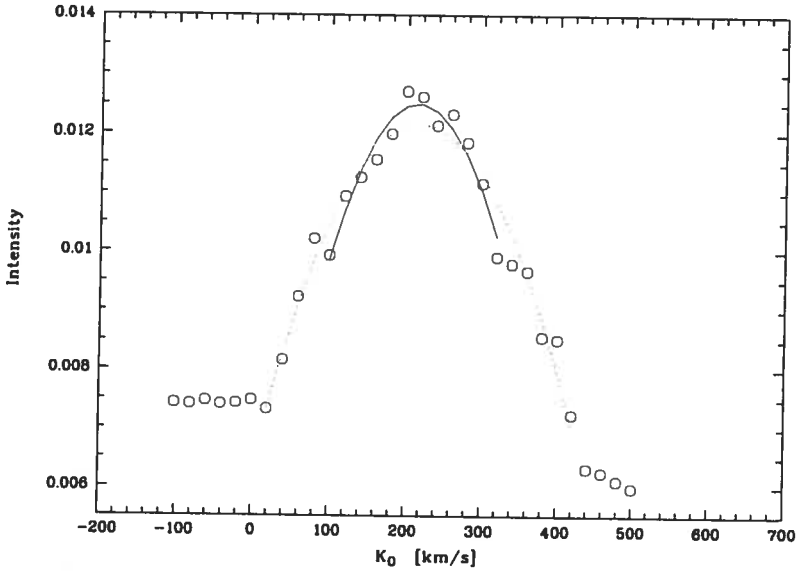

FIGURE 3.10 – Same as before, but for the HeIIλ4542 absorption line. See text for more details.

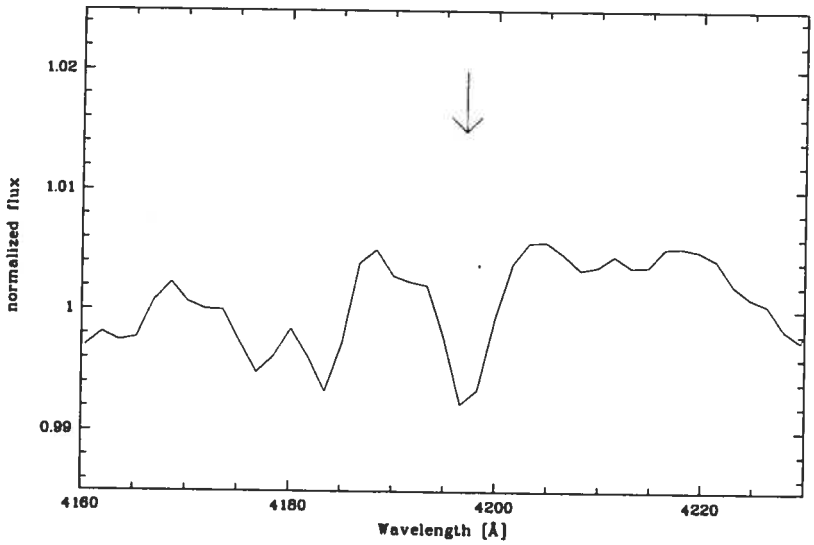

FIGURE 3.11 – Co-added residual spectra for HeIIλ4200 after being shifted into the O-star's frame of reference, using the best solution for K_O (see text for more details). The position of the HeIIλ4200 absorption line is indicated by the arrow.

and thus no correction factor required), the WN component would be the most massive star ever weighed by quite some margin; so far, the record holders are the two WN6ha stars in the Galactic binary WR20a with 83 and 82 $M_{\odot}$, respectively (Rauw et al. 2004, 2005; Bonanos et al. 2004). The total absolute visual magnitude of R145, completely dominated by the WN6h component, is $M_v = -7.0$, (Breysacher 1986), i.e. brighter than the M_v obtained for each component of WR20a (-6.5, Rauw et al. 2005, 2007), and in the range of the central WN6ha stars of NGC 3603 (-6.9 to -7.7 mag; see Moffat et al. 1994). Thus, if one compares R145 and WR20a in terms of absolute magnitude, it follows that R145's significantly higher mass could be consistent with its brighter absolute magnitude, given that the ~same bolometric correction both for R145 and WR20a applies. However, we do not have very reliable orbital parameters for R145. The problem with the inclination angle persists, and more both spectroscopic and polarimetric data are required.

3.4.6 The Mass-Loss Rate of the WN Star

Following the prescription of Moffat et al. (1998; also see references therein), we can obtain a rough estimate of the mass-loss rates $\dot{M}_{\rm WR}$ of the WN6h star in R145. Using

$$\tau = 23\sigma_T f_c \dot{M}_{\rm WR}(1+\cos^2 i)/(16\pi)^2 m_p v_\infty a,$$

where σ_T is the Thompson electron scattering cross-section, $f_c = I_{\rm O}/(I_{\rm WR}+I_{\rm O})$ the intensity ratio between the O star and the total luminosity, m_p the proton mass, and v_∞ the wind terminal velocity. For f_c, we use the light ratio ~ 0.1 as derived above from the absorption-line strength of the O star companion with respect to single early-type O stars. From tailored atmosphere analysis of R144, Crowther & Dessart (1998) found $v_\infty = 1350$ kms^{-1}. S07 report that the FWHM of the HeIIλ4686 emission line in R145 is only slightly smaller than in R144; assuming that both stars are similar enough that the FWHM of HeIIλ4686 can act as a reasonable proxy of the terminal wind velocity, we adopt for R145 a value of $v_\infty = 1300$ kms^{-1}.

The inclination angle i, γ and τ are obtained from the polarimetry (see Table 3.5).

Inserting those values in the equation given above, we obtain a mass-loss rate of $\dot{M}_{\rm WR} \sim 2.9 \times 10^{-4}$ $M_{\odot}yr^{-1}$. Crowther & Dessart (1998) report a *lower* value of $\dot{M}_{\rm WR} = 1.5 \times 10^{-4}$ $M_{\odot}yr^{-1}$ for the *more luminous* star R144. Therefore, the two methods agree to within a factor of two, which is quite encouraging, given the uncertainties involved. The agreement becomes even better if the true inclination angle is higher than 39°. For $i = 90°$, our derived value of the mass-loss rate would decrease by a factor of ~1.6; however, this high inclination angle is ruled out by the fit to the polarization curve (see above).

3.4.7 Wind-Wind Interaction Effects

It is well known that in WR+O binaries, where both stars have strong winds, wind-wind collisions (WWC) occur, and a shock cone is formed as the contact discontinuity between the two winds wraps around the star with the weaker wind, which is usually the O star. (More precisely, the wind momentum of the O star is smaller than that of the WR star, since both winds are ~equally fast, but the WR wind is an order of magnitude denser than the O star's wind.) As the shocked matter flows with high velocities along the contact discontinuity, it cools, giving rise to excess emissions which can be seen atop some optical emission lines of the WR star. Since the flow velocity seen by an observer adds vectorially to the orbital velocity of the star, the position of the excess bumps atop the emission lines depends on the orientation of the flow. The shock-cone acts like a beacon of a lighthouse: if it is pointing towards the observer, the excess emission will be blue-shifted, and half an orbit later, the matter will be flowing away from the observer, resulting in a red-shifted excess emission.

To study this behavior in more detail in R145, we followed the recipe described in S07 (see Section 2.5.8), which we briefly recapitulate here. All spectra were shifted into the rest frame of the WR star. Then, a minimum spectrum was subtracted from all spectra of the time series, and the residuals were shifted back into the observer's frame of reference. However, rather

than constructing a pixel-by-pixel minumum spectrum as did S07, we opted to use spectra that were observed around apastron, i.e. around $\phi \sim 0.5$, when the WWC excess emissions are weakest. Due to gaps in phase coverage, two spectra taken around $\phi \sim 0.53$ were chosen, averaged, and subtracted from all spectra. Then, the residuals were folded into the corresponding phase of the binary period, and a dynamic spectrum was constructed, where the intensities are coded in greyscales, white being the strongest emission. Forty phase-bins were used for good resolution, covering one orbital phase centered on $\phi = 0$, at which periastron passage (PP) occurs. The result is shown in Figure 3.13.

As can be seen from Figure 3.13, the WWC excess emission is by far strongest at periastron passage, i.e. when the two stars are closest to each other, and quickly drops when the separation between the stars increases. Since it has been shown by Stevens et al. (1992) that the WWC zone of relatively wide binaries can be treated as adiabatic even at periastron, assuming the WWC excess emission in HeIIλ4686 to be optically thin, we can thus expect a rise and fall of the emissitivity which $\propto d^{-1}$ (Usov 1992; Stevens et al. 1992), where d is the relative separation between the WR and the O star, given by

$$d/d_{\rm min} = \frac{1+e}{1+e\cos v},$$

where v is the true anomaly of the orbital ellipse and $d/d_{\rm min} = 1$ at periastron ($v = 0$, $\phi = 0$), and consequently $d/d_{\rm min} = (1+e)(1-e)$ at apastron ($v = \pi$, $\phi = 0.5$).

Following the prescriptions of Marchenko et al. (2003), we measured the equivalent widths (EWs) of the WWC excess emission component in the HeIIλ4686 emission line at different orbital separations (i.e., the EW of the residuals after subtraction of the minimum spectrum), and normalized them so that $EW_{\rm max} = 1$, which was expected to occur near $\phi = 0$.

In Figure 3.14, we have plotted the normalized EWs of the WWC excess emission versus

the orbital phase. Also given are the the emissivity curves one would expect from a d^{-1} dependence (solid line) and a steeper d^{-2} dependnce (dotted line) of the emissivity. Unfortunately, our data are not very clean, nor are there many spectra covering the critical time of periastron passage; in particular, there seems to be a double peak on either side of $\phi = 0$, which makes it very difficult to properly assess the peak emissivity. However, the preliminary conclusion may be drawn that, assuming the orbital parameters are correct, our data are consistent with an emissivity dependence that lies somewhere between d^{-1} and d^{-2}. If the true peak emissivity is (considerably) higher than our highest data point, the correct flux normalization could bring down our data points to lower flux values, so that our data would even be *less* consistent with the theoretically expected d^{-1} curve. (Note that a change of inclination angle from $i = 39°$ would not introduce any change in the emissivity curves since they have been computed using *normalized* separations.) This is in accord to the results Marchenko et al. (2003) obtained for the Galactic WR binary WR 140 (WC7+O); they found that a d^{-2} curve fitted their data much better, although this could be partly due to an adopted value of orbital eccentricity that is too low. Furthermore, since after all, energetic X-ray photons as well as excess light in HeIIλ4686 do escape the shock zone, thereby radiatively cooling the flow, it might be that the approximation of purely adiabatic cooling is invalid. However, for a conclusive treatment of this issue, more and better data are required.

3.5 Summary and Conclusion

We have combined previously published radial velocity (RV) data from Moffat (1989) with data obtained by Schnurr et al. (2007; see Chapter 2), along with previously unpublished polarimetric data, for the two WN6h stars R144 and R145 in the LMC. While the former star was first suspected to be binary by Schnurr et al. (2007), the latter had already been identified as binary by Moffat (1989).

While our study could not yield a periodicity for R144, we have, for the first time, established the full set of orbital parameters for R145. The orbital period was found to be

$P = 158.8 \pm 0.1$ days, in contrast to the preliminary estimate of 25.4 days by Moffat (1989), based on the assumption of a circular orbit. From our analysis of the polarimetric data for R145, the inclination angle of the orbital system was found to be $i = 39 \pm 6$ degrees. By applying a modified version of the shift-and-add method published by Demers et al. (2002), we were able to isolate the spectral signature of the O-star companion. We found the RV amplitude of the primary (WN) star to be $K_{\rm WN} = 93 \pm 21$ kms^{-1}, while the RV amplitude of the secondary (O) star was found to be $K_{\rm O} = 214 \pm 19$ kms^{-1}. We derived the masses of the WR and the O component to be, respectively, $M_{\rm WN} \sin^3 i = 126 \pm 32 M_{\odot}$ and $M_{\rm O} \sin^3 i = 55 \pm 21 M_{\odot}$. This leads to a large mass ratio $q = M_{\rm WR}/M_{\rm O} \sim 2.3 \pm 1.1$, compatible with the strong dilution of the O-companion's absorption lines. It also leads to extremely high masses, if one takes i at face value. We also estimated a high value of the mass-loss rate for the WR component, of $\sim 2.9 \times 10^{-4}$ M$_{\odot}$yr^{-1}, in line with its high luminosity and presence of optical emission lines, even it is a (near) main-sequence object. From analysis of the HeIIλ4686 excess emission from WWC, we find a somewhat steeper dependence of the excess strength compared to that expected from theory of adiabatic winds, $\propto d^{-1}$.

Given the very large uncertainties on the values derived from our data, our findings cannot be considered other than preliminary. However, given the fact that R145 seems to contain one of the most luminous and thus probably also most massive stars known in the Local Group, we feel that any additional effort is well deserved to obtain more reliable results. Therefore, we are currently carrying out a long-term monitoring of this system, along with R144, but we strongly encourage independent studies of this potential cornerstone object.

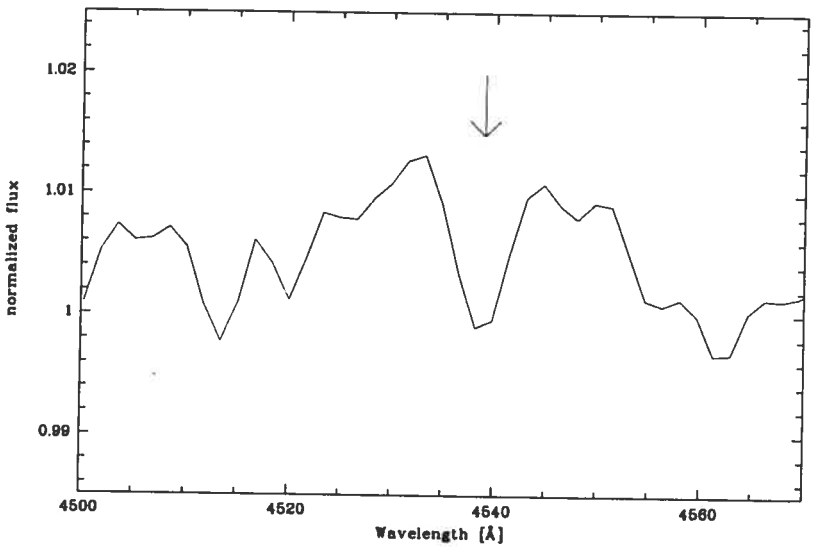

FIGURE 3.12 – Same as Figure 3.11, but for HeIIλ4542. See text for more details.

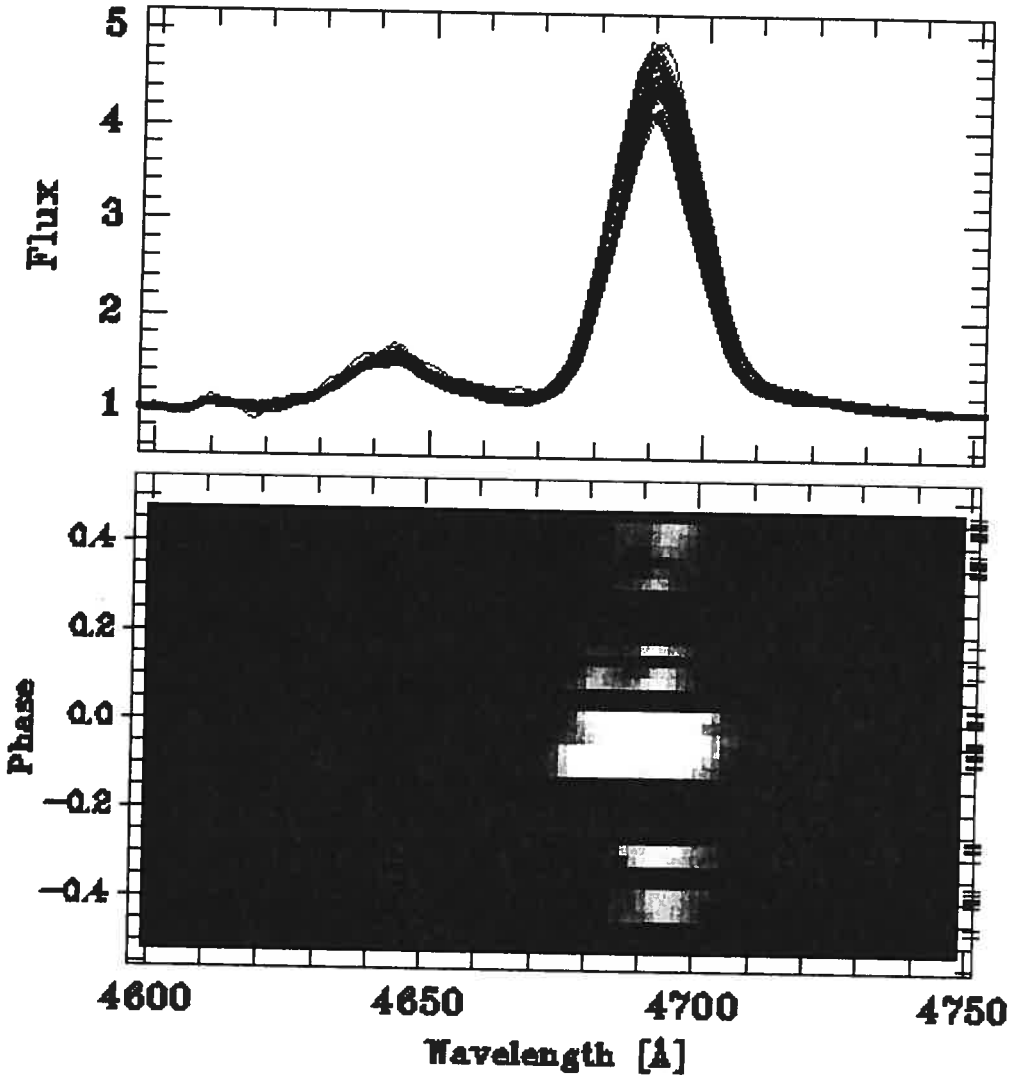

FIGURE 3.13 – Overplot of the original spectra (in grey) and the minimum profile (in thick black, taken around apastron), both in the WR star's frame of reference (*upper panel*). While the HeIIλ4686 emission line is highly variable, the strongest increase occurs around pariastron passage ($\phi = 0$). The WR star passes in front at $\phi = 0.5$ and it can (if just) be seen that it is at this phase that the WWC excess emission displays the largest redshift (*lower panel*). Black areas correspond to empty phase bins.

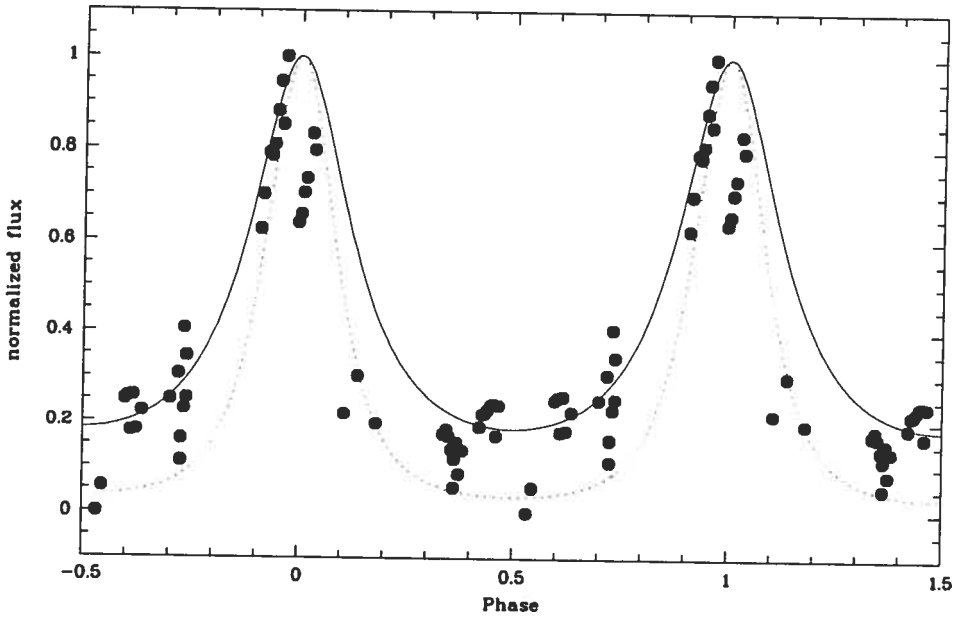

FIGURE 3.14 – Normalized equivalent widths of the excess emissions atop HeIIλ4686 folded into the phase corresponding to the orbital period of $P = 158.8$ days. Overplotted are the hypothetical emissivity curves of the WWC as a function of orbital phase; the solid line represents an emissivity rising and falling with d^{-1}, whereas the dotted line is for a steeper d^{-2} law.

Chapter 4

Summary, Conclusion, and Perspectives

The motivation for this study arose from the hypothesis that the binary frequency of WR stars was higher at lower Z. The reason for this assumption was that in evolution models, the metal-dependent mass-loss rates through radiatively-driven, stellar winds could not produce enough WR stars from single O stars, compared to the observed WR populations, especially at low metallicities (Maeder & Meynet 1994).

We have thus carried out an intense, spectroscopic survey of 41 of the 47 known WNL stars in the LMC in order to identify the binaries among them through RV variability due to orbital motion. Our study is the third and last one of its kind, because it concludes a decade-long effort of the Montréal Massive Star Group to obtain the true binary frequency among *all* WR stars in the Magellanic Clouds.

Furthermore, we have also included publicly available MACHO photometry and both *Chandra* and *ROSAT* X-ray observations. For some of our program stars, we were hence able to establish X-ray luminosities. Unfortunately, the photometric data covered only one WNL binary, and this system did not show any eclipses deep enough to be detectable at the achieved noise level.

Our results can be summarized as follows:

— We identify four previously unknown binaries, three of which, BAT99-12, 95, and 113, have orbital periods shorter than 5 days. One new binary, BAT99-99, is an intermediate-period binary with $P = 92.2$ days.

— It is however possible that BAT99-12 is not a binary, but rather a rapid rotator whose cyclic line-profile variation in the strategic HeIIλ4686 line mimics orbital motion. While we currently count BAT99-12 as binary, more data are required to secure its binary status.

— We show than one star, BAT99-107, which was reported to show long-term RV variations (Moffat 1989) and to be a binary, is indeed single.

— For one star, BAT99-119, reported to be a 25.4-day binary by Moffat (1989), we confirmed strong RV variability; however, from our RV data alone, we were unable to establish its binary nature. It was only after combination with published spectroscopic data (and ultimately unpublished polarimetric data) that we were able to obtain the correct orbital period (see below).

— This brings the total number of known WNL binaries in the LMC to nine, and the total number of WR binaries to nineteen. The overall WR frequency of binaries with $P \lesssim 200$ days in the LMC is thus $19/126 = 15\%$. We furthermore find that the binary frequencies among different subtypes in the LMC (i.e., WNL, WNE, WC/WO) are perfectly consistent with each other. That is, while Maeder & Meynet (1994) noted that most likely RLOF would preferably produce earlier WR types, we do not find that early-type WR stars show significantly larger binary frequencies. This might be another indication that at least in the LMC, RLOF has not taken place in the observed binary population.

— We have built a Galactic comparison sample containing 67 WR stars at a Galactocentric

distance of R = [6.5kpc;9.5kpc] and with a distance from the Sun of $d \leq 4$ kpc, to account for the radial metallicity gradient in the Milky Way. Among these 67 WR stars, we find an overall binary frequency ($P \lesssim 200$ days) of 22% (15 stars). We thus find that the binary frequency among WR stars in the LMC is statistically consistent with the binary frequency obtained in the Galaxy. Any numerical difference can easily be explained by small-number statistics.

— By analyzing the photometric and X-ray data, and by searching for correlations among the respective data sets and the stellar properties of our program stars, we were able to identify one excellent binary candidate, BAT99-118, which coincidentally is also the most luminous known WR star in the Local Group (Crowther & Dessart 1998). While we were unable to establish an orbital period, this system shows clear and significantly large RV variability, and an X-ray luminosity that is consistent with colliding winds in a WR+O binary system. This star merits a closer look, and is currently being monitored.

— We have found that virtually all our binaries display to some degree line-profile variabilities due to wind-wind collisions (WWC); these WWC produce excess emission in the plasma as it cools down in the flow along the discontinuity shock zone between the two stellar winds. What renders these WWC important is, next to being a high-energy phenomenon as such, that they offer the possibility to measure the orbital inclination angle using only very simple assumptions (Luehrs 1997).

— The star with one of the highest X-ray luminosities ever observed in a WR star, BAT99-116, was found to display significant line-profile variability; however, we were not able to find a periodicity in the RV or equivalent-width data. From brightness considerations, we argued that this star most likely is not in a normal, WWC-displaying binary (i.e. with a stellar companion), but rather in a system with a compact companion (neutron star or black hole) whose mass might be too small to induce a variability that we can detect in our RV data. Therefore, this system very much merits a closer look.

— From the correlation among our different data sets, we have also confirmed once more that the only reliable way to identify WR binaries and measure their masses is to monitor the stars spectroscopically in order to detect cyclical RV variability. All other, indirect methods, such as brightness considerations or large X-ray luminosities, are not reliable enough. These findings might be somewhat unpopular with telescope-time allocation committees, but they are of great importance when it comes to determining the multiplicity status of unresolved, stellar sources.

It has become obvious that the results of our study confirm what the results obtained by Bartzakos et al. (2001) and Foellmi et al. (2003) already indicated, namely that the importance of WR formation through binary interaction does not seem to increase when the metallicity is lowered from the Galactic to the LMC value. However, one has to be aware of the fact that this result alone is *not at all* strong evidence against RLOF dominating the WR formation at very low (say, 1/50 $Z_{\odot}$) metallicity. Since 1994, massive-star evolution models have constantly been updated with the latest input physics, in particular rotation. Recent calculations suggest that rotation has a much stronger effect on stellar evolution than was anticipated beforehand; in fact, new models of the Geneva group can explain WR populations at different Z entirely without the need to resort to RLOF binaries; also, these updated models explain much better other observed phenomena, as e.g. the RSG/BSG ratio at different Z, or the occurence of transition-type WN/WC stars, which represent the transition between the WN and the WC phase and which can only be reproduced by rotating models (e.g. Meynet & Maeder 2005).

However, not only do these models still lack important input physics as e.g. the influence of magnetic fields or proper convective treatment, but recent observational evidence also indicates that the canonical mass-loss rates of OB stars have still to be lowered by factors of ~ 10 and maybe even up to 100 in some cases (e.g. Fullerton et al. 2006). Obviously, we are still far from a consistent picture of massive single-star evolution. Unfortunately, this has a direct consequence for the expected binary frequencies. As we have pointed out, it might simply be that any evolutionary effects related to Z might be too small to be observable when one

changes the metallicity from solar to only LMC ($Z_{\rm LMC} \sim 1/3 Z_{\odot}$); the smaller the differences, the larger the required number of studied WR stars in order to obtain a good "S/N ratio". It might thus very well be that we do run into some kind of sophisticated "small-number limit" when we rely on the LMC results only. Thus, we cannot consider the issue settled. Unfortunately, the WR population in the SMC is too small to grant reliable statistics, and there are so far no *complete and sufficiently large* WR populations at very low Z known.

We have, however, made great strides towards identifying and weighing the most massive stars known. As a most remarkable result of our study, with the exception of one case, all WNL binaries in the LMC are not classical WR stars, but rather very luminous WN5-7ha stars. There is ample evidence that these stars are among the most massive stars known, very possibly even the most massive ones (Rauw et al. 1996; Crowther & Dessart 1998; Schweickhardt et al. 1999; Rauw et al. 2004, 2005; Bonanos et al. 2004). Since our study has greatly enlarged the sample of known binaries which harbor such extreme stars, we have paved the way to directly "weigh" an unprecedented number of very massive stars using highly model-independent, Keplerian orbits.

One such case, BAT99-119, has alread been studied by us in greater detail. By combining our RV data with RVs previously published by Moffat (1989), and with previously unpublished polarimetric data, we have, for the first time, established the full set of orbital parameters for this very massive system. By applying a modified version of the shift-and-add method published by Demers et al. (2002), we were able to isolate the spectral signature of the companion. Thus, we have now all the orbital parameters required to obtain the absolute masses. We find for the WN and the O component, respectively, $M_{WN} \sin^3 i = 126 \pm 32 M_{\odot}$ and $M_O \sin^3 i = 55 \pm 21 M_{\odot}$. If the inclination angle is actually $\sim 40°$, the true masses are even higher; however, the errors are very large. Thus, while we potentially have weighed the most massive star known so far, more and better data are required to firmly establish the nature of this cornerstone system. Once the masses are determined with good precision, we can proceed to reliably calibrate stellar models.

Bibliography

Alcock, C., Allsman, R.A., Axelrod, T.S., et al. 1996, ApJ, 461, 84

Aspin, C., Simmons, J.F.L., Brown, J.C. 1981, MNRAS, 194, 283

Auer, L.H., van Blerkom, D. 1979, ApJ, 178, 175

Balucinska-Church, M., McCammon, D. 1992, ApJ, 400, 699

Bartzkos, P., Moffat, A.F.J., Niemela, V.S. 2001, MNRAS, 324, 18

Blauuw, A. 1961, BAN, 15, 265

Bonanos, A.Z., Stanke, K.Z., Udalski, A., et al. 2004, ApJ, 611 L33

Bouret, J.-C., Lanz, T., Hillier, J.D. 2005, A&A 438, 301

Breysacher, J. 1986, A&A, 160, 185

Breysacher, J., Azzopardi, M, Testor, G. 1999, (BAT99), A&AS, 137, 117

Brown, J.C., McLean, I.S., Emslie, A.G. 1978, A&A, 68, 415

Brown, J.C., Aspin, C., Simmons, J.F.L., McLean, I.S. 1982, MNRAS 198 787

Burgasser, A.J., Kirkpatrick, J.D., Reid, I.D., et al. 2003, ApJ, 586, 512

Caron, G., Moffat, A.F.J., St-Louis, N., Wade, G.A., Lester, J.B. 2003, AJ, 126, 1415

Chiosi, C., Maeder, A. 1986, ARA&A, 24, 329

Clark, J.S., Negueruela, I., Crowther, P.A., Goodwin, S.P. 2005, A&A, 434, 949

Conti, P.S. 1976, Mem. Soc. Sci. Liège, 6ième série, Tome IX, 193

Crowther, P.A. 2000, A&A 356, 191

Crowther, P.A., Hillier, D.J., Smith, L.J. 1995, A&A, 302, 457

Crowther, P.A., Bohannan, B. 1997, A&A, 317, 532

Crowther, P.A., Smith L.J. 1997, A&A, 320, 500

Crowther, P.A., Dessart, L. 1998, MNRAS, 296, 622

Crowther, P.A., Hadfield, L. 2006, A&A, 449, 711

Crowther, P.A., Dessart, L., Hillier, D.J., Abbott, J.B., Fullerton, A.W. 2002, A&A, 392, 653

Crowther, P.A., Hadfield, L.J., Clark, J.S., Negueruela, L., Vacca, W.D. 2006, MNRAS, 372, 1407

Deeming, T.J. 1975, Ap&SS, 36, 137

de Donder, E, Vanbeveren, D., van Bever, J. 1997, A&A, 318, 812

de Donder, E., Vanbeveren, D. 1999, New Astron., 4, 167

Demers, H., Moffat, A.F.J., Marchenko, S.V., Gayley, K.G., Morel, T. 2002, ApJ, 577

Duquennoy, A., Mayor, M., Halbwachs, J.-L. 1991, A&AS, 88, 281

Evans, C.J., Smartt, S.J., Lee, J.-K., Lennon, D.J., et al. 2005, A&A, 437, 467

Eversberg, T., Lepine, S., Moffat, A.F.J. 1998, ApJ, 494, 799

Figer, D.F. 2005, Nature, 434, 192

Foellmi, C., Moffat, A.F.J., Guerrero, M.A. 2003a, MNRAS, 338, 360

Foellmi, C., Moffat, A.F.J., Guerrero, M.A. 2003b, MNRAS, 338, 1025

Foellmi, C. 2004, A&A, 416, 291

Fullerton, A.W., Massa, D.L., Prinja, R.K. 2006, ApJ, 637, 1025

Gamen, R., Gosset, E., Morrell, N.I., et al. 2006, A&A, in press

Groh, J.S., Hillier, D.J., Damineli, A. 2006, ApJ, 638, L33

Guerrero, M.A.R., Chu, Y.-H. 2006b, in: *Massive Stars and High-Energy Emission in OB Associations*, Proc. JENAM 2005, eds. Rauw, G., Nazé, Y., Blomme, R., Gosset, E.

Guerrero, M.A.R., Chu, Y.-H. 2006a, submitted to ApJS

Hamann, W.-R., Gräfener, G., Liermann, A. 2006, A&A, 457, 1015

Harries, T.J., Howarth, I.D. 1996, A&A, 310, 235

Herrero, A., Kudritzki, R.P., Vilchez, J.M., et al. 1992, A&A, 261, 209

Herrero, A., Puls, J., Najarro, F. 2002, A&A, 396, 949

Hill, G.M., Moffat, A.F.J., St-Louis, N. 2002, MNRAS, 335, 1069

Humphreys, R.M., Davidson, K. 1979, ApJ, 232, 409

Humphreys, R.M., Davidson, K. 1994, PASP, 106, 1025

Ignace, R., Gayley, K.G. 2002, ApJ, 568, 954

Kaastra, J.S., Mewe, R. 1993, A&AS, 97, 443

Kaufer, A. 1996, PhD Thesis, Karl-Ruprechts-Universität Heidelberg

Kaufer, A., Stahl, O., Wolf, B., Gaeng, T., et al. 1996, A&A, 305, 887

Keller, S.C. 2004, PASA, 21, 310

Keller, S.C., Wood, P.R. 2006, ApJ, 642, 834

Kim, S., Staveley-Smith, L., Dopita, M. A., Freeman, K. C., Sault, R. J., Kesteven, M. J., McConnell, D. 1998, ApJ, 503, 674

Kippenhahn, R., Weigert, A. 1967, Zeitschrift f. Astronomie, 65, 251

De Koter A., Heap S.R., Hubeny I. 1997, ApJ, 477, 792

Kouwenhoven, T. 2006, PhD Thesis, University of Amsterdam

Kreyszig, E. 1975, Statistische Methoden und ihre Anwendungen, Vandenhoeck & Ruprecht, Göttingen

Lamers, H.J.G.L.M., Maeder, A., Schmutz, W., Cassinelli, J.P. 1991, ApJ, 368, 538

Lamontagne, R., Moffat, A.H.J., Drissen, L., Robert, C., Matthews, J.M. 1996, AJ, 112, 2227

Langer, N. 1995, *Leben und Sterben der Sterne*, Verlag C.H. Beck, München

Langer, N. 1998, A&A, 329, 551

Langer, N., Hamann, W.-R., Lennon, M., Najarro, F., Pauldrach, A.W.A., Puls J. 1994, A&A, 290, 819

Langer, N., Maeder, A. 1995, A&A, 295, 685

Levesque, E.M., Massey, P., Olsen, K.A.G., Plez, B., Josselin, E., Maeder, A., Meynet, G. 2005, ApJ, 628, 973

Liedahl, D.A., Osterheld, A.L., Goldstein, W.H. 1995, ApJ, 438, 115L

Lomb, N.R. 1976, Ap&SS, 39, 447

Lucy, L.B., White, R.L. 1980, ApJ, 241, 300

Luehrs, S. 1997, PASP, 109, 504

Maeder, A. 1998, in: *Fundamental Stellar Properties*, Proc. IAU Symp. 189, p. 313

Maeder, A. 1999, A&A, 347, 185

Maeder, A. 2002, A&A, 392, 575

Maeder, A., Conti, P.S. 1994, ARA&A, 32, 227

Maeder, A., Grebel, E.K., Mermilliod, J.-C. 1999, A&A, 346, 459

Maeder, A., Meynet, G. 1994, A&A, 287, 803

Maeder, A., Meynet, G. 2000a, ARA&A, 38, 143

Maeder, A., Meynet, G. 2000b, A&A, 361, 159

Maeder, A., Meynet, G. 2003, A&A, 411, 543

Maeder, A., Meynet, G. 2004, A&A, 422, 225

Magalhães, A.M., Benedetti E., Roland, E.H. 1984, PASP, 96, 383

Marchenko, S.V., Moffat, A.F.J., Koenigsberger, G. 1994, ApJ, 422, 810

Marchenko, S.V., Moffat, A.F.J., Eversberg, T. Morel, T., Hill G.M., Tovmassian, G.H., Seggewiss, W. 1998, MNRAS, 294, 642

Marchenko, S.V., Moffat, A.F.J, Grosdidier, Y. 1999, ApJ, 522, 433

Marchenko, S.V., Moffat, A.F.J., Ballereau, D., Chauville, J., et al. 2003, ApJ, 596, 1295

Martins F., Schaerer D., Hillier D.J., Meynadier F., Heydari-Malayeri M., Walborn N.R. 2005, A&A 441, 735

Mason B.D., Gies D.R., Hartkopf W.I., Bagnulo W.G., Brummelaer T.T., McAlister, H.A. 1998, AJ, 115, 821

Massey, P. 2003, ARA&A, 41, 15

Massey, P., Hunter, D.A. 1998, ApJ, 493, 180

Massey, P., Duffy, A.S 2001, ApJ, 550, 713

Massey, P., Penny, L.R., Vukovich, J. 2002, 565, 982

Massey, P., Olson, K.A.G., DeGioia-Eastwood, K. 2003, PASP, 115, 1265

Massey, P, Bresolin, F., Kudritzki, R.P., Puls, K., Pauldrach, A.W.A. 2004, ApJ, 608, 1001

Massey, P, Puls, J., Pauldrach, A.W.A., Bresolin, F., Kudritzki, R.P., Simon, T. 2005, ApJ, 627, 477

Massey, P., Plez, B., Levesque, E.M., et al. 2007, to appear in *Massive Stars. Fundamental Parameters and Circumstellar Interactions*, RevMexAA Proc. Series.

Meynet, G., Maeder, A. 2005, A&A, 429, 581

Miller, I., Freund, J.E., Johnson, R.A. 1990, *Probability and Statistics for Engineers*, Prentice-Hall

Moffat, A.F.J. 1989, ApJ, 347, 373 (M89)

Moffat, A.F.J. 1991, A&A, 244, L9

Moffat, A.F.J., Michaud, G. 1981, ApJ, 251, 133

Moffat, A.F.J., Seggewiss, W. 1987, ApJ, 309, 714

Moffat, A.F.J., Niemela, V.S., Phillips, M.M., Chu, Y.-H., Seggewiss, W. 1987, ApJ, 312, 612

Moffat, A.F.J., Drissen, L., Shara, M.M. 1994, ApJ, 436, 183

Moffat, A.F.J., Corcoran M.F., Stevens I.R., et al. 2002, ApJ, 573, 191

Moffat, A.F.J., Marchenkov, S.V., Bartakos, P., et al. 1998, ApJ, 497, 896

Mokiem M.R., de Koter A., Evans C.J., et al. 2006, A&A, 456, 1131

Nakamura, F., Umemura, M. 2001, ApJ, 548, 19

Niemela, V.S, Seggewiss, W., Moffat, A.F.J. 2001, A&A, 369, 544

Nikolaev, S., Drake, A.J., Keller, S.C., et al. 2004, ApJ, 601, 260

Nota, A., Pasquali, A., Drissen, L., et al. 1996, ApJS, 102, 383

Nugis T., Lamers, H.J.G.L.M. 2000, A&A, 360, 227

Oskinova, L. 2005, MNRAS, 361, 679

Ostriker, J.P., Gnedin, N.Yu. 1996, ApJ, 472, L63

Owocki S.P., Cohen, D.H. 2001, ApJ, 559, 1108

Paczinsky, B. 1967, Acta Astronomica, 17, 355

Pasquali, A., Langer, N. Schmutz, W., et al. 1997, ApJ, 478, 340

Penny, L.R. 1996, ApJ, 463, 737

Penny, L.R., Sprague, A.J., Seago, G., Gies, D.R. 2004, ApJ, 617, 1316

Petrovic, J., Langer, N., van der Hucht, K.A. 2005, A&A, 435, 1013

Prilutskii, O., Usov, V.V. 1976, Soviet Astronomy, 20, 2

Rauw, G, Vreux, J.-M., Gosset, E., Hutsemékers, D., Magain, P., Rochowitz, K. 1996, A&A, 306, 771

Rauw, G., De Becker, M., Nazé, Y., Crowther, P.A., et al. 2004, A&A 420, L9

Rauw, G., Crowther, P.A., de Becker, M., et al. 2005, A&A, 432, 985

Rauw, G., Manfroid, J., Gosset, E., et al. 2007, A&A, 463, 981

Robert, C., Moffat, A.F.J., Drissen. L., et al. 1992, ApJ, 397, 277

Roberts, D.H., Lehar, J., Dreher, J.W. 1987, AJ, 93, 968

St-Louis, N., Moffat, A.F.J., et al. 1993, ApJ, 410, 342

Salpeter, E.E. 1955, ApJ, 212, 161

Scargle, J.D. 1982, ApJ, 263, 835

Schaerer, D. Vacca, W.D. 1998, ApJ, 497, 618

Schaerer, D. 2002, A&A 382, 28

Scheffler, H., Elsässer, H. 1990, *Physik der Sterne und der Sonne*, BI Verlag, Mannheim

Schnurr, O., Moffat, A.F.J., St-Louis, N., Morrell, N.I. 2007, to be submitted to MNRAS (S07; see also Chapter 2).

Schwarz, U.J. 1978, A&A, 65, 345

Schwarzenberg-Czerny, A. 1989, in: *Proc ESO Conference and Workshop*, eds. Grobol, P.J., Ruijsscher, R.C.E. 1993

Schweickhardt, J., Schmutz, W., Stahl, O., Szeifert, Th., Wolf B. 1999, A&A, 347, 127

Seggewiss, W., Moffat, A.F.J., Lamontagne, R. 1991, A&ASS, 89, 105

Selman, F.J., Melnick, J. 2005, A&A 443, 851

Seward, F.D., Chlebowski, T. 1982, AJ, 256, 530

Simmons, J.F.L., Aspin, C., Brown, J.C. 1982, MNRAS, 198, 45

Simmons, J.F.L., Boyle, C.B. 1984, A&A, 134, 368

Smith, L.F., Shara, M.M., Moffat, A.F.J. 1996, MNRAS, 281, 163

Smith, L.F., Maeder, A. 1998, A&A, 334, 845

Smith N., Owocki, S.P. 2006, ApJ, 645, L45

Spruit, H.C. 1999, A&A, 349

Spruit, H.C. 2002, A&A, 381

Stahl, O. 1987, A&A, 182, 229

Stahl, O, Wolf B., Klare G., Cassatella A., Krautter J., Oersi P., Ferrari-Toniolo M. 1983, A&A, 127, 49

Stahl, O., Buzzoni, B., et al. 1986, ESO Messenger, 46, 23

Stegmann, I.M. 2002, in: *Interacting Winds from Massive Stars*, APS Conf. Series, Vol. 260, eds. Moffat, A.F.J., St-Louis, N.

Stellingwerf, R.F. 1978, ApJ, 224, 953

Stevens, I.R., Blondin, J.M., Pollock, A.M.T. 1992, ApJ, 386, 265

Udalski, A., Szymanski M., Kubiak M., et al. 2000, Acta Astronomica 50, 307

Usov, V.V. 1992, ApJ, 389, 635

Vanbeveren, D., Conti, P.S. 1980, A&A, 88, 230

Vanbeveren, D., de Loore, C., van Rensbergen, W. 1998, A&AR, 9, 63

van der Hucht, K.A., Hidayat, B., Admiranto, A.G., Supelli, K.R., Doom, C. 1988, A&A, 199, 217

van der Hucht, K.A. 2001, New Astronomy Review, 45, 135

Villar-Sbaffi, A., St-Louis, N., Moffat, A.F.J., Piirola, V. 2006, ApJ, 640, 995

Vink, J.S., de Koter, A., Lamers, H.J.G.L.M. 2000, A&A, 362, 295

Vink, J.S., de Koter, A., Lamers, H.J.G.L.M. 2001, A&A, 369, 574

Vink, J.S., de Koter, A. 2005, A&A, 442, 587

Walborn N. 1986, in: *Luminous Stars and Associations in Galaxies*, Proc. IAU Symp. 116, eds. de Lorre, C., Willis, A.J., Laskarides, P., Reidel, Dordrecht, p. 185-196; Discussion, p. 197, 198.

Walborn, N.R., Fitzpatrick, E.L. 1990, PASP, 102, 379

Walborn N., Fitzpatrick, E.L. 2000, PASP, 112, 50

Walborn, N, Howarth, I.D., Lennon D.J., et al. 2002, AJ, 123, 2754

Weidner, C., Kroupa, P. 2004, MNRAS, 348, 187

Wellstein, S., Langer, N.,1999, A&A, 350, 148

Willis, A.J., Stevens, I.R. 1996, A&A, 310, 577

Wolf, B., Appenzeller, I., Cassatella, A. 1980, A&A, 88, 15

Wolf, C., Rayet, G. 1867, Comptes Rendues, 65, 292

Wolinski, K.G., Dolan, J.F. 1994, MNRAS, 267, 5

Woosley, S.E., Bloom, J.S. 2006, ARA&A, 44, 507

Zahn, J.-P. 1977, A&A, 57, 383